

High-throughput and modeling technologies for process development in antibody purification

zur Erlangung des akademischen Grades eines
DOKTORS DER INGENIEURWISSENSCHAFTEN (Dr.-Ing.)

der Fakultät für Chemieingenieurwesen und Verfahrenstechnik des
Karlsruher Instituts für Technologie (KIT)

genehmigte
DISSERTATION

von
Thiemo Huuk, M.Sc.
aus Wuppertal

Referent: Prof. Dr. Jürgen Hubbuch
Korreferent: Prof. Dr. Matthias Franzreb
Tag der mündlichen Prüfung: 26.02.2016

"HIER KÖNNTE IHRE WERBUNG STEHEN" :-)

Danksagung

Für die Unterstützung während meiner Promotion möchte ich mich insbesondere bei den folgenden Personen bedanken:

Prof. Jürgen Hubbuch für die Betreuung meiner Arbeit und die Freiheit mich in verrückten Projekten austoben zu können.

Prof. Matthias Franzreb für die Übernahme des Korreferats.

Meinem Kollegen Dr. Tobias Hahn für die geniale Zusammenarbeit in den letzten 4 Jahren, die mich sowohl fachlich als auch menschlich geprägt hat.

Meinen Studenten ohne die ich meine Forschungsthemen nicht so breit hätte streuen können und mit denen ich mir meine Neugier bewahren konnte. Vielen Dank an Anna Bogutzki, Mareike Kühner, Daniel Büchler, Alex Dieudonné, Jacqueline Göpper, Zoé Pena, Gang Wang, Barbara Schmiege, Eva Donner, Till Briskot und Alexander Gutzler.

Meinem Kollegen Dr. Pascal Baumann der mich in meiner Arbeit unterstützt hat und mit mir legendäre Dienstreisen überstanden hat :-)

Meiner Kollegin Nina Brestrich für die fachlichen Diskussionen und die tatkräftige Unterstützung im Labor.

Meinen Kollegen und ehemaligen Kollegen am MAB.

Dr. Stefan Hepbildikler, Dr. Jan Griesbach, Dr. Susanne Nath, Dr. Ferdinand Stückler und Katharina Doninger von Roche, die mich finanziell getragen haben und mir immer mit Rat und Tat zur Seite standen.

Zusammenfassung

Biopharmazeutische Proteine sind eine der am schnellsten wachsenden Medikamentenklassen. In 2012 waren 14 der 37 durch die US Arzneimittelbehörde FDA zugelassenen Medikamente Biopharmazeutika. Innerhalb des Produktionsprozesses von Biopharmazeutika muss im Anschluss an die Biosynthese des Proteins mittels genetisch veränderten Zellen, das Zielprotein aufgereinigt werden. Dieses sog. *Downstream Processing* muss gewährleisten, die extrem vielfältigen Typen an Verunreinigungen zu entfernen. Hierzu zählen Zellen und Zellbruchstücke, verschiedenste Proteine die auf die Wirtszelle zurückzuführen sind, stark geladene Nukleinsäuren, sowie unerwünschte Produktvarianten.

Die Verkürzung der Entwicklungszeiten für diese Reinigungsprozesse steht im engen Zusammenhang mit der Etablierung standardisierter Vorgehensweisen in der Prozessentwicklung. Für die Reinigung von monoklonalen Antikörpern wurden hierzu, auf Grundlage von bestehendem Prozesswissen, sogenannte Plattformprozesse etabliert. Typische Plattformprozesse zur Reinigung von Antikörpern beginnen mit einer Fest-Flüssig-Trennung um Feststoffe aus der Prozesslösung zu entfernen. Diese würden nachfolgende Prozessschritte beeinträchtigen. Nach der Abreicherung von Feststoffen, wird die Prozesslösung mit einer Protein A Chromatographie weiter verarbeitet. In dieser kann der Antikörper selektiv aus der Prozesslösung gebunden werden ohne das eine weitere Vorbehandlung notwendig ist. Die meisten Wirtsproteine und die Nukleinsäuren binden nicht an den Liganden der Protein A Säule und fließen während des Beladens oder eines nachgelagerten Waschschrittes durch die Säule. Die Elution des Antikörpers erfolgt über eine Absenkung des pH Wertes, der eine Abstoßung induziert. Der gesammelte saure Produktpool wird als nächstes einer Virusinaktivierung unterzogen, um die Virussicherheit zu gewährleisten. Im Anschluss erfolgt die weitere Reinigung mittels einer Kationenaustauscher-Chromatographie (CEX) die in einer binde und elutions Betriebsweise eingesetzt wird, um produktähnliche Kontaminanten, wie z.B. Produktaggregate oder Buchstücke abzutrennen. In der Regel beinhaltet ein Plattformprozess einen dritten chromatographischen Schritt. Im Vergleich zu den zuvor beschriebenen Schritten ist dieser relativ flexibel. Die finale Feinreinigung erfolgt dabei häufig mittels einer Anionenaustauscher-Chromatographie (AEX) die in einer Durchfluss-Betriebsweise eingesetzt wird. Bei dieser Betriebsweise bindet das Produkt nicht an die Säule und fließt ungehindert durch diese hindurch. Die verbleibenden Kontaminanten binden hingegen an die Säule. Zum Schluss erfolgt eine Virusfiltration aus Gründen der Sicherheitsanforderungen und eine Ultra-/Diafiltration um die Flüssigkeit in der das Produkt gelöst ist in eine Matrix zu überführen, die für die Anwendung beim Menschen geeignet ist oder für die nachfolgende Formulierung benötigt wird.

Für hoch konservierte Molekülklassen, wie z.B. Antikörper, besteht die derzeitige Entwicklung von Reinigungsprozessen in der Adaption der bestehenden Plattformprozesse an

neue Moleküle. In der Regel erfolgt dies auf Grundlage von sog. *Design of Experiments* (DoE), wobei die Planung der Experimente auf einer statistischen Grundlage erfolgt und die Daten im Anschluss an empirische Korrelationen, wie z.B. lineare oder quadratische Funktionen angepasst wird. Der größte Teil der Entwicklungsaufwendungen entfällt hierbei, aufgrund der vielen Freiheitsgrade, auf die Optimierung der Chromatographie Schritte. Im Folgenden werden wir uns daher auf die Betrachtung der Chromatographie Schritte beschränken.

Unter dem Konzept von *Quality by Design* (QbD) stellen die regulatorischen Behörden ein neuartiges Konzept der Prozessentwicklung vor. Zuvor basierten die Zulassungsverfahren auf engen Bereichen für Prozessparameter und einer Kontrollstrategie, auf deren Grundlage Abweichungen von den vorgegebenen Parametern erkannt werden müssen. Wenn ein Prozess den vorgegebenen Parameterbereich verlässt, wird die entsprechende Produktionscharge verworfen. QbD bedeutet in diesem Zusammenhang den Aufbau eines detaillierteren Prozessverständnisses auf einer mechanistischen Grundlage. Dies umfasst das Verständnis wie die Parameter des Produktionsprozesses die Qualität des finalen Produktes beeinflussen. Für den Aufbau dieses mechanistischen Verständnisses wird den Firmen im Gegenzug die Zulassung flexiblerer Prozesse in Aussicht gestellt.

Um über die Möglichkeiten von DoE und empirischen Korrelationen hinausgehend das im Rahmen von QbD erforderliche Prozessverständnis aufzubauen, steht der Einsatz einer Hochdurchsatz-Prozessentwicklung (HTPD) und einer Prozessentwicklung basierend auf mechanistischen Modellen im Raum. Beide Technologien werden derzeit meist unabhängig voneinander eingesetzt, obwohl es offensichtliche synergistische Effekte gibt. HTPD bezieht sich auf den Dreiklang aus Miniaturisierung, Automation und Parallelisierung von experimentellen Abläufen. HTPD hat seinen Weg in die Industrie gefunden und ist mittlerweile ein fester Bestandteil im Methodenportfolio für erste Screening-Experimente, wie z.B. die Auswahl von Adsorbentien oder von Salzen.

Aufgrund der technologischen Komplexität wird eine mechanistische Modellierung vorwiegend im akademischen Kontext eingesetzt. In Abgrenzung gegenüber statistischen Modellen, wie DoE oder der alleinigen Erhöhung der Menge an Daten im HTPD, basiert mechanistische Modellierung auf zugrundeliegenden mechanistischen Prinzipien, wie z.B. Diffusionsgesetzen.

Die mechanistische Modellierung umfasst eine fluide mobile Phase, die durch eine feste stationäre Phase gepumpt wird. Die stationäre Phase besteht dabei aus porösen Adsorbentpartikeln, um die Oberfläche zu vergrößern, welche über ihre Funktionalisierung für die Adsorption verantwortlich ist. Die Kombination von verschiedenen Modellen erlaubt sowohl die Berücksichtigung von Effekten die im interpartikulären Volumen auftreten, wie z.B. Konvektion und axiale Dispersion und von Mechanismen die auf die poröse Struktur der Partikel zurückzuführen sind (z.B. Film- und Porendiffusion). Eine Isothermengleichung wird genutzt um den Proteintransfer aus der flüssigen Phase auf die Oberfläche des Adsorbentens zu beschreiben.

In der ersten Publikation stellen wir die am Institut entwickelte Chromatographie Modellierungssoftware ChromX vor und wie diese in einem Lehrumfeld eingesetzt werden kann. In dem hier vorgestellten Bachelor-Praktikum wurde eine modellbasierte Prozessentwicklung für einen einzelnen Chromatographie Schritt durchgeführt, um einen monoklonalen Antikörper aus einer Mischung aus drei Modellproteinen aufzureinigen. Die Software ChromX

wurde in den folgenden Publikationen als Werkzeug für die modellbasierte Prozessentwicklung eingesetzt.

Eine modellbasierte Prozessentwicklung erfordert einen schnellen und zuverlässigen Weg zur Bestimmung der zahlreichen Modellparameter. Diese Parameter teilen sich in solche auf, welche die Säule beschreiben und solche die sich auf die einzelnen Proteine beziehen. Die ionische Kapazität ist z.B. eine Säuleneigenschaft, welche die Konzentration von Liganden auf der Oberfläche eines Ionentauschers beschreibt. Der traditionelle Weg zu experimentellen Bestimmung der ionische Kapazität ist die Säure-Base-Titration. Einer der Hauptnachteile diese Methode ist die Beeinträchtigung mancher industriell relevanter Adsorber und die mangelnde Übertragbarkeit auf roboterbasierte Hochdurchsatzexperimente. Um diese Einschränkungen zu umgehen, haben wir eine alternative Methode zur Bestimmung der ionischen Kapazität entwickelt, die auf der Adsorption der natürlichen, im UV Licht detektierbaren Aminosäure Histidin beruht. Die Methode stellen wir im zweiten Artikel vor. Diese nicht-invasive, photometrische Methode kann sowohl in der konventionellen Säulenchromatographie, als auch in roboterbasierten Hochdurchsatzexperimenten eingesetzt werden. In der Folge ermöglicht dies die Kalibrierung von mechanistischen Chromatographiemodellen, basierend auf verschiedenen experimentellen Systemen und eröffnet so den Weg zu Hybridansätzen aus HTPD und mechanistischer Modellierung. Zusätzlich ermöglicht die Methode die Bestimmung der Adsorbervolumen in der sog. *batch* Chromatographie und verbessert somit deren Datenqualität.

Die proteinbezogenen Parameter in der mechanistischen Modellierung werden in der Regel mittels Schätzungen basierend auf experimentellen Daten und von Peakfitting bestimmt. Diese Parameter beschreiben z.B. die Anzahl an Ladungs-Patches die ein Protein besitzt. Bisher werden die Experimente für die Parameterschätzung meist nach persönlichen Erfahrungen und Daumenregeln geplant. Im dritten Manuskript stellen wir eine Methode namens *Optimal Experimental Design* (OED) vor. Diese ist ein zentraler Bestandteil eines ausgereifteren Vorgehens zur Planung von Experimenten. OED erlaubt die nüchterne Bestimmung eines nächsten Experimentes, basierend auf einer Maximierung des Informationsgehaltes dieses Experimentes.

Chromatographie Prozesse werden meist über im Flussweg befindliche UV Detektoren überwacht und kontrolliert. Da die mechanistische Chromatographiemodellierung auf molaren bzw. Massenkonzentrationen beruht, ist eine Sensorkalibrierung erforderlich, um die UV Signale zu konvertieren. Weiterhin müssen die molaren Konzentrationen in der Prozesslösung bekannt sein. Die Erstellung solcher Kalibrierungen und die Untersuchung der Prozesslösung ist in Folge der zahlreichen Komponenten in einem industriellen Produktionsprozess eine große Herausforderung und daher zumindest in der Frühphase der Prozessentwicklung nicht vorhanden. Im vierten Artikel stellen wir einen universellen Ansatz vor, die Parameter einer Sensorkalibrierung von dem Minimierungsproblem in die Isothermen-Gleichung zu verschieben. Dies ermöglicht eine Modellkalibrierung basierend auf UV Signalen anstelle von molaren Konzentrationen.

Der Einsatz von HTPD in der Prozessentwicklung stellt eine große Herausforderung an den Probendurchsatz einer nachgelagerten Analytik dar. Im fünften Artikel untersuchen wir die Möglichkeiten einer nicht-invasiven analytischen Methode, die auf den Unterschieden in den Proteinspektren und einer multivariaten Datenanalyse beruht, einen Limitierung der HTPD aufgrund der Analytik zu verhindern. Der vorgestellte Ansatz ermöglicht die

integrierte Aufnahme von Multikomponenten *batch* Isothermen auf einem Pipettierroboter. Das beobachtete kompetitive Bindungsverhalten konnte dabei basierend auf einer mechanistischen Modellierung erklärt werden.

Die beiden letzten Manuskripte beschäftigen sich mit angewandten Prozessoptimierungsfallstudien. Im sechsten Manuskript wird eine klassische DoE basierte und eine modellbasierte Prozessentwicklung miteinander verglichen. Die Untersuchung erfolgt dabei anhand der Reinigung eines monoklonalen Antikörpers aus einem industriellen Produktstrom. Der Kationentauscher soll dabei Spezies mit größerem, als auch kleinerem Molekulargewicht erfassen. In dem experimentellen Ansatz wird eine lineare Gradientenelution, 5 Stufenelutionen und die entsprechenden Fraktionsanalytiken (SEC) genutzt. Im modellbasierten Ansatz erfolgt die Kalibrierung auf Grundlage des Gradienten, zweier Stufen und der Fraktionsdaten. Der Prozess wurde mit beiden Methoden hinsichtlich einer Zielfunktion bestehend aus einer Monomer Reinheit von mindestens 90%, einer Ausbeute von mindestens 80% und einem maximalen Fraktionsvolumen von 5 Säulenvolumen (Einschränkung der technischen Infrastruktur) optimiert. Beide Ansätze führten zu optimalen Stufenelutionen im Bereich von 200 bis 210mM Salz. Somit konnte gezeigt werden dass die mechanistische Modellierung eine Alternative oder sogar ein Ersatz für eine experimentelle Prozessentwicklung sein kann.

Die vorherige Arbeit beschränkte sich auf einen eine Säule umfassenden Prozess. Industrielle Reinigungsprozesse bestehen jedoch meist auf mehreren solchen Operationen, die nacheinander angeordnet sind. Die Optimierung solcher Mehr-Säulen-Prozesse wird in der Regel nacheinander durchgeführt, um die experimentelle Komplexität gering zu halten. Nichtsdestotrotz wird vermutet, dass die konzertierte Optimierung von aufeinanderfolgenden Chromatographien Vorteile hinsichtlich der Identifikation eines globalen Prozessoptimums birgt, anstelle des Auffindens von zwei Einzeloptima. Im siebten Manuskript kalibrierten wir ein mechanistisches Modell für einen CEX und einen AEX und eine Mischung aus drei Modellproteinen. Zuerst optimierten wir die beiden Prozessfließschemata (CEX→AEX und AEX→CEX) in einem konzertierten Ansatz. Hierbei wird nur die Reinheit, Ausbeute und Konzentration in der letzten Säule ausgewertet. Die Kombination CEX→AEX zeigte sich der anderen Alternative überlegen. Um die Relevanz der konzertierten Optimierung zu untersuchen, wiederholten wir die Optimierung des gleiches Prozessschemas, basierend auf einer sequentiellen Optimierung der beiden Säulen. Bei einer reinen Betrachtung des Zwischenergebnissen zwischen den beiden Säulen, zeigt sich die sequenzielle Optimierung im Vorteil. Das insgesamt überlegende Prozessoptimum wird hingegen in dem konzertierten Ansatz gefunden.

Abstract

Biopharmaceutical proteins constitute one of the fastest growing classes of drugs. 14 out of 37 drugs approved by the US Food and Drug Administration (FDA) in 2012 are biopharmaceuticals. Within the production process of biopharmaceutical proteins, subsequently to the biological synthesis of the protein using cellular systems and genetic engineering technologies, the target protein has to be purified out of the very heterogenous cultivation media. This *downstream processing* has to cope with an extreme wide range of impurities, such as cells and cell fragments, a manifold mixture of host cell proteins, highly charged nucleic acids, and undesired product variants.

The shortening of industrial *downstream process development* (DSP) timelines is closely related to the standardization of the development workflows. For the purification of monoclonal antibodies so called *platform processes* have been derived from historical process knowledge. Typical mAb platform downstream processes start with a solid-liquid separation to deplete solid impurities from the product feed stream and to prevent a deterioration of the subsequent unit operations. The particle-free product feed stream is directed to an affinity protein A chromatography, which is capable to bind the mAb selectively from the feed without further preconditioning. Most of the host cell proteins (HCP) and the residual DNA do not adsorb to the ligand and flow-through the column during the loading or a subsequent wash step. The elution of the mAb is triggered by a decrease of the pH value, inducing a charge repulsion effect. The collected acidic product pool is commonly directed to a virus inactivation procedure, to guarantee viral safety. Afterwards, a cation exchange chromatography (CEX) is commonly operated in bind and elute mode to remove product-related impurities such as aggregates and fragments. In most cases, platform processes contain a third chromatographic operation. This third chromatography is quite flexible compared to the previously mentioned process flow-sheet. As a final polishing chromatography an anion exchange chromatography (AEX) operated in flow-through mode is a frequently used option. In a flow-through operation, the product does not adsorb to the AEX and flows freely through the column, whereas residual contaminants adsorb to the AEX. Finally, a virus filtration is used to guarantee viral safety and an ultra-/diafiltration is used to exchange the matrix against a buffer system which is suitable for the application in humans or the subsequent formulation process.

The current status of industrial downstream process development for highly conserved classes of biopharmaceuticals such as antibodies, is dominated by the adaptation these platform processes to new molecules. In most cases this is carried out by *Design of Experiments* (DoE) approaches, which rely on a statistically motivated experimental planning and the fitting of empirical correlations, such as linear or quadratic functions. To a great

extend, the process development effort is attributed to the chromatographic operations, due to the numerous operational parameters. Therefore, we will focus on chromatographic processes in the following.

Under the concept of *Quality by Design* (QbD), the regulatory agencies proposed a new concept of process development. Before, the filing of a production process was predominantly based on narrow parameter ranges and a control strategy to detect an operation outside the filed process ranges. In case of an “out of specification” operation, the production lot was rejected. QbD means the establishment of a more detailed mechanistic process understanding. This comprises the understanding, how operational parameters of the production process, influences the quality of the final product. By providing this kind of mechanistic understanding, the filing of more flexible process will be possible.

Exceeding the capabilities of DoE and empirical correlations, high-throughput process development (HTPD) and process development based on mechanistic models are two technologies which are considered to provide the process understanding requested by the QbD concept. Both technologies are commonly used independently from each other, despite their synergistic potential. HTPD refers to the triad of miniaturization, automation, parallelization of experimental workflows and has made its way into industries standard repertoire for initial experimental screenings, such as the discrimination between different adsorbers or types of salt.

Due to its technological complexity, mechanistic modeling has been predominantly used in the academic context for a long time. In contrast to statistical modeling approaches such as DoE or the sole increase of data in HTPD, mechanistic modeling is based on underlying mechanistic principles, such as diffusion laws.

Mechanistic modeling of chromatography accounts for the fluid mobile phase that is pumped through a solid stationary phase. The stationary phase consists of porous adsorber beads, to increase the adsorber surface, which is functionalized to modulate the adsorption process. The combination of different models, allows for the consideration of effects occurring in the volume between the particles, such as convection and axial dispersion, or mechanisms arising from the porous structure of the stationary phase, such as film or pore diffusion. Finally, an isotherm equation is used to describe the transition of protein species from the mobile phase onto the adsorber surface.

In the 1st publication, we presented the in-house developed chromatography modeling software ChromX and its capabilities in academic teaching. The undergraduate students laboratory course presented in this article focused on the model-based optimization of a single column chromatography process, to purify a monoclonal antibody from an artificial three component mixture. The software ChromX was utilized in the following publications as a tool for model-based process development.

Model-based process development requires a rapid and reliable way to determine the numerous model parameters. These parameters can be divided in column-related properties and protein-related ones. The ionic capacity is a column-related properties, which describes the concentration of the ligands on the surface of an ion exchange adsorber. The traditional method to determine the ionic capacity is an acid-base titration. One of the major drawbacks of this method is the deterioration of some kinds of industrial-relevant adsorbers and the impossibility to transfer the method to high-throughput experiments on

robotic work stations. To overcome the constraints of acid-base titration, we developed an alternative method to determine the ionic capacity based on the adsorption of the natural, uv-detectable amino acid histidine. The method is presented in the 2nd paper. This non-invasive, photometric method can be used in conventional column chromatography and in robotic high-throughput experiments. Therefore, it enables the calibration of mechanistic models for chromatography in various experimental systems and it opens up the way for a hybrid approach of robotic high-throughput chromatography and mechanistic chromatography modeling. In addition, it enables the reliable determination of the exact adsorber volumes in batch chromatography and improves the data quality in batch chromatography.

The protein-related parameters for mechanistic modeling are commonly estimated based on experimental data and a peak fitting approach. These parameters describe for example the number of charged patches of a protein. The way of generating the experimental data for parameter estimation is predominantly based on personal experience and rules of thumb. In the 3rd manuscript, we present a method called *Optimal Experimental Design* (OED), which is a central part of a more sophisticated way of estimating model parameters. OED enables the rational determination of the experiment which should be carried out next, based on a maximization of the added information content of this experiment.

Chromatographic process monitoring and control is commonly based on in-line uv detectors. Since mechanistic chromatography modeling requires molar or mass concentrations, a sensor calibration for the conversion of uv signals to molar concentrations and the molar composition of the feed solution are a prerequisite for model-based process development. The establishment of sensor calibrations for the numerous species in an industrial purification challenge and the analysis of the exact feed composition can be quite time consuming and therefore it is unusual to establish these calibrations in the early stages of industrial process development. In the 4th article, we present a generic approach to shift the parameters for the sensor calibrations from the minimization problem to the isotherm equation. This enables a model calibration based on uv signals instead of molar concentrations.

The integration of high-throughput experiments in the purification process development can be quite challenging with respect to the demands on the throughput for the subsequent analytical methods. In the 5th article, we evaluated the capabilities of a non-invasive analytical method based on the different uv spectra of proteins and multivariate statistics, to prevent an analytical bottleneck in high-throughput process development. The presented analytical approach enables the integrated generation of multi-component batch isotherms on a robotic work station. The observed competitive binding behavior could be explained based on a mechanistic modeling approach.

The last two manuscripts cover two types of process optimization case studies. The 6th manuscript presents a study comparing traditional DoE-driven process development and process development based on mechanistic modeling. This work is focusing on the purification of a monoclonal antibody (mAb) out of an industrial feed solution containing two higher molecular and one lower molecular species, using cation exchange chromatography. The experimental approach comprises a linear salt gradient elution and 5 step elutions with different salt concentrations, complemented with a peak fraction analysis using analytical size exclusion chromatography. In the model-based optimization approach parameters were estimated from a linear salt gradient experiment, two salt step elutions, and the corresponding fraction analysis data. The process was optimized with the objective of a

monomer purity of at least 99%, a yield of at least 80%, and a maximal fraction volume of 5 column volumes due to constraints in the technical infrastructure, using the experimental and the model-based approach. Both optimization approaches result in steps elutions of 200 to 210mM salt, meeting the three constraints. Therefore, it could be demonstrated that mechanistic modeling is a suitable alternative or complement for experimental driven process development.

The previously mentioned work focused on single column purification processes. However, industrial downstream processes commonly consist of several chromatographic operations, which are arranged in a sequential manner. The optimization of these multi-column processes is commonly carried out one after each other, to keep the experimental complexity manageable. Nevertheless, the concerted optimization of two consecutive chromatographies is supposed to be beneficial, e.g. through the identification of an overall process optimum, rather than two single chromatography optima. In the 7th manuscript, we calibrated a mechanistic chromatography model for an artificial three component protein mixture on a cation (CEX) and an anion exchange adsorber (AEX). First, we optimized the two possible process flowsheets (CEX→AEX and AEX→CEX) using a concerted optimization approach. For this, the purity, recovery, and concentration derived from the last column were evaluated based on an objective function. The CEX→AEX flowsheet outperforms the alternative process flowsheet. To evaluate the impact of a concerted process optimization, we repeated the optimization of the CEX→AEX flowsheet, optimizing the columns one after each other. This sequential optimization approach showed a superior intermediate result after the first column, but resulted in an inferior overall performance.

Contents

1	Introduction	1
1.1	Downstream Process Development	1
1.2	High-throughput Process Development	4
1.3	Model-based Process Development	5
1.4	Research Proposal	9
1.5	Outline	11
2	Simulating and Optimizing Preparative Protein Chromatography with ChromX	15
	T. Hahn, T. Huuk, V. Heuveline, J. Hubbuch	
2.1	Introduction	16
2.2	Theory	17
2.3	ChromX Features	19
2.4	Software Exercises	20
2.5	Laboratory Course Structure	20
2.6	Laboratory Results	22
2.7	Pedagogical Aspects	22
2.8	Conclusion	24
3	A Versatile Noninvasive Method for Adsorber Quantification in Batch and Column Chromatography Based on the Ionic Capacity	27

T. Huuk, T. Briskot, T. Hahn, J. Hubbuch	
3.1	Introduction 28
3.2	Theory 29
3.3	Materials and Methods 31
3.4	Results 37
3.5	Discussion 43
3.6	Conclusion 45
4	Optimal Experimental Design for the Determination of Isotherm Parameters of Glucose Oxidase using Mixed Mode Column Chromatography 49
T. Hahn, G. Wang, T. Huuk, V. Heuveline, J. Hubbuch	
4.1	Introduction 50
4.2	Theory 51
4.3	Materials and Methods 55
4.4	Results and Discussion 58
4.5	Conclusions 64
5	UV Absorption-based Inverse Modelling of Protein Chromatography 67
T. Hahn, P. Baumann, T. Huuk, V. Heuveline, J. Hubbuch	
5.1	Introduction 68
5.2	Materials and Methods 69
5.3	Results and Discussion 76
5.4	Concluding Remarks 79
6	Deconvolution of High-throughput Multi-component Isotherms Using Multivariate Data Analysis of Protein Spectra 81
P. Baumann*, T. Hahn*, T. Huuk*, A. Osberghaus, J. Hubbuch (* contributed equally)	
6.1	Introduction 82
6.2	Materials and Methods 83
6.3	Results and Discussion 86
6.4	Concluding Remarks 91

7 Calibration-free Inverse Modeling of Ion-exchange Chromatography in Industrial Antibody Purification	93
T. Hahn, T. Huuk, A. Osberghaus, K. Doninger, S. Nath S. Hepbildikler, V. Heuveline, J. Hubbuch	
7.1 Introduction	94
7.2 Materials and Methods	95
7.3 Results and Discussion	99
7.4 Concluding Remarks	103
8 Model-based Integrated Optimization and Evaluation of a Multi-step Ion Exchange Chromatography	105
T. Huuk, T. Hahn, A. Osberghaus, J. Hubbuch	
8.1 Introduction	106
8.2 Theory	108
8.3 Materials	110
8.4 Methods	111
8.5 Results	115
8.6 Discussion	124
8.7 Conclusion	128
9 Conclusion and Outlook	131
A Supporting Information	133
A.1 Simulating and Optimizing Preparative Protein Chromatography with ChromX	133
A.2 A Versatile Noninvasive Method for Adsorber Quantification in Batch and Column Chromatography Based on the Ionic Capacity	141
A.3 Deconvolution of High-throughput Multi-component Isotherms Using Multivariate Data Analysis of Protein Spectra	145
Bibliography	147

1 | Introduction

Biopharmaceuticals constitute one of the fastest growing classes of drugs. 14 out of 37 drugs approved by the US Food and Drug Administration (FDA) in 2012 are biopharmaceuticals [128]. The term biopharmaceuticals can refer to proteins (e.g. antibodies or insulin), nucleic acids (to be used in future gene therapies), or whole cells for cell-therapies. This work will focus on biopharmaceuticals belonging to the group of proteins, with a special attention to monoclonal antibodies (mAbs).

In contrast to chemically produced molecules, biopharmaceutical proteins are produced by cellular systems, due to their molecular complexity. These expression systems can be simple microbial systems such as *E.coli* or *S.cerevisiae*, or even more complex systems such as plants or mammalian cells [103; 138; 169]. Using genetic engineering technologies, these expression systems are empowered to produce the desired protein [107].

The production process of biopharmaceuticals starts with the cultivation of these cells, called Upstream Processing (USP) [25]. During the USP, the cells express the protein in huge amounts and transport them to an intracellular compartment in case of most bacterial systems, or secrete them into the extracellular cultivation media for most mammalian systems. USP ends up with a very heterogeneous mixture of cultivation media components, the cellular expression system and its metabolites, proteins and nucleic acids related to the expression system, and the biopharmaceutical protein in its functional conformation and undesired product variants [40; 99]. The contaminants related to the expression system or the production process are called process-related impurities, those related to unwanted product variants are called product-related impurities. The biopharmaceutical protein has to be purified out of this crude product feed stream in the so called Downstream Processing. The following section will focus on the Downstream Processing of monoclonal antibodies.

1.1 Downstream Process Development

The shortening of industrial *Downstream Process Development* (DSP) timelines is closely related to the standardization of the development workflows. For the purification of monoclonal antibodies so called *platform processes* have been derived from historical process knowledge [39; 100; 145]. Different mAbs have similar physico-chemical properties as a consequence of their similar molecular structure. This kind of framework protein sequence enables the implementation of a platform process which can be easily adapted to different mAbs.

Typical mAb platform downstream processes start with a solid-liquid separation to deplete solid impurities from the product feed stream and to prevent a deterioration of the subsequent unit operations. These solid impurities are attributed to the cellular expression system and cell fragments (*debris*) due to cell disruption within the cultivation process. The removal of cells is commonly carried out via centrifugation, followed by a depth filtration to remove the remaining debris [100]. The particle-free product feed stream is directed to an affinity protein A chromatography. The protein A chromatography is capable to bind the mAb selectively from the feed without further preconditioning [39]. The adsorption is attributed to the protein A ligand which is originally derived from *Staphylococcus aureus* [114]. Most of the host cell proteins (HCP) and the residual DNA do not adsorb to the ligand and flow-through the column during the loading or a subsequent wash step. HCP remaining after the protein A chromatography are frequently attributed to an interaction with the adsorbed mAb and to a lesser extent with the ligand itself [98]. The elution of the mAb is triggered by a decrease of the pH value, inducing a charge repulsion effect.

The collected acidic product pool is commonly directed to a virus inactivation procedure, to guarantee viral safety. Viral safety is a critical concern of biopharmaceutical production processes and addressed by the regulatory agencies [73]. Viruses might be introduced to the product feed stream by the cellular expression system, by process solutions containing for example animal derived components, or by employees during the production process. To ensure the absence of viruses in the final product, two dedicated processes to inactivate viruses and to remove viruses have to be present in the purification scheme. In addition, other purification steps not primarily intended to remove viruses have to be evaluated with respect to their capability to remove possible apparent viruses. In a mAb platform process the virus inactivation is commonly implemented as a low pH incubation process. Due to the acidity of the protein A eluate, a subsequent low pH hold is reasonable [39; 100; 145]. After the low pH incubation the pH value of the product feed stream is conditioned to a moderate pH which is suitable for storage and the subsequent unit operations.

Following the virus inactivation, a cation exchange chromatography (CEX) is commonly operated in bind and elute mode to remove product-related impurities such as aggregates and fragments [39]. Aggregates commonly adsorb more strongly to the CEX adsorber due to their increased number of charges and the increased molecular size. In addition, CEX is capable to concentrate the product feed stream, thereby reducing the demands for the subsequent facility sizing [49].

In most cases, platform processes contain a third chromatographic operation. This third chromatography is quite flexible compared to the previously mentioned process flow-sheet. As a final polishing chromatography an anion exchange chromatography (AEX) operated in flow-through mode is a frequently used option. In a flow-through operation, the product does not adsorb to the AEX and flows freely through the column, whereas residual contaminants adsorb to the AEX. The operation of the final chromatography in flow-through mode provides the advantage, just to bind the remaining trace contaminants and not the almost pure antibody. Therefore, the sizing of the column is less expensive [39].

As an alternative to AEX, hydrophobic interaction chromatography (HIC) [43; 155] or combined interaction mechanisms called mixed-mode chromatography (MMC) [26; 43] are possible. The use of membrane adsorbers instead of packed-bed chromatographic columns is gaining increasingly relevance [135; 170].

Finally, a virus filtration is used to guarantee viral safety [24] and an ultra-/diafiltration is used to exchange the matrix against a buffer system which is suitable for the application in humans or the subsequent formulation process.

To a great extent, these platform processes are fixed within a company and the adaptation to new antibodies is standardized. For each unit operation a small number of process parameters are adapted to the new molecule, such as the pH value, the elution salt concentration, and the boundaries for the eluate collection in CEX [39]. This adaptation process is commonly based on *Design of Experiments* (DoE) to maximize the information content, while keeping the number of experiments fixed [148; 152].

Platform processes solely exist for molecule classes which are highly conserved on a molecular level. Therefore, for other molecule classes, DSP has to start to develop purification processes from scratch, constituting a greater challenge with respect to a reduction of development timelines. Similarly, the intensified development of antibody-derived molecules, such as Fabs poses new challenges to the standardized DSP workflows [49]. Chemically modified molecules such as antibody-drug-conjugates [130] require additional chemical reactions with specialized subsequent purification steps.

1.1.1 Regulatory Framework

Downstream process development (DSP) refers to the process of implementing purification processes, which are capable to ensure a specified quality of pharmaceutical products. The regulatory framework given by the regulatory agencies specifies these quality requirements of purification processes [76]. The regulatory agencies in the US, EU, and Japan started a harmonization of their quality requirements and proposed a new approach to develop processes under the term *Quality by Design* (QbD) [74; 75]. Previously, regulation was predominantly based on a fixed process which had to be specified in detail and analytical techniques to detect process deviations. An operation outside the filed process specifications led inevitably to a rejection of the production lot.

Under the concept of QbD the regulatory agencies demand for the development of a detailed mechanistic process understanding and granting the companies the permission to file more flexible processes in return. The term *mechanistic process understanding* has been specified by the regulatory agencies within their ICH guidelines [74]. The *Quality Target Product Profile* (QTPP) specifies the characteristics of the product, to ensure the intended quality, safety, and efficacy in the patient. The different characteristics specified in the QTPP are evaluated concerning their criticality. The most critical attributes of the product are classified as *Critical Quality Attributes* (CQA). Criticality includes the potential impact on the patient safety, the probability of occurrence, and the probability of detecting deviations of the CQA. Subsequently, process parameters or parameter combinations which influence the CQA have to be identified. These process parameters, are called *Critical Process Parameters* (CPP). The term *mechanistic process understanding* refers to the understanding of how CPP influence the CQA.

1.2 High-throughput Process Development

High-throughput process development (HTPD) is one of the recent technologies that found its way into biopharmaceutical DSP. HTPD refers to the triad of miniaturization, automation, parallelization of experimental workflows. The miniaturization of experimental systems is of outstanding importance to be able to start process development in an earlier stage of the product life cycle, when the amount of material is still limited. The automation of the experimental workflows is essential to reduce labor intensive and prone to error manual work. Automation in DSP is commonly achieved by the use of pipetting robots, called liquid handling station. Beside of the automation, these systems allow for the execution of numerous experiments in parallel, enabling the rapid generation of huge amounts of experimental data.

In the following we will focus on HTPD of chromatographic processes, although other topics such as solubility studies [166], protein folding studies [105], and aqueous extraction methods [14] have been reported in literature.

The two most common techniques to chromatographic HTPD are batch chromatographic experiments and the use of miniaturized robotic columns. Batch chromatography is commonly used for the initial parameter screenings, due to the experimental throughput, the experimental simplicity, and the low sample volume required. In batch chromatography, adsorber volumes in the range of 6.8 to 50 μL per well [90] are filled into a 96 wells plate. Based on this plates, three different types of batch chromatographic experiments are commonly used in DSP. In batch adsorption isotherm experiments, different mobile phase protein concentrations are incubated with the adsorber until equilibrium is reached. The resulting adsorption isotherms give an insight into the strength of the adsorption and the maximum binding capacity, with respect to the mobile phase conditions (e.g. pH, salt concentration, or type) [88; 90; 120; 167]. Stopping the incubation of protein and adsorber at several points in time, before the equilibrium is reached, provides batch kinetic data. These batch kinetics provide an insight into the adsorption rate and can give a first guidance for the residence time in column chromatography [15; 31; 57]. Performing one or several elution steps after the two before mentioned experimental types results in a batch bind and elute experiment that gives an insight into both, the adsorption and the desorption process. One of the critical concerns using batch chromatography is the determination of the exact adsorber volume in batch chromatography. The pipetting of the adsorber slurry is prone to error due to the rapid sedimentation of the particles and the viscosity of the suspension. An overview of how to implement a slurry pipetting procedure is given by Barker et. al [7]. Devices such as the MediaScout ResiQuot device (Atoll, Weingarten, Germany), in which the adsorber is first forced into a stainless steel grid and afterward transferred to the wells of a 96 well plate intend to prevent these prone to error pipetting operations [67].

When using miniaturized chromatographic systems, there is always a trade-off between experimental simplicity/throughput and experimental complexity/comparability to conventional chromatographic formats. Batch chromatography is unable to cover effects arising from the fluid flow in a packed bed column or the different kind of diffusion effects occurring in a column.

In the case, a higher degree of experimental complexity is necessary, miniaturized chromatographic columns (RoboColumns, Atoll, Weingarten, Germany) have been developed

[167]. The basic concept of high-throughput column chromatography (HTCC) is to miniaturize conventional chromatographic columns, to install them on a robotic work station, and to carry out the fluid flow operations by linking a robotic liquid handling arm to the column inlet. At the column outlet, the eluate can be collected drop-wise in 96 well plates. Experiments to determine the dynamic binding capacity (DBC) from isocratic robotic breakthrough experiments are technically straightforward and have been frequently published, e.g. [167]. Susanto et al. [149] extended the simple experimental determination of DBC based on HTCC by modeling of the robotic process. Baumgartner et al. [11] evaluated the impact of mixed salts on the DBC in hydrophobic interaction HTCC. Summing up, the full exploitation of HTPD can shorten the development timelines and increase the amount of experimental data derived from a limited amount of sample.

1.3 Model-based Process Development

In contrast to statistical modeling approaches such as DoE or the sole increase of data in HTPD, this section will focus on modeling based on underlying mechanistic principles. Mechanistic modeling of chromatography considers effects arising from the fluid flow through a packed bed column, the porosity of the adsorbent, and the diverse interactions between proteins and the adsorber surface. The predictive capabilities of statistical modeling and DoE are restricted to the interpolation within the calibrated parameter range and strongly depend on the complexity of the utilized statistical model (e.g. linear or quadratic interpolations). Mechanistic modeling is not restricted by the calibrated parameter range [127]. Even process parameters outside the calibrated range can be predicted, assuming no additional effects arising from the operation outside the calibrated range. A detailed review of mechanistic modeling of chromatography is given in the textbooks of Guiochon and Schmidt-Traub [55; 141].

A chromatographic separation process is characterized by a fluid mobile phase that is pumped through a solid stationary phase. The stationary phase consists of porous adsorber beads, to increase the adsorber surface, which is functionalized to modulate the adsorption process. The porosities of the packing can be characterized by tracer injections. The total porosity ε_{Tot} , the column porosity ε_{Col} , and the adsorber bead porosity ε_{Bead} can be calculated from the retention volume of a non-interacting pore-penetrating tracer $V_{tracer,small}$, a non-interacting non-pore-penetrating tracer $V_{tracer,large}$, and the geometric column volume CV :

$$\varepsilon_{Tot} = \frac{V_{tracer,small}}{CV}$$

$$\varepsilon_{Col} = \frac{V_{tracer,large}}{CV}$$

$$\varepsilon_{Bead} = \frac{V_{tracer,small} - V_{tracer,large}}{CV - V_{tracer,large}}$$

The resulting volumes within the chromatographic column are illustrated in Fig.1.1a-c. On a molecular level different effects take place in the different volumes in the chromatographic column. These effect will be explained in the next sections.

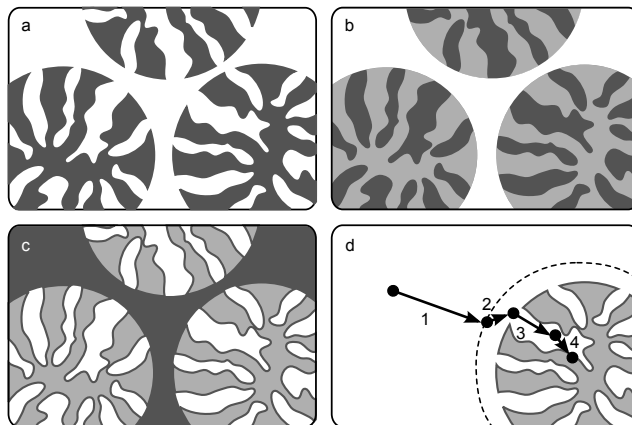


Figure 1.1: Structure of packed beds (a-c) and adsorption process (d). The total column volume is divided into the volume of the stationary phase (a), the volume of mobile phase in the pore system (b), and the interstitial volume of the mobile phase (c). Molecules are transported through the interstitial volume (d.1), pass a boundary layer (also referred to as film) around the beads (d.2), diffuse within the pore system (d.3), and adsorb onto the surface (d.4).[59]

1.3.1 Column Model

The column model describes the effects within the interstitial volume of the mobile phase on a macroscopic level. The equations describing these effects are of convection-diffusion-reaction type, whereas the reaction is the mass transfer out of the interstitial mobile phase volume. For reasons of simplicity and to ensure fast computation, the three dimensional column is reduced to one dimension along the longitudinal axis of the column. The model describes the change of the protein concentration c over the time t at a longitudinal position x in the column. The simplest column model assumes a direct contact of the interstitial volume with the adsorber surface, neglecting the pore volume. This *equilibrium dispersive model* (EDM) is shown in Eq. (1.1). The flow velocity of the mobile phase u and the total porosity of the volume ε_{Tot} form the convection term. The apparent diffusion coefficient D_{app} covers all axial diffusion effects which lead to a peak broadening. Due to the direct coupling of interstitial volume and the adsorber surface, the change in the adsorbed protein concentration q is scaled by $\frac{1-\varepsilon_{Tot}}{\varepsilon_{Tot}}$.

$$\frac{\partial c}{\partial t}(x, t) = \underbrace{-\frac{u(t)}{\varepsilon_{Tot}} \frac{\partial c}{\partial x}(x, t)}_{\text{Convection}} + \underbrace{D_{app} \frac{\partial^2 c}{\partial x^2}(x, t)}_{\text{Diffusion}} - \underbrace{\frac{1-\varepsilon_{Tot}}{\varepsilon_{Tot}} \frac{\partial q}{\partial t}(x, t)}_{\text{Mass transfer}} \quad (1.1)$$

To introduce a higher level of complexity to the column model, a pore volume with a protein concentration c_p can be introduced between the interstitial volume and the adsorber surface. This *transport dispersive model* (TDM) is depicted in Eq. (1.2). The apparent diffusion coefficient D_{app} from the EDM reduces to an axial dispersion coefficient D_{ax} covering the peak broadening effect occurring in the interstitial volume. The peak broadening effects arising from the mass transfer from the interstitial volume to the pore volume are covered by an effective mass transfer coefficient k_{eff} . The mass transfer is scaled with

$\frac{1-\varepsilon_{Col}}{\varepsilon_{Col}} \frac{3}{r_p}$ with r_p being the radius of the adsorber bead. EDM and TDM are complemented with Danckwerts boundary condition at the column in and outlet [34].

$$\frac{\partial c}{\partial t}(x, t) = \underbrace{-\frac{u(t)}{\varepsilon_{Col}} \frac{\partial c}{\partial x}(x, t)}_{\text{Convection}} + \underbrace{D_{ax} \frac{\partial^2 c}{\partial x^2}(x, t)}_{\text{Diffusion}} - \underbrace{\frac{1-\varepsilon_{Col}}{\varepsilon_{Col}} \frac{3}{r_p} k_{eff} (c(x, t) - c_p(x, t))}_{\text{Mass transfer}} \quad (1.2)$$

1.3.2 Pore Model

The TDM introduces a protein concentration c_p within the pore volume. A simple *lumped rate pore mode* (Eq. (1.3)) assumes a uniform concentration within the pore. The change of the protein concentration in the pore c_p results from the mass transition from the interstitial volume to the pore and from the mass within the pore adsorbing to the surface of the adsorber.

$$\frac{\partial c_p}{\partial t}(x, t) = \underbrace{\frac{3}{r_p} \frac{k_{eff}}{\varepsilon_{Bead}} (c(x, t) - c_p(x, t))}_{\text{Interstitial} \leftrightarrow \text{Pore}} - \underbrace{\frac{1-\varepsilon_{Bead}}{\varepsilon_{Bead}} \frac{\partial q}{\partial t}(x, t)}_{\text{Pore} \leftrightarrow \text{Adsorption}} \quad (1.3)$$

The more complex *general rate model* (GRM) introduces a radial dimension r of the adsorber particle. The GRM is depicted in Eqs. 1.4 and 1.5. The effective mass transfer coefficient k_{eff} from the lumped rate model is splitted in a film transfer coefficient k_{film} referring to the mass transfer over the boundary layer and a pore diffusion coefficient D_{pore} covering the diffusion along the radial pore position within the bead.

$$\frac{\partial c_p}{\partial t}(x, r, t) = D_{pore} \left(\frac{\partial^2 c}{\partial r^2} + \frac{2}{r} \frac{\partial c}{\partial r} \right) - \frac{1-\varepsilon_{Bead}}{\varepsilon_{Bead}} \frac{\partial q}{\partial t}(x, r, t) \quad (1.4)$$

$$\frac{\partial c_p}{\partial r}(x, r_p, t) = \frac{1}{D_{pore}} \frac{k_{film}}{\varepsilon_{Bead}} (c(x, t) - c_p(x, r_p, t)). \quad (1.5)$$

1.3.3 Adsorption Model

The adsorption model describes the mass transition from the pore c_p onto the surface of the adsorber q . The steric mass action (SMA) isotherm [23] is frequently used for ion exchange chromatography. The isotherm assumes that a macro molecule exhibiting ν charged patches, adsorbes to the ion exchange resin thereby replacing an equal amount of counter ions from the adsorber surface. The adsorber is characterized by a ligand concentration Λ , called the total ionic capacity. The equilibrium of the adsorption desorption process is captured by a coefficient $k_{eq} = k_{ads} \cdot k_{des}^{-1}$ and the velocity of the reaction by the coefficient $k_{kin} = k_{des}^{-1}$. The macro molecule adsorbed to the surface replaces ν counter-ions

and shields σ ligands by steric effects. This steric shielding of binding sites reduces the apparent binding capacity of the adsorber in the non-linear range of the isotherm. Operation in the non-linear range of the isotherm is common for preparative chromatography. The SMA isotherm for n proteins is shown in Eq. (1.6) and the corresponding equation for the replaced salt ions is given in Eq. (1.7).

$$k_{kin,i} \frac{\partial q_i}{\partial t}(x,t) = k_{eq,i} \underbrace{\left(\Lambda - \sum_{j=1}^n (\nu_j + \sigma_j) q_j(x,t) \right)}_{\bar{q}_{salt}^{\nu_i}}^{\nu_i} c_{p,i}(x,t) - c_{p,salt}^{\nu_i}(x,t) q_i(x,t) \quad (1.6)$$

$$q_{salt}(x,t) = \Lambda - \sum_{j=1}^n \nu_j q_j(x,t). \quad (1.7)$$

1.4 Research Proposal

The current status of industrial downstream process development (DSP) for highly conserved classes of biopharmaceuticals such as antibodies, is dominated by platform technology. The way of adapting these generic processes to new molecules is standardized to the greatest possible extent, to shorten the development timelines and to ensure a predictable expenditure of time. In most cases the adaptation is carried out by *Design of Experiments* (DoE) approaches, which rely on a statistically motivated experimental planning and the fitting of empirical correlations, such as linear or quadratic functions. Under the concept of *Quality by Design* (QbD), the regulatory agencies proposed a new concept of process development. Before, the filing of a production process was predominantly based on narrow parameter ranges and a control strategy to detect an operation outside the filed process ranges. In case of an “out of specification” operation, the production lot was rejected.

Under the QbD concept, the regulatory agencies propose the establishment of a more detailed mechanistic process understanding. This comprises the understanding, how operational parameters of the production process, influences the quality of the final product. By providing this kind of mechanistic understanding, the filing of more flexible process will be possible.

Exceeding the capabilities of DoE and empirical correlations, high-throughput process development (HTPD) and process development based on mechanistic models are two technologies which are considered to provide the process understanding requested by the QbD concept. Both technologies are commonly used independently from each other, despite their synergistic potential. HTPD has made its way into industries standard repertoire for initial experimental screenings, such as the discrimination between different adsorbers or types of salt. Due to its technological complexity, mechanistic modeling has been predominantly used in the academic context for a long time.

The objectives of this thesis were the identification of the major obstacles for process development based on mechanistic modeling and the development of additional techniques to overcome them. Particular attention was given to the synergistic potential of modeling and HTPD. To pave the way for model-based process development, we lowered the first hurdle for this new technology by the introduction of a modeling technology package. In addition to the software ChromX, this technology package addressed several challenges. Model-based process development requires a rapid and reliable way to determine the model parameters. These parameters can be divided in column-related properties and protein-related ones. The former method to determine the column-related ionic capacity based on an acid-base titration was prone to deteriorate some chromatographic adsorbers. Therefore, we had to develop a new method to overcome these limitations.

Due to the lack of pure protein samples in industrial process development scenarios, protein-specific model parameters are commonly estimated from experimental data. The generation of these data was based on experience and rules of thumb. We implemented and evaluated a model-based concept of planning experiments.

In most industrial and academic purification tasks, the exact molar concentrations in the product feed stream are unknown or they are not accessible with reasonable effort. Mechanistic modeling is traditionally based on known molar concentration.

To overcome this limitation, we had to develop an approach to calibrate mechanistic models based on commonly available uv signals instead of molar concentrations.

To demonstrate the capabilities of mechanistic modeling in comparison to conventional DoE approaches, we had to carry out a comparative study on these technologies.

Most academic modeling case studies focused on single column processes, although industrial purification schemes are commonly based on multiple chromatographic operations. Therefore we had to extend the commonly employed single column modeling to the multi-column optimization of a complete process flow sheet.

HTPD and mechanistic modeling are commonly used separately. Batch chromatography is frequently used for initial parameter or adsorber screenings. The reason for this restriction to initial screenings is the complexity of predicting column chromatography based on batch data, the problem of adsorber volume definition in batch experiments, and the analytical bottleneck that may arise from HTPD. To resolve these limitations, we addressed the problem of adsorber volume definition in batch experiments by the development of a method to quantify the adsorber in batch chromatography and the adaptation of a photometric method to analyse multi-protein mixtures in batch experiments. The challenge of predicting column chromatography based on batch data, was addressed by the use of mechanistic models.

1.5 Outline

1.5.1 Building Blocks

1. Simulating and Optimizing Preparative Protein Chromatography with ChromX

T. Hahn, T. Huuk, V. Heuveline, J. Hubbuch

In this publication, the in-house developed chromatography modeling software ChromX and its capabilities in academic teaching are presented. ChromX offers various mechanistic models for the macroscopic mass transport through the column, the diffusion processes within the different volumes within the column, and several adsorption models. The undergraduate students laboratory course presented in this article focused on the model-based optimization of a single column chromatography process, to purify a monoclonal antibody from an artificial three component mixture. The course covered the design and execution of the laboratory experiments to calibrate the models, the estimation of the isotherm parameters, and the model-based process optimization.

The software ChromX was utilized in the following publication as a tool for model-based process development.

Article accepted in Journal of Chemical Education.

2. A Versatile Noninvasive Method for Adsorber Quantification in Batch and Column Chromatography Based on the Ionic Capacity

T. Huuk, T. Briskot, T. Hahn, J. Hubbuch

In this paper, a new method for the determination of the ionic capacity Λ is introduced. The ionic capacity is a key characteristic of ion-exchange chromatographic adsorbers, which quantifies the amount of ligands per adsorber volume. The ionic capacity is a column parameter which is required within the commonly used steric mass action isotherm. The traditional method to determine the ionic capacity experimentally is an acid-base titration (AcB). AcB requires an inline conductivity probe and is therefore not applicable for robotic high-throughput chromatography. In addition, AcB deteriorates the packing of some chromatographic adsorbers, such as Poros adsorbers. Poros is a popular chromatographic adsorber, used in several of the following industrial case studies. To overcome the constraints of AcB, we developed an alternative method to determine the ionic capacity based on the adsorption of the natural, uv-detectable amino acid histidine. This non-invasive, photometric method can be used in conventional column chromatography and in robotic high-throughput experiments. Therefore, it enables the calibration of mechanistic models for chromatography in various experimental scales and it opens up the way for a hybrid approach of robotic high-throughput chromatography and mechanistic chromatography modeling. In addition, it enables the reliable determination of the exact adsorber volumes in batch chromatography and improves the data quality in batch chromatography.

Article submitted to Biotechnology Progress.

3. Optimal Experimental Design for the Determination of Isotherm Parameters of Glucose Oxidase using Mixed Mode Column Chromatography

T. Hahn, G. Wang, T. Huuk, V. Heuveline, J. Hubbuch

With the intensified utilization of mechanistic modeling in industrial process development scenarios and the advancing complexity of mechanistic models, the procedure of how to determine model parameter gains more and more attention. This article deals with a method called *Optimal Experimental Design* (OED), which is a central part of a more sophisticated way of estimating model parameters. Currently model parameters are commonly estimated based on experimental data, which are generated in a trial and error way or by rules of thumb. OED enables the rational determination of the experiment which should be carried out next, based on a maximization of the added information content of this experiment. We demonstrate the capabilities of OED based on a case study using a single model protein and three different adsorbers. The anion exchange adsorber Capto Q and its hydrophobic counterpart Capto phenyl represent single interaction mechanism adsorbers. The ligand of the mixed-mode adsorber Capto adhere is a combination of the two single interaction adsorbers.

Article in preparation.

4. UV Absorption-based Inverse Modelling of Protein Chromatography

T. Hahn, P. Baumann, T. Huuk, V. Heuveline, J. Hubbuch

Chromatographic process monitoring and control is commonly based on in-line uv detectors. Since mechanistic chromatography modeling requires molar or mass concentrations, a sensor calibration for the conversion of uv signals to molar concentrations and the molar composition of the feed solution are a prerequisite for model-based process development. The establishment of sensor calibrations for the numerous present species and the analysis of the exact feed composition can be quite time consuming and therefore it is unusual to establish these calibrations in the early stages of industrial process development.

In this article, we present a generic approach to shift the parameters for the sensor calibrations from the minimization problem to the isotherm equation. This enables a model calibration based on uv signals instead of molar concentrations. The approach is exemplified for an anion exchange chromatography using a modified steric mass action isotherm and an *E.coli* feed containing 11 lumped impurities beside to the target protein.

Article accepted in Engineering in Life Sciences.

5. Deconvolution of High-throughput Multi-component Isotherms Using Multivariate Data Analysis of Protein Spectra

P. Baumann*, T. Hahn*, T. Huuk*, A. Osberghaus, J. Hubbuch (* contributed equally)

The integration of high-throughput experiments in the purification process development can be quite challenging with respect to the demands on the throughput for the subsequent analytical methods. In this article, we evaluated the capabilities of a non-invasive analytical method based on the different uv spectra of proteins and multivariate statistics, to prevent an analytical bottleneck in high-throughput process development. As a case study we prepared batch adsorption isotherms with the cation exchanger SP Sepharose FF and two model proteins at several salt concentrations and pH values. The presented analytical approach enables the integrated generation of multi-component batch isotherms on a robotic work station. The observed competitive binding behavior is in agreement with a fitted steric mass action model. Therefore, the presented method opens up the possibility for future hybrid approaches, combining high-throughput and model-based process development technologies.

Article accepted in Engineering in Life Sciences.

1.5.2 Process Case Studies

6. Calibration-free Inverse Modeling of Ion-exchange Chromatography in Industrial Antibody Purification

T. Hahn, T. Huuk, A. Osberghaus, K. Doninger, S. Nath S. Hepbildikler, V. Heuveline, J. Hubbuch

In this case study, the purification of a monoclonal antibody (mAb) out of an industrial feed solution containing two higher molecular and one lower molecular species, using cation exchange chromatography was optimized based on a traditional experimental driven approach and a model-based approach. The experimental approach comprise a linear salt gradient elution and 5 step elutions with different salt concentrations, complemented with a peak fraction analysis using analytical size exclusion chromatography.

The model-based optimization approach employed a general rate model for the macroscopic protein transport and a uv absorbance-based version of the steric mass action isotherm. The model parameters were estimated from a linear salt gradient experiment, two salt step elutions, and the corresponding fraction analysis data.

The process was optimized with the objective of a monomer purity of at least 99%, a yield of at least 80%, and a maximal fraction volume of 5 column volumes due to constrains in the technical infrastructure, using the experimental and the model-based approach. Both optimization approaches result in steps elutions of 200 to 210mM salt, meeting the three constrains. Therefore, it could be demonstrated that mechanistic modeling is a suitable alternative or complement for experimental driven process development.

Article accepted in Engineering in Life Sciences.

7. Model-based Integrated Optimization and Evaluation of a Multi-step Ion Exchange Chromatography

T. Huuk, T. Hahn, A. Osberghaus, J. Hubbuch

The previously mentioned work focused on single column purification processes. However, industrial downstream processes commonly consist of several chromatographic operations, which are arranged in a sequential manner. The optimization of these multi-column processes is commonly carried out one after each other, to keep the experimental complexity manageable. Nevertheless, the concerted optimization of two consecutive chromatographies is supposed to be beneficial, e.g. through the identification of an overall process optimum, rather than two single chromatography optima.

In this article, we calibrated a transport dispersive lumped rate model complemented with a steric mass action isotherm for an artificial three component mixture on cation (CEX) and anion exchange adsorbers (AEX). First, we optimized the two possible process flowsheets (CEX→AEX and AEX→CEX) using a concerted optimization approach. For this, the purity, recovery, and yield derived from the last column were evaluated based on an objective function. The CEX→AEX flowsheet outperforms the alternative process flowsheet. To evaluate the impact of a concerted process optimization, we repeated the optimization of the CEX→AEX flowsheet, optimizing the columns one after each other. This sequential optimization approach showed a superior intermediate result after the first column, but resulted in an inferior overall performance.

Article accepted in Separation and Purification Technology.

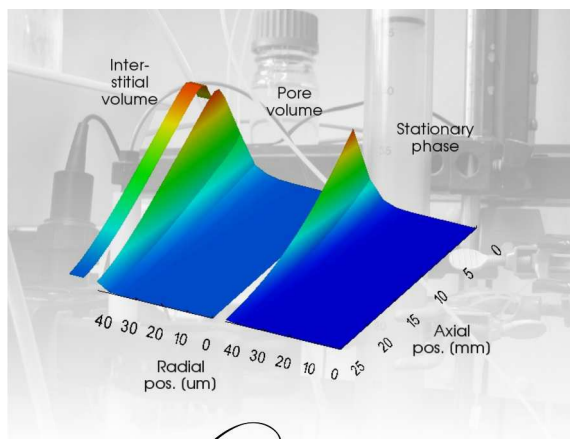
2 | Simulating and Optimizing Preparative Protein Chromatography with ChromX

Tobias Hahn¹, Thiemo Huuk¹, Vincent Heuveline², Jürgen Hubbuch¹

¹ Karlsruhe Institute of Technology (KIT), Institute of Process Engineering in Life Sciences, Section IV: Biomolecular Separation Engineering, Karlsruhe, Germany

² Heidelberg University, Interdisciplinary Center for Scientific Computing, Engineering Mathematics and Computing Lab, Heidelberg, Germany

Abstract



ChromX.org

Industrial purification of biomolecules is commonly based on a sequence of chromatographic processes, which are adapted slightly to new target components, as the time to market is crucial. To improve time and material efficiency, modeling is increasingly used to determine optimal operating conditions, thus providing new challenges for current and future bioengineers.

At the Karlsruhe Institute of Technology (KIT), mechanistic modeling of protein chromatography has long been part of the curriculum of the Bioengineering master's degree program, supported by exercises using simulation software. Emphasis lies on nonlinear preparative chromatography,

where the result strongly depends on the sample concentration. For undergraduate students to gain hands-on experience in model-based optimization, a three-week, in-depth laboratory course was designed on the purification of a ternary mixture of proteins using

ion-exchange chromatography and mechanistic modeling. Students apply in-house software ChromX, which is made available for download, together with tutorials on numerics and practical applications.

This article presents the working principle of ChromX and results of the laboratory course for undergraduate students.

2.1 Introduction

In a biopharmaceutical production sequence, the biggest expenditure is associated with the purification of the target component from a very heterogeneous mixture, so-called downstream processing (DSP). Industrial DSP development, especially for monoclonal antibodies (mAb), is commonly based on a sequence of chromatographic processes, which are adapted slightly to new target components [100; 145].

In order to find optimal process parameters, modeling tools are increasingly gaining the attention of the pharmaceutical industry [62]. For using these tools, bioengineers are needed to acquire a new set of skills. Statistics, numerical mathematics, scientific computing, and data mining will play an increasing role in the future.

In the fourth semester of the bioengineering bachelor's degree program at the Karlsruhe Institute of Technology (KIT), students choose a three-week in-depth laboratory course in enzyme technology, biochemical engineering, or downstream processing. The DSP course applies cation-exchange chromatography to purify an antibody from a ternary protein mixture. Previously, a systematic trial-and-error approach was pursued for this purpose, which can be misleading as unexpected non-linear effects may occur. In contrast to analytical chromatography, where diluted samples are injected, industrial production processes are performed in the so-called nonlinear or preparative mode. The maximum binding capacity of the chromatographic medium is approached by injecting a large amount of concentrated feed solution. This leads to concentration-dependent *nonlinear* retention, as well as to competition of the species in the feed for binding sites.

Although many research groups developed their own simulation tools and published results generated with it, only few simulators are publicly available. The six simulators found for nonlinear chromatography are: Aspen Chromatography [5], CADET [41], Chromulator [154], ChromWorks [28], gProms [134], and pcs [102]. Aspen, ChromWorks, and gProms are commercial Windows applications that cannot be downloaded directly. They are not considered further because students should be able to use the software outside the university on their own. Nevertheless, Aspen has been used successfully by instructors to teach chromatography [163]. CADET is the most advanced noncommercial simulator in terms of numerical methods, but its C++ code must be compiled manually and does not offer a graphical interface. pcs is based on MATLAB, which usually is not taught in undergraduate programs. Moreover, MATLAB licenses become expensive once students graduate. Chromulator software was used in the KIT master's degree program in the past. As it became more troublesome to run the software on current versions of Microsoft Windows, we decided to extend our simulation code for research, ChromX [72], with a user-friendly interface and also to use it in undergraduate courses as a "black box". We are

convinced the separation processes will be designed almost entirely in a computer-assisted fashion in the future and, hence, want to provide our students with the opportunity to gain first experience.

ChromX for Microsoft Windows is available for download with step-by-step tutorials on the different phenomena occurring in liquid chromatography [84]. In addition, a set of MATLAB files explains the numerical methods. A short overview of models and their numerical solutions is given in the Chap. 1, the Supporting Information A.1 contain some exemplary exercises from the master's degree program. A comprehensive introduction to preparative and nonlinear chromatography is in the text book by Schmidt-Traub [109], and more in-depth analyses are presented in the book by Guiochon et al. [55].

2.2 Theory

2.2.1 Chromatography Models

In column liquid chromatography, the sample is dissolved in a liquid (mobile phase) and flows through a packed bed of porous particles or a monolithic column (stationary phase). For simplicity, a bed of uniformly sized spherical particles is assumed in the following sections. The physical or chemical properties of the stationary phase and the different components are utilized in a way that some components are retained more strongly than others. As illustrated in Figure 2.1, molecules are transported through the fluid outside of the particles, and then enter the particle's pore system and diffuse inside the pores. Adsorption and desorption are followed by diffusion out of the particle. The mass transport through the column and pores is described by modeling the fluid dynamics effects, while the retention of the species is described by empirical or mechanistic models for adsorption/desorption and/or reaction [55; 109].

For a large molecule that cannot enter the pore system, transport in flow direction depends on the pump speed and bed porosity (alias, *column porosity*). All diffusive effects in the interstitial volume leading to the broadening of an injected pulse are assumed to follow Fick's law of diffusion with a lumped *axial dispersion* coefficient. For smaller non-interacting molecules, additional effects are included, depending on the model complexity chosen. These include a *film transfer* coefficient that models the inhibition of transition into and out of the pores by the boundary layer, and a *pore diffusion* coefficient that accounts for intra-particle diffusion. Diffusion on the surface is usually neglected [55].

Adsorption onto the surface is modeled by an *isotherm* equation that describes the concentration of adsorbed protein as a function of the protein concentration in the mobile phase at constant temperature. For ion-exchange chromatography, the steric mass action (SMA) isotherm [23] was employed, as described in Chap. 1. It allows for modeling the influence of the counter-ion concentration in the mobile phase on the sorption behavior of proteins.

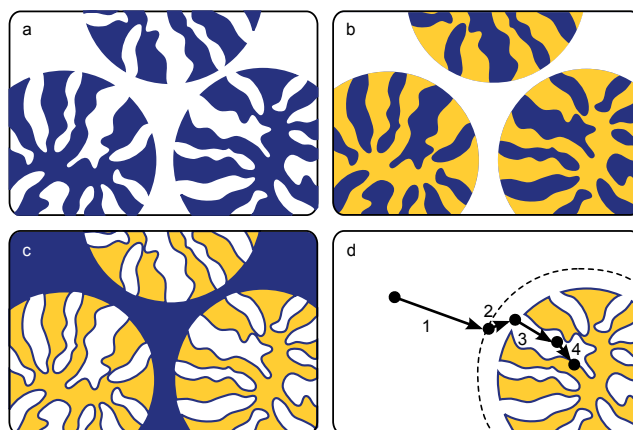


Figure 2.1: Structure of packed beds (a-c) and adsorption process (d). The total column volume is divided into the volume of the stationary phase (a), the volume of mobile phase in the pore system (b), and the interstitial volume of the mobile phase (c). Molecules are transported through the interstitial volume (d.1), pass a boundary layer (also referred to as film) around the beads (d.2), diffuse within the pore system (d.3), and adsorb onto the surface (d.4).

2.2.2 Numerical Solution

For each species, a system of partial differential equations must be solved: a convection-diffusion equation for the interstitial volume of the mobile phase, a diffusion equation for the pore volume, and an isotherm equation for adsorption/desorption. As all species are coupled via the isotherm in nonlinear chromatography, no closed-form solution is available and numerical solutions must be computed. When only linear chromatography is considered, specialized tools provide for a higher performance [20; 142; 147].

The tutorials distributed with ChromX describe the step-by-step solution of the equations with MATLAB and ChromX. First, convection and diffusion problems are solved in axial or radial flow systems. Pore diffusion models are added next, before adsorption and desorption are simulated.

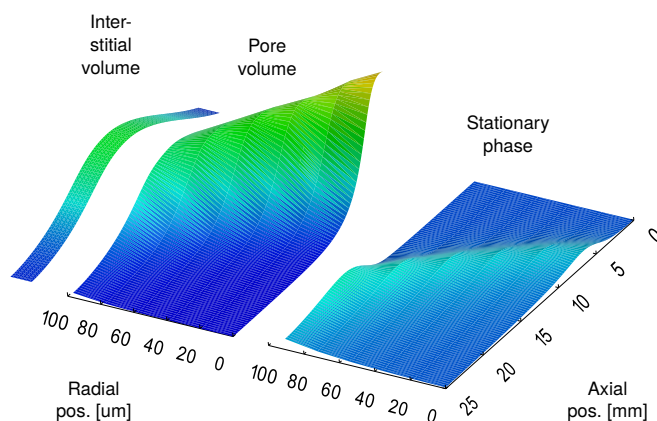


Figure 2.2: Qualitative visualization of intra-column and intra-particle concentrations during a step elution with ParaView.

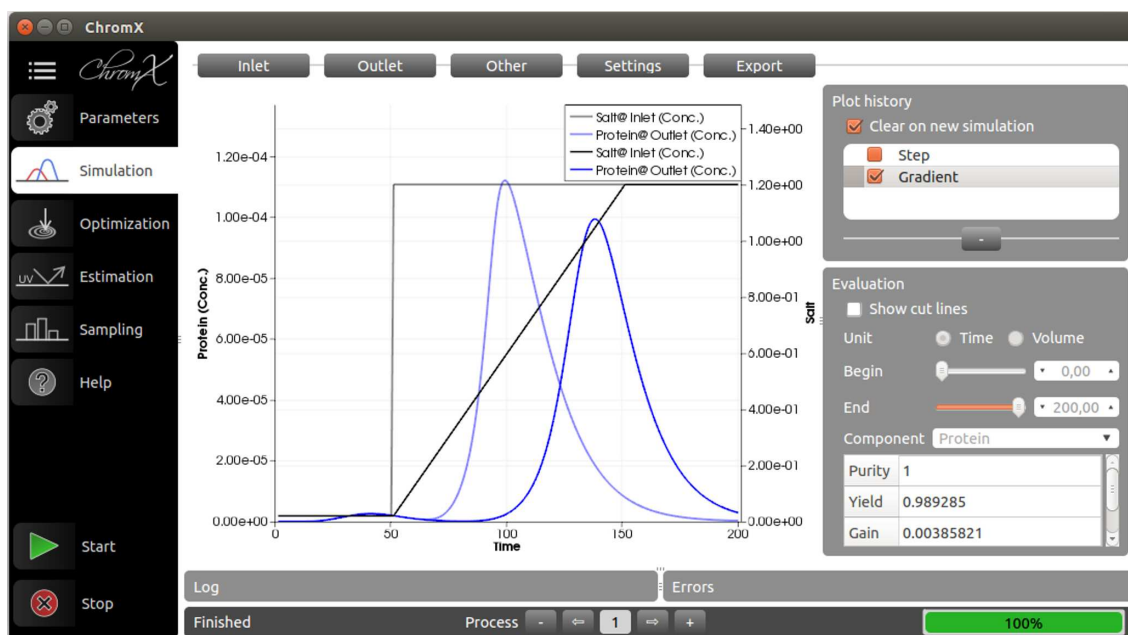


Figure 2.3: ChromX user interface: Comparison of peak shapes when switching from step (semi-transparent lines) to gradient elution (solid lines).

2.3 ChromX Features

The core of ChromX is the modular equation solver. The version used for teaching hides most of the parameters (types of finite elements, solver tolerances, matrix formats, hardware-specific settings, etc.) to simplify the program for new users. Fixed units were not prescribed for various reasons. Simple binding models, such as the Langmuir isotherm, can be used with any unit that is able to quantify concentrations, e.g., M, mg/mL or even absorption units [109]. Moreover, switching from CADET using meter as a standard unit of length or from Chromulator that uses non-dimensional formulations to other tools is facilitated. The embedded Help page provides information in the form “film transfer coefficient k_f [length/time]” in the section on models; recommendations are given in the Supporting Information A.1.

Column and component-specific parameters can be edited easily. Complex injection and elution profiles are defined in terms of concentration events, e.g., a salt step, followed by a gradient and a final high-salt step. Proteins can be added, removed, and sorted in the interface. The number of proteins is only limited by the computer’s memory.

A process setup can be cloned to simulate two or more chromatography runs in parallel with, e.g., different gradient lengths or slopes. This is done during parameter estimation, where several experiments are necessary to determine all isotherm parameters by chromatogram fitting. ChromX contains built-in heuristic and deterministic optimization routines for this task.

When all protein parameters are determined, optimization can be performed with respect to a chosen objective function. Alternatively, hypercube sampling [12] can be used to

study the dependence of the objective function on system parameters, such as batch, variations, etc.

ChromX includes extensive evaluation and export functions. How simulation results can be evaluated and compared easily is illustrated in Figure 2.2. First, a step elution is simulated with the SMA isotherm model and compared to a gradient elution. The results are plotted in a semi-transparent manner and each curve can be evaluated in terms of yield, purity, and peak area.

All results can be exported as a bitmap, vector graphic or spread sheet in XLS format. Intra-column time series can be exported in the VTK format and represented with, e.g., the open source visualization software ParaView [2] (Figure 2.3). This is explained in a dedicated tutorial [84].

2.4 Software Exercises

Software exercises accompany the lecture series on chromatography modeling and are intended to provide a deeper understanding of the mathematical operators and parameters in the differential equations and their effect on the chromatogram. System characteristics are to be pre-calculated with correlations for setups with and without dispersion and film kinetic effects. The calculated breakthrough and retention times are validated with the simulation software and Langmuir isotherm:

- Effects of a change in the feed concentration, i.e., switching from linear chromatography to preparative settings
- Axial dispersion affecting the shape of a breakthrough curve
- Shape changes for breakthroughs and isocratic elutions with different film kinetic effects and pore diffusion limitations
- Multi-component settings that demonstrate that superimposition of single-component simulations do not approximate a mixture in preparative chromatography.

Exemplary exercises and solutions are included in the Supporting Information A.1.

2.5 Laboratory Course Structure

In the DSP course, cation-exchange chromatography is used to purify an antibody from a ternary protein mixture. Students are in three groups of two students each. The first group performs process development with a statistical design of experiments, the second applies model-based process optimization, and the third conducts the necessary analytics for quality assessment. This sharing of tasks between process development and analytics mimics DSP development at pharmaceutical companies where different departments interact. For the mutual exchange of experience among the groups, daily progress meetings

are organized. The course starts with presentations on the theory, methods, and proposed proceeding, followed by two weeks of lab work. The course finishes with a poster presentation of the results and a preparation of a report of 25-30 pages. The total time students have to invest is estimated to be 120 hours. The only prerequisite is a course on biotechnological separation processes that introduced the principle of chromatography.

The objectives of the model-based process optimization group are to calibrate a model using tracer experiments, as well as step and gradient elutions, to perform simulations outside of the lab to optimize the separation of proteins, and to validate these simulation results. Excerpts from the lab assignments are given in Boxes 1 and 2. The lab course results are available as a case study, including all measurements and parameter files.

Box 1. Excerpts from Laboratory Assignments: Process Development with a Statistical Design of Experiments.

The students are to use an ion exchange step to purify the given feedstock, which contains the target protein (monoclonal antibody) and two other proteins as impurities. The concentration of the antibody is about 3.8 g/L. The concentrations of the impurities are unknown. The two impurities have theoretical isoelectric points of 7 and 11 and molecular weights of 17 kDa and 14 kDa. The first impurity has a chromophore group, which accounts for the dark color of the solution. The feedstock has a pH of about 8 and a conductivity of about 5 mS/cm. They are to reach the highest possible purity, yield, production rate, and concentration of the antibody. First, the type of ion exchanger and an appropriate adsorbent and buffer are to be selected. For regulatory reasons, the choice of buffers is to be limited to the use of simple buffer salts and NaCl. Both batch binding experiments and column chromatography may be performed. The process is to be carried out in a 1 mL column with a fast protein liquid chromatography (FPLC) system. The flow rate is to be chosen such that the contact time is roughly equivalent to 1 min (empirical value). All other process parameters, such as the elution mode (step or gradient), gradient length, ionic strengths, load volume, and pooling criteria, may be chosen freely. To optimize the development process, a statistical design of experiments (DoE) is to be made, with the parameters being varied by a software provided. The experiments are to be analyzed in cooperation with the analytics group. For evaluation of the DoE and in order to find the optimal process parameter combination, an objective function consisting of the goals listed above is to be found. This is to be done in agreement with the model-based development group.

Box 2. Excerpts from Laboratory Assignments: Model-based Process Development

The students are given the same separation task and the same feedstock as described in Box 1. However, the process is to be designed in a model-based manner. For the characterization of the column as well as of the feedstock, additional experiments will be required. The column selection is to be done by the first group. For this purpose, experiments are to be planned, which provide the basic information needed for modeling. Afterwards, the component-specific model parameters of the individual components of the feedstock are to be determined. With these values, process simulation is to be performed, considering the above recommendation for the flow rate. The students are to find a combination of elution mode (step or gradient), gradient length, ionic strengths, load volume, and pooling criteria, by means of which a high purity, yield, production rate, and concentration of the antibody can be achieved. Finally, a validation run is to be performed under the optimal conditions identified. The results are to be compared to those of the first group.

2.6 Laboratory Results

Initial experiments were conducted to determine system properties such as dead volumes, column and bead porosity, and the ionic capacity of chromatography resin. Afterwards, four experiments in the bind/elution mode were performed for parameter estimation, i.e., one step elution and two gradient elutions with a low sample volume, as well as one gradient elution with a large sample volume. The proceeding is described in detail in the Supporting Information A.1.

Exemplary results are shown in Figures 2.4a and 2.4b. A small breakthrough of nonbinding myoglobin and antibody was accurately modeled in the beginning. This also applied to the elution far beyond the detector limit in the experiment with a high sample volume.

Finally, the calibrated model was used for process optimization. The objective of the laboratory course was to find a compromise between the production rate and yield, while achieving a high purity. There is no unique solution to this problem. Students decided in favor of a very fast process, which concentrates the antibody at the same time (sample volume 3.6 mL, collected volume 2 mL). The step elution shown in Figure 2.4c reaches a purity above 99 % at 80 % yield. The results were subsequently validated experimentally in the lab.

2.7 Pedagogical Aspects

The DSP laboratory course for undergraduate students was taught for the third time in the 2014/2015 winter semester. Students appeared to learn preparative chromatography in more depth compared to the previously used trial-and-error approach. The course goals described above were met with this teaching format, although undergraduate students were familiarized with the models necessary for this particular task (SMA for ion-exchange chromatography) only. Because of the small number of students, statistical statements

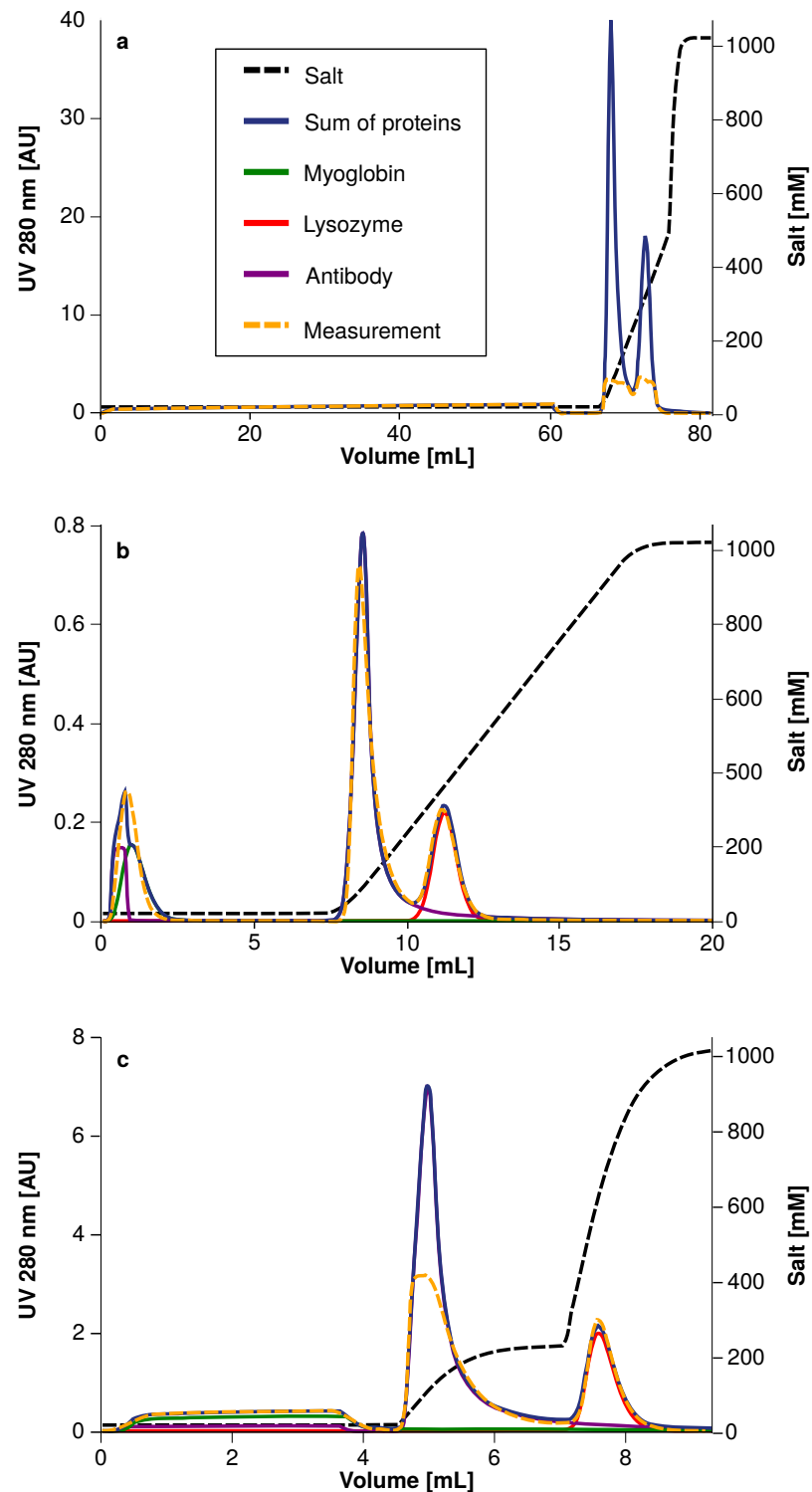


Figure 2.4: Comparison of simulated and measured chromatograms for the experiments with 60 mL sample volume and 20 - 520 mM salt gradient (a), 0.5 mL sample volume and 20 - 1020 mM salt gradient (b), and optimization result with 3.6 mL sample volume and 230 mM salt step elution (c). The UV detector was saturated at 3 AU such that the elution peaks in (a) and (c) were not completely recorded. Single component curves were omitted in (a) for reasons of clarity.

cannot be made, but statistics on the lecture series of the master's degree program are encouraging and given in the Supporting Information A.1.

Compared to conventional process optimization, ChromX provided an immediate feedback that might mislead students into trying setups without first anticipating results. An experiment that takes 30 minutes or longer has to be considered more carefully in order not to waste time and material. Hence, the grading scheme reflected the conception of the lab course: 20 % project plan presentation, 40 % practical work, 20 % report, and 20 % poster and poster presentation. For grading, the course of process design rather than the actual results were considered. Nevertheless, the solutions found by the model-based optimization group were almost identical to those of the group focusing on process optimization with a statistical design of experiments. The long runtime of the experiments and the daily progress meetings allowed for an extensive exchange among the groups and joint learning.

2.8 Conclusion

In pharmaceutical practice, preparative chromatography is of highest importance. To demonstrate the differences from analytical chromatography, a user-friendly interface was developed for use in a simulation toolbox for research and focused on models with a reasonable level of detail, i.e., where changes in model parameters directly related to peak properties. Easy visualization and export of results were other design criteria. This allowed us to establish an undergraduate laboratory course on the purification of a ternary protein mixture using mechanistic modeling.

The feedback from students was very positive. ChromX allowed them to study the influence of system and model parameters on the outcome of experiments. It also prepared them for the challenges lying ahead in industrial bioengineering.

Associated content

Supporting Information

ChromX for Microsoft Windows is available free of charge for academia [84]. On the ChromX webpage, we offer introductory material that explains the underlying models, their mathematical solution, and parameter estimation for MATLAB and ChromX. In this way, instructors can incorporate ChromX into their existing classroom and laboratory activities. ChromX will be further developed. We welcome any feedback and suggestions concerning the software, the tutorials as well as the case studies.

Mathematical background, working principle of ChromX and the MATLAB tutorials, software exercises with Langmuir isotherm, and experimental results of the laboratory course. This material is available free of charge via the Internet at <http://pubs.acs.org>.

Acknowledgment

We gratefully acknowledge the support of Matthias Franzreb. We would also like to thank all students who participated in the 2013/2014 laboratory course on protein purification using chromatography. The research leading to these results was funded partly by EURO-TRANS-BIO (grant agreement no. 0316071B, EC's Seventh Framework Programme).

3 | A Versatile Noninvasive Method for Adsorber Quantification in Batch and Column Chromatography Based on the Ionic Capacity

Thiemo Huuk¹, Till Briskot¹, Tobias Hahn¹, Jürgen Hubbuch¹

¹ Karlsruhe Institute of Technology (KIT), Institute of Process Engineering in Life Sciences, Section IV: Biomolecular Separation Engineering, Karlsruhe, Germany

Abstract

Within the Quality by Design (QbD) framework proposed by the International Conference on Harmonisation (ICH), high-throughput process development (HTPD) and mechanistic modeling are of outstanding importance for future biopharmaceutical chromatography process development. In order to compare the data derived from different column scales or batch chromatographies, the amount of adsorber has to be quantified with the same noninvasive method.

Similarly, an important requirement for the implementation of mechanistic modeling is the reliable determination of column characteristics such as the ionic capacity Λ for ion-exchange chromatography with the same method at all scales and formats.

We developed a method to determine the ionic capacity in column and batch chromatography, based on the adsorption/desorption of the natural, uv-detectable amino acid histidine. In column chromatography, this method produces results comparable to those of classical acid-base titration.

In contrast to acid-base titration, this method can be adapted to robotic batch chromatographic experiments. We are able to convert the adsorber volumes in batch chromatography to the equivalent volume of a compressed column.

In a case study, we demonstrate that this method increases the quality of SMA parameters fitted to batch adsorption isotherms, and the capability to predict column breakthrough experiments.

3.1 Introduction

Chromatography is a key unit operation in the downstream processing (DSP) of biopharmaceuticals [100; 145]. The optimization of chromatography is a complex task due to the numerous operational parameters and their interactions.

DSP development is continuously facing the demand of accelerating the process development, reducing the 'time to market' [122], and meeting the evolving demands of regulatory authorities, such as a detailed process understanding proposed by the Quality by Design (QbD) initiative [27; 74].

To comply with these QbD requirements, new process development technologies have to be incorporated in the current portfolio of methods. There are two possible approaches to obtain a detailed process understanding: The massive expansion of the data basis by the implementation of high-throughput process development techniques (HTPD), and process modeling to gain mechanistic process insights. Currently, these two technologies are often used independently despite the obvious synergistic potential [122; 125].

HTPD for chromatography is commonly based on batch chromatography or miniaturized chromatographic columns [122; 167]. Both techniques are compatible with pipetting robots, enabling the parallelization and automation of experimental workflows. A key challenge for implementing high-throughput experimental systems is the proof of comparability to classical column chromatography at the laboratory and production scales. Effects arising from the complex flow behavior within a chromatographic column, e.g. axial peak broadening, are not found in batch chromatography. Therefore, batch chromatography is predominantly used at the early stages of DSP development, e.g. for the screening of different adsorbers [13; 15; 120] or the selection of salts or pH value [150].

Using a combination of multiple experimental formats such as batch, robotic columns, and classical columns, it is crucial to determine the adsorber volume in the different formats with the same method to enable comparability.

Disregarding the technical simplifications related to high-throughput experiments, one remaining drawback of these experiments is the limited mechanistic insight into the processes. HTPD itself just increases the amount of data and enables the creation of black-box models such as response-surface models or DoE studies. Although, these empirical models are frequently used with good results, they are restricted with respect to the provided mechanistic process insight [15; 65; 131]. In contrast to mechanistic models, they are not based on first principle natural laws, such as Fick's law of diffusion within a column model and do not allow extrapolation [127].

Another technology proposed in the ICH guidelines within the QbD framework [74], is mechanistic modeling to gain a fundamental insight into chromatographic processes. While mechanistic modeling becomes more common in DSP development [18; 30; 122], one of the major challenges regarding the implementation is the quality of data derived from high-throughput experiments or classical column chromatography and the comparability of data in different column formats and bed volumes.

In summary, one method to quantify the adsorber volume in all formats is a prerequisite to increase the quality of HTPD data and to prove the comparability of different chromatographic formats. Furthermore, to be able to use mechanistic IEX modeling in different formats, it is necessary to determine parameters such as the ionic capacity in all formats with the same noninvasive method.

To resolve this issue, we established a noninvasive photometric method for the determination of the ionic capacity in column chromatography. The method is based on the total

histidine capacity of the adsorber. The determined ionic capacities are comparable to conventional acid-base-titrations.

We automated the method on a liquid handling station and adapted it to batch chromatography. Using the same adsorber lot and assuming a constant bead voidage, the method can be adapted to quantify the adsorber volume in batch chromatography.

Based on the adsorber quantification in batch chromatography, we are able to predict a column breakthrough curve based on a single batch adsorption isotherm.

3.2 Theory

Conventional chromatography columns are packed by gravity settling or by applying a defined flow or pressure to the adsorber bed. 96-well filter plates filled with equal volumes of adsorber can be purchased [15] or individually prepared by slurry dispensing or 'mechanical approaches' such as the ResiQuot device (Atoll, Weingarten, Germany). Slurry dispensing requires optimized slurry mixing and calibrated pipetting procedures to ensure reliable adsorber volumes. Calibrations are commonly based on the adsorber dry mass or the settled adsorber volume as a reference [7; 31]. Other approaches aim to correct the differences between the wells in batch chromatography [90], or evaluate the influence of the adsorber surface area [69]. Especially for highly compressible adsorbers, the difference between the settled-bed volume and the volume of a compressed column is obvious. In addition, the influence of neighboring adsorber particles in packed-bed chromatography can lead to a change in pore structure at the contact spots [71].

Using the ResiQuot device, an adsorber suspension is filled into a grid with defined geometries by application of a vacuum. Afterwards, these adsorber plaques can be transferred to a 96-well (filter) plate. The variation of adsorber volumes in between the plaques has been shown to be less than 2% [67]. As in the case of slurry dispensing, the difference in compression between the ResiQuot and a packed column is obvious.

As a consequence of the different packing procedures and the differences in adsorber compression [87], application of a method for quantifying the adsorber volume within different chromatographic formats is a precondition for comparing data derived from these chromatographic formats [64].

The ionic capacity Λ is of high importance for the mechanistic modeling of ion-exchange chromatography (IEX) and describes the amount of ligands on the adsorber surface. For example, the commonly used stoichiometric displacement (SDM) or steric mass action (SMA) isotherms [23; 159] are based on the exchange of charged groups of a protein and salt ions on the surface of an adsorber with a characteristic ionic capacity. Experimental methods to determine the ionic capacity of an adsorber are the transition pH method [46; 96; 97] or a simple acid-base titration [68].

Fig. 3.1 A provides a summary of the acid-base titration.

First, the counter ions bound to the cation-exchange adsorber (CEX) are exchanged by protons, exposing the adsorber to a HCl solution. At low pH values, the interaction of the ligand with a proton is preferred to e.g. sodium ions. Afterwards, the remaining acid in the interstitial and pore volume is removed by a prolonged treatment with ultra-pure water. Subsequently, the ligands can be titrated with a sodium hydroxide solution with a known molar concentration. While the column is titrated, water is formed within the column. When all protons are exchanged to sodium ions, sodium hydroxide breaks through the

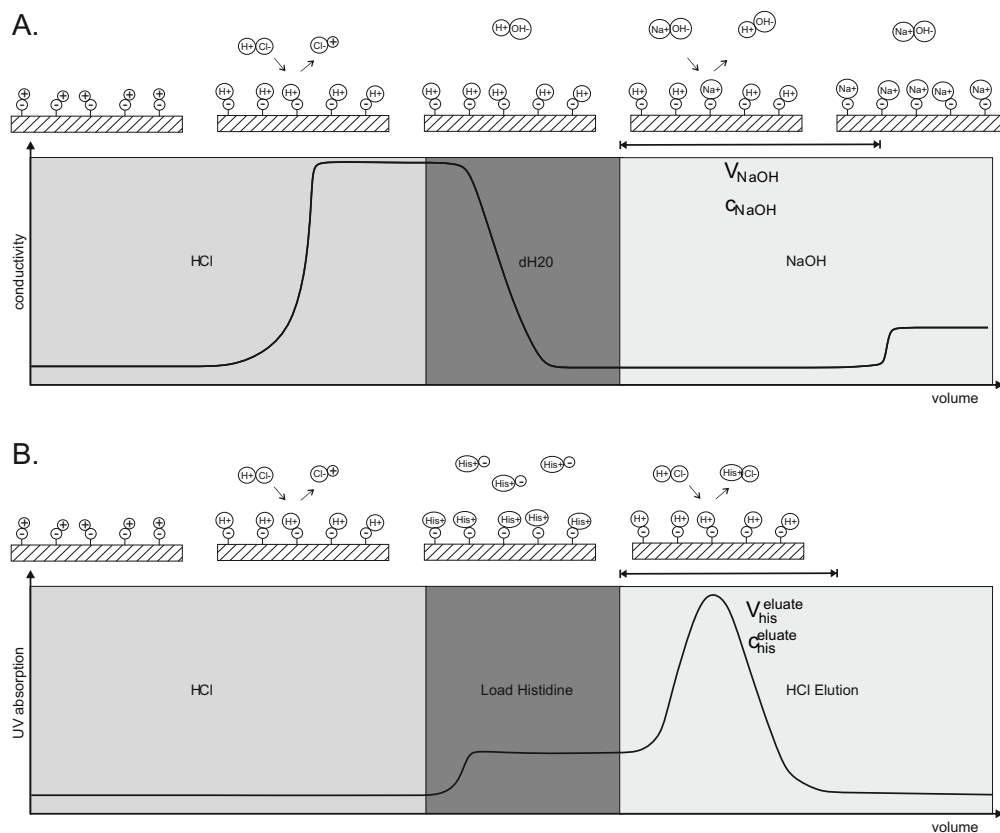


Figure 3.1: Experimental acid-base titration (A) and histidine capacity determination (B) on a cation exchange adsorber. The methods are sketched on a molecular level and with regard to the in-line traces recorded by the column chromatography system.

column, that can be detected in the in-line conductivity trace of a HPLC system. From the volume of the titrant and its concentration, it is possible to quantify the amount of exchanged ions.

The acid-base titration exhibits several disadvantages. The volume of the titrant has to be determined from the in-line conductivity or pH traces. These signals are available for most HPLC systems, but are not available in standard robotic systems. Another disadvantage is the exposure of the adsorber to ultra-pure water and a possible deterioration of the packing (comp. Fig. 3.2).

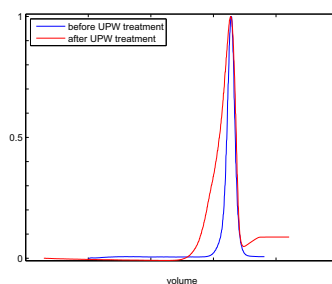


Figure 3.2: Deterioration of packing quality of a 16mL Poros 50HS column due to contact to ultra-pure water (UPW). The diagram shows salt pulse injections before and after UPW treatment. The data are normalized and peak centered.

To avoid these limitations, we developed a method based on the histidine capacity. Histidine is a natural amino acid and a buffer substance that is used in biopharmaceutical formulations [139; 140]. Therefore, it can be assumed safe to expose a laboratory- or production-scale column to histidine.

The method is presented in Fig. 3.1 B. First, the adsorber is equilibrated with a HCl solution to exchange the counter ions to protons. Afterwards, the column is loaded with histidine for a prolonged period of time. After this point, all ligands of the adsorber are saturated with histidine and the interstitial and pore volumes of the adsorber are filled with the histidine loading solution. Afterwards, histidine can be eluted from the adsorbent by applying HCl to the column and collecting the complete eluate. The histidine in the eluate refers to the histidine bound to the adsorber, the one in the interstitial, and pore volumes filled with a histidine solution with a concentration equal to the load solution. Using a low histidine concentration in the load prevents multi-layer adsorption.

The histidine in the eluate can be quantified photometrically at 230nm and an in-line uv trace is not necessary. The method can be adopted to high-throughput experiments and no UPW is needed.

3.3 Materials and Methods

3.3.1 Adsorbers and chemicals

This study was carried out using two different strong cation exchange adsorbers. The agarose-based SP Sepharose FF (GE Healthcare, Buckinghamshire, GB) was selected as a model for highly compressible adsorber beads. Poros 50HS (Applied Biosystems, Carlsbad,

CA, USA) consists of an almost incompressible crosslinked poly(styrene-divenylbenzene) bead, and its packing can be altered by salt-free solutions. Sepharose FF and Poros 50 have an average particle size of 90 and $50\mu m$, respectively.

All chemicals were of analytical grade and purchased from Sigma Aldrich (St. Louis, MO, USA) and Merck Millipore (Darmstadt, Germany). All solutions were prepared with ultra-pure water.

3.3.2 Column chromatography

All lab scale experiments were carried out on an Äkta purifier 10 controlled by Unicorn 5.31 (both GE Healthcare). For column packing, the Poros adsorber was buffer-exchanged into an aqueous $0.1\frac{mol}{L}$ sodium chloride solution, the Sepharose was packed with storage solution. The adsorbers were packed into glass columns with an inner diameter of $6.6mm$ and different bed heights (Omnifit, Danbury, CT, USA). The Sepharose and Poros adsorbers were packed at a maximum pressure drop of $2bar$ and $3bar$, respectively. The qualification of the column packing and the determination of the voidages was carried out by $25\mu L$ injections of a 1%(v/v) acetone (for Sepharose) or $1\frac{mol}{L}$ NaCl solution (for Poros) as pore-penetrating tracer $V_{acetone}$ and a $10g/L$ dextrane (MW 2000kDa, Sigma Aldrich) as non-pore-penetrating tracer $V_{dextrane}$. The dead volumes of the Äkta LC and the empty column were determined using acetone as a tracer V_{dead} . All tracer experiments were carried out as triplicates. The flow rate for all column experiments was kept at $0.2mL/min$. The porosities were calculated from the tracer experiments and the geometric column volume (CV).

$$\begin{aligned}\varepsilon_{column} &= \frac{V_{dextrane} - V_{dead}}{CV} \\ \varepsilon_{particle} &= \frac{V_{acetone} - V_{dextrane}}{CV - V_{dextrane}} \\ \varepsilon_{total} &= \frac{V_{acetone} - V_{dead}}{CV}\end{aligned}\quad (3.1)$$

The order of the subsequent adsorber quantification experiments was histidine capacity, acid-base-titration, and gravimetry. The first two were carried out as triplicates.

3.3.2.1 Histidine capacity

For the determination of the histidine capacity, the column was equilibrated with 5CV of a $0.5\frac{mol}{L}$ HCl solution. Afterwards, the column was loaded with 20CV of a $0.03\frac{mol}{L}$ aqueous histidine solution c_{his}^{load} . Subsequently, the histidine was eluted using a $0.5\frac{mol}{L}$ HCl solution. The elution can be detected at 230nm and the eluate was collected in a pre-balanced tube. The volume of the collected eluate V_{his}^{eluate} was determined from its weight and the density of the solution. The absorption at 230nm (A_{230}) of the collected eluate was determined with a NanoDrop 2000c spectrophotometer (Thermo Fisher Scientific, Waltham, MA, USA). The molar concentration of histidine c_{his}^{eluate} in $0.5\frac{mol}{L}$ HCl solution was calculated according to the law of Lambert-Beer and a calibration that was carried out on the same spectrophotometer. The amount of histidine found in the collected fraction n_{his}^{eluate} relates to the amount of histidine bound to the adsorber n_{his}^{ads} , the histidine in the

total hold up volume of the LC system, and the mobile phase in the column. Due to the prolonged load volume, the concentration of histidine within this hold-up volume is assumed to be equal to c_{his}^{load} .

$$n_{his}^{ads} = V_{his}^{eluate} \cdot c_{his}^{eluate} - V_{dead} \cdot c_{his}^{load} - CV \cdot \epsilon_{total} \cdot c_{his}^{load} \quad (3.2)$$

The histidine capacity per adsorber skeleton and geometric column volume is calculated according to

$$\Lambda_{his}^{skeleton} = \frac{n_{his}^{ads}}{CV \cdot (1 - \epsilon_{total})} \quad (3.3)$$

and

$$\Lambda_{his}^{CV} = \frac{n_{his}^{ads}}{CV}. \quad (3.4)$$

3.3.2.2 Acid-base titration

The acid-base titration (AcB titration) was carried out after the determination of the histidine capacity. The column was equilibrated for 10CV with a $0.5 \frac{mol}{L}$ HCl solution to exchange the counter-ions against protons. Afterwards, the unbound HCl was removed by flushing the column extensively with ultra-pure water (UPW) for 25CV. Finally, the adsorber was titrated with a $0.01 \frac{mol}{L}$ NaOH solution c_{NaOH} . The titration volume V_{NaOH} was calculated from the increase of the in-line conductivity trace and the system dead volume. The amount of exchanged sodium ions n_{Na^+} was calculated according to

$$n_{Na^+} = V_{NaOH} \cdot c_{NaOH} \quad (3.5)$$

. Subsequently, the total ionic capacity based on acid-base titration was calculated as

$$\Lambda_{AcB}^{skeleton} = \frac{n_{Na^+}}{CV \cdot (1 - \epsilon_{total})} \quad (3.6)$$

and

$$\Lambda_{AcB}^{CV} = \frac{n_{Na^+}}{CV}. \quad (3.7)$$

3.3.2.3 Gravimetry

The invasive gravimetric determination of the adsorber dry weight was carried out as an orthogonal reference method. After flushing the column with UPW, the adsorber was completely transferred to a pre-balanced tube and dried until a constant weight m_{dry} was reached.

3.3.3 Batch chromatography

Batch chromatographic experiments were carried out on an EVO Freedom 200 liquid handling station equipped with an eight-tip liquid handling arm, a plate-moving arm,

an orbital shaker (operated at 1000min^{-1}), a vacuum station (operated at a vacuum of 300mbar), and a spectrophotometer. The system was controlled by EVOware 2.5 (all from Tecan, Männedorf, CH). The batch experiments were carried out in 'MultiScreenHTS DV Filter Plates' with a pore size of $0.65\mu\text{m}$ purchased from Merck Millipore (Billerica, MA, USA). Equal adsorber volumes were distributed to the 96-wells with a ResiQuot device (Atoll, Weingarten, Germany), equipped with a $20.8\mu\text{L}$ plaque grid ($V_{batch}^{uncorrected}$). The device was operated at a maximum vacuum of 300mbar .

3.3.3.1 Histidine capacity

The histidine capacities of the 96 adsorber plaques were determined in analogy to the method for columns in triplicate. The experimental procedure is illustrated in Fig. 3.3.

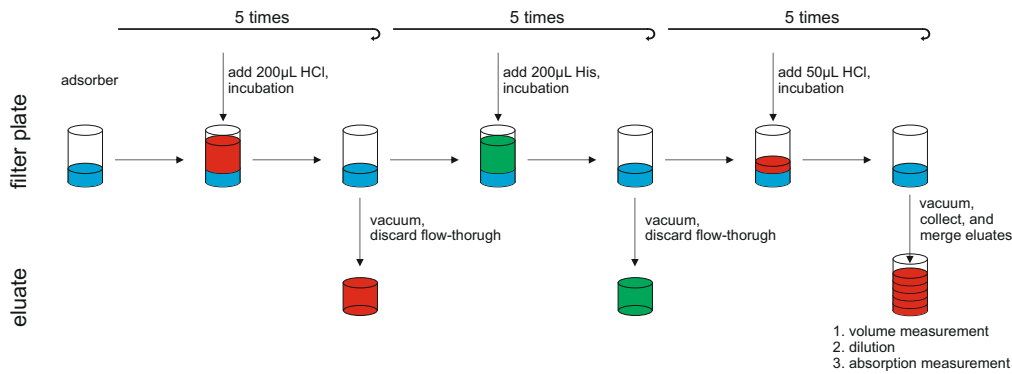


Figure 3.3: Adaptation of the experimental procedure to determine the histidine capacity in batch chromatography.

First, the adsorber plaques were equilibrated five times with $200\mu\text{L}$ $0.5\frac{\text{mol}}{\text{L}}$ HCl solution for 5 minutes on the orbital shaker and removed by vacuum. Afterwards, the adsorber plaques were loaded five times with $200\mu\text{L}$ $0.03\frac{\text{mol}}{\text{L}}$ histidine solution c_{his}^{load} for 5 minutes on the orbital shaker and removed by vacuum. Finally, the bound histidine was eluted from the plaques by applying five times a volume of $50\mu\text{L}$ of a $0.5\frac{\text{mol}}{\text{L}}$ HCl solution per well, a three-minutes incubation, and the removal by vacuum. The complete eluate of $250\mu\text{L}$ was collected in a 96-UVStar plate (Greiner Bio-One, Kremsmünster, Austria). This collection plate and a five-fold diluted plate (dilution with $0.5\frac{\text{mol}}{\text{L}}$ HCl solution) were directed to the spectrophotometer, and absorptions at 230, 900, and 995nm were recorded. The absorptions at 230nm (A_{230}) were corrected to a pathlength of 10mm using the 900 and 995nm signals (A_{900} , A_{995}) [94; 125].

$$A_{230\text{nm},10\text{mm}} = 0.1617 \cdot \frac{A_{230}}{A_{995} - A_{900}} \quad (3.8)$$

The molar histidine concentrations c_{his}^{eluate} were calculated according to the law of Lambert-Beer and a calibration that was carried out on the same spectrophotometer: The exact volumes of the 96 collected fractions V_{his}^{eluate} were determined using the 900 and 995nm signals.

The amount of histidine found in the collected fractions n_{his}^{eluate} refers to the histidine

adsorbed n_{his}^{ads} and present within the pores of the beads n_{his}^{pore} . Due to the prolonged vacuum application, the histidine in the volume in between the beads is assumed to be negligible. The hold-up volume of the membrane of the filter plate after the vacuum process was determined to be negligible.

$$n_{his}^{eluate} = V_{his}^{eluate} \cdot c_{his}^{eluate} = n_{his}^{ads} + n_{his}^{pore} \quad (3.9)$$

n_{his}^{eluate} values deviating more than three times the standard deviation from the mean of the 288 measurements (3.96) per adsorber, were classified as outliers and excluded from the further data processing.

3.3.4 Equivalent column volume

The approach presented in Sec. 3.3.2.1 for the histidine capacity in column chromatography correlates the histidine bound to the adsorber $n_{his,column}^{ads}$ with the column volume CV . Based on the voidages of the column and the adsorber particle, it is also possible to correlate the sum of histidine bound to the adsorber $n_{his,column}^{ads}$ (comp. Eq. (3.2)) and present in the pore volume of the bead $n_{his,column}^{pore}$ (comp. Eq. (3.10)) with the column volume.

$$n_{his,column}^{pore} = (1 - \varepsilon_{column}) \cdot \varepsilon_{particle} \cdot CV \cdot c_{his}^{load} \quad (3.10)$$

$$\Lambda_{his,column}^{CV+pore} = \frac{n_{his,column}^{ads} + n_{his,column}^{pore}}{CV} \quad (3.11)$$

Assuming an equal particle voidage and ionic capacity (e.g. equal adsorber lot) in column and batch chromatography, it is possible to use this correlation derived from column chromatography to calculate an *equivalent column volume* $V_{batch}^{corrected}$ of the adsorber plaque based on the amount of histidine found in the eluate $n_{his,batch}^{eluate}$.

$$V_{batch}^{corrected} = \frac{n_{his,batch}^{eluate}}{\Lambda_{his,column}^{CV+pore}} \quad (3.12)$$

3.3.5 Validation

The adsorption of the model protein lysozyme on SP Sepharose FF was used as a case study to demonstrate the ability of the histidine capacity, to predict a breakthrough curve in column chromatography from batch adsorption data.

3.3.5.1 Experimental settings

A 30.28g/L lysozyme (Sigma Aldrich) stock solution in $0.02 \frac{mol}{L}$ sodium phosphate buffer at pH 7 was used for both chromatographic formats.

For the column experiments, the voidages and the histidine capacity of a $711 \mu L$ column were determined as described previously. Subsequently, a breakthrough curve was recorded at a flow of 0.2mL/min using the lysozyme stock solution as a sample. The experiment

was carried out using an Äkta LC equipped with a diode array detector (Thermo Fisher Scientific) with a pathlength of 0.4mm to prevent detector saturation. A detailed review of the system setup is given elsewhere [21; 22]. The mass of the adsorbed lysozyme was calculated from the area between the concentration trace and the stock solution concentration. Dynamic binding capacities per adsorber skeleton volume were calculated based on a 10% and 100% breakthrough (10%DBC, 100%DBC).

Batch isotherm data were recorded based on filter plates filled with SP Sepharose FF, prepared as described previously. Based on a serial dilution of the 30.28g/L lysozyme stock solution, initial lysozyme concentrations in the range of 3 to 30.28g/L were prepared. 200 μ L of this protein solutions were added to the filter plates and incubated for 2h. The filtrate was collected and the lysozyme concentration c_{eq} was determined with a NanoDrop 2000c spectrophotometer. The adsorbed lysozyme masses were calculated from the initial and equilibrium lysozyme masses.

3.3.5.2 Model-based data analysis

A steric mass action isotherm [23] Eq. (3.13) was fitted to the batch data. The isotherm accounts for a protein, exhibiting ν charged patches which interact with the adsorber, displacing an equal amount of counter ions. The adsorber is characterized by an ionic capacity Λ . The adsorbed protein sterically shields σ further ligands of the adsorber, decreasing the apparent binding capacity. The adsorption/desorption process is characterized by an equilibrium constant k_{eq} and is modulated by the salt concentration c_{salt} . Attention should be paid to the fact that in addition to the mobile phase salt concentration $c_{salt,0}$, the adsorption/desorption process releases additional salt ions (comp. Eq. (3.14)). The parameter estimation and calculation of 95% confidence intervals for the batch data were carried out with Matlab R2015a (Mathworks, Natick, MA, USA).

$$q = k_{eq} \left(\frac{\Lambda - (\nu + \sigma)q}{c_{salt}} \right)^\nu c \quad (3.13)$$

$$c_{salt} = c_{salt,0} + \frac{(1 - \varepsilon_{total})}{\varepsilon_{total}} \cdot \nu \cdot q \quad (3.14)$$

The maximum binding capacity in $\frac{g}{L}$ is calculated with the molecular weight MW according to

$$q_{max} = \frac{\Lambda}{\nu + \sigma} \cdot MW. \quad (3.15)$$

Occasionally, the maximum binding capacity q_{max} is also referred to as static or equilibrium binding capacity. Subsequently, the isotherm parameters derived from batch chromatography, were used to predict the breakthrough curve on a chromatographic column. The simulation of a chromatographic column was carried out with the software ChromX (Karlsruhe Institute of Technology (KIT), Karlsruhe, Germany) [59; 84], using a transport-dispersive column model, a general-rate pore model, and the steric mass action isotherm in its kinetic formulation [60]. Additional information on the model parameters are given in the Supporting Information.

3.3.6 Data processing

Calculations, data processing, and graphics were prepared with Excel 2013 (Microsoft, Redmond, WA, USA), Matlab R2015a (Mathworks, Natick, MA, USA), and Corel Draw X5 (Corel Corp., Ottawa, CA).

3.4 Results

3.4.1 Column chromatography

3.4.1.1 Poros 50HS

Five different column volumes ranging from 164 to 566 μL were packed with Poros 50HS. The determined voidages of the adsorber bed are presented in the Supporting Information (Tab. 1). Afterwards, the ionic capacity was calculated as a function of geometric column volume based on the histidine capacity Λ_{his}^{CV} and per adsorber skeleton $\Lambda_{his}^{skeleton}$ as triplicate. On the basis of the five different column volumes, $\Lambda_{his}^{skeleton}$ was calculated to $0.387 \pm 0.011 \frac{\text{mol}}{\text{L}}$ and Λ_{his}^{CV} to $0.113 \pm 0.007 \frac{\text{mol}}{\text{L}}$. Subsequently, the ionic capacity was determined based on acid-base titration. The ionic capacity based on acid-base titration per column volume Λ_{AcB}^{CV} was determined to be $0.08 \pm 0.0056 \frac{\text{mol}}{\text{L}}$ and per adsorber skeleton $\Lambda_{AcB}^{skeleton}$ to be $0.276 \pm 0.042 \frac{\text{mol}}{\text{L}}$. Finally, the columns were unpacked and the adsorber dry weight was determined. The data for the Poros 50HS columns are summarized in the Supporting Information (Tab. 1). The corresponding linear regressions and the parameters of the fits are plotted in Fig. 3.4 on the left hand side. Figure 3.4 A presents the data for the histidine capacity $n_{his}^{ads}(CV)$, figure C the data for the acid-base titration, and figure E the adsorber dry weight data.

The coefficients of determination R^2 for the linear regressions are 98.1, 98.5, and 99.8% for the histidine capacity, the acid-base titration, and the dry weight, respectively.

3.4.1.2 SP Sepharose FF

The experimental procedure presented for Poros 50HS was repeated for the SP Sepharose FF adsorber (SPSFF). Five different column volumes ranging from 173 to 487 μL were packed with SPSFF. The determined voidages of the adsorber bed are presented in the Supporting Information (Tab. 2). Afterwards, the ionic capacity was calculated as a function of geometric column volume based on the histidine capacity Λ_{his}^{CV} and per adsorber skeleton $\Lambda_{his}^{skeleton}$ as triplicate. On the basis of the five different column volumes, $\Lambda_{his}^{skeleton}$ was calculated to $5.269 \pm 0.21 \frac{\text{mol}}{\text{L}}$ and Λ_{his}^{CV} to $0.285 \pm 0.018 \frac{\text{mol}}{\text{L}}$. Subsequently, the ionic capacity was determined based on acid-base titration. The ionic capacity based on acid-base titration per column volume Λ_{AcB}^{CV} was determined to be $0.213 \pm 0.018 \frac{\text{mol}}{\text{L}}$ and per adsorber skeleton $\Lambda_{AcB}^{skeleton}$ to be $3.929 \pm 0.21 \frac{\text{mol}}{\text{L}}$. Finally, the columns were unpacked and the adsorber dry weight was determined. The data for the SPSFF columns are summarized in the Supporting Information (Tab. 2). The corresponding linear regressions and the parameters of the fits are plotted in Fig. 3.4 on the right hand side. Figure 3.4 B

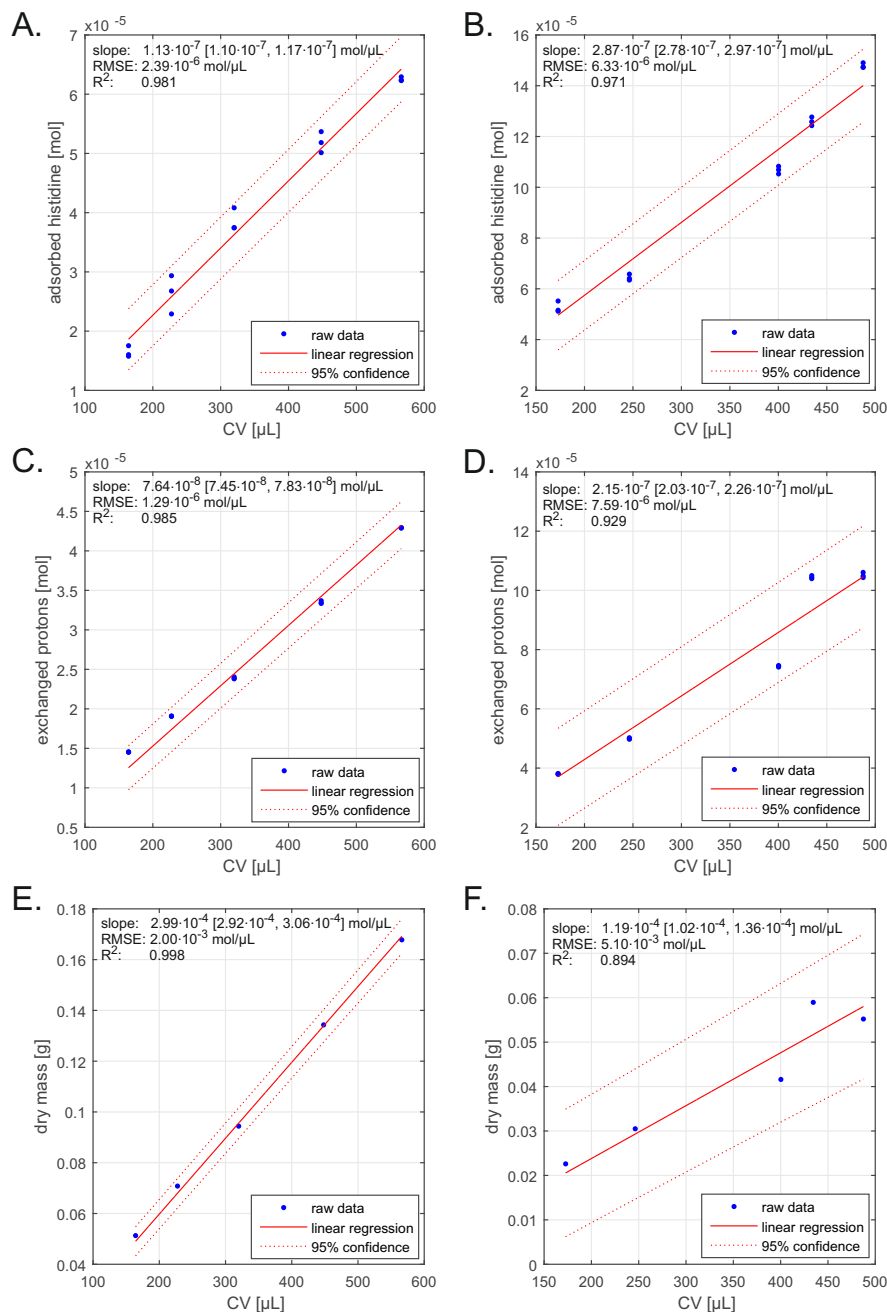


Figure 3.4: Column chromatography data fits for Poros 50HS (left) and SP Sepharose FF (right). The figures A, C, and D present the linear fits of the measurements through the origin, for the histidine capacity, the acid-base titration, and gravimetry, for Poros. The figures B, D, and E show the respective fits for Sepharose: the slope of the fit with 95% confidence intervals, the RMSE, and the R^2 .

presents the data for the histidine capacity $n_{his}^{ads}(CV)$, figure D the data for the acid-base titration, and figure F the adsorber dry weight data. The coefficients of determination R^2 for the linear regressions are 97.1, 92.9, and 89.4% for the histidine capacity, the acid-base titration, and the dry weight, respectively.

The results from the three methods correlate linearly with the column volume. It has to be noted that the method of unpacking the column and drying the adsorbent is invasive and therefore usually not applicable for characterizing a column. The acid-base titration and the histidine capacity are both suitable for determining the ionic capacity of a column.

3.4.2 Batch chromatography

In batch chromatography on robotic work stations, acid-base titration is not feasible due to the lack of a conductivity detector in standard robotic hardware. The determination of adsorber dry weights for standard 96-well setups would be very labor-intensive, prone to errors due to a lot of manual work, and inappropriate due to its invasive nature. Therefore, the histidine capacity can be used in column and batch chromatography alike.

Using the histidine capacity in batch chromatography, it is impossible to distinguish experimentally between the adsorbed histidine n_{his}^{ads} and the histidine in the pore volume n_{his}^{pore} .

From the known voidages determined in the column tracer experiments (comp. Eqs. (3.1)), it is possible to determine the sum of n_{his}^{ads} and the histidine in the pore volume n_{his}^{pore} and to correlate this amount of histidine to the column volume. This adjusted correlation derived from the column chromatography data can be used to convert the sums of n_{his}^{ads} and n_{his}^{pore} determined in batch chromatography to *equivalent column volumes* per plaque. These adjusted correlations for the column chromatography with Poros 50HS and SPSFF are presented in Fig. 3.5.

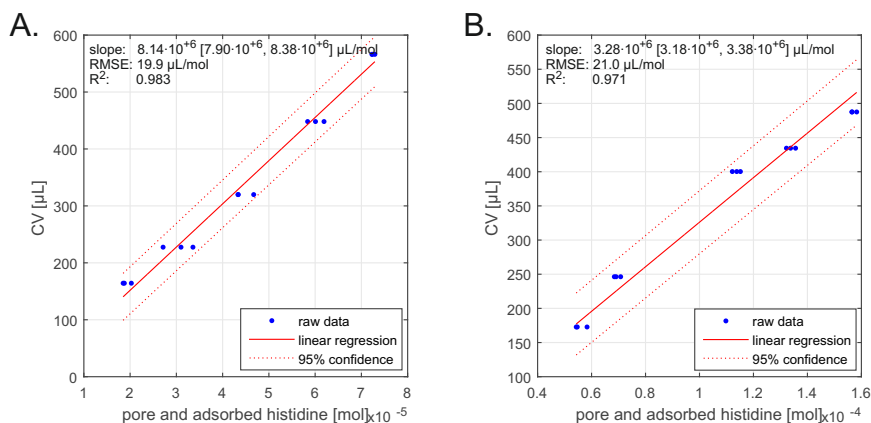


Figure 3.5: Experimental data for Poros 50HS (A) and SPSFF (B) columns. Plot of column volume vs. the histidine adsorbed and in the pore volume. Each figure shows the slope of the fit with 95% confidence intervals, the RMSE, and the R^2 .

Fig. 3.6 presents the experimental batch results for Poros 50HS (A, C) and for SPSFF (B, D). The figures A and B show the distribution of the *equivalent column volumes* of the adsorber plaques to the 96 wells of the filter plate. The figures C and D depict the

distribution of the *equivalent column volumes*. For SPSFF, the mean *equivalent column volume* of the 96 wells measured as triplicates is determined to be $13.9 \pm 0.6 \mu\text{L}$. Based on the voidages determined in the column experiments, the *equivalent column volume* corresponds to an adsorber skeleton volume of $0.7 \mu\text{L}$.

For Poros 50HS, the mean *equivalent column volume* of the 96 wells measured as triplicates is determined to be $14.8 \pm 2.7 \mu\text{L}$ (6 single measurements out of 288 excluded as outliers due to a membrane defect). Based on the voidages determined in the column experiments, the *equivalent column volume* corresponds to an adsorber skeleton volume of $4.3 \mu\text{L}$.

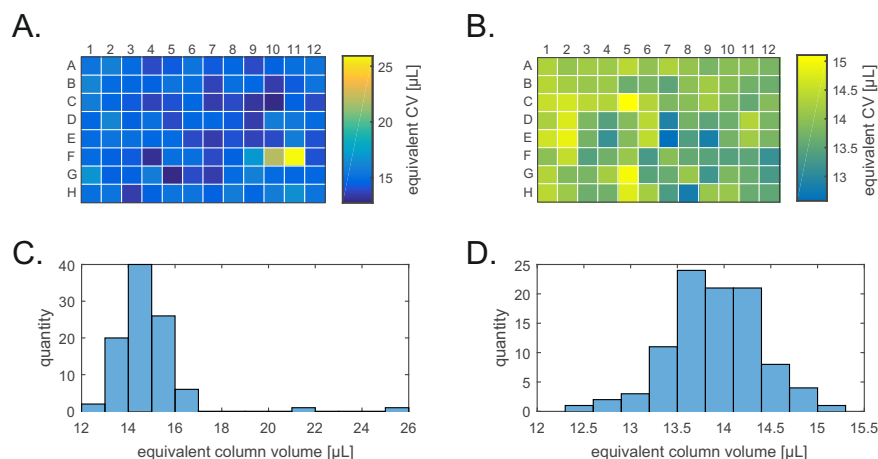


Figure 3.6: Calculated *equivalent column volume* of adsorber plaques. The distribution of the *equivalent column volume* for Poros 50HS is plotted in the figures A and C. B and D show the data for SPSFF, respectively.

3.4.3 Validation

As case study for validation, we recorded a single batch adsorption isotherm of lysozyme on SP Sepharose FF, estimated SMA parameters based on this batch data, and predicted an experimental column breakthrough curve.

The results of the batch adsorption isotherms are presented in Fig. 3.7 (left). The red dots represent the isotherm data without correction using the histidine capacity. The red curves represent the SMA isotherm fitted to the data. The blue curves represent the fits to the data with correction of the adsorber volume using the histidine capacity. The estimated SMA parameters are summarized in Tab. 3.1. The maximum binding capacities per skeleton volume (q_{max}) without and with histidine correction are 900g/L and 1042g/L , respectively. The calculation of q_{max} is carried out according to Eq. (3.15). The histidine correction increases the adsorbed concentrations. This effect is captured by the SMA parameters with a decreasing steric shielding σ . The equilibrium parameter is hard to determine due to the restriction to a single condition isotherm, but k_{eq} has little influence on the prediction of the subsequent column breakthrough curve.

The estimated SMA parameters derived from the batch experiment were complemented with a General Rate Model and used for the *in silico* prediction of breakthrough curves.

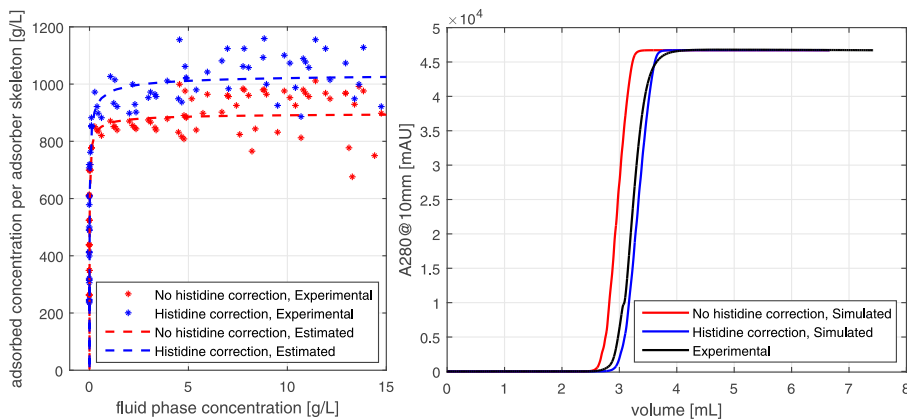


Figure 3.7: Batch adsorption isotherm of lysozyme on SP Sepharose FF, based on the adsorber skeleton volume (left). The red and blue dots represent the data without and with correction using the histidine capacity, respectively. The outlier detection applied to the data is explained in section 3.3. The red curves show the SMA isotherm fitted to the data without histidine correction. The blue curves are SMA fits with correction using the histidine capacity. The simulation of column breakthrough curves of lysozyme on SP Sepharose FF, based on SMA parameters from batch adsorption isotherms is shown on the right hand side. The black curve represents the experimental breakthrough curve. The red curve is derived from the parameters without histidine correction and the blue curve is based on SMA parameters with additional histidine correction.

Table 3.1: SMA parameters estimated from batch isotherm data without and with additional correction using the histidine capacity. Parameters are related to the adsorber skeleton volume and shown with 95% confidence intervals (CI).

	Unit	No histidine correction	CI	Histidine correction	CI
k_{eq}		203	[200; 206]	93	[72; 114]
ν		1.68	[1.66; 1.70]	1.83	[1.56; 2.11]
σ		27.9	[27.8; 28.1]	23.8	[22.8; 24.7]
q_{max}	$\frac{g}{L}$	900.7	[896.5; 904.7]	1042.0	[994.4; 1093.9]

The simulation results are presented in Fig. 3.7 (right). The simulated curve based on the SMA parameters without correction using the histidine capacity is shown in red. The experimental breakthrough curve is shown in black. The retention volumes of the simulated break through decreased compared to the experimental curve. The area-based calculations of the 10% and 100% dynamic binding capacities (DBC) per adsorber skeleton are shown in Tab. 3.2. The simulated curves without histidine correction result in 10% and 100% DBCs being 7.4 and 8.5% smaller than their experimental counter parts. The simulated curve based on the SMA parameters with correction using the histidine capacity is shown in blue. The histidine correction increases the break through retention volume. The calculated 10% and 100% DBCs are 3.8 and 2.6% larger than their experimental counter parts. The shape of the two simulated curves is almost identical, both are steeper than the experimental one.

Table 3.2: Dynamic binding capacities based on a 10% and 100% breakthrough (10%DBC, 100%DBC) of the load solution. DBCs are calculated for the experimental breakthrough curve and for the simulations with and without histidine correction, shown in Fig. 3.7. DBCs are given as absolute value per skeleton volume, and in relation to the experimental value.

	Unit	No histidine correction	Histidine correction	Experimental
10%DBC	$\frac{g}{L}$	1061.1	1189.6	1146.3
	%	-7.4	3.8	
100%DBC	$\frac{g}{L}$	1145.3	1283.6	1251.1
	%	-8.5	2.6	

3.5 Discussion

3.5.1 Column chromatography

For Poros 50HS, the ionic capacity per geometric column volume based on five packed columns is $0.08 \frac{\text{mol}}{\text{L}}$ for the acid-base titration and $0.113 \frac{\text{mol}}{\text{L}}$ for the histidine capacity. For SP Sepharose FF, the ionic capacity per geometric column volume based on five packed columns is $0.213 \frac{\text{mol}}{\text{L}}$ for the acid-base titration and $0.285 \frac{\text{mol}}{\text{L}}$ for the histidine capacity. This results in histidine-based ionic capacities being 1.4 and 1.3 times larger than the capacities determined by acid-base titration for Poros and Sepharose, respectively. In the following we discuss possible causes which might contribute to this difference between the two methods. Afterwards, we focus on the impact of the differences on the methods usability for chromatography modeling.

The quality of the acid-base titration mainly depends on the concentration of the titrant and the titration volume recorded by the LC system. The impact of the recorded titration volume is minimized by keeping the titrant concentration low (0.01M). For the histidine capacity, the volume of the eluate fraction and its histidine concentration are foremost of importance. The volume is hereby determined by gravimetry and a density measurement of the eluate pool.

The low bed heights used in this study have an identical impact on acid-base titration and histidine capacity-based ionic capacities. Assuming an uncertainty of the caliper-based measurement of the bed height of 0.5mm, this corresponds to an uncertainty of the ionic capacities in the range of 10 to 3% depending on the different column volumes. Since both methods are carried out using the same column packing and bed height measurement, this explanation is not sufficient.

The main operational difference between acid-base titration and histidine capacity is that titration is a type of dynamic capacity measure based on recording a dynamic breakthrough of the titrant. In contrast, the histidine capacity relies on a static measure for the histidine capacity, consisting of a prolonged loading with the histidine solution and the complete elution of the bound histidine and subsequent measurement. Figuratively, acid-base titration is to histidine capacity as dynamic binding capacity is to static binding capacity. This consideration is consistent with the proportionality of ionic capacity and binding capacity described in Eq. (3.15).

Staby et al. [146] quantified the differences in static binding capacities (SBC) and dynamic binding capacities (10% and 50% DBC) using the model protein lysozyme and different types of adsorbers. For Poros 50HS, Staby et al. determined the SBC to be 1.1 to 1.8 fold larger than the DBC, depending on the flow rate. This range is in line with the ratio of the dynamic acid-base titration and the static histidine capacity of 1.4. Instead of SP Sepharose FF, Staby et al. analyzed the closely related XL adsorber, exhibiting additional dextrane surface extenders compared to the FF adsorber. The factor between SBC and DBC was quantified to be in the range of 1.6 to 1.9 for the XL adsorber. This range is close to the factor of 1.3, here determined for the two titration methods and the FF adsorber.

Model parameter estimations based on different ionic capacities will differ. Therefore, estimated parameters have to be complemented with information on the underlying method, the ionic capacity was determined with. The criterion for deciding in favor of acid-base titration and histidine capacity is rather the applicability to different chromatographic formats, the non-invasive nature of the method, and the methodical simplicity.

3.5.2 Batch chromatography

The histidine capacity does not require an in-line conductivity detector and can, thus, be adopted to batch chromatography.

As a test case, we prepared 96-well filter plates with Poros 50HS and SP Sepharose FF, using a ResiQuot device equipped with a $20.8\mu L$ grid. Using the histidine capacity method, it is possible to determine the amount of histidine adsorbed to the resin and within the pore volume of the adsorber particle. The amount of histidine can be converted into an *equivalent column volume* value, based on a calibration carried out in column chromatography.

The method is not restricted to a correction of the volume of adsorber plaques prepared with the ResiQuot device as it was done in this work. The ResiQuot device was used in this case study to compare the results to existing reports from literature, since alternative approaches such as slurry pipetting highly depend on the individual experimental setup. For Poros 50HS and SP Sepharose FF, the mean *equivalent column volumes* were determined to be $14.8 \pm 2.7\mu L$ and $13.9 \pm 0.6\mu L$, respectively. Therefore, the presented histidine method results in *equivalent column volumes* being smaller than the grid volume by a factor of 1.4 and 1.5 for Poros and Sepharose.

The difference between a settled bed and a flow compressed packed bed is reported in literature for different adsorber materials. For a polystyrene-divenylbenzene (PS-DVB) adsorber backbone, Nash et al.[116] found a factor describing this effect of 1.01 to 1.03 depending on the applied flow rate. Poros is composed of a PS-DVB backbone. Lee et al. [95] reported a factor of 1.06 for the corresponding anion exchange adsorber used in this work. A factor of 1.06 is also reported in the manual provided by the adsorber supplier [3]. For SP Sepharose FF, Dziennik et al. [38] found a factor of 1.09, and Nash et al. [116] reported a factor of 1.05. For the corresponding anion exchange adsorber, Lee et al. [95] found a factor of 1.15. Therefore, the reported flow compression effect can only partly explain the measured difference between grid volume and *equivalent column volume*.

This conclusion is backed-up by the work of Bergander and Lacki [16] on the impact of adsorber volume definition in batch chromatography. Bergander et al. compared the adsorber volumes prepared with a ResiQuot device to a packed bed column, based on an invasive dry weight approach. They found batch adsorber volumes to be reduced by a factor of 1.6 compared to the grid volume (for a ResiQuot device and several different GE adsorbers). These results are in good agreement with the results presented in this work. According to Bergander et al., the underlying effects contributing to the different packing densities in column and batch chromatography are related to different pressure drops, slurry concentrations, durations of the packing process, and adsorber specific properties.

3.5.3 Validation

Bergander et al. [16] emphasize the necessity to account for the exact adsorber volume in batch chromatography, in case that a quantitative prediction of column chromatography is needed. To evaluate the impact of the histidine correction on the data quality of batch experiments, especially on the capability to predict column chromatographic experiments, we predicted column breakthrough curves based on the data derived from a single condition batch adsorption isotherm.

Correcting the batch adsorber volumes using the histidine capacity minimizes the offset

between the simulated and the experimental 100%DBC from 8.5% to 2.6%. The remaining offset between the histidine corrected simulated trace and the experimental data, can be attributed to several factors. The experimental breakthrough curve exhibits a minor peak shoulder at the initial increase. This shoulder can be explained by impurities in the lysozyme solution. These minor impurities are not considered in the simulation approach and therefore increase the DBC offset. The steeper shape of the simulated curve is another factor, contributing to the offset between the simulated and experimental DBCs. It should be recalled, that the simulation approach is based on a single condition adsorption isotherm. This approach can only provide information on the thermodynamics of the interaction and not on the kinetics or fluid dynamics. The latter effects could be accessed experimentally by batch kinetics or further column experiments. In addition, the origination of the simulation approach from a single condition adsorption isotherm, is sophisticated with respect to the estimation of a unique set of isotherm parameters. The estimation of the characteristic charge ν and the shielding parameter σ seem to be less impacted by this limitation, than the equilibrium parameters k_{eq} . The latter one is not determinable uniquely from the single condition batch data.

3.6 Conclusion

To fulfill the QbD requirements, the pharmaceutical industry has to incorporate new technologies such as HTPD and mechanistic modeling.

Mechanistic modeling of ion exchange chromatography requires the determination of the ionic capacity Λ of the adsorber. Standard techniques to determine the ionic capacity, such as acid-base titration, are not compatible with high-throughput experimental systems. The presented histidine capacity avoids the pitfalls of acid-base titration, namely the need to have a conductivity probe in high-throughput experimental systems and the restriction to adsorbers which tolerate salt-free solutions.

Another limitation of current batch high-throughput experiments is the inadequately addressed problem of adsorber quantification. Most of the existing methods relate the batch adsorber volume to the settled bed volume or the dry weight. Using the same adsorber lot in column and batch chromatography and assuming an unaltered bead voidage, the presented histidine capacity is capable of correlating the batch adsorber volume to the *equivalent volume* of a packed-bed column.

In a case study, we demonstrated the possibility to predict a column breakthrough curve based on a single condition batch adsorption isotherm, using the histidine capacity. As a consequence, the usability of batch isotherm data can be extended from the measurement of partition coefficients of different protein species derived from the initial isotherm slope to determination of binding capacities which highly depend on a reliable determination of the adsorber volume.

The presented case study can be extended from batch isotherms to batch kinetics or batch bind-elute experiments, strengthening the role of batch data in conventional and *in silico* process development.

The presented work has been focusing on CEX, but an adaptation to AEX is possible. Modifications to characterize e.g., hydrophobicity in hydrophobic- or multi-modal chromatography using another molecule instead of histidine e.g., an aromatic amino acid, are conceivable. We presented data for lab-scale column and batch chromatography, but in principle, the method is also applicable to miniaturized robotic columns.

Acknowledgment

The authors gratefully acknowledge financial support and technical advice by Roche Diagnostics GmbH (Penzberg, Germany).

The research leading to these results has partly received funding from EUROTRANS-BIO (grant agreement no. 0316071B, EC's Seventh Framework Program).

Nomenclature

Abbreviation	Unit	Definition
ϵ_{column}	–	column voidage
$\epsilon_{particle}$	–	particle voidage
ϵ_{total}	–	total voidage
$V_{dextrane}$	μL	retention volume of dextrane injection, as non-pore-penetrating tracer
$V_{acetone}$ or V_{NaCl}	μL	retention volume of acetone or NaCl injection, as pore-penetrating tracer
A_{230}	AU	absorption measured at 230nm
$A_{230,10mm}$	AU	absorption measured at 230nm, pathlength 10mm
A_{900} or A_{995}	AU	absorption measured at 900nm or 995nm, respectively
CV	μL	geometric column volume
V_{his}^{eluate}	μL	volume of eluate in the histidine capacity
n_{his}^{eluate}	mol	amount of histidine in the eluate
n_{his}^{ads}	mol	amount of adsorbed histidine
c_{his}^{load}	$\frac{mol}{L}$	histidine concentration in the load solution
c_{his}^{eluate}	$\frac{mol}{L}$	histidine concentration in the eluate
$\Lambda_{his}^{skeleton}$	$\frac{mol}{L}$	ionic capacity per volume of adsorber skeleton, determined with the histidine capacity
Λ_{his}^{CV}	$\frac{mol}{L}$	ionic capacity per column volume, determined with the histidine capacity
n_{Na+}	mol	amount of exchanged sodium ions
V_{NaOH}	μL	volume of titrant NaOH
c_{NaOH}	$\frac{mol}{L}$	concentration of titrant
$\Lambda_{AcB}^{skeleton}$	$\frac{mol}{L}$	ionic capacity per volume of adsorber skeleton, determined by acid-base titration
Λ_{AcB}^{CV}	$\frac{mol}{L}$	ionic capacity per column volume, determined by acid-base titration
m_{dry}	g	adsorber dry weight
$V_{batch}^{uncorrected}$	μL	volume of the uncorrected adsorber plaque, defined by the geometric volume of the plaque grid ($20.8\mu L$)
$V_{batch}^{corrected}$	μL	calculated equivalent column volume of the adsorber plaque
V_{dead}	μL	dead volume of Äkta LC and column housing
q^{CV}	$\frac{g}{L}$ or $\frac{mol}{L}$	adsorbed protein concentration based on the geometric column volume
$q^{skeleton}$	$\frac{g}{L}$ or $\frac{mol}{L}$	adsorbed protein concentration based on the adsorber skeleton volume
q_{max}^{CV}	$\frac{g}{L}$	maximum binding capacity per geometric column volume
$q_{max}^{skeleton}$	$\frac{g}{L}$	maximum binding capacity per adsorber skeleton volume
c_{eq}	$\frac{g}{L}$ or $\frac{mol}{L}$	equilibrium fluid phase concentration of the protein
k_{eq}		equilibrium parameter in the SMA isotherm
ν		charge parameter in the SMA isotherm
σ		shielding parameter in the SMA isotherm
c_{salt}	$\frac{mol}{L}$	apparent salt concentration (incl. displaced salt)
$c_{salt,0}$	$\frac{mol}{L}$	buffer salt concentration
MW	$\frac{g}{mol}$	molecular weight

4 | Optimal Experimental Design for the Determination of Isotherm Parameters of Glucose Oxidase using Mixed Mode Column Chromatography

Tobias Hahn¹, Gang Wang¹, Thiemo Huuk¹, Vincent Heuveline², Jürgen Hubbuch¹

¹ Karlsruhe Institute of Technology (KIT), Institute of Process Engineering in Life Sciences, Section IV: Biomolecular Separation Engineering, Karlsruhe, Germany

² Heidelberg University, Interdisciplinary Center for Scientific Computing, Engineering Mathematics and Computing Lab, Heidelberg, Germany

Abstract

Nowadays' models in chromatography include many parameters that are hard to measure experimentally, e.g. thermodynamic activity coefficients in models for hydrophobic interaction and mixed mode chromatography. In practical applications, it is hard to predict, how many and which experiments to conduct for model calibration.

Optimal Experimental Design (OED) first determines the experimental set-up with highest probable information content. Using this approach, the model parameters with the highest statistical quality are found using the least number of experiments. This is especially valuable when low sample volume is available for screening.

We present OED for column chromatography of proteins including the computation of approximate covariances and confidence intervals. A case study with the model protein glucose oxidase investigates identifiability of adsorption isotherm parameters on three resins by GE Healthcare: Capto™ Q, Phenyl, and adhere. An extended General Rate Model was developed to account for salt-dependent diffusion phenomena.

The results underline the improved reliability using OED at potentially much less time and material consumption compared to manual experimental design. From the covariance matrices it is further possible to gain insight into the models' ability to describe the protein's sorption behavior for the various resins.

4.1 Introduction

Mixed mode resins offer multiple binding interactions and are increasingly used in the purification of antibodies [52; 160], oligosaccharides [117] and many other molecules. By adjusting the operational conditions the binding modes can be reduced to a single interaction [70; 89] or used together to effect the separation. The mixed mode chromatography (MMC) ligands often include features of ion-exchange chromatography (IEC) and of hydrophobic interaction chromatography (HIC) ligands. They are highly suitable for application in pH-tunable hydrophobic [81] or high salt conditions [78], and for capturing specific proteins under physiological conditions [53].

As for other chromatographic methods, the fundamentals of mixed mode chromatography can be understood and improved by creating reliable models [29]. The Steric Mass Action model (SMA) [23] was employed successfully for mixed mode chromatography [83]. Mollerup's thermodynamic framework [110; 111] increased the understanding of IEC as well as HIC [113] and the optimisation of purification processes [112]. Based on this, Nfor *et al.* developed a model for protein adsorption in IEC/HIC mixed mode chromatography [120]. These models include many parameters, which are hard to measure experimentally, for example thermodynamic activity or interaction coefficients. Especially in multi component settings, it is hard to predict how many experiments to conduct for model calibration and which ones will have the highest information content. Conventional Design of Experiments (DoE) approaches will most probably include unnecessary experiments that do not add certainty to the parameter estimates.

As mathematical models are available that describe the dynamics of the system, sensitivity analysis allows to find optimal experiments for model calibration. While the objective of parameter estimation is to find model parameters which minimize the disagreement of simulation and measurement, Optimal Experimental Design (OED) [6] takes one step backward and first determines the experimental set-up with highest probable information content. Here, the objective is to minimize the uncertainty of the parameters measured via the parameter covariance matrix. Using this approach, the model parameters with the highest statistical quality are found using the least number of experiments. This is especially valuable when low sample volume is available for screening.

The technique was described for nonlinear ordinary differential equations by Schlöder *et al.* and applied to the reaction of urethane [9]. The same methodology was used by Arellano-Garcia for SO₂ oxidation [4]. A fed-batch reactor and the Lotka Volterra fishing problem were approached with OED by Tenen *et al.* [151]. In the context of chromatography, Wozny *et al.* [8] investigated the optimal determination of SMA parameters for β -lactoglobulin using static batch experiments

Here, we present OED for column chromatography of proteins, including the computation of approximate covariances and confidence intervals. A case study compares parameter estimation with manually chosen experimental conditions and OED for the model protein glucose oxidase on IEC, HIC and MMC resins to gain a deeper understanding of the differences in sorption behavior. With Capto™ adhere, GE Healthcare provides a mixed-mode adsorbent that chemically combines the anion-exchange adsorbent Capto™ Q, and the hydrophobic interaction adsorbent Capto™ Phenyl and is hence chosen for this task.

4.2 Theory

4.2.1 Adsorption Models

The employed models for ion-exchange, hydrophobic interaction, and mixed mode chromatography are structurally very similar and presented in the following sections

4.2.1.1 Ion-exchange Chromatography

A protein molecule unit P in solution is assumed to bind to ν ligands L , exchanging ν units of salt counter-ions SL :



The Steric Mass Action model [23] considers that the number of available ligands is further reduced by steric shielding effects that are mostly caused by protein-protein repulsion [93]. The multi-component equilibrium formulation of the mobile phase concentrations c and stationary phase concentrations q of m proteins and salt is given by

$$\frac{q_i}{c_i} = k_{eq,i} \left(\frac{\bar{q}_{salt}}{c_{salt}} \right)^{\nu_i} \quad i = 1, \dots, m, \quad (4.2)$$

where \bar{q}_{salt} is the concentration of available ligands, given by

$$\bar{q}_{salt} = \Lambda_{IEC} - \sum_{i=1}^m (\nu_i + \sigma_i) q_i. \quad (4.3)$$

Here, Λ_{IEC} is the total concentration of binding sites in the stationary phase and σ_i accounts for the steric shielding of protein i .

The concentration of counter-ions in the stationary phase is analogously given by

$$q_{salt} = \Lambda_{IEC} - \sum_{i=1}^m \nu_i q_i. \quad (4.4)$$

Jackobsson *et al.* [77] introduced binding kinetic rate constants k_{ads} and k_{des} with $k_{eq} = k_{ads}/k_{des}$, here given in the formulation with $k_{kin} = k_{des}^{-1}$:

$$k_{kin,i} \frac{\partial q_i}{\partial t} = k_{eq,i} \bar{q}_{salt}^{\nu_i} c_i - c_{salt}^{\nu_i} q_i \quad i = 1, \dots, n. \quad (4.5)$$

4.2.1.2 Hydrophobic Interaction Chromatography

Mollerup established a model based on fundamental chemical thermodynamics [111]. In contrast to IEC, a protein molecule unit P in solution is assumed to bind to n ligands L , forming a protein ligand complex:



Here, the equilibrium formulation is written in terms of the activity coefficients of the species

$$\frac{q_i}{c_i} = k_{eq,i} \left(\frac{\bar{q}_L}{c_v} \right)^{n_i} \frac{\gamma_P \gamma_L}{\gamma_{PN_n}} \quad i = 1, \dots, m, \quad (4.7)$$

where γ_L and γ_{PN_n} are assumed to be unity and the molarity of the solution in the pore volume c_v is constant. The protein solute activity coefficient is modeled as

$$\gamma_{P,i} = \exp(K_{s,i} c_{salt} + K_{p,i} c_i) \gamma_{P,i}^{\infty,w} \quad i = 1, \dots, m, \quad (4.8)$$

where K_s and K_p are constant interaction parameters and $\gamma_P^{\infty,w}$ is the activity coefficient at infinite dilution.

Similarly to SMA, the concentration of available ligands \bar{q}_L , given by

$$\bar{q}_L = \Lambda_{HIC} - \sum_{j=1}^m (n_j + s_j) q_j, \quad (4.9)$$

with a steric shielding coefficient s .

In the classical form [111], $\Lambda_{HIC}^{n_i}$ is lumped into k_{eq} such that the loading is described with the help of the single-component saturation concentrations $q_{max,i} = \Lambda_{HIC}/(n_i + s_i)$:

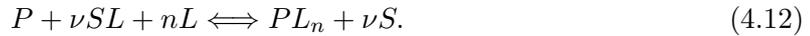
$$\bar{q}_L = \Lambda_{HIC} \bar{q}'_L = \Lambda_{HIC} \left(1 - \sum_{i=1}^m \frac{q_i}{q_{max,i}} \right) \quad i = 1, \dots, m, \quad (4.10)$$

In the kinetic formulation, c_v and $\gamma_P^{\infty,w}$ are lumped in the equilibrium constant:

$$k_{kin,i} \frac{\partial q_i}{\partial t} = k_{eq,i} \bar{q}'_{L,i}{}^{n_i} \exp(K_{s,i} c_{salt} + K_{p,i} c_i) c_i - q_i. \quad (4.11)$$

4.2.1.3 Mixed Mode Chromatography

Nfor *et al.* developed a model for protein adsorption in IEC/HIC mixed mode chromatography by assuming both adsorption modes to happen at the same time [120]:



The equilibrium formulation was derived to be

$$\frac{q_i}{c_i} = k_{eq,i} \left(\frac{\bar{q}_{salt}}{c_{salt}} \right)^{\nu_i} \left(\frac{\bar{q}_L}{c_v} \right)^{n_i} \gamma_p \quad (4.13)$$

with the additional counter-ion balance known from SMA, Eq. (4.4).

The kinetic form is likewise:

$$k_{kin,i} \frac{\partial q_i}{\partial t} = k_{eq,i} \bar{q}'_{salt}{}^{\nu_i} \bar{q}'_L{}^{n_i} \exp(K_{s,i} c_{salt} + K_{p,i} c_i) c_i - c_{salt}^{\nu_i} q_i. \quad (4.14)$$

The similarity to Eqs. (4.5) and (4.11) is apparent. When switching hydrophobic effects off, i.e. $n = K_s = K_p = 0$, Eq. (4.14) reduces to Eq. (4.5). For $\nu = 0$, we recover Eq. (4.11).

4.2.2 Column Model

The General Rate Model (GRM) [55] is employed to describe the macroscopic protein transport through the column. The systems are of Convection Diffusion Reaction (CDR) type. Eq. (4.15) describes the rate of change of a concentration $c_i(x, t)$ in the interstitial phase of a column with length L to consist of convective mass transport in space with the average interstitial velocity of the fluid u , peak broadening effects that are modeled as dispersion in axial direction with respect to a coefficient D_{ax} , and transition from the interstitial concentration into the particle pore concentration $c_{p,i}$ which depends on the porosity of the bed ε_b , the radius of adsorber particles r_p and a component-specific film transfer coefficient $k_{film,i}$. The model is complemented with Danckwerts boundary conditions, Eqs. (4.15),(4.17).

$$\frac{\partial c_i}{\partial t} = -u(t) \frac{\partial c_i}{\partial x} + D_{ax} \frac{\partial^2 c_i}{\partial x^2} - \frac{1 - \varepsilon_b}{\varepsilon_b} k_{film,i} \frac{3}{r_p} (c_i - c_{p,i}) \quad (4.15)$$

$$\frac{\partial c_i}{\partial x}(0, t) = \frac{u(t)}{D_{ax}} (c_i(0, t) - c_{in,i}(t)) \quad (4.16)$$

$$\frac{\partial c_i}{\partial x}(L, t) = 0 \quad (4.17)$$

The GRM, Eq. (4.18), introduces a radial dimension $r \in [0, r_p]$ for the particles and a component-specific pore diffusion coefficient D_p to model diffusion-driven mass transfer in the pore system.

$$\frac{\partial c_{p,i}}{\partial t} = \begin{cases} \frac{1}{r^2} \frac{\partial}{\partial r} \left(r^2 D_{p,i} \frac{\partial c_{p,i}}{\partial r} \right) - \frac{1 - \varepsilon_p}{\varepsilon_p} \frac{\partial q_i}{\partial t} & \text{for } r \in (0, r_p) \\ \frac{k_{film,i}}{\varepsilon_p D_{p,i}} (c_i - c_{p,i}) & \text{for } r = r_p, \\ 0 & \text{for } r = 0. \end{cases} \quad (4.18)$$

The high salt concentrations used in the experiments influence the kinetic effects. It was impossible to find $D_{p,i}$ values that lead to sufficiently well fitting simulated chromatograms for experiments with salt concentrations above 1 M (data not shown). Similarly, a strong increase of the *HETP* value (height-equivalent of a theoretical plate) starting at 1 M salt was reported for HIC resins [115] that could be modeled with an exponential function of the form

$$HETP = a + b \exp(c \cdot c_{salt}). \quad (4.19)$$

We also observed different *HETP* values for pulse injections of small tracers dissolved in low and high salt buffer, such that the adsorption related terms in the *HETP* cannot be the cause of the effect. The most influential term remaining in the *HETP* value for a GRM is pore diffusivity [55]. Assuming the other contributors to be constant, the relation is given by $HETP = c_1 + c_2 \cdot D_{p,i}^{-1}$ with two constants c_1, c_2 [55]. Combining this with the *HETP* correlation of [115] and rearranging, we formulate the salt concentration-dependent pore diffusion coefficient with three constants D_{p0}, D_{p1}, D_{p2} as

$$D_p(c_{salt}) = D_{p0} \frac{1 + D_{p1}}{1 + D_{p1} \cdot \exp(D_{p2} \cdot c_{salt})}. \quad (4.20)$$

The formulation in this paper is chosen such that $D_p(0) = D_{p0}$ and values of different species can be compared easily. For parameter estimation, we work the numerically favorable equation

$$D_p(c_{salt}) = \frac{D'_{p0}}{1 + D_{p1} \cdot \exp(D_{p2} \cdot c_{salt})} \quad (4.21)$$

with $D'_{p0} = D_{p0}(1 + D_{p1})$ in order to avoid rounding errors in the division.

4.2.3 Model Calibration

Estimation of an unknown parameter set $\hat{\theta}$ solves the least squares optimization problem

$$\hat{\theta} = \arg \min_{\theta} \sum_{k=1}^{N_{exp}} \sum_j \left(\frac{c_{meas,k}(t_j) - c_{sim,k}(t_j; \theta)}{\sigma_k} \right)^2, \quad (4.22)$$

where $c_{meas,k}(t_j)$ and $c_{sim,k}(t_j)$ are the measured and simulated sum signals of experiment k at the column outlet at point in time t_j . σ_k is the variance of the measurement error of the respective experiment. Assuming the noise of the parameter estimates to be zero-mean Gaussian and isotropic, solving the least squares problem is identical to Maximum Likelihood estimation.

4.2.4 Statistical Analysis

As a measure of parameter certainty, an estimate of the covariance matrix is used. The diagonal elements of the covariance matrix represent the variance of the estimates. Obtaining the exact covariance matrix is a complex mathematical problem that leads most studies to use a Jacobian matrix [9] or a Fisher information matrix (FIM) instead [153; 162]. The asymptotic variance of the maximum likelihood estimator is given by the Cramer-Rao lower bound [33; 48], the reciprocal of the Fisher information:

$$Cov(\theta) \geq FIM(\theta)^{-1} = \left(\sum_{k=1}^{N_{exp}} FIM_k(\theta) \right)^{-1}. \quad (4.23)$$

with the Fisher information matrix of each experiment k being defined with the parameter sensitivities of a Function $F_k(t)$ [137] :

$$FIM_k(\theta) = \frac{1}{\sigma_k^2} \int_T \frac{\partial F_k}{\partial \theta_j} \frac{\partial F_k^T}{\partial \theta_j} dt \quad (4.24)$$

In our case, two function F are of interest, the model $F_k(t) = c_{sim,k}(t)$ and the least squares error $F_k = (c_{meas,k}(t) - c_{sim,k}(t))^2$.

4.2.4.1 Confidence Intervals

The confidence intervals contain the true parameter of interest with an a priori defined probability. If not stated otherwise, confidence intervals with a probability of 95 % are

calculated. Given an estimate of the covariance matrix created from $F_k = (c_{meas,k}(t) - c_{sim,k}(t))^2$, a confidence intervals for θ_j is given by

$$\theta_j \pm c\sqrt{\text{diag}(\text{Cov}(\theta))} \quad (4.25)$$

where c is the respective quantile of the Student's t-distribution.

4.2.4.2 Optimal Experimental Design

The purpose of optimal experimental design is to identify the process set-ups that facilitate parameter estimation. Hence, the parameter sensitivity of the model is to be maximized. Here, we use $F_k(t) = c_{sim,k}(t)$ to determine the parameter covariance matrix of the designed experiments and aim to minimize it [33; 48].

For this purpose, a scalar function of the covariance matrix has to be defined. A discussion of proposed functions is given in [151]. In the following, the D-criterion is used that minimizes the determinant of the covariance matrix and thus the volume of the confidence ellipsoid.

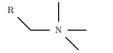
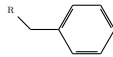
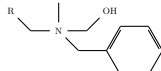
$$D(\text{Cov}) = \ln \det(\text{Cov}) \quad (4.26)$$

4.3 Materials and Methods

4.3.1 Chromatographic Instrumentation

The chromatographic experiments were carried out using an ÄKTApurifier 10 fast protein liquid chromatography (FPLC) system equipped with pump P-903, UV (10mm path length), conductivity and pH monitor UPC-900, an autosampler A-905 and a fraction collector Frac-950 (all GE Healthcare, Little Chalfont, Buckinghamshire, UK). The instrument was controlled with UNICORN 5.31 (GE Healthcare, Little Chalfont, Buckinghamshire, UK).

Table 4.1: Overview of chromatography resins.

Capto™	Ligand	Structure	Binding
Q	Quaternary amine		ionic
Phenyl	Phenyl		hydrophobic
adhere	N-benzyl-n-methyl ethanolamine		ionic, hydrophobic, hydrogen bonds

4.3.2 Adsorbers, Buffers, and Protein

All resins were acquired pre-packed by ATOLL as 1 ml miniChrom columns with dimension $5\text{ cm} \times 0.2\text{ cm}^2$. The three different resins used are shown in Tab. 4.1. Capto™ Q is a strong

anion exchange resin and Capto™ Phenyl is a hydrophobic interaction media. They are used for capture or intermediate purification steps of proteins. Capto™ adhere combines the features of both Capto™ Q and Capto™ Phenyl. All columns were stored in 20% ethanol at 4 °C.

20 mM 1-methylpiperazine buffers (Sigma-Aldrich, St. Louis, MO, USA) with 0 and 4 M NaCl (Merck, Darmstadt, Germany) were used at pH 4.5 for all experiments. The different salt profiles were mixed from these two buffers. To regenerate the single mode columns, the concentration of sodium chloride was increased to 4 M in case of Capto™ Q and decreased to 0 M in case of Capto™ Phenyl. Because of the hydrophobic and ionic features of Capto™ adhere, the pH was reduced to 3 in a regeneration step by applying 50 mM NaH₂PO₄ (VWR, Darmstadt, Germany) to induce the charge repulsion effect. For cleaning-in-place 1 M NaOH (Merck, Darmstadt, Germany) was used. All buffers were 0.22 μ m-filtrated and degassed by sonification.

Glucose Oxidase (from *Aspergillus niger*, no. G7141, Sigma-Aldrich, St. Louis, MO, USA) was used as model protein. The protein was prepared using the respective running buffer and 0.22 μ m-filtrated prior to usage.

4.3.3 System Characterization

To determine the system characteristics, experiments with tracer substances were carried out. The flow rate was kept at 0.2 ml/min. The UV signal at 300 nm and conductivity signal were recorded.

The FPLC dead volume was determined by tracer injections without a column attached to the system. All other data were corrected with respect to this dead volume. The column void volume was calculated from injections of a pore-penetrating, non-interacting (acetone) and a non-pore-penetrating, non-interacting tracer (dextrane 2000 kDa). The total ionic capacity was determined by acid-base titration.

4.3.4 Initial Model Calibration

Initial model calibration was performed with manually designed experiments. Thereafter, optimal experimental design was repeated until the the D-criterion value did not change significantly. If not stated otherwise, the sample concentration and volume were kept constant at 0.06 mM and 0.5 ml for low salt binding, 0.02 mM and 1 ml for high salt binding, because of solubility constraints.

In case of Capto™ Q, three bind-elute runs were performed: two gradient and one step elution. The gradients were ran from 0 M to 0.20 M NaCl, and 0 M to 4 M NaCl; the step height was set to 0.1 M. The gradients and steps were initiated after 6 ml and the length of the gradients was chosen to be 20 ml.

For Capto™ Phenyl, three step elutions with varying binding buffer salt concentrations were performed: 4 M, 2 M, and 1 M NaCl. All steps went down to 0 M NaCl and were initiated after 6, 6, and 25 ml.

In case of Capto™ adhere, three experiments with low-salt binding and three with high-salt binding were performed, two steps and one gradient in each case. The steps had final concentrations of 1 and 2 M NaCl and were again initiated after 6 ml. As before, the gradients started at 6 ml, had a length of 20 ml and were ran from 0 to 2 M, and 4 to 0 M NaCl.

Table 4.2: Measured (top) and calculated (bottom) column parameters.

Parameter	Symbol	Unit	Proceeding	Capto™ Q	Capto™ Phenyl	Capto™ adhere
Length	L	mm	From manufacturer	50	50	50
Volume	V	ml	From manufacturer	1	1	1
Bead radius	r_p	mm	From manufacturer	0.045	0.0375	0.0375
System dead volume	V_d	ml	Acetone pulse without column	0.078	0.078	0.078
Retention volume acetone	V_{RetAc}	ml	Acetone pulse with column	0.9	1.07	1.02
Retention volume dextran	V_{RetDex}	ml	Dextran pulse with column	0.42	0.5	0.47
HETP	$HETP$	mm	UNICORN peak integration	0.366	0.283	0.182
Volume of HCl	V_{HCl}	ml	Acid/base titration	24.2		13.28
Molarity of HCl	c_{HCl}	M	Manually controlled	0.01		0.01
Flow rate	u	$\frac{mm}{s}$	Manually controlled	0.167	0.167	0.167
Total column porosity	ε_t		$V_{RetAc} - V_d$	0.822	0.992	0.942
Bed porosity	ε_b		$V_{RetDex} - V_d$	0.342	0.422	0.392
Particle porosity	ε_p		$\frac{\varepsilon_t - \varepsilon_c}{1 - \varepsilon_c}$	0.729	0.986	0.905
Interstitial flow	u_{int}	$\frac{mm}{s}$	u/ε_b	0.487	0.395	0.426
Axial dispersion	D_{ax}	$\frac{mm^2}{s}$	$u_{int}/2 \cdot HETP$	0.089	0.056	0.036
Ionic capacity	Λ	M	$\frac{c_{HCl} \cdot V_{HCl}}{V_c(1 - \varepsilon_t)}$	1.36		2.29

4.3.5 Numerical Methods

The simulations were performed using the in-house software package ChromX [59]. A finite element method with linear Streamline-Upwind-Petrov-Galerkin elements was used here. The discretization in time is performed with the fractional step θ -scheme. The non-linearity of the equation system introduced by the isotherm was treated with Picard iteration. The resulting linear systems are solved by LU factorization.

The estimation process was performed sequentially. First, the measurements of a single run were used for model calibration. After every completed estimation, the next experiment was added to monitor the change of the confidence intervals for manually chosen experimental set-ups. ChromX currently uses forward finite differences to compute the parameter covariance matrix and confidence intervals.

The optimal experimental design procedure was implemented in MATLAB® R2014a that was coupled to ChromX for chromatogram generation. For highest accuracy, the sensitivities were directly calculated by differentiating the model equations. All equations are

Table 4.3: Initial calibration of pore diffusion models.

Species	Capto™	$k_{film}[mm/s]$	$D_{p0}[mm^2/s]$	D_{p1}	$D_{p2}[M^{-1}]$
Glucose oxidase	Q	$7.38 \cdot 10^{-4} \pm 18\%$	$3.37 \cdot 10^{-6} \pm 12\%$	-	-
	Phenyl	$2.72 \cdot 10^{-4} \pm 1.5\%$	$2.70 \cdot 10^{-6} \pm 6.5\%$	$0.05 \pm 45\%$	$2.45 \pm 11\%$
	adhere	$5.61 \cdot 10^{-4} \pm 20\%$	$1.29 \cdot 10^{-6} \pm 41\%$	$0.16 \pm 143\%$	$1.04 \pm 31\%$
Salt	Q	$5.68 \cdot 10^{-3} \pm 187\%$	$2.61 \cdot 10^{-5} \pm 76\%$	-	-
	Phenyl	$1.43 \cdot 10^{-4} \pm 3.9\%$	$3.75 \cdot 10^{-6} \pm 9.3\%$	$0.07 \pm 65\%$	$0.96 \pm 17\%$
	adhere	$1.15 \cdot 10^{-4} \pm 12\%$	$1.24 \cdot 10^{-5} \pm 91\%$	$13.9 \pm 110\%$	$0.58 \pm 42\%$

Table 4.4: Initial isotherm parameter estimation results.

Capto™	$k_{kin}[sM^{-1}]$	k_{eq}	ν	σ	$q_{max,HIC}[M]$
Q	$3.94 \cdot 10^{-5} \pm 28\%$	$2.21 \cdot 10^{-6} \pm 25\%$	$4.79 \pm 1.2\%$	$143 \pm 375\%$	-
Phenyl	$1.00 \pm 432\%$	$54.8 \pm 5.6\%$	-	-	$0.51 \pm 62k\%$
adhere	$0.21 \pm 45\%$	$0.16 \pm 104\%$	$2.54 \pm 3.2\%$	$283 \pm 198\%$	-
Capto™	n	s	$k_s[M^{-1}]$	$k_p[M^{-1}]$	
Phenyl	$0.14 \pm 62k\%$	-	$3.71 \pm 0.9\%$	$-32.9 \pm 20\%$	
adhere	$0.25 \pm 463\%$	$291 \pm 1875\%$	$3.68 \pm 3.6\%$	$-8.01 \pm 76\%$	

sufficiently smooth to fulfill the Schwarz integrability condition. Hence, time and parameter derivative can be interchanged and the sensitivities can be integrated over time with the same numerical methods.

4.4 Results and Discussion

4.4.1 Column Characterization

The dead and void volumes given in Table 4.2 were determined from the pulse injections responses of acetone and dextran. The bead size of Capto™ Q is slightly larger, leading to a higher axial dispersion. Furthermore, its structure seems to differ as indicated by the significantly lower bead porosity compared to the other adsorbents. Capto™ Q also features dextran surface extenders which shall increase the binding capacity. Indeed, the volume of HCl needed for titration was almost twice as large as for Capto™ adhere. However, its lower porosity results in a lower ionic capacity per solid volume.

4.4.2 Initial Parameter Estimation

As described in section 4.2.2, different pore diffusion equations were employed to model the measured chromatograms. For HIC and MMC, the GRM with salt-dependent pore diffusion was used.

The estimated GRM and isotherm parameters are listed in Tables 4.3 and 4.4. The resulting plots are displayed in Figure 4.1 and show very good agreement with the measurements. The measurements have not been post-processed and include buffer effects. The simulated sum signal consists of the protein's UV trace and a linear contribution of the salt concentration.

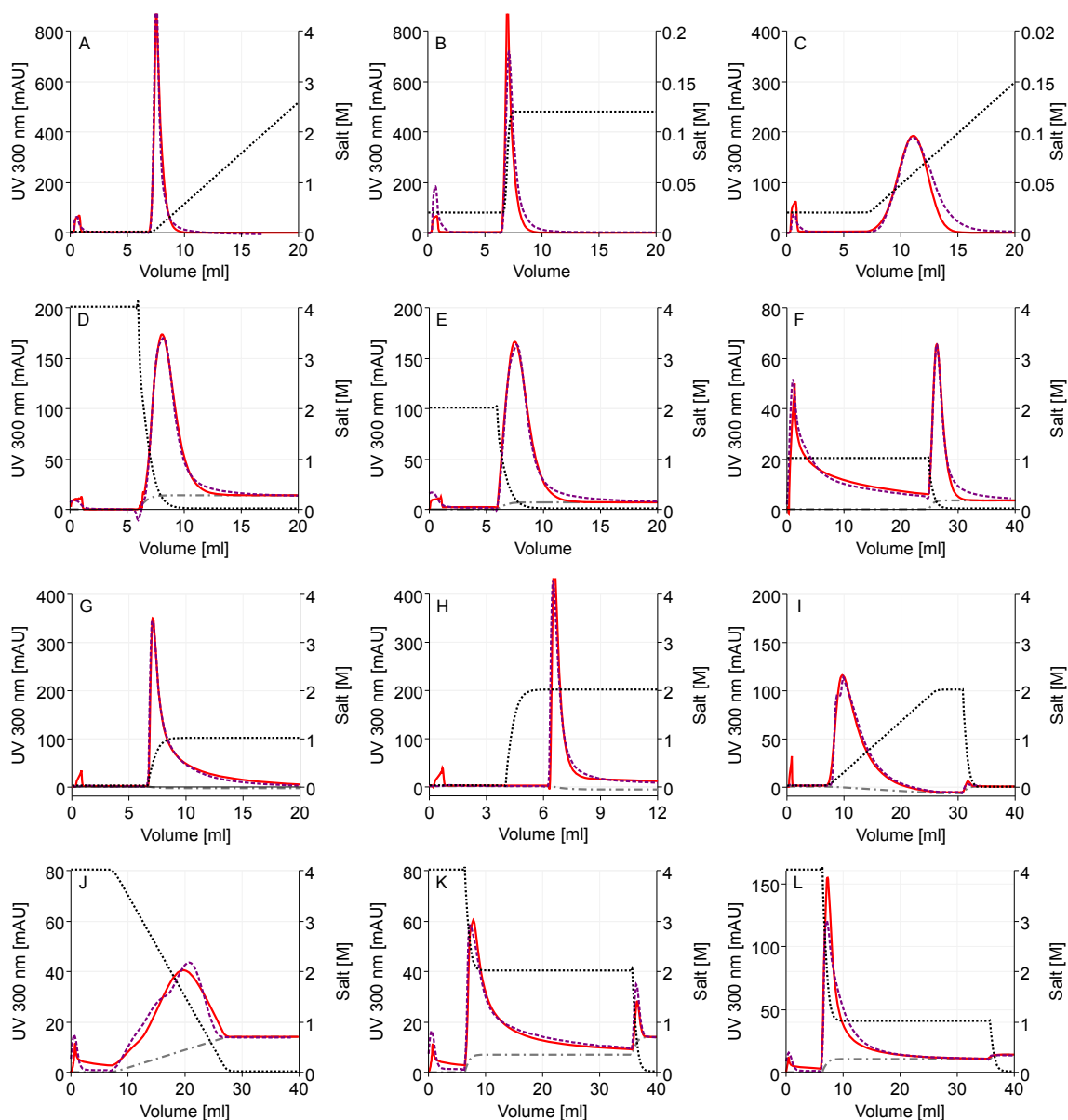


Figure 4.1: Comparison of measured chromatogram (---) and simulated sum signal (—) for the salt elutions (···) used for initial calibration of the IEC (A-C), HIC (D-F) and MMC (G-L) model. Measurements have not been post-processed and include buffer effects. The simulated sum signal consists of the protein’s UV trace and include a baseline shift (---).

It is interesting to note, that the two gradients on Capto™ adhere show shoulders and almost double peaks. As the peak shape is identical in the other recorded wavelengths 280 and 457 nm, it is unlikely that impurities are the cause of this. Similar phenomena have been reported in the literature: Karger *et al.* described two peaks resulting from the injection of papain through HPLC and explained this two-peak phenomenon with a metastable state of adsorbed protein after conformational change [82]. McNay *et al.* demonstrated the partial unfolding of lysozyme adsorbed on hydrophobic surfaces with nuclear magnetic and isotope-exchange techniques [108]. By applying an empirical approach, Jungbauer *et al.* studied protein conformational change during hydrophobic interaction chromatography depending on ligand type and salt concentration in the mobile phase [80].

From the parameter estimates, it is unlikely that glucose oxidase unfolds during high salt binding on the mixed mode resin. The characteristic parameter n is rather small. Instead, we could observed the forming of shoulders in the simulation by varying the pore diffusion parameters. The intra-column concentration show that during elution, part of the desorbed protein starts to diffuse deeper into the particles, supported by the faster diffusion rate due to decreasing salt concentration. This phenomenon continues as long as a concentration gradient in the pores exists and the mobile phase salt concentration still allows for binding. Numerical errors are unlikely, the simulations were performed on a fine grid of 50 nodes in the radial dimension and did not change after further refinement.

4.4.3 Confidence Estimates

The 95% confidence intervals were determined from the respective global covariance matrix including all fluid dynamic and isotherm parameter. They reveal that the remaining uncertainty in the linear isotherm parameter estimates for glucose oxidase is still up to $\pm 30\%$, $\pm 20\%$ for the film transfer and pore diffusion coefficients, and the steric shielding is completely undetermined. The influence of the parameter σ is only visible in the non-linear range of the isotherm. It is safe to assume that the injected sample amount was not sufficient to reach it. Furthermore, the correlation matrix contains some high entries which means that the respective parameters correlate with each other and the experiments did not contain information that only relates to a single one, e.g. $(k_{kin}, k_{eq}) = 0.45$, $(k_{kin}, \nu) = -0.71$ and $(k_{eq}, \nu) = -0.67$.

For HIC, only k_{eq} and some of the GRM parameters could be determined with reasonable certainty. As for IEC, the nonlinear range was not reached, n and q_{max} are undetermined with confidence intervals $\pm 62,000\%$. Similar results were obtained for MMC. σ , n , and s , the parameters that are only influential in the nonlinear range have the highest uncertainty.

It is interesting to note, that the estimated k_p values are negative for both, HIC and MMC. The parameter k_s and k_p were introduced by Mollerup depending on protein, salt and pH [112]. The estimated values $k_s > 1$ indicates that the water-protein interactions are stronger than the salt-protein interactions under the given circumstances. The value $k_p < 0$ implies that the protein-protein interactions are stronger than the water-protein interactions.

4.4.4 Optimal Experimental Design

In order to reduce the parameter uncertainty, three experiments were designed consecutively for each resin.

For IEC, the proposed bind/elution conditions were

- Exp. 4: a step from 0.0419 M to 4.02 M,
- Exp. 5: a gradient from 0.02 M to 3.05 M over 20 CV and
- Exp. 6: a gradient from 0.1642 to 0.4959 M over 20 CV.

Table 4.5: Final calibration of pore diffusion models.

Species	Capto™	$k_{film}[mm/s]$	$D_{p0}[mm^2/s]$	D_{p1}	$D_{p2}[M^{-1}]$
Glucose Oxidase	Q	$6.15 \cdot 10^{-3} \pm 116\%$	$1.60 \cdot 10^{-6} \pm 6.0\%$	-	-
	Phenyl	$2.43 \cdot 10^{-4} \pm 1.1\%$	$2.51 \cdot 10^{-6} \pm 21\%$	$0.03 \pm 12\%$	$2.45 \pm 0.6\%$
	adhere	$3.74 \cdot 10^{-4} \pm 10\%$	$1.26 \cdot 10^{-6} \pm 66\%$	$0.18 \pm 156\%$	$0.94 \pm 45\%$
Salt	Q	$5.70 \cdot 10^{-3} \pm 19\%$	$3.23 \cdot 10^{-5} \pm 24\%$	-	-
	Phenyl	$1.79 \cdot 10^{-4} \pm 3.7\%$	$3.88 \cdot 10^{-6} \pm 19\%$	$0.06 \pm 18\%$	$0.96 \pm 9.2\%$
	adhere	$1.52 \cdot 10^{-4} \pm 14\%$	$6.62 \cdot 10^{-5} \pm 1308\%$	$3.23 \pm 1233\%$	$0.66 \pm 129\%$

Table 4.6: Final isotherm parameter estimation results.

Capto™	$k_{kin}[sM^{-1}]$	k_{eq}	ν	σ	$q_{max}[M]$
Q	$1.02 \cdot 10^{-4} \pm 15\%$	$5.60 \cdot 10^{-6} \pm 12\%$	$4.81 \pm 0.6\%$	$48.4 \pm 370\%$	-
Phenyl	$1.00 \pm 1462\%$	$50.4 \pm 7.8\%$	-	-	$0.13 \pm 83\%$
adhere	$0.15 \pm 63\%$	$0.15 \pm 232\%$	$2.90 \pm 9\%$	$291 \pm 83\%$	-
Capto™	n	s	$k_s[M^{-1}]$	$k_p[M^{-1}]$	
Phenyl	$2.68 \pm 109\%$	-	$3.58 \pm 1.1\%$	$3577 \pm 422\%$	
adhere	$0.24 \pm 984\%$	$348 \pm 171\%$	$3.80 \pm 9.8\%$	$-20.2 \pm 51\%$	

Over the course of OED, the logarithm of the determinant reduced as from

Exp. 1–3: $\ln(\det(Cov)) = -123$ to

Exp. 1–4: $\ln(\det(Cov)) = -127$,

Exp. 1–5: $\ln(\det(Cov)) = -130.5$, and finally

Exp. 1–6: $\ln(\det(Cov)) = -130.9$.

The last experiment was not able to improve the objective value significantly indicating that the model cannot be improved under the given constraints.

All parameters are in the same order of magnitude. The film transfer values now attain the maximum and kinetics are even faster. The charge value changed only slightly and steric shielding increased by 25%. While the confidence intervals could be narrowed significantly, not all correlations improved the same. $(k_{kin}, \nu) = -0.19$ and $(k_{eq}, \nu) = -0.19$ improved clearly, but $(k_{kin}, k_{eq}) = 0.40$ did not. A very shallow salt gradient could have improved the certainty further, but was not proposed by OED. A narrower design space would have been beneficial, avoiding unnecessary high salt concentrations.

For HIC, most confidence intervals improved significantly. The optimally designed experiments were two gradients from 4 M to 0.02 M and 3.04 M to 0.23 M, and a step from 3.1 M to 0.47 M. The k_p value, which is now positive is still not well determined and could be removed from the equation when staying within the explored design space. The k_{kin} value of 1 is at the natural upper bound but the fit would have improved further for higher values. This indicates that the desorption term of the kinetic isotherm equation should be smaller. The cause could be further salt concentration dependencies or a hysteresis of adsorption and desorption kinetics. Further studies are necessary to investigate the kinetics of HIC binding under different salt concentrations.

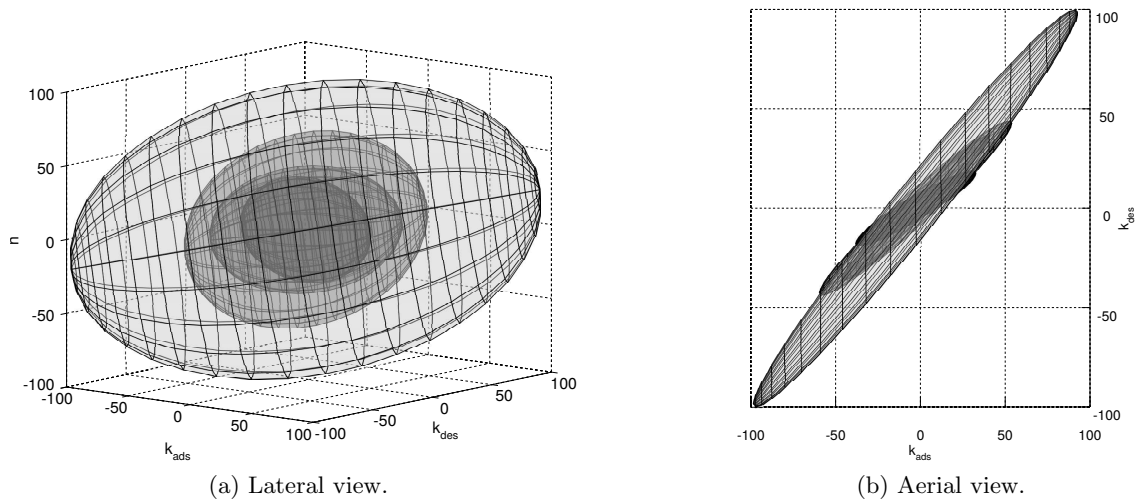


Figure 4.2: Ill-posed model equations lead to a suboptimal shape of the confidence ellipsoid. HIC isotherm parameters n , $k_{ads} = k_{eq}/k_{kin}$ and $k_{des} = k_{kin}^{-1}$ were estimated with the optimum being located skew to the parameter axes which show the remaining size of the confidence interval in percent compared to the first estimation.

Plotting the confidence ellipsoids can be beneficial when assessing the quality of the estimates. To demonstrate this, we performed parameter estimation for the HIC model again, but with the (k_{ads}, k_{des}) formulation instead of (k_{eq}, k_{kin}) . In a previous study for SMA [61], it was shown that deterministic solvers fail when the direction of decent is skew to the parameter axes. For the HIC model parameters k_{ads} , k_{des} , and n , we obtained the ellipsoids plotted in Fig. 4.2 for Exp. 1–3, 1–4, 1–5, and 1–6. While the lateral view shows the relative shrinking of confidence intervals, the aerial view shows a similar result as in [61] for SMA. The deterministic optimizer was not able to move away from the initial estimate and the confidence ellipsoid is long drawn skew to the axes. From the plot it would have been obvious that the ratio k_{ads}/k_{des} must be considered to minimize the volume of the ellipsoid.

Completely different results were obtained for MMC. Unfortunately, some of the confidence intervals became larger after applying OED. This does not necessarily mean, that the actual values are worse only that the fit is not as sensitive anymore to small changes in the parameter values. The three additional runs were all gradient elutions from 0.17 M to 4.02 M, 0.22 M to 1.84 M and 3.5 M to 0.65 M.

The correlation matrix shows three clusters (Fig. 4.3). The GRM parameters of glucose oxidase correlate strongly with each other, the same applies to salt. This could be caused by the high salt concentrations of the first two OED gradients that lead to a significant flow-through peak which do not seem to be sensitive to changes in the GRM parameters. The third cluster spans all isotherm parameters.

While the fit is certainly very good and even shoulders could be simulated, only k_s and ν have acceptable confidence intervals. For comparison, the average error reported in [120] for protein parameters determined from batch isotherms are $k_{eq} > 25\%$, $\nu > 10\%$, $n > 40\%$, $k_p > 40\%$, $k_s > 25\%$, $q_{max} > 15\%$.

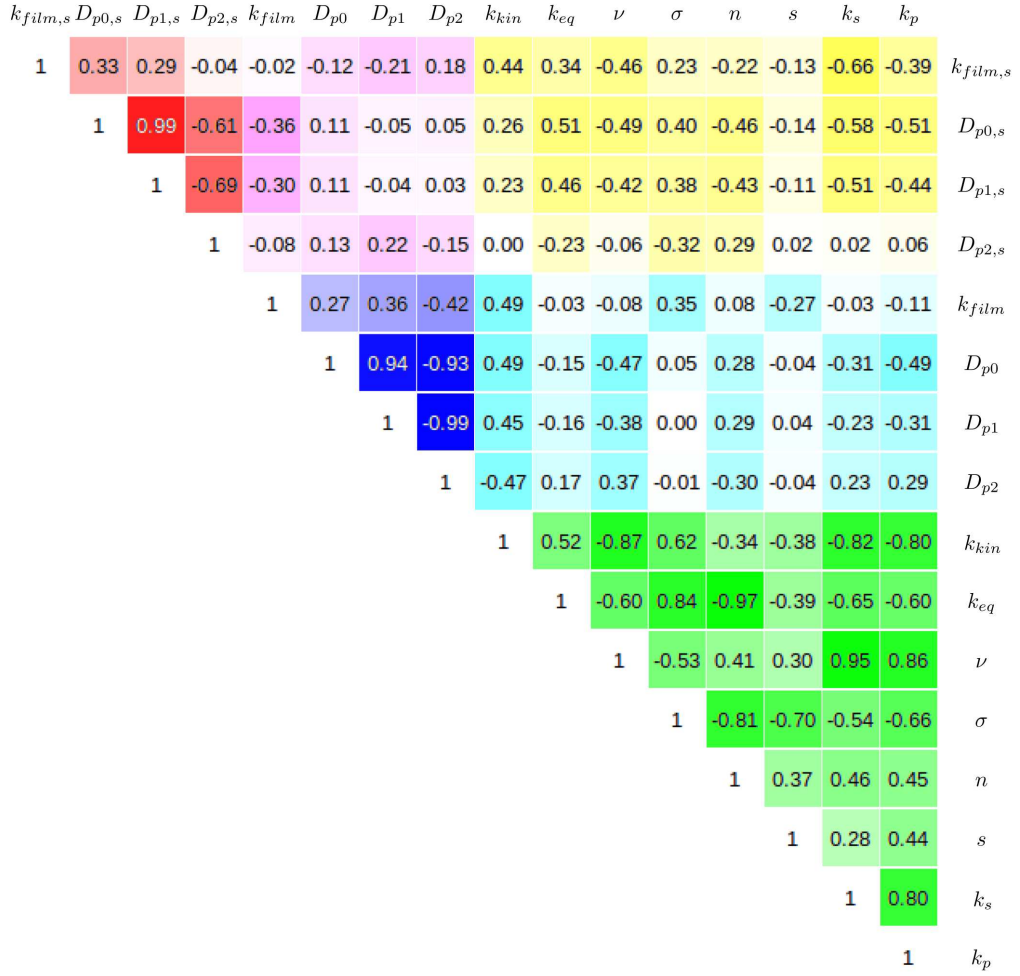


Figure 4.3: Visualization of the correlation matrix of the MMC model parameters after applying OED. The range of correlation coefficients is $[-1, 1]$ with higher absolute values indicating stronger correlations.

4.4.5 Interpretation of Isotherm Parameters

Many SMA parameter sets have been reported in literature, e.g. [60; 72; 126]. The order of magnitude of the parameters found here is reasonable: k_{kin} is small in order to generate a steep elution peak front and $\nu \approx 5$ means that the 160 kDa molecule binds to approximately 5 ligands at once. The k_{eq} values given here are taken with respect to the adsorber skeleton. To interpret the magnitude easier, approximate values per column volume can be calculated. This is achieved via a transformation of the equilibrium isotherm:

$$\begin{aligned}
 q &= k_{eq} (\Lambda - (\nu + \sigma) q)^\nu c_s^{-\nu} c \\
 &= k_{eq} \left(\frac{1 - \varepsilon_t}{1 - \varepsilon_t} \Lambda - (\nu + \sigma) q \right)^\nu c_s^{-\nu} c \\
 &= k_{eq} (1 - \varepsilon_t)^{-\nu} ((1 - \varepsilon_t) \Lambda - (1 - \varepsilon_t) (\nu + \sigma) q)^\nu c_s^{-\nu} c \\
 &=: k_{eq,CV} (\Lambda_{CV} - (\nu + \sigma_{CV}) q)^\nu c_s^{-\nu} c.
 \end{aligned}$$

We obtain a reasonable value of

$$k_{eq,CV} = k_{eq}(1 - \varepsilon_t)^{-\nu} = 0.023$$

that fits to the immediate desorption observed with slightly increased salt concentration. The steric shielding parameter is unfortunately undetermined.

The GRM parameters of the HIC model are the best in terms of certainty. The same applies to the non-linear parameters n and q_{max} . The usually lower capacity of HIC resins seems to be beneficial in this case. However, the high uncertainty in the kinetic parameter combined with the tendency to attain values greater than one indicates that the model is not perfectly formulated.

The confidence and correlation analysis of the MMC model parameters shows that the nonlinear parameters could not be determined under the given constraints. Nevertheless, OED was able to improve the remaining correlations in a way that GRM and isotherm parameters mostly correlate among themselves.

4.5 Conclusions

The resin Capto™ adhere offers the ion-exchange and hydrophobic interaction modes of Capto™ Q and Capto™ phenyl but the employed model protein glucose oxidase shows a very unique binding behavior. Models based on the SMA, Mollerups's HIC, and Nfor's MMC model were calibrated initially by three (IEC and HIC) or six (MMC) chromatograms obtained under manually selected conditions. As none of the models supports a change in pH, only elution by varying of the salt concentration could be applied.

Based on these initial models, new experimental set-ups were designed by minimizing the confidence ellipsoid according to the D-optimality criterion Eq. (4.26). After sequentially conducting the new experiments, the size of the confidence ellipsoid could be reduced. The results underline the potential of OED to reduce time and material consumption compared to DoEs, where additional experiments do not necessarily improve the confidence.

To evaluate the reliability of estimates, approximate confidence intervals were calculated for each estimated parameter after including the measurements of a new experiment. After three OED runs, IEC and HIC parameter estimates became more reliable, MMC still showed strong correlations and uncertainties.

The model parameters were analyzed to gain information on the adsorption of glucose oxidase on Capto™ Q, phenyl and adhere under the investigated experimental conditions. In the literature, only non-negative estimates for the mixed-mode isotherm parameter k_p were reported, when modeling the adsorption between Capto™ adhere and proteins with similar pI and size as glucose oxidase [120]. Here, we obtained highly negative values for both MMC and HIC, indicating that protein-protein interactions dominate over water-protein interactions. This results should be subject of further studies.

Furthermore, peak distortions were observed during HIC and MMC elution. On the one hand, these observations match with descriptions of partial unfolding of proteins during

interaction with hydrophobic ligands in the literature [80; 108]. But this phenomenon is currently not taken into account when modeling HIC and MMC mechanistically. On the other hand, the characteristic HIC parameter n is too small to justify the assumption of unfolding and we could trigger the forming of shoulders by introducing salt-dependent pore diffusion.

In summary, mixed mode chromatography offers a broad operating window under high and low salt conditions. The OED approach was used successfully to improve the reliability of isotherm parameter estimates in two of three cases investigated, IEX and HIC. For MMC it became obvious that an excellent fit does not necessarily imply a well-calibrated model. In future, the OED approach could be used for automated process development while enhancing the reliability and robustness of downstream-processing when implementing the Quality by Design approach. However, expert knowledge is still necessary to define a reasonable parameter space. Otherwise, OED might propose infeasible or unsuitable experiments at the boundaries.

Acknowledgments

The research leading to these results was partly funded by EUROTRANS-BIO (grant agreement no. 0316071B, EC's Seventh Framework Programme).

5 | UV Absorption-based Inverse Modelling of Protein Chromatography

Tobias Hahn¹, Pascal Baumann¹, Thiemo Huuk¹, Vincent Heuveline², Jürgen Hubbuch¹

¹ Karlsruhe Institute of Technology (KIT), Institute of Process Engineering in Life Sciences, Section IV: Biomolecular Separation Engineering, Karlsruhe, Germany

² Heidelberg University, Interdisciplinary Center for Scientific Computing, Engineering Mathematics and Computing Lab, Heidelberg, Germany

Abstract

UV absorbance measurements play an important role in bioprocess development. Yield and purity are often evaluated in terms of peak percentages in analytical size exclusion chromatography or ion-exchange chromatography. Also, industrial chromatography steps are usually controlled based on UV data with pooling decisions according to absorbance thresholds.

Model-based process development would make elaborate screening experiments redundant, once the model has been calibrated to the specific process step. So far, absorbance measurements could not be used directly for modelling chromatography steps as the commonly applied models rely on mass or molar concentration. This study presents mechanistic modelling of an industrially relevant chromatography setting without any knowledge of the feed composition. The model equations were re-written to employ boundary conditions in UV absorbance units, the absorption coefficients were shifted into the isotherm, and standard parameter estimation procedures could be applied. An anion-exchange chromatography case study of a target protein expressed in *Escherichia coli* and eleven lumped impurity peaks demonstrated practical applicability. The target protein concentration in the feed material was estimated from chromatograms. Using this method, initially unknown feed concentrations can be determined a posteriori for ion-exchange and multi-modal chromatography from single-component absorbance curves.

Practical Application

This study explores the feasibility of modelling ion-exchange chromatography without knowledge of feed composition in terms of molar or mass concentration. This is especially valuable in early-stage process development when no information is available on the impurities. It was shown that all model parameters can be determined uniquely from single-component elution curves. Here, the concentration of Cherry-tagged glutathione-S-transferase within a crude feedstock could be determined from chromatograms at a particular wavelength.

5.1 Introduction

Industrial downstream processing (DSP) faces the challenge of efficiently purifying a product out of a very heterogeneous mixture. The purification sequence is commonly based on platform processes that are only slightly adapted to new target components to accelerate process development [100; 145]. Prior to this, high-throughput screening methods are often used to find promising initial conditions for platform processing [17]. Mechanistic modelling is a favorable alternative, provided the model parameters can be determined with less effort, allowing identification of optimal process parameters *in silico*.

The common models in liquid chromatography describe the mass transport in the column by so-called Convection Diffusion Reaction (CDR) equations, where the reaction term models phase transitions and, eventually, the retention of the species. With no a priori knowledge about the components' behavior, the inverse method is a suitable option which alters parameters in a systematic fashion to achieve a match of the recorded chromatogram and the model prediction.

The potential of mathematical modelling and numerical optimization of chromatography has already been demonstrated in academic set-ups for mixtures of small molecules [1; 42], model proteins [127] and antibodies [35; 85], and also for industrial process steps [30; 112]. All applications have in common, that molar concentrations in the feed were known and sensor calibrations existed for all components.

Cornel et al. [32] determined absorption coefficients for a two-component mixture directly from the simulated concentration curves by choosing the best fitting values in each iteration of the estimation procedure. No sensor calibration was necessary, but mass concentrations in the feed were known a priori.

In the following sections, we describe a mechanistic modelling approach for an industrially relevant chromatography setting that does not require prior knowledge of the feed composition in terms of molar or mass concentrations. We re-write the model equation for boundary conditions in UV absorbance units and aim at determining the unknown feed concentrations a posteriori by taking advantage of the particular structure of stoichiometric exchange models. Standard parameter estimation procedures can be applied if single-component absorption curves are available.

A case study based on an anion-exchange chromatographic (AEX) process step (Q Sepharose FF, GE Healthcare) demonstrates the applicability. The mixture fed into AEX is a crude feed stock of *Escherichia Coli SE 1*, including the Cherry-tagged enzyme Glutathione-S-Transferase as the product.

Table 5.1: Measured column parameters.

Parameter	Symbol	Value	Unit	Proceeding
Diameter	d	7	mm	From manufacturer
Length	L	25	mm	From manufacturer
Bead radius	r_p	0.045	mm	From manufacturer
System dead volume	V_d	0.07	ml	Acetone injection without column
Retention volume Acetone	V_{RetAc}	0.96	ml	Acetone peak injection with column
Retention volume dextran	V_{RetDex}	0.34	ml	Dextran peak injection with column
Standard deviation of dextran	σ_{Dex}	0.029	ml	Äkta peak integration
Volume of HCl	V_{HCl}	1.48	ml	Acid/base titration
Molarity of HCl	c_{HCl}	0.01	M	Manually controlled
Flow rate	u	0.2	$\frac{mm}{s}$	Manually controlled

5.2 Materials and Methods

5.2.1 Column Parameter Determination

To model the mass transport in the chromatography system, the column properties listed in Tables 5.1 and 5.2 must be determined by pulse injections of non-interacting tracer molecules [109]. A 1 ml column (effective volume 0.962 ml), with Q Sepharose Fast Flow Resin (GE Healthcare, Freiburg, Germany) was analyzed firstly with an 1 % acetone (Merck, Darmstadt, Germany) pulse and secondly with a dextran pulse from *leuconostoc spp.* MW 2,000,000 (Sigma Aldrich, Steinheim, Germany) using an Äkta Purifier system (GE Healthcare, Little Chalfont, UK) controlled with Unicorn 5.2 (GE Healthcare, Uppsala, Sweden) to determine the essential system parameters [109] presented in Table 5.1. Acid-base titration was carried out to determine the total ionic capacity: the column was flushed with a 0.5 M NaOH solution (Merck, Darmstadt, Germany) until a constant UV and conductivity signal was achieved. Afterwards, the column was washed with ultra pure water until a constant UV and conductivity baseline was reached. Then, the column was titrated at a flow of 0.64 ml/min with a 0.01 M HCl solution (Merck, Darmstadt, Germany) until an increase in the conductivity signal was recorded. From the Cl-ion concentration of the titrant and the volume of the applied titrant, the total number of exchangeable ions was calculated. All chemicals used were obtained in highest quality.

With this set of parameters, all system-specific parameters occurring in the mathematical model can be fixed as given in Table 5.2.

5.2.2 Sample Production

The applied sample consisted of an *Escherichia Coli SE 1* lysate, including Cherry-tagged Glutathione-S-Transferase (GST) as a product. The Cherry-tag, which can be fused to any

Parameter	Symbol	Value	Unit	Proceeding
Volume	V	0.962	ml	$\frac{1}{4} \cdot \pi \cdot d^2 \cdot L$
Fluid volume	V_f	0.89	ml	$V_{RetAc} - V_d$
Interstitial volume	V_{int}	0.27	ml	$V_{RetDex} - V_d$
Total column porosity	ε_t	0.925		$\frac{V_f}{V}$
Interstitial porosity	ε_b	0.28		$\frac{V_{int}}{V}$
Particle porosity	ε_p	0.896		$\frac{V_f - V_{int}}{V - V_{int}}$
Interstitial flow	u_{int}	0.714	$\frac{mm}{s}$	$\frac{u}{\varepsilon_b}$
Axial dispersion	D_{ax}	0.1	$\frac{mm^2}{s}$	$\frac{1}{2} \cdot L \cdot u_{int} \cdot \left(\frac{\sigma_{Dex}}{V_{int}} \right)^2$
Ionic capacity	Λ	0.22	M	$\frac{c_{HCl} \cdot V_{HCl}}{V(1-\varepsilon_b)(1-\varepsilon_p)}$

Table 5.2: Calculated column parameters.

target protein, allows for straightforward product analytics by VIS absorbance measurements [10]. The cultivation was performed for 24 h in 800 ml standard TB (terrific broth) medium at 37 °C and 180 rpm rotational speed in 2.5 l Tunair flasks (Sigma Aldrich). Cell disruption was performed by sonication of the cell pellet in 20 ml of 50 mM Tris buffer (pH 8), including 1X Sigma FAST protease inhibitor (Sigma Aldrich), in a Branson Digital Sonifier (70 % pulse amplitude, 10 X 15 s pulse duration, 30 s resting on ice between pulses). The lysate was centrifuged at 12000 rpm for 60 min at 10 °C using a 5810 R centrifuge (Eppendorf, Germany) followed by a second clarification step using 0.2 µm sterile PES filters (VWR, Germany). Finally, the permeate was 10 times diluted in 50 mM Tris buffer (pH 8).

5.2.3 Sample Characterisation

For comparison, the product concentration was determined in the Caliper LabChip GX II capillary gel electrophoresis system with LabChip GX 3.1 software (Perkin Elmer, Hopkinton, USA). The HT Protein Express and Pico LabChip was run with the HT Protein Express LabChip reagent kit using the HT Protein Express 200 assay. Cherry-tagged GST was identified using the sample ladder from the reagent kit. The product was quantified by peak-baseline integration of the fluorescence signals (Fig. 5.1) and scaling to an external lysozyme protein standard of 1 mg/ml.

5.2.4 Bind-elute Experiments

The component-specific isotherm parameters are determined from bind-elute experiments. The general approach is identical to concentration-based parameter estimation [35; 85; 127]. A 50 mM Tris-HCl buffer, pH 8 was employed as the mobile phase during binding and the same buffer supplemented with 1 M NaCl was used for elution. Different salt gradients were generated from these two buffers. After the 0.5 ml sample was injected (12.4 ml for the breakthrough experiment), the column was washed with low-salt buffer for 3 ml of 50 mM Tris-HCl buffer, before initiating linear gradient (0 to 1 M NaCl) elution over 5, 10, 15 and 20 ml. On gradient completion the columns were irrigated with 2 ml of 50 mM Tris-HCl + 1 M NaCl before re-equilibrating with 5 ml of 50 mM Tris-HCl buffer. The linear phase linear velocity employed was 0.2 mm/s throughout.

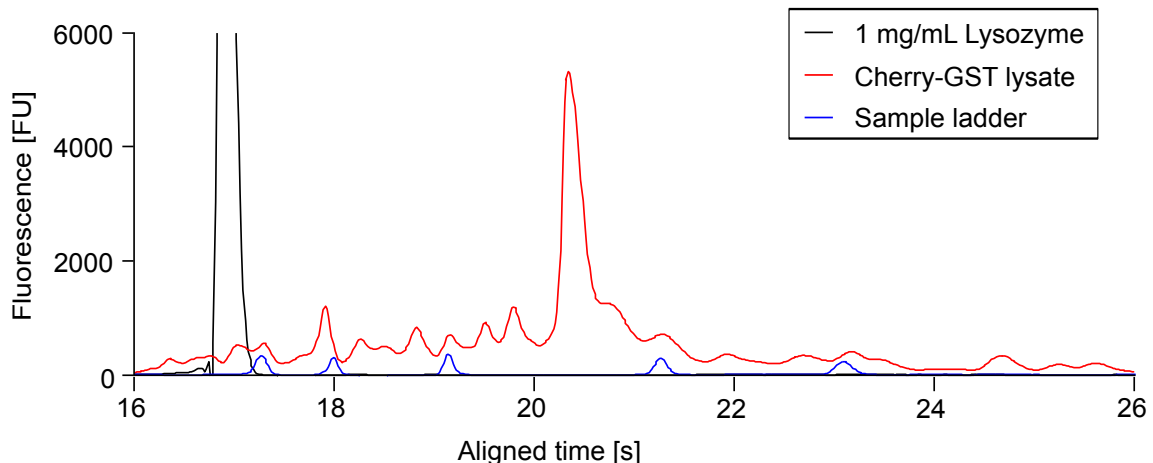


Figure 5.1: Capillary gel electrophoresis analysis of feed material.

5.2.5 Parameter Estimation

In general, estimation of an unknown parameter set \bar{p} solves the least squares optimization problem

$$\min_{\bar{p}} \sum_j \left(m(t_j) - \sum_{i \geq 1} c_i(L, t_j; \bar{p}) \cdot a_i \right)^2, \quad (5.1)$$

where $m(t_j)$ is the measured chromatogram value at time t_j , typically given in milli absorbance units [mAU]. This measurement might also contain noise, which can be neglected when assuming the noise to be zero-mean Gaussian and isotropic.

$c_i(L, t)$ is the simulated mass or molar concentrations at the outlet of the column with length L . The transformation into absorbance units is performed with a scaling factor a_i . According to Beer's law, the absorption coefficient a_i consists of an extinction coefficient and UV cell path length. It is unknown in this case.

5.2.6 Chromatography Model

The Transport Dispersive Model (TDM) [109] in Eqs. (5.2) and (5.3) is used to model the macroscopic protein transport through the column. For simplicity, the component-specific internal and external diffusion effects are lumped in an effective mass transfer coefficient.

The system is of Convection Diffusion Reaction (CDR) type. Eq. (5.2) describes the rate of change of the concentration $c_i(x, t)$ of component i in the interstitial volume of a column with length L , which consists of convective mass transport in space with the average interstitial velocity of the fluid u . Peak broadening effects are modelled as dispersion in axial direction with respect to a coefficient D_{ax} . The exchange between the interstitial concentration and the particle pore concentration $c_{p,i}(x, t)$ depends on the porosity of the bed ε_b , the radius of adsorber particles r_p , and a component-specific effective mass transfer coefficient $k_{eff,i}$. The model is one-dimensional in space, such that the concentrations

depend on the axial position in the column and time. Equation (5.3) models the accumulation of mass in the pore volume $c_{p,i}$ and stationary phase q_i as a function of the particle porosity ε_p . The model is complemented by Danckwerts boundary conditions Eqs. (5.4), (5.5), including the applied inlet concentration $c_{in,i}$, and an isotherm equation modelling the stationary phase concentration q_i .

$$\frac{\partial c_i}{\partial t} = -u(t) \frac{\partial c_i}{\partial x} + D_{ax} \frac{\partial^2 c_i}{\partial x^2} - \frac{1 - \varepsilon_b}{\varepsilon_b} k_{eff,i} \frac{3}{r_p} (c_i - c_{p,i}) \quad (5.2)$$

$$\frac{\partial c_{p,i}}{\partial t} = -\frac{1 - \varepsilon_p}{\varepsilon_p} \frac{\partial q_i}{\partial t} + k_{eff,i} \frac{3}{\varepsilon_p r_p} (c_i - c_{p,i}) \quad (5.3)$$

$$\frac{\partial c_i}{\partial x} (0, t) = \frac{u(t)}{D_{ax}} (c_i(0, t) - c_{in,i}(t)) \quad (5.4)$$

$$\frac{\partial c_i}{\partial x} (L, t) = 0 \quad (5.5)$$

The steric mass action isotherm (SMA) [23] is a commonly used semi-mechanistic isotherm in ion-exchange chromatography. It is capable of reproducing the influence of counter ions on the retention behavior of protein species using the proteins' characteristic charges ν_i . In addition, it considers adsorber properties such as the total ionic capacity Λ and steric shielding effects σ_i of the protein covering an amount of binding sites, greater than the actual number of sites it interacts with. The kinetic SMA isotherm is given in Eq. (5.6) for k proteins, with q_i and $c_{p,i}$ being the concentration of the protein $i \in \{1, \dots, k\}$ adsorbed and in solution, respectively. $c_{p,salt}$ is the salt concentration of the solution. $k_{ads,i}$ and $k_{des,i}$ are the constants of the adsorption and desorption rate.

$$\frac{\partial q_i}{\partial t} = k_{ads,i} \left(\Lambda - \sum_{j=1}^k (\nu_j + \sigma_j) q_j \right)^{\nu_i} c_{p,i} - k_{des,i} c_{p,salt}^{\nu_i} q_i \quad (5.6)$$

$$q_{salt} = \Lambda - \sum_{j=1}^k \nu_j q_j \quad (5.7)$$

The model is chosen because of its capability of simulating the whole chromatographic process, including elution, by changing the induced salt concentration at the inlet. The model is based on molar concentrations, such that the boundary conditions of the TDM must be set in terms of molarities.

5.2.7 Transformation

As the SMA model is based on molar concentrations [M], interstitial and pore volume concentrations must be given in [M] as well. This also applies to the boundary conditions. Here, the exact molar concentrations in the feed are unknown, as are the scaling factors for UV absorbance. We will re-write the equations to directly incorporate UV absorbance values.

First, the injected protein concentrations are transformed into absorbance values:

$$c'_{in}[mAU] = a [mAU/M] \cdot c_{in}[M]. \quad (5.8)$$

These can be determined later from the respective peak area in the chromatogram.

The equations for the interstitial and pore volume as well as the boundary conditions are linear in c . These can be multiplied by a to obtain

$$a_i \frac{\partial c_i}{\partial t} = a_i \left[-u \frac{\partial c_i}{\partial x} + D_{ax} \frac{\partial^2 c_i}{\partial x^2} - \frac{1 - \varepsilon_c}{\varepsilon_c} k_f (c_i - c_{p,i}) \right] \quad (5.9)$$

$$\iff \frac{\partial c'_i}{\partial t} = -u \frac{\partial c'_i}{\partial x} + D_{ax} \frac{\partial^2 c'_i}{\partial x^2} - \frac{1 - \varepsilon_c}{\varepsilon_c} k_f (c'_i - c'_{p,i}) \quad (5.10)$$

$$\frac{\partial c'_i}{\partial x}(0, t) = \frac{u}{D_{ax}} (c'_i(0, t) - c'_{in,i}(t)) \quad (5.11)$$

$$\frac{\partial c'_i}{\partial x}(L, t) = 0 \quad (5.12)$$

We obtain equations for $c'_i = a_i \cdot c_i$ that use $c'_{p,i} = a_i \cdot c_{p,i}$. This is calculated from the scaled lumped rate model

$$\varepsilon_p \frac{\partial c'_{p,i}}{\partial t} + (1 - \varepsilon_p) \frac{\partial q'_i}{\partial t} = k_{eff,i} \frac{3}{r_p} (c'_i - c'_{p,i}). \quad (5.13)$$

Again, we require an equation for $q'_i = a_i \cdot q_i$. Scaling the kinetic SMA formulation yields

$$a_i \frac{\partial q_i}{\partial t} = a_i \left[k_{ads,i} \left(\Lambda - \sum_{j=1}^k (\nu_j + \sigma_j) q_j \right)^{\nu_i} c_{p,i} - k_{des,i} c_s^{\nu_i} q_i \right] \quad (5.14)$$

$$\iff \frac{\partial q'_i}{\partial t} = k_{ads,i} \left(\Lambda - \sum_{j=1}^k (\nu_j + \sigma_j) q_j \right)^{\nu_i} c'_{p,i} - k_{des,i} c_s^{\nu_i} q'_i \quad (5.15)$$

$$\iff \frac{\partial q'_i}{\partial t} = k_{ads,i} \left(\Lambda - \sum_{j=1}^k (\nu_j + \sigma_j) \frac{a_j}{a_j} q_j \right)^{\nu_i} c'_{p,i} - k_{des,i} c_s^{\nu_i} q'_i \quad (5.16)$$

$$\iff \frac{\partial q'_i}{\partial t} = k_{ads,i} \left(\Lambda - \sum_{j=1}^k \frac{\nu_j + \sigma_j}{a_j} q'_j \right)^{\nu_i} c'_{p,i} - k_{des,i} c_s^{\nu_i} q'_i. \quad (5.17)$$

Here, we multiplied by $\frac{a_j}{a_j}$ in step (5.15)→(5.16) to transform the remaining q into q' . Essentially, we shifted the unknown scaling factor from the least-squares problem (5.1) into the isotherm.

We are left with Eq. (5.7), which can be altered to include q' as above:

$$q_{salt} = \Lambda - \sum_{j=1}^k \nu_j q_j \quad (5.18)$$

$$= \Lambda - \sum_{j=1}^k \nu_j \frac{a_j}{a_j} q_j \quad (5.19)$$

$$= \Lambda - \sum_{j=1}^k \frac{\nu_j}{a_j} q'_j. \quad (5.20)$$

The transformation procedure is also applicable to other isotherms with stoichiometric exchange, e.g. the mixed-mode isotherm in [120].

Binding models of Langmuir type and isotherms without an additional equation for counterions, e.g. for hydrophobic interaction chromatography (HIC) [112], can be treated as above, but due to the missing second equation, a will remain hidden within other constants. In case of the kinetic Langmuir isotherm, we obtain

$$\frac{\partial q_i}{\partial t} = k_{ads,i} q_{max,i} \left(1 - \sum_{j=1}^k \frac{q_j}{q_{max,j}} \right) c_{p,i} - k_{des,i} q_i \quad (5.21)$$

$$\Leftrightarrow \frac{\partial q'_i}{\partial t} = k'_{ads,i} q'_{max,i} \left(1 - \sum_{j=1}^k \frac{q'_j}{q'_{max,j}} \right) c'_{p,i} - k_{des,i} q'_i, \quad (5.22)$$

with $k'_{ads,i} = k_{ads,i}/a_i$ and $q'_{max,i} = q_{max,i} \cdot a_i$. These parameters can be used for UV-based modelling but not for determining absorption coefficients and molar concentrations.

Other convection-diffusion models, such as the general rate model [109] or models of radial flow chromatography [50], are also linear in the concentration variables and can be treated as the TDM above.

5.2.8 Uniqueness

In this section, it is shown that the transformation does not affect the parameter determination.

The linear range of the isotherm is uninfluenced by the transformation. For $\Lambda \gg \sum_{j=1}^k \frac{\nu_j + \sigma_j}{a_j} q'_j$, we obtain

$$\frac{\partial q'_i}{\partial t} \approx k_{ads,i} \Lambda^{\nu_i} c'_{p,i} - k_{des,i} c_s^{\nu_i} q'_i. \quad (5.23)$$

Consequently, all methods to determine the linear SMA parameters k_{ads} , k_{des} , and ν can be employed here. It has been shown that the characteristic charge ν and equilibrium coefficient, defined as $k_{eq} = \frac{k_{ads}}{k_{des}}$, determine the retention time in gradient elution [143]. At least two gradients with different lengths and/or slopes are necessary to uniquely determine the two values. The kinetic parameter k_{des} can be identified from the peak shape [85]. This method is also applicable to multi-component settings, as no protein-protein interactions are assumed to happen in the linear range.

The non-linear parameter σ is typically determined by a frontal experiment or from batch isotherms. Both methods rely on determining the saturation capacity $q_{max} = \frac{\Lambda}{\nu + \sigma}$ and calculating

$$\sigma = \frac{\Lambda}{q_{max}} - \nu. \quad (5.24)$$

If the [mAU] equivalent q'_{max} was determined, the equation becomes

$$\sigma = \frac{\Lambda \cdot a}{q'_{max}} - \nu. \quad (5.25)$$

With known ν and a , σ can be uniquely determined. Alternatively, the steric factor can be identified from the peak shape in non-linear chromatography [44], again with known ν and a . This method allows for including additional steric shielding effects in multi-component settings.

To determine a , one of the original methods for identifying the characteristic charge can be used. It relied on measuring the increase in conductivity caused by freed counter-ions [23]. In the UV-based case, the amount of freed counter-ions can be determined from the second isotherm equation (5.20):

$$\int_0^L \sum_{j=1}^k \frac{\nu_j}{a_j} q'_j dx. \quad (5.26)$$

If ν has been determined, e.g. from gradient elutions as above, a can be identified uniquely from the increase in conductivity in single-component adsorption. In non-linear multi-component settings, the increase of conductivity will be visible in the chromatogram. The a -dependent locally varying counter-ion concentration in the pores due to adsorbing proteins will lead to a different adsorption behaviour.

Summarizing, every parameter plays a distinct role and can be determined from single-component absorbance curves. If only the chromatogram is available in multi-component settings, the parameters might be correlated.

5.2.9 Numerical Solution

The numerical simulation is performed using the in-house software package ChromX [84]. Following the method of lines, the equation system is first discretized in space using the Finite Element Method (FEM). A Streamline-Upwind-Petrov-Galerkin (SUPG) ansatz was used here with linear basis and test functions. The discretisation in time is performed with the fractional step θ -scheme, a semi-implicit procedure providing second-order accuracy [47]. Finally, the non-linearity of the equation system introduced by the isotherm must be treated with an iterative procedure, here, Picard iteration. The resulting linear systems are solved by LU factorization.

A variety of algorithms is available for the solution of the optimisation problem in Eq. (5.1). We employed a heuristic method, the genetic algorithm implementation GALib [161], and a deterministic Levenberg-Marquardt implementation CMinpack [37]. Genetic algorithms prevent local minimums by performing random jumps and, hence, explore a larger area of the search space. The result of the genetic algorithm is then refined with the deterministic algorithm. To support this, we divide the kinetic isotherm by k_{des} and use the formulation with equilibrium coefficient k_{eq} . Working with k_{ads} would require to always change k_{des} at the same time to keep the retention time constant. This is unsuitable for the deterministic algorithm that only uses first derivatives [61].

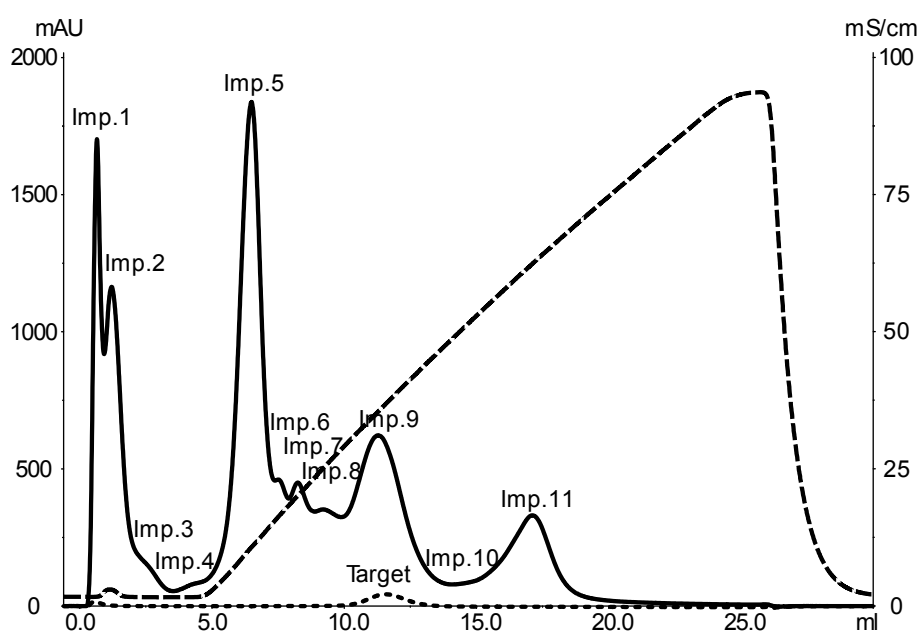


Figure 5.2: Result of the 20 ml gradient elution: UV 280 nm (solid line), UV 536 nm (dotted line) and conductivity (dashed line). 11 impurities were identified with peak maxima at 0.65 ml (imp. 1), 1.21 ml (imp. 2), 1.96 ml (imp. 3), 5 ml (imp. 4), 6.5 ml (imp. 5), 7.5 ml (imp. 6), 8.23 ml (imp. 7), 9.21 ml (imp. 8), 11.28 ml (imp. 9), 15.52 ml (imp. 10), 17.11 ml (imp. 11). The target component is clearly visible in the 536 nm signal, with the peak maximum at 11.54 ml.

5.3 Results and Discussion

5.3.1 Bind-elute Experiments

Five experiments in bind/elution mode were performed. Figure 5.2 shows the result obtained with a 20 ml gradient. Several impurity peaks could be resolved. The first one is a breakthrough at 0.65 ml. The second peak occurs slightly later at 1.21 ml, followed by two shoulders (impurities 3 and 4) and a high peak at 6.50 ml. The signal continues with three lower peaks (imp. 6, 7, 8), followed by a larger one at 11.28 ml that is also visible at 536 nm. It is identified to be the target component. The fact that this peak's maximum is reached 0.26 ml earlier at 280 nm leads to the assumption that a impurity (imp. 9) is eluting slightly before. A small shoulder (imp. 10) and a final peak at 17.1 ml (imp. 11) complete the elution profile.

5.3.2 Protein Parameter Estimation

The components' peak areas were determined with Unicorn peak integration from the 280 nm signal of the 20 ml gradient chromatogram. The resulting areas in mAU·ml were divided by the sample volume of 0.5 ml to obtain the inlet absorbance values for modelling c'_{in} in mAU. Hence, the estimated absorption coefficients a refer to 280 nm. The same bounds of integration were used for the 300 nm signal. No additional simulation was necessary, the simulated 280 nm peaks were scaled according to the ratio of 300 nm and

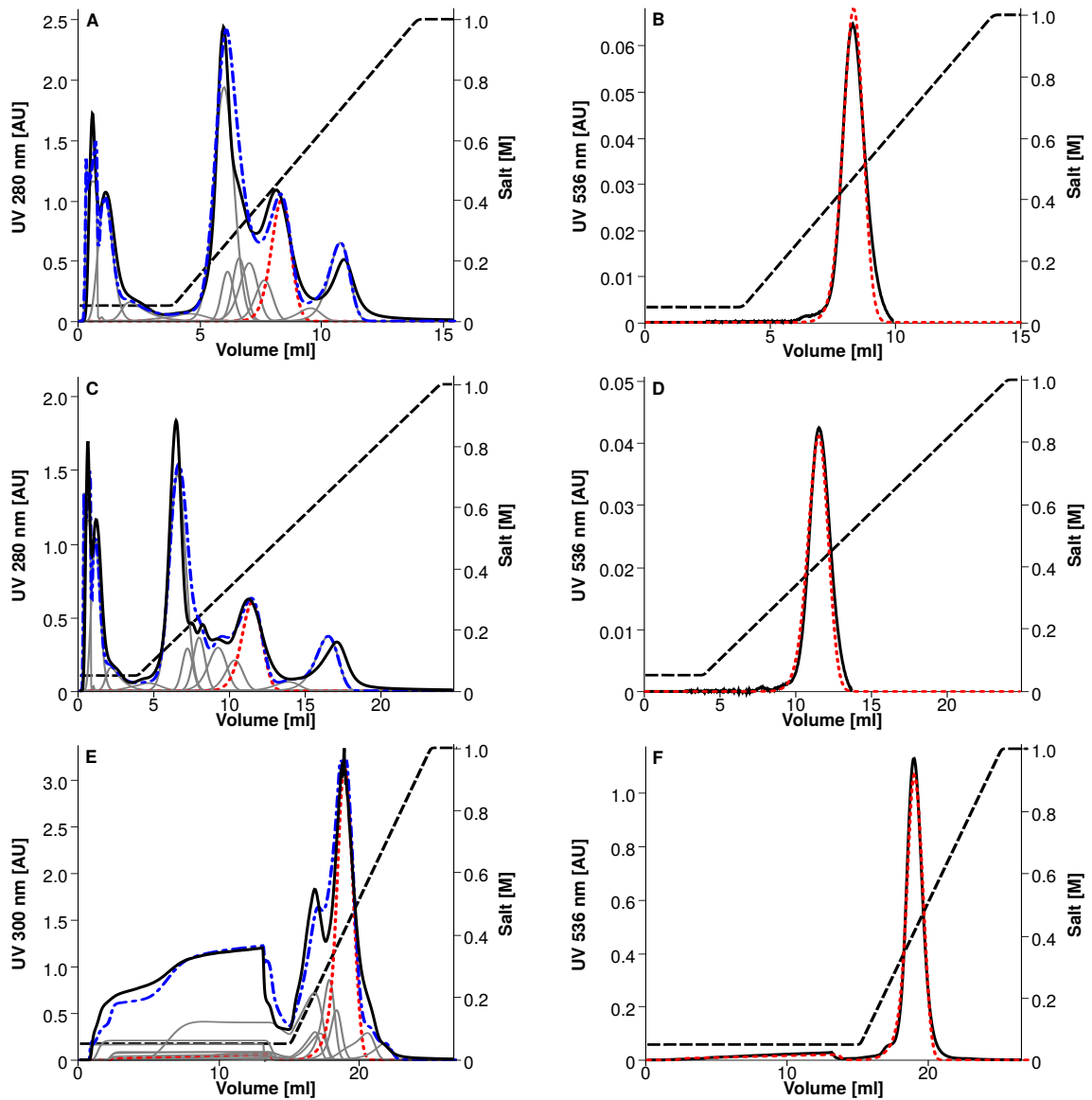


Figure 5.3: Comparison of measured and simulated chromatograms with UV signals (solid lines), conductivity measurement (dashed lines), simulated Cherry-GST absorbance (dotted lines), impurity traces (light solid lines), and sum of simulated proteins (dot-dashed lines). Plots A and B show the 10 ml gradient elution, C and D the 20 ml gradient elution, and E and F the breakthrough experiment.

Table 5.3: Estimated component-specific model parameters.

Component	$k_{eff}/10^{-3}$	k_{des}^{-1}	k_{eq}	ν	σ	$a/10^8$
Impurity 1	0.010	-	-	-	-	-
Impurity 2	2.090	1	0.004	0.066	157.1	0.600
Impurity 3	5.006	0	3.939	1.293	102.5	0.056
Impurity 4	5.586	0.050	22.46	0.566	6.325	0.130
Impurity 5	15.00	0.151	32.36	0.866	1.895	41.37
Impurity 6	13.00	0	21.54	1.890	0.001	0.150
Impurity 7	12.08	0	32.22	1.930	1.702	13.24
Impurity 8	7.077	0.066	75.83	4.135	0	1.967
Impurity 9	7.100	0.070	175.8	4.289	0.022	42.91
Cherry-tagged GST	9.271	0.208	334.0	4.000	0.035	0.865
Impurity 10	14.98	0.424	3084.3	5.350	2.241	2.396
Impurity 11	7.131	0.235	152227	7.968	0.025	30.00

280 nm peak areas. The 300 nm signal was used for modeling the breakthrough experiment. Here, the 280 nm signal was incomplete due to sensor saturation.

As the genetic algorithm performs random jumps, admissible parameter ranges have to be set. First estimates of ν and k_{eq} were obtained from the correlation of retention times in gradient elution as in [145] for all binding species. The resulting large equilibrium parameter values in the order of 10^6 fit well to the observed retention. k_{des} has to reside in the natural range $k_{des}^{-1} \in [0, 1]$ and the upper limit for k_{eff} is given by $3 \cdot k_{eff}/r_p = 1$. The steric factor was assumed to be in a range of $\sigma \in [0, 200]$ as it scales approximately with the molecular weight [86] and we expect HCPs of 100 kDa and above. The range of absorption coefficients was chosen large, $a \in [10^5, 10^{10}]$. Eventually, the curve fitting was refined using the Levenberg-Marquardt algorithm.

Selected results are presented in Figure 5.3. The left column shows the simulated components, their sum, and the chromatograms at 280 nm for the 10 and 20 ml gradient as well as the 300 nm chromatogram of the breakthrough experiment. The right column shows the same curves at 536 nm. The 15 ml gradient result looks very similar. In the 5 ml gradient chromatogram, highly overlapping impurities lead to only three distinct peaks (data not shown). The corresponding model parameters are given in Table 5.3. As the first peak is not retained, isotherm parameters could not be determined. The second and third impurity are only slightly retained and the correlation from [145] cannot be used. Furthermore, there might be other parameter combinations of k_{eq} and ν that lead to the same retention volume, and combinations of σ and a with the same amount of occupied ligands. Certainty can be increased by using different low-salt buffer concentrations or including samples with different impurity ratios. But parameter determination for components in the flow-through is not in the focus of this study. The other linear parameters lead to good agreement of simulation and measurement in the first and second row of Fig. 5.3. As the species do not interact, the four linear parameters can be determined well from the four gradient experiments. The experiment with 12.4 ml sample volume shows good agreement as well, in particular in UV 536 nm. Thanks to this visibility of Cherry-tagged GST in UV 536 nm, a single-component adsorption curve is available that allows for an accurate estimation of the absorption coefficient.

5.3.3 Capillary Gel Electrophoresis

The target protein can be identified easily in the capillary gel electrophoresis result because of its high fluorescence value. The determined concentration was $3.73 \cdot 10^5$ M, resulting in an absorption coefficient of $7.86 \cdot 10^7$ mAU/M at 280 nm. This is smaller than the estimated value by approximately 9%. The estimate of a is very good, considering the number of interacting species.

Although capillary gel electrophoresis identified even more species, the lumped peaks found by Unicorn peak integration were sufficient to model the elution behavior of the protein components at all investigated wavelengths.

5.4 Concluding Remarks

This study demonstrates that mechanistic modelling can be applied to an anion-exchange step of a crude feed stock, even if the molar concentrations of the feed components are unknown. The model equations were re-written to define injection with respect to the peak areas determined from chromatograms at a chosen wavelengths. The unknown absorption coefficients that scale molar concentration to absorbance units then occur in the isotherm equation. The counter-ion balance of stoichiometric exchange models can be used for estimating these factors using the inverse method. For the steric mass action model, it was shown theoretically that this additional parameter can be uniquely determined in single-component settings.

In a multi-component case study, the molar concentration of the target protein, Cherry-tagged GST, estimated by chromatogram fitting was only 9 % less than the value measured by capillary gel electrophoresis. Here, a single-component absorbance curve was available through the absorbance of the Cherry-tag in UV 536 nm. For the other components, a correlation of the steric shielding factor and the absorption coefficient persists. Only the total counter-ion concentration on the adsorber surface is measurable, but not the exact amounts displaced per-component.

Additional reliability can be achieved by including samples with different impurity proportions or fraction analyses that only need to provide peak percentages in one of the observed wavelengths. In preparative chromatography process development, these fraction analyses are performed on a regular basis, e.g. with size-exclusion chromatography [85] or ion-exchange HPLC [30], such that no additional experiments are required.

Acknowledgment

The research leading to these results was partly funded by EUROTRANS-BIO (grant agreement no. 0316071B, EC's Seventh Framework Programme). The authors also acknowledge the support by DelphiGenetics (Belgium).

The authors have declared no conflicts of interest.

6 | Deconvolution of High-throughput Multi-component Isotherms Using Multivariate Data Analysis of Protein Spectra

Pascal Baumann^{1,*}, Tobias Hahn^{1,*}, Thiemo Huuk^{1,*}, Anna Osberghaus¹, Jürgen Hubbuch¹

¹ Karlsruhe Institute of Technology (KIT), Institute of Process Engineering in Life Sciences, Section IV: Biomolecular Separation Engineering, Karlsruhe, Germany

* Contributed equally to this work

Abstract

Gaining a more profound understanding of biopharmaceutical downstream processes is a key demand of the Quality by Design (QbD) guideline. One of the most dominant approaches to gain process understanding is the extensive use of experimental high-throughput formats, such as batch chromatography on robotic liquid handling stations. Using these high-throughput experimental formats, the generation of numerous samples poses an enormous problem to subsequent analytical techniques.

Here, a high-throughput case study for batch chromatographic multi-component isotherms is presented. To debottleneck the subsequent analytics, a non-invasive technique using UV spectra and multivariate statistics was adapted to a batch chromatographic format. Using this approach, it was possible to integrate the entire analytical setup into the robotic work flow.

As a case study, batch isotherms for SP Sepharose FF and the model proteins cytochrome c and lysozyme at various pH values and ionic strengths were recorded. A successful examination of the quality of the analytical procedure compared to classical single wavelength photometry was carried out. To address the growing demand for a more profound process understanding, the experimental data were fitted to the steric mass action isotherm, getting a more detailed insight into the competitive binding behavior at various pH values and ionic strengths.

Practical application

This case study explores the usability of UV spectra and multivariate statistics to prevent an analytical bottleneck in high-throughput batch chromatography, incorporating multiple protein species. The presented approach enables integration of the analytical setup in the batch chromatographic work flow, using a standard UV/VIS spectrophotometer. The quality of the analytical data was sufficient to fit steric mass action isotherms at various pH values and ionic strengths and get a mechanistic insight into the competitive binding behavior.

6.1 Introduction

Nowadays, biopharmaceutical downstream process (DSP) development is mainly based on chromatographic separation techniques. Chromatography, as many other separation techniques for biopharmaceuticals, is influenced by numerous operational parameters that affect process performance. The growing need for a deeper mechanistic understanding of the technical process on a molecular level and the impact of the process on the product quality, demanded by the Quality by Design (QbD) approach, pose a great challenge to biopharmaceutical DSP [27; 74]. The requested process understanding can be generated by several approaches. One very obvious approach is the systematic experimental evaluation of the impact of different operational parameters on the downstream process performance.

A possibility to support the exploration of the design space, as basis for many statistical DoE approaches, is the use of high-throughput techniques [88]. These approaches enable miniaturization of the experimental systems and parallelization and automation of the experimental work flow allowing for full factorial experimental designs [13; 123; 167]. Therefore, high-throughput techniques enable a reduction of time and material consumption. In the context of chromatographic process development, there are several experimental systems adapted to robotic high-throughput experiments.

Batch chromatography can be implemented very easily on a liquid handling station using a defined adsorber volume provided in a 96-well plate. The batch chromatographic systems can be used for resin screening [88], batch bind-elute studies or the measurement of adsorption isotherms [30; 88; 120; 121] and kinetic data [31].

One major disadvantage of these experimental high-throughput formats is that the above-mentioned experimental bottleneck is not prevented but often only shifted to subsequent analytics. In the simplest case, when only single protein data have to be recorded, a photometric measurement within the robotic work flow is possible. This simple analytical approach is restricted to the quantification of a single protein species or several protein species with different exclusive absorption maxima beside 280 nm [10]. The major advantage of photometric assays is the high sample throughput, which can easily cope with the amount of samples generated in robotic high-throughput experiments and the non-invasive nature of the technique.

In pharmaceutical high-throughput process development, a simple photometric measurement will be unable to differentiate between several protein species. In this case, more

sophisticated analytics have to be performed. Such advanced analytics might be e.g., analytical high-performance liquid chromatography (HPLC) and product-specific immunoassays [104; 157]. The time requirement of these immunoassays is still high in comparison to that of the chromatographic experiments. HPLC assays are predominant in the characterization of the size and charge heterogeneity of a target protein. One major drawback of processing high-throughput experimental samples with HPLC assays is the low sample throughput of HPLC techniques. Despite the mentioned drawbacks, HPLC and other analytical techniques such as immunoassays bear the major disadvantage of an invasive nature.

An ideal analytical technique in the context of high-throughput experimental work flows would be a photometric assay that can be carried out in standard UV/VIS plate readers typically installed on robotic workstations. This assay has to be protein species-specific and quantitative. Such an assay, based on the measurement of UV spectra and subsequent multivariate statistics, was introduced by Hansen *et al.* in 2011 [63]. When using protein mid-UV (200 – 300 nm) spectra, the absorption of different protein species is strongly influenced by properties of peptide bonds and amino acid residues. A partial least squares - projection to latent structures (PLS) regression enables subsequent quantitative evaluation of mixtures of different protein species.

Here, we present a case study on the high-throughput generation of multi-component isotherm data. We combine a high-throughput method for the collection of multi-component isotherms in an automated batch format with a non-invasive protein-specific quantification method based on the measurement of mid-UV spectra. The collected data are subsequently fitted using the steric mass action isotherm including competitive protein binding introduced by Brooks and Cramer [23].

6.2 Materials and Methods

6.2.1 Materials

6.2.1.1 Disposables & Reaction Vessels

As a strong cation exchange adsorber, sulfopropyl (SP) sepharose fast flow (FF) provided by GE Healthcare Life Sciences, Sweden, was used. Binding experiments were carried out in 2 mL 96-well square deep well plates (VWR, Germany). Absorption and protein spectra measurements were carried out in 96-well flat bottom UV-Star microplates (Greiner Bio-One, Germany). Buffers were filtered using 0.2 μm cellulose acetate filters supplied by Sartorius, Germany.

6.2.1.2 Chemicals & Buffers

Binding experiments at pH 5 were carried out in 20 mM acetate buffer consisting of acetic acid (Merck, Germany) and sodium acetate (Sigma-Aldrich, USA). For experiments at pH 7, a 20 mM phosphate buffer consisting of di-sodium hydrogen phosphate and sodium

di-hydrogen phosphate (Sigma-Aldrich, USA) was used. The ionic strength of the applied buffers was adjusted to 42, 65, 90, 115, and 150 mM using sodium chloride (AppliChem, Germany). The model proteins lysozyme from chicken egg white and cytochrome c from equine heart were purchased from Sigma-Aldrich, USA. Calibrations for the multivariate data analysis model of the two-component system were carried out using a 2.4 mg/mL protein solution. For binding experiments, a 10 mg/mL stock solution with 70 % cytochrome c and 30 % lysozyme was used.

6.2.1.3 Instrumentation & Software

For pH adjustment of all buffers, a HI-3220 pH meter (Hanna Instruments, USA) was used. The instrument was calibrated using high-precision standards from Hanna Instruments (USA). For generation of equal amounts of adsorber per well, a Media Scout Resi Quot System (Atoll, Germany) was applied. For pressure adjustment, a vacuum pump with pressure regulation was used. For the batch isotherms, a Freedom EVO® 200 liquid handling station (Tecan, Germany) was used, operated with EvoWare 2.1. The system is equipped with eight fixed tips, a plate-moving arm and an orbital shaker (Tecan, Germany). A Rotanta 46RSC centrifuge (Hettich, Germany) and an Infinite M200 UV plate spectrophotometer (Tecan, Germany) are integrated in the system. The spectrometer was controlled by i-control 1.9 (Tecan, Germany). Data processing and creation of figures was performed in Matlab R2011a (MathWorks, USA).

6.2.2 Experimental Setup

6.2.2.1 Model Calibration and Validation

The multivariate data analysis calibration [63] was based on a four-level D-optimal onion design generated with MODDE (Umetrics, Sweden) with additional data points added at low concentration levels. The model included 7 mixing ratios (1:0; 2.5:1; 2:1; 1:1; 1:2; 1:2.5; 0:1) and 15 concentration levels (concentration levels correspond to the protein concentration of cytochrome c and lysozyme in total) from 0 to 1.2 g/L (each 5 concentrations in a range of 0 to 0.1, 0.1 to 0.5, and 0.5 to 1.2 g/L). For example, a mixing ratio of 2:1 means that the mixture contains 2/3 of cytochrome c and 1/3 of lysozyme. For a total concentration level of 1.2 mg/mL at a mixing ratio of 2:1, the solution contains 0.8 mg/mL cytochrome c and 0.4 mg/mL lysozyme. In total, 32 samples were used for model calibration.

8 samples were added as a test set for model validation. The cytochrome c and lysozyme stock solutions were pipetted in the desired mixing ratios and diluted with the respective buffers on the liquid handling station. All 40 samples were prepared as 1.8 mL solutions in 96 deep-well plates to avoid small pipetted volumes. 300 μ L of each sample were transferred to 96-well flat bottom UV-Star microplates. Sample absorption spectra were measured in a range of 240 – 300 nm in 2 nm steps. The spectral data of the 32 samples mentioned above were used for model calibration in Matlab R2011a, using the PLS toolbox (Eigenvector Research, USA). 5 samples out of 32 were used as an internal cross validation. The regression model was then validated on the external test set of additional 8 samples and used for the concentration determination of unknown samples.

6.2.2.2 Generation of Equal Adsorber Volumina

Generation of equal 20.8 μL adsorber amounts was achieved using the Media Scout Resi Quot system (Atoll, Germany) described by Herrmann et al. [67]. The system was equipped with a pressure-controlled vacuum pump and the working pressure was set to 800 mbar. To remove the adsorber storage solution, the adsorber plaques were washed twice with deionized water and the applied binding buffer of the respective experiment. The equilibrated plaques were transferred into a 2 mL 96-well square deep well plate and suspended in 100 μL binding buffer. The plate was then stored until use on the liquid handling station. The outer wells were not used for isotherm experiments due to the largest variance in adsorber volume on the plate [124].

6.2.2.3 Isotherm Experiments

Isotherms covering 10 different starting concentrations c_{in} were generated on the liquid handling station. As only the inner 60 wells were used for the experiments, 6 isotherms could be created per sample plate. Each adsorber plate was used for one pH level including 5 different salt level isotherms (42, 65, 90, 115, and 150 mM) and one isotherm as duplicate for investigating the repeatability of isotherm data.

The investigated pH levels were pH 5 and 7. 10 mg/mL stock solutions of 70 % cytochrome c and 30 % lysozyme in the respective buffers were applied. The starting concentrations c_{in} of the isotherm experiments were set to 2, 2.5, 3, 3.5, 4, 4.5, 5, 6, 7, and 8 mg/mL with a final volume of 800 μl per well (including 100 μL adsorber storage buffer from plaque generation). The adsorber plate was closed with a lid by the robotic plate-moving arm and placed in the orbital shaker for 2 h. Kinetic studies for lysozyme [38] and a monoclonal antibody [13] have shown that an incubation time of 20 to 40 min is sufficient for reaching the binding equilibrium on SP Sepharose FF. Afterwards, the plate was centrifuged for 10 min at 1000 rpm in the Rotanta 46RSC centrifuge. 300 μL of the resulting supernatant was transferred to a 96-well flat bottom UV-Star microplate. As for model calibration, sample absorption spectra were measured in a range of 240–300 nm in 2 nm steps. The spectral data were processed using the previously calibrated regression model. Lysozyme and cytochrome c concentrations could be determined selectively. The validity of cytochrome c levels was additionally assured by comparison to 527 nm absorption measurements.

6.2.2.4 Isotherm Fitting

The purpose of isotherm fitting is to validate, whether the observed measurements follow the theoretical framework for protein adsorption in ion-exchange chromatography. The adsorption model applied is the semi-mechanistic steric mass action isotherm (SMA) introduced by Brooks and Cramer [23]. It incorporates effects of counter-ions on the retention behavior of proteins and includes characteristic charges of proteins ν_i . Additionally, steric shielding effects of proteins are considered as a parameter σ_i , representing sterically hindered binding sites without electrostatic interactions. As a final factor, the total ionic capacity Λ of the applied adsorber represents the total number of electrostatic binding

sites. The isothermal form of the SMA isotherm for a mixture of two proteins is shown in Eq. (6.1) and Eq. (6.2), with q_i and $c_{eq,i}$ being the concentration of the protein i adsorbed and in solution, respectively. The effective pore salt concentration is described by c_{salt} . $k_{eq,i}$ is the equilibrium constant of adsorption and desorption.

$$q_1 = k_{eq,1} \left(\frac{\Lambda - (\nu_1 + \sigma_1)q_1 - (\nu_2 + \sigma_2)q_2}{c_{salt}} \right)^{\nu_1} c_{eq,1} \quad (6.1)$$

$$q_2 = k_{eq,2} \left(\frac{\Lambda - (\nu_2 + \sigma_2)q_2 - (\nu_1 + \sigma_1)q_1}{c_{salt}} \right)^{\nu_2} c_{eq,2} \quad (6.2)$$

The SMA model allows for fitting isotherm data, including concurring binding behavior and varying salt concentrations. The fitting procedure was carried out in Matlab R2011a using the least squares data fitting function `lsqcurvefit` (trust-region-reflective algorithm). The estimated parameters include the equilibrium constant $k_{eq,i}$, the characteristic charge ν_i , and the steric shielding σ_i .

6.3 Results and Discussion

6.3.1 Model Generation & Experimental Performance

Partial least squares regression (PLS) is used to reduce data sets and finding significant variance for correlating several input variables (e.g. wavelengths) with output variables (e.g. concentrations). Input variables of similar information content are lumped as so-called latent variables (LVs) leading to a data reduction. The first LV carries the highest information content, whereas each additional LV added leads to less and less improvement of the model. At a certain number of LVs, further addition of LVs then leads to incorporation of measurement noise into the system which needs to be avoided.

For generation of the MVDA model, the optimal number of latent variables was found to be 5, yielding normally distributed residues for the cross validation of all 32 samples. This setup was found identical for both pH 5 and pH 7. The generated MVDA models were then applied to the external test set consisting of 8 samples. The maximal relative deviation in concentration was determined as 3.9 % for pH 5 and 5.3 % for pH 7. Hence, the model performed well for a set of samples that were not used for the calibration experiments.

Besides testing the performance of the MVDA model, also the repeatability of the experimental data was investigated. The duplicates of the isotherms in the presence of 90 mM ionic strength at pH 5 and pH 7 are shown in Supplementary Fig. A.2 for cytochrome c (left) and lysozyme (right). The protein bound to the adsorbent is plotted versus the residual protein in free solution for equilibrium conditions. The trends of the duplicates (cross/diamond) agree well for both investigated pH values and proteins. Also, the absolute values of the duplicates are in good agreement considering the experimental difficulties when working with low adsorbent and liquid volumes. Consequently, both the obtained MVDA model and the experimental data were of high quality and were used in the presented study.

6.3.2 Multi-component Isotherms

To prove the applicability of the MVDA model for real isotherm data in a mixture of proteins, the concentrations of cytochrome c derived from the MVDA are compared to the values of a selective 527 nm analytical wavelength (see Supplementary Fig. A.3). The data points from the MVDA model, plotted over the selective 527 nm wavelength measurements, are shown in a parity plot. It has to be noted that the MVDA model was calibrated in the UV range (240 – 300 nm) whereas the selective wavelength for cytochrome c is at a much higher wavelength in the VIS region. For pH 5 (Supplementary Fig. A.3A) as well as for pH 7 (Supplementary Fig. A.3B), the isotherm data agree well with coefficients of determination of the data points for all investigated ionic strengths (ISs) of 99.74 % for pH 5 and 99.34 % for pH 7. Thus, the MVDA model was applicable to this large data set for straightforward HTS applications.

The isotherm data for both lysozyme and cytochrome c are shown in Fig. 6.1 as 2D (left) and 3D (right) scatter plots. The experimental data are illustrated as markers and the fitted SMA model is shown as curves and planes. For all data sets, the binding of proteins decreases with increasing ionic strength (from 42 mM to 150 mM IS). For cytochrome c (red), both pH conditions (pH 5 – Fig. 6.1A and pH 7 – Fig. 6.1B) show a similar trend for all ionic strengths: The isotherm data increase for low starting concentrations c_{in} and decrease for higher values of c_{in} . However, the overall binding of cytochrome c at pH 5 (Fig. 6.1A) is slightly increased when compared to pH 7 (Fig. 6.1B). E.g., in the setups of 42 mM IS, the maximum binding capacity $q_{Cyt\ c}$ was determined to be 63.98 mg/mL for pH 5 and 50.13 mg/mL for pH 7. Again, for lysozyme (bottomblue), both pH conditions behave similarly for all ISs. In contrast to cytochrome c, the isotherm data increase consistently with the starting concentrations c_{in} . The overall binding behavior of lysozyme at pH 5 (Fig. 6.1A) is slightly decreased when compared to pH 7 (Fig. 6.1B). The maximum binding capacity q_{Lys} at 42 mM IS was determined to be 67.48 mg/mL for pH 5 and 74.77 mg/mL for pH 7. Although the initial amount of lysozyme in the mixture was much lower (30 %) compared to cytochrome c (70 %), the maxima of q_{Lys} exceed those of $q_{Cyt\ c}$.

The experimental results encountered follow the expected trends. As observed for all investigated setups, an increase in ionic strength causes a weakening of the electrostatic binding in ion exchange chromatography. Cytochrome c showed a strong increase in protein binding for low starting concentrations c_{in} , starting to decrease with higher values of c_{in} . This indicates a displacement of cytochrome c by lysozyme when the binding process approaches the maximal binding capacity of the adsorber. This assumption was confirmed by the trends encountered for lysozyme. Here, a continuous increase in protein binding was observed towards a maximum for the highest starting concentrations c_{in} . This displacement under all investigated conditions agrees with the isoelectric points of the two proteins being 10 to 10.5 for cytochrome c and 11.4 for lysozyme (compare data sheet Sigma-Aldrich) yielding a higher net charge for lysozyme and thus a stronger binding to the cation exchange resin. This also explains the enhancement of the displacement reaction for pH 7 compared to pH 5 due to cytochrome c being closer to its nominal pI.

6.3.3 SMA Data Fitting

For SMA data fitting, the total ionic capacity Λ for the adsorber plaques was estimated first. A packed 1 mL of SP Sepharose FF has a total ionic capacity of 800 mM [124].

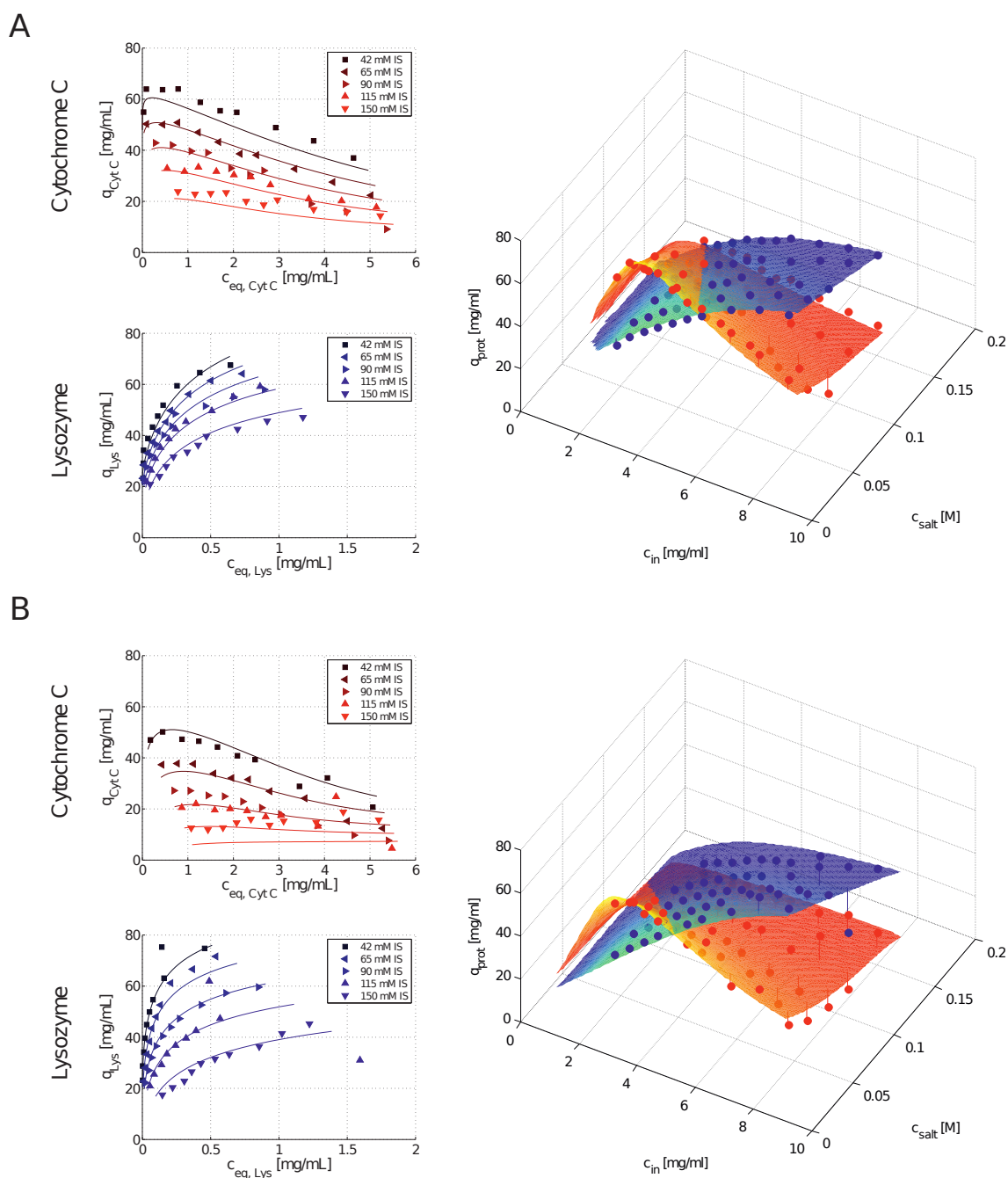


Figure 6.1: Isotherm data derived from the MVDA model-based equilibrium concentrations for both cytochrome c (red) and lysozyme (blue) and the corresponding SMA isotherm fitting curves. The experimental results at pH 5 (A) and pH 7 (B) are illustrated for all investigated ionic strengths in a range of 42 mM to 150 mM. The experimental data points are highlighted as markers and the SMA isotherm fitting curves are illustrated as solid lines for 2D plots and as planes for 3D plots.

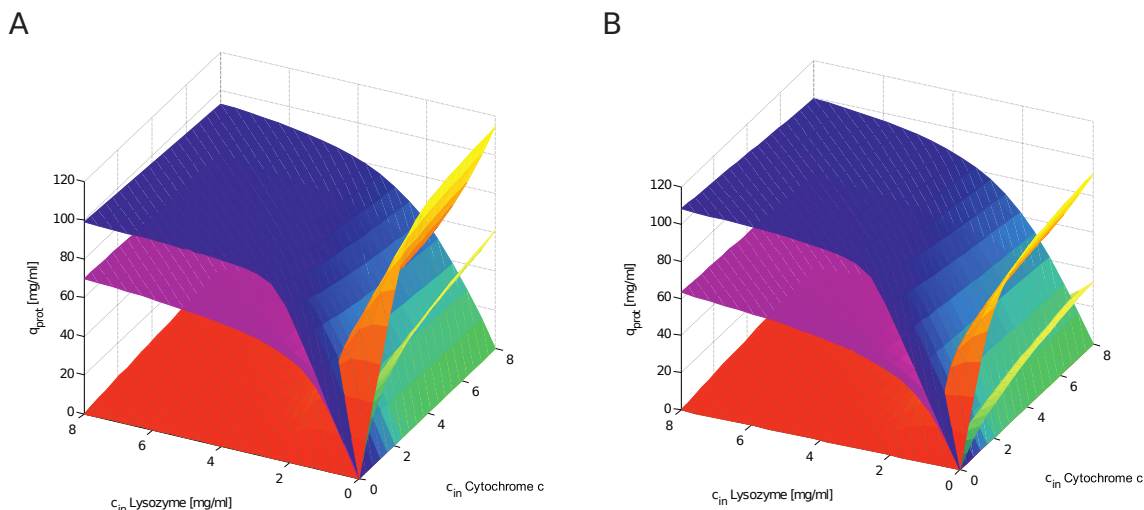


Figure 6.2: predicted SMA model for different concentrations and mixing ratios of cytochrome c and lysozyme at pH 5 (A) and pH 7 (B). Lysozyme is shown in blue (42 mM IS) and pink (150 mM IS), cytochrome c is illustrated in red (42 mM IS) and yellow (150 mM).

Table 6.1: SMA parameters of cytochrome c and Lysozyme at pH 5 and pH 7 determined by least squares fitting of the MVDA isotherm data.

Protein	pH	$k_{eq,i}$	ν_i	σ_i
Cytochrome c	5	0.010	9.955	45.775
Cytochrome c	7	0.040	4.827	36.877
Lysozyme	5	0.632	7.945	48.278
Lysozyme	7	0.454	5.834	51.871

The calculation of the equivalent Λ for the adsorber plaques being 0.504 mM followed the description by Hermann et al. using the packed-bed porosity factor [67]. The data fitting was performed in Matlab R2011a using q_i and $c_{eq,i}$ being the concentration of the protein i adsorbed and in solution inside the pore as input variables according to Eqs. (6.1), (6.2). The corresponding SMA fitting functions are illustrated in Fig. 6.2 by solid lines plotted combined with the respective MVDA data points. The fits were found to be of good agreement, the experimental isotherm points are matched well and the competitive binding trends were conserved.

The resulting SMA parameter sets for both proteins under the investigated conditions are listed in Table 6.1. The lysozyme equilibrium constants $k_{eq,i}$ are much higher (ranging from 0.454 to 0.632) compared to cytochrome c (0.010 to 0.040) for both pH 5 and pH 7. Comparable values and trends were reported by Gallant et al. for both proteins at pH 6 ($k_{eq,Lys} = 0.124$, $k_{eq,Cyt c} = 0.006$) [45]. As shown in Table 6.1, the characteristic charge ν_i of cytochrome c was determined to be 20 % higher than for lysozyme at pH 5 whereas for pH 7, the same trend is shown inversely. ν_i values given by Gallant et al. at pH 6 ($\nu_{Lys} = 5.95$, $\nu_{Cyt c} = 6.15$) as the center point between pH 5 and pH 7 indicated an identical charge characteristic for both proteins agreeing well with this inversion of ν_i from pH 5 to pH 7 shown in this study. Also, the absolute values for ν_i match well. The steric shielding parameters σ_i shown in Table 6.1 are similar for all proteins under all conditions ranging from 36.877 to 51.871. Those values are in accordance with Gallant et al. for cytochrome c (53.4) and Osberghaus et al. for lysozyme (29.7 – 36.8) and

cytochrome c (28.7 – 40.8) [124].

The overall model quality depends on the identifiability of isotherm parameters from the chosen experiments. To determine the range of the design space used for model calibration, the total concentration of occupied binding sites in equilibrium Λ_{bound} is calculated:

$$\Lambda_{bound} = \Lambda - \sum_i (\nu_i + \sigma_i) q_i \quad (6.3)$$

Pairs $(q_{Cyt\ c}, q_{Lys})$ can be taken from the experimental data in [mg/mL] and divided by the respective molecular weights. $MW_{Cyt\ c} = 12.38$ kDa and $MW_{Lys} = 14.30$ kDa were taken from the Sigma Aldrich data sheet and the SMA parameters for pH 5 and pH 7 are given in Table 6.1. For the lowest salt concentration and highest initial concentration at pH 5, Λ_{bound} adds up to 432.5 mM (166.7 mM cytochrome c, 265.8 mM lysozyme) and for pH 7 to 371.5 mM. For the lowest initial concentration, we obtain $\Lambda_{bound, pH5} = 338.7$ mM and $\Lambda_{bound, pH7} = 302.7$ mM. Comparing these values to the total ionic capacity of Λ of 504 mM, the loading is in a range of 60 % to 86 %.

This could be an explanation for the deviation of the equilibrium constants from literature values. As the linear range of the isotherms is not covered by the experiments, the 95 % confidence intervals for k_{eq} are the largest ($k_{eq, Cyt\ c, pH5}$ 94 %, $k_{eq, Cyt\ c, pH7}$ 233 %, $k_{eq, Lys, pH5}$ 68 %, $k_{eq, Cyt\ c, pH7}$ 187 %). However, it should be noted that Gallant et al. were investigating cytochrome c and lysozyme at pH 6 and not at pH 5 and 7. Absolute values were thus not comparable but relative trends were conserved. The confidence intervals for the steric shielding parameter were the smallest ($\sigma_{Cyt\ c, pH5}$ 13 %, $\sigma_{Cyt\ c, pH7}$ 34 %, $\sigma_{Lys, pH5}$ 11 %, $\sigma_{Cyt\ c, pH7}$ 28 %) as they can be read from the concentration in the saturated state. For the characteristic charge we determined slightly larger intervals ($\nu_{Cyt\ c, pH5}$ 20 %, $\nu_{Cyt\ c, pH7}$ 42 %, $\nu_{Lys, pH5}$ 21 %, $\nu_{Cyt\ c, pH7}$ 41 %). As the parameters are still correlated, additional experiments could be done to minimize the uncertainty, e.g. following [8]. Nevertheless, it can be concluded that the SMA model is able to reproduce the observed binding behavior.

Finally, the fitted SMA model was plotted for different protein concentration levels c_{in} of both proteins for pH 5 (Fig. 6.2A) and pH 7 (Fig. 6.2B). Lysozyme is shown in blue (42 mM IS) and pink (150 mM IS), cytochrome c is illustrated in red (42 mM IS) and yellow (150 mM). Data points along the x and y axes (0 mg/mL lysozyme or cytochrome c) are the single component isotherms showing a linear slope for low concentrations and resulting in a maximum (q_{max}) at the adsorber saturation. The model predicts an almost constant maximal binding capacity at pH 5 and pH 7 at both ISs for lysozyme whereas the binding of cytochrome c is enhanced at pH 5 especially for 150 mM IS compared to pH 7. Furthermore the model in Fig. 6.2 predicts that already 2 mg/mL of lysozyme present in the mixture suppresses the binding of cytochrome c on the adsorber for both pH setups. These findings agree with the experimental data which indicated a diminished binding of cytochrome c (Fig. 6.1) though being the species of excess concentration in the mixture (70 % cytochrome c/ 30 % lysozyme).

6.3.4 SMA Parameters vs. Experimental Data

The equilibrium constant $k_{eq, i}$ as a factor describing the binding affinity of proteins under given conditions being over 10-fold higher for lysozyme compared to cytochrome c (compare Table 6.1) is in accordance with the isotherms given in Fig. 6.1. The displacement

of cytochrome c by lysozyme at higher starting concentrations c_{in} was discussed above. Surprisingly, the corresponding characteristic charge ν_i is not the crucial factor driving this phenomenon. E.g., for pH 5, ν_{Lys} of 7.945 is lower than $\nu_{Cyt c}$ of 9.955 but still the equilibrium is strongly shifted towards lysozyme. However, the above-discussed effects of increased displacement of cytochrome c at pH 7 (towards the pI of both proteins) agree with the change in characteristic charge from pH 5 to pH 7 which decreases strongly for cytochrome c from 9.955 to 4.827 whereas lysozyme is much less affected. In summary, the equilibrium constant was found to be a factor for indicating displacement phenomena whereas the characteristic charge shows the extent. The shielding factors σ_i being similar for both proteins were expected as lysozyme and cytochrome c are similar in size. Lysozyme as the slightly larger molecule ($MW_{Lys} = 14.30$ kDa, $MW_{Cyt c} = 12.38$ kDa) resulted in marginally higher σ_i values.

6.4 Concluding Remarks

It was demonstrated that multivariate data analysis (MVDA) of protein spectra is a straightforward method of determining accurate concentration levels for protein mixtures for HTS applications such as batch isotherms. The data points were of high quality and were thus usable for modeling purposes. Based on the MVDA data, accurate SMA fits were found that coincide with literature values.

Analyzing the presented amount of samples using a standard analytical method, such as analytical chromatography takes approximately 5 min per sample or above. Using the presented MVDA method, in contrast, 10-15 s per sample are sufficient. The time requirement per sample is one of the key aspects in the concept of QbD, as the bottleneck of HTS and exploring the design space is shifted to the analytics. Besides this, the major advantage over traditional analytical tools, its non-invasive nature, is very convenient in the context of performing experiments on robotic work stations, making sampling obsolete. The proposed methodology can be used for any multi-component mixture that do show differences in single-component absorption spectra. Brestrich *et al.* used the methodology for a distinction between antibody monomers, aggregates and lower molecular weight species though being spectrometrically similar [8; 22]. Such species can be distinguished due to an increase or decrease of exposed amino acid residues and by included scattering effects for larger aggregates. The analytical technology based on MVDA of protein spectra might become a standard tool for robotic work stations and in-line analytics[21; 22]. The technique of model calibration might be extended to more complex protein compositions and proteins which are not available as pure components.

Acknowledgments

The authors acknowledge the financial support by the German Federal Ministry of Education and Research (BMBF) - funding code 0316071B. This research work is part of the project 'ERA Net Euro Trans Bio - 6: Development of an integrated strategy for a high-throughput process development platform on a micro-scale format - FORECAST'. The authors acknowledge Dr. Sigrid Hansen for the kind introduction to multivariate data analysis. The authors are completely responsible for the content of this publication.

The authors have declared no conflicts of interest.

7 | Calibration-free Inverse Modeling of Ion-exchange Chromatography in Industrial Antibody Purification

Tobias Hahn¹, Thiemo Huuk¹, Anna Osberghaus¹, Katharina Doninger², Susanne Nath², Stefan Hepbildikler², Vincent Heuveline³, Jürgen Hubbuch¹

¹ Karlsruhe Institute of Technology (KIT), Institute of Process Engineering in Life Sciences, Section IV: Biomolecular Separation Engineering, Karlsruhe, Germany

² Pharmaceutical Biotech Production, Roche Diagnostics GmbH, Penzberg, Germany

³ Heidelberg University, Interdisciplinary Center for Scientific Computing, Engineering Mathematics and Computing Lab, Heidelberg, Germany

Abstract

The identification of optimal process parameters for the isolation of a target component from multi component mixtures is especially challenging in industrial applications. With constantly increasing time to market pressure, screening a large parameter space is not feasible and Design-Of-Experiment approaches with few experiments might fail due to dynamic and nonlinear reactions to small parameter changes.

Model-based optimization can determine optimal operating conditions, once the model has been calibrated to the specific process step. In this work, parameters for the Steric Mass Action model are estimated for the target protein and three impurities of an industrial antibody cation-exchange purification step using only chromatograms at different wavelengths and additional fraction analyses with size exclusion chromatography. Information on the molar or mass concentrations in the feed are not available. The model-based optimization results coincide with conventional chromatogram-based optimization.

Practical Application

This paper demonstrates that model-based optimization can be applied to an industrial cation-exchange step, even if the molar concentrations of the feed components are unknown. Based on a few experiments, which might be already available from previous screenings, the model can be calibrated. For differentiating components eluting hidden in the sum signal, single components elution curves must be generated for peak fitting. This is accomplished by SEC fraction analyses at the same wavelength as the chromatogram.

7.1 Introduction

Biopharmaceutical products currently constitute one of the fastest growing markets for the pharmaceutical industry [91]. Industrial downstream processing (DSP) faces the challenge of efficiently purifying a product out of a very heterogeneous mixture. Especially for monoclonal antibodies (mAb), the purification sequence is commonly based on platform processes that are only slightly adapted to new target components [100; 145]. This approach ensures fast process development and reduces the time to market, but it is probable that the reduced exploration of design space leads to suboptimal processes [118]. Process understanding is hence a sensible and important addition to the use of platform processes [66]. As the integration of modeling tools into process development is also an essential part of the strategy for the implementation of the Quality by Design (QbD) approach [27; 74], modeling tools are increasingly gaining the attention of the pharmaceutical industry. It ensures time and material-efficient process optimization as long as the model parameters can be determined reliably with less effort.

For some sorption sub-models, such as the Steric Mass Action (SMA) model for ion-exchange chromatography of proteins [23], model calibration protocols for pure components exist [23], which allow for determining the component-specific parameters in a consecutive fashion. With no a priori knowledge about the components' behavior within mixtures, the inverse method is a suited option, which alters parameters in a systematic fashion to achieve a match of measured chromatogram and model prediction. In a comparative study [126], the direct approach and the inverse method were found to reach equal prediction quality such that the latter is recommended for fast process development.

The potential of mathematical modeling and numerical optimization of chromatography has been demonstrated in academic set-ups for mixtures of small molecules [1; 42], model proteins [127] and antibodies [35; 85], as well as for industrial process steps [30; 112]. All applications have in common, that sensor calibrations existed for all components, allowing to transform UV absorption values into mass or molar concentrations. This paper discusses the challenges when applying mechanistic modeling and numerical optimization to a data-set of industrial preparative chromatography without knowledge of feed composition in terms of molar concentrations. Additional experiments and analyses are avoided by employing a modeling approach that estimates the absorption coefficients from the recorded UV data.

The case study bases on a cation-exchange chromatographic (CEX) process step (Poros 50 HS resin). The antibody mixture fed into CEX is a protein A eluate after low pH

incubation and conditioning. The mixture contains several antibody variants differing in size and charge, that all elute in a common peak. Fraction collection and analysis has to be performed to obtain information on the location of the impurities. Using size exclusion chromatography, the targeted monomer and three impurities can be distinguished, two high molecular weight (HMW) and one low molecular weight (LMW) species. The found model parameters were used for *in silico* optimization and eventually coincide with conventional optimization by chromatogram evaluation.

7.2 Materials and Methods

Initial experiments were conducted to determine system properties, thereafter six experiments in bind/elution mode were performed. The following sections describe the experimental set-up, data processing and parameter estimation.

7.2.1 Column Parameter Determination

A 20 ml column, with Poros 50 HS (Applied Biosystems, Carlsbad, CA, USA) resin was analyzed first with an acetone pulse and second with dextran using an Äkta Avant system (GE Healthcare, Little Chalfont, UK) to determine the essential model parameters as described in [109] and presented in Table 7.1. Acid-base-titration was carried out to determine the total ionic capacity: The column was flushed with a 0.5 M HCl solution until a constant UV and conductivity signal was achieved. Afterwards the column was washed with ultrapure water until a constant UV and conductivity baseline was reached. After that the column was titrated at a flow of 100 cm/h with a 0.01 M NaOH solution until an increase in conductivity signal was recorded. From the Na-ion concentration of the titrant and the volume of the applied titrant, the total number of exchangeable ions was calculated. All chemicals used were obtained highest quality.

With this set of parameters all system specific parameters occurring in the mathematical model can be fixed as also given in Table 7.1.

7.2.2 Bind-elute Experiments

As system liquid a 50 mM acetate buffer was used at pH 4.95, for elution a high-salt buffer of 50 mM acetate and 750 mM NaCl was employed. The different salt profiles in the following were mixed from these two buffers.

A sample volume of 81.3 ml = 4.2 column volumes (CV) was injected for each experiment. First, the gradient experiment was ran from 50 mM (0 % high salt buffer) to 550 mM (66 % high-salt buffer), with the gradient starting at 8.4 CV and ending at 18.1 CV. As the elution peak reached its maximum at a total salt concentration of 210 mM, five step elutions with concentrations 190, 200, 210, 220 and 230 mM were performed for optimization. Each step was induced at 7 CV and was followed by a wash with 100 % high-salt buffer as soon as the 280 nm UV signal fell below a threshold of 100 mAU.

Table 7.1: Measured (top) and calculated (bottom) column parameters.

Parameter	Symbol	Value	Unit	Proceeding
Diameter	d	10	mm	From manufacturer
Length	L	246	mm	Manual measurement
Bead radius	r_p	0.025	mm	From manufacturer
System dead volume	V_d	1.98	ml	Acetone injection without column
Retention volume Acetone	V_{RetAc}	16.94	ml	Acetone peak injection with column
Retention volume dextran	V_{RetDex}	10.29	ml	Dextran peak injection with column
Standard deviation of dextran	σ_{Dex}	0.161	ml	Äkta peak integration
Volume of $NaOH$	V_{NaOH}	130.2	ml	Acid/base titration
Molarity of $NaOH$	c_{NaOH}	0.01	M	Manually controlled
Flow rate	u	0.69	$\frac{mm}{s}$	Manually controlled
Volume	V	19.32	ml	$\frac{1}{4} \cdot \pi \cdot d^2 \cdot L$
Fluid volume	V_f	14.96	ml	$V_{RetAc} - V_d$
Interstitial volume	V_{int}	6.43	ml	$V_{RetDex} - V_d$
Total column porosity	ε_t	0.77		$\frac{V_f}{V}$
Interstitial porosity	ε_b	0.43		$\frac{V_{int}}{V}$
Particle porosity	ε_p	0.6		$\frac{V_f - V_{int}}{V - V_{int}}$
Interstitial flow	u_{int}	1.61	$\frac{mm}{s}$	$\frac{u}{\varepsilon_b}$
Axial dispersion	D_{ax}	0.124	$\frac{mm^2}{s}$	$\frac{1}{2} \cdot L \cdot u_{int} \cdot \left(\frac{\sigma_{Dex}}{V_{int}} \right)^2$
Ionic capacity	Λ	0.3	M	$\frac{c_{NaOH} \cdot V_{NaOH}}{V_c(1-\varepsilon_b)(1-\varepsilon_p)}$

The elution peaks of all experiments were captured in 3 ml samples and analyzed by SEC to determine the relative contribution of the two HMW species, the monomer, and the LMW species to the sum signal. In the case of the step elutions, the peak occurring during the subsequent wash was also fractionated and analyzed. The same analysis was performed for the feed material.

As the gradient elution resulted in a blunt top (Figure 7.2) and not a distinct peak, a longer gradient elution was performed to check for charge variants.

7.2.3 Mathematical Model

The UV absorbance based model as developed in [58] is used in the following. The General Rate Model (GRM) [109] models the macroscopic protein transport through the column. The system is of Convection Diffusion Reaction (CDR) type. Eq. (7.1) describes the rate of change of a concentration $c_i(x, t)$, measured in [M] for salt and [mAU] for proteins, in the interstitial volume of a column with length L to consist of convective mass transport in space with the average interstitial velocity of the fluid u , peak broadening effects that are modeled as dispersion in axial direction with respect to a coefficient D_{ax} , and transition from the interstitial concentration into the particle pore concentration $c_{p,i}(x, r, t)$ which

depends on the porosity of the bed ε_b , the radius of adsorber particles r_p and a component-specific film transfer coefficient $k_{film,i}$. The model is complemented with Danckwerts boundary conditions, Eqs. (7.2),(7.3). Equations (7.4)-(7.6) model the accumulation of mass in the pore volume $c_{p,i}$ and stationary phase q_i depending on the particle porosity ε_p and the component-specific pore-diffusion coefficient D_p .

$$\frac{\partial c_i}{\partial t} = -u(t) \frac{\partial c_i}{\partial x} + D_{ax} \frac{\partial^2 c_i}{\partial x^2} - \frac{1 - \varepsilon_b}{\varepsilon_b} k_{film,i} \frac{3}{r_p} (c_i - c_{p,i}) \quad (7.1)$$

$$\frac{\partial c_i}{\partial x}(0, t) = \frac{u(t)}{D_{ax}} (c_i(0, t) - c_{in,i}(t)) \quad (7.2)$$

$$\frac{\partial c_i}{\partial x}(L, t) = 0 \quad (7.3)$$

$$\frac{\partial c_p}{\partial t}(x, r, t) = \frac{1 - \varepsilon_p}{\varepsilon_p} \frac{\partial q}{\partial t}(x, r, t) + \frac{1}{r^2} \frac{\partial}{\partial r} \left(r^2 D_p \frac{\partial c_p}{\partial r}(x, r, t) \right) \quad (7.4)$$

$$\frac{\partial c_p}{\partial r}(x, r_p, t) = \frac{k_{film}}{\varepsilon_p D_p} (c(x, t) - c_p(x, r_p, t)) \quad (7.5)$$

$$\frac{\partial c_p}{\partial r}(x, 0, t) = 0 \quad (7.6)$$

The steric mass action isotherm (SMA) [23], modified by [58], is a commonly used semi-mechanistic isotherm in ion-exchange chromatography. It is capable of reproducing the influence of counter ions on the retention behavior of protein species using the proteins' characteristic charges ν_i . In addition, it considers adsorbent properties such as the total ionic capacity Λ and steric shielding effects σ_i of the protein i covering an amount of binding sites, greater than the actual number of sites it interacts with. The UV absorbance-based kinetic SMA isotherm is given in Eq. (7.7), with q_i and $c_{p,i}$ being the concentration of the protein i adsorbed and in solution respectively. $c_{p,salt}$ is the salt concentration of the solution. $k_{eq,i}$ and $k_{des,i}$ are the constants of equilibrium and desorption rate, and a_i the absorption coefficient that scales molar concentrations to absorbance units, according to Lambert-Beer law. The factors a_i consist of extinction coefficient and UV cell path length, where the extinction coefficients are unknown for the impurities and cannot be determined easily as the components are not available in pure form.

$$k_{des,i}^{-1} \frac{\partial q_i}{\partial t} = k_{eq,i} \left(\Lambda - \sum_{j=1}^k \frac{\nu_j + \sigma_j}{a_j} q_j \right)^{\nu_i} c_{p,i} - c_{p,salt}^{\nu_i} q_i \quad (7.7)$$

$$q_{salt} = \Lambda - \sum_{j=1}^k \frac{\nu_j}{a_j} q_j \quad (7.8)$$

The model is chosen because of its capability of simulating the whole chromatographic process, including elution, by changing the induced salt concentration at the inlet.

7.2.4 Numerical Solution

The numerical simulation is performed using the in-house software package ChromX. Following the method of lines, the equation system is first discretized in space on given nodes,

using the Finite Element Method (FEM). FEM is a highly versatile method with strong mathematical foundation and well suited for CDR equations. The solutions procedure starts with the weak formulation, incorporating the boundary conditions and representing the variables with basis functions from the respective spaces. A Streamline-Upwind-Petrov-Galerkin (SUPG) method was used here with linear basis and test functions. The discretization in time is performed with the fractional step θ -scheme, a semi-implicit procedure providing second-order accuracy [47]. Finally, the non-linearity of the equation system introduced by the isotherm must be treated with an iterative procedure, here, Picard iteration. The resulting linear systems are solved by LU factorization.

7.2.5 Parameter Estimation

Estimation of an unknown parameter set \bar{p} solves the least squares optimization problem

$$\min_{\bar{p}} \sum_j \left(m(t_j) - \sum_{i \geq 1} c_i(L, t_j; \bar{p}) \right)^2, \quad (7.9)$$

where $m(t_j)$ is the measured chromatogram value at point in time t_j . The measurements might also contain noise, which can be neglected when assuming the noise to be zero-mean Gaussian and isotropic. The concentration c_i is simulated in absorbance units. Linear scaling to molar concentrations was checked with concentrated feed samples.

The sensor signal is approximately proportional to the feed concentration up to the saturation limit in UV 280, as suggested by Lambert-Beer law. Furthermore, UV 300 nm captures approximately four times higher concentrations than UV 280 nm (data not shown). The chromatograms were also corrected by the influence of the salt concentration in the mobile phase.

A variety of algorithms is available for the solution of this optimization problem. In this work, we employed a heuristic method based on a genetic algorithm (GAlib ver. 2.4.7 [161]). Genetic algorithms avoid local minimums by performing random jumps and hence explore a larger area of the search space.

As the UV sensor is quickly saturated at 280 nm, we consider additional absorbance measurements at 260 and 300 nm to capture the complete peak shape. In addition, we include size-exclusion chromatography (SEC) analyses of fractions at a common wavelength, such that the contributions to the UV sum signal can be quantified. This data enters the least squares problem Eq. (7.9): m is extended with additional entries of the contributions for each fraction and species and c is extended accordingly with entries only including those simulated concentrations that belong to the respective contribution.

The estimation procedure using SEC data relies on pseudo absorbance profiles $m_i(t_j)$ for all components i that are generated by multiplying the UV signal with the component's fraction percentage in the corresponding time interval. Figure 7.1 shows the pseudo profiles for the step elution with lowest salt concentration. A HMW1 peak is visible during the high-salt step following elution, while LMWs are only visible at the beginning of the elution peak.

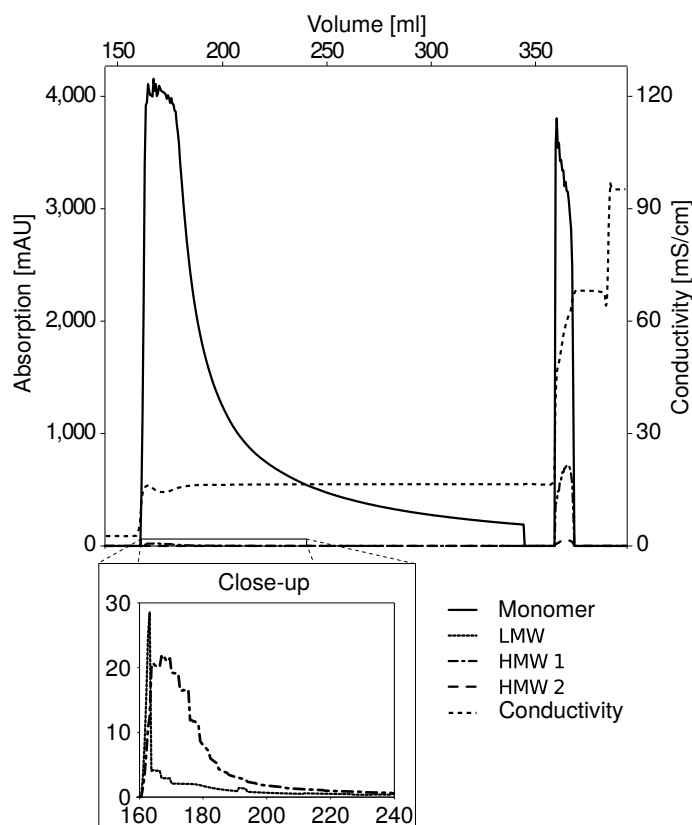


Figure 7.1: Single-component absorption profiles at UV 280 nm for the 190 mM salt step elution. The curves are generated by multiplying the chromatogram by component ratios found by fraction analysis with SEC.

7.3 Results and Discussion

7.3.1 Bind-elute Experiments

The feed analysis by SEC showed 96.79 % monomer, 2.95 % + 0.17 % species with higher molecular weight (HMW 1 and HMW 2) and 0.09 % species with lower molecular weight (LMW) at 280 nm. Further IEC analysis revealed, that the exact composition of the monomer is 15.4 % acidic, 63.3 % main and 21.3 % basic variant. An example of a step elution result is presented in Figure 7.1. It shows a steep front, long tailing and a considerable peak after the final high salt step. The gradient elution result in Figure 7.2 shows a blunt top, indicating that the monomer variants elute differently.

7.3.2 Reference Optimum

When not using model-based optimization in combination with reliable feed concentrations or alternative assays, the optimum has to be defined using only UV absorbance data. Purity is defined as average SEC target peak area of involved fractions divided by total absorbance and yield is similarly defined as ratio of collected peak area by total area. Because of process performance requirements, only step elution scenarios are considered

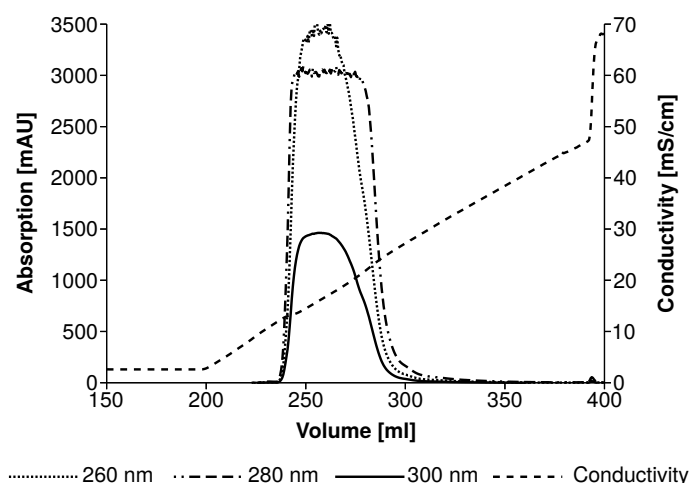


Figure 7.2: Gradient elution peak recorded at UV 260, 280 and 300 nm. Only the 300 nm signal shows the entire top. The peak shape indicates that the monomer consists of differently eluting charge variants.

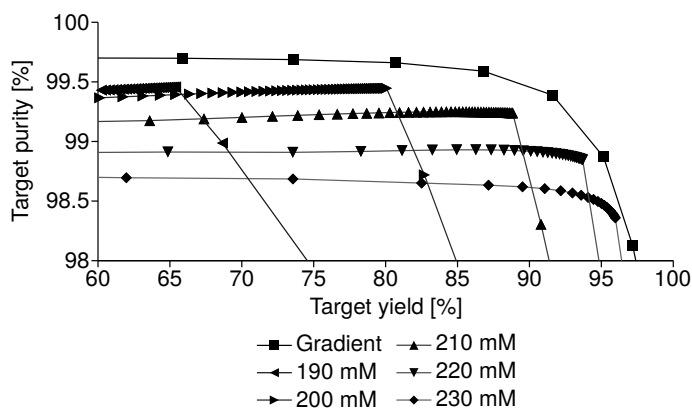


Figure 7.3: Monomer purity over yield when collecting fractions consecutively. Higher steps lead to co-eluting contaminants and lower purity. Lower steps allow to separate contaminants but do not collect all of the target component.

that achieve at least 99 % purity and 80 % yield with fraction size smaller than 5 column volumes.

Figure 7.3 shows the development of monomer purity over yield when starting to collect from the first fraction of the elution peak and successively adding the other fractions. Based on this data, the 200 and 210 mM steps perform best. Gradient elutions are undesired in the final process and were not considered. When collecting the first 33 fractions (= 99 ml \approx 5 CV), the 210 mM step achieves a purity of 99.3 % and 86.5 % yield. The 200 mM step achieves a slightly better purity of 99.5 %, but only 80 % yield. The 220 mM step reaches a higher yield with fewer fractions but does not attain the desired purity.

7.3.3 Protein Parameter Estimation

The estimation algorithm employed is a genetic algorithm, to quickly cover a large search space. The inlet absorbance values are set for all components using the known peak area

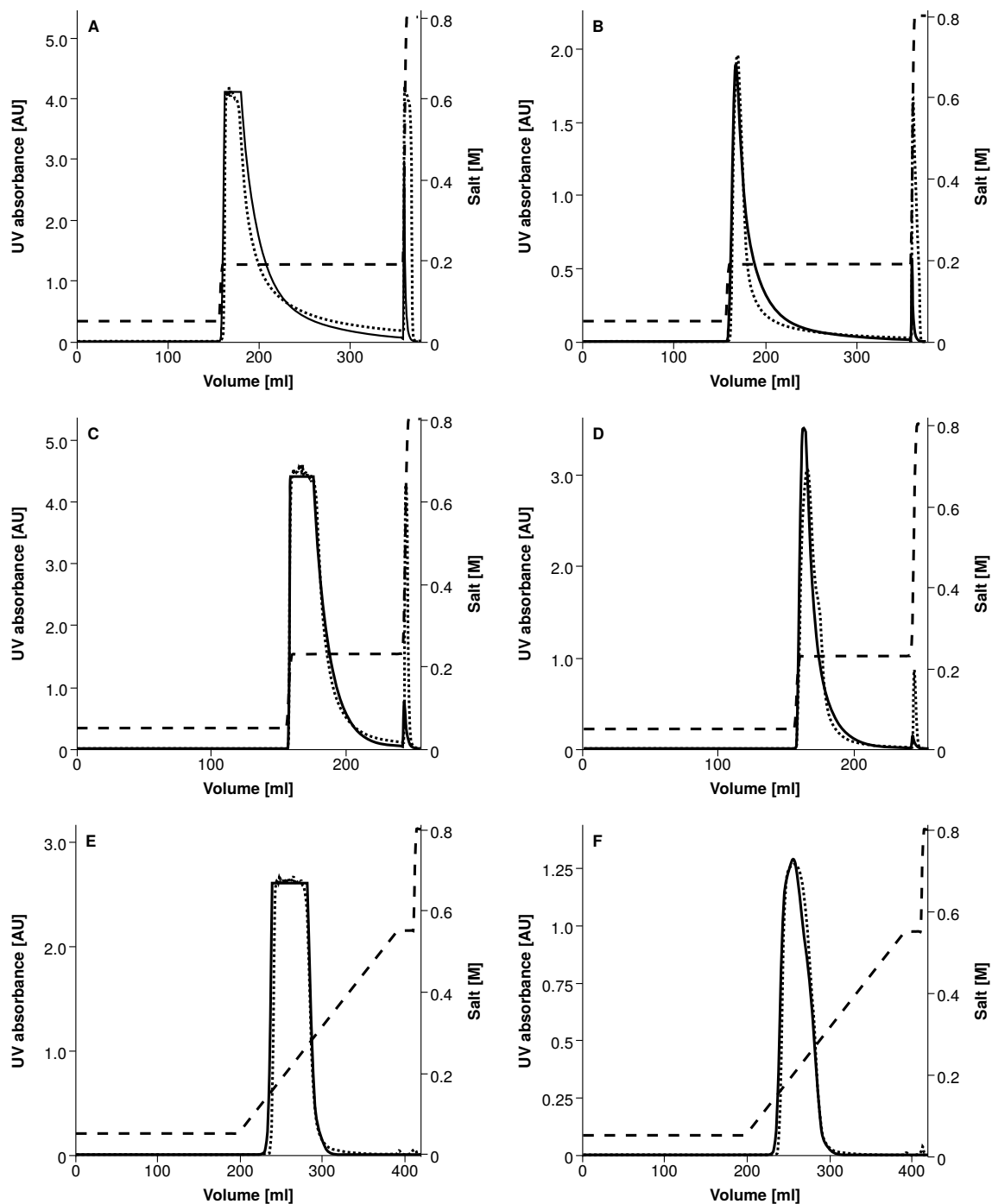


Figure 7.4: Comparison of measured chromatogram (\cdots) and simulated sum signal ($-$) for the salt elutions ($--$) used for model calibration.

Table 7.2: Estimated model parameters.

Component	k_{film}	D_p	k_{des}^{-1}	k_{eq}	ν	σ	a
Salt	0.0083	$7.00 \cdot 10^{-04}$	-	-	-	-	-
LMW	0.0083	$3.49 \cdot 10^{-06}$	$1.61 \cdot 10^{-2}$	1.70	3.32	65.0	$4.4 \cdot 10^7$
Monomer Acidic	0.0083	$2.10 \cdot 10^{-05}$	$9.00 \cdot 10^{-5}$	1.98	3.05	75.3	$8.22 \cdot 10^7$
Monomer Main	0.0083	$5.34 \cdot 10^{-06}$	$1.90 \cdot 10^{-3}$	1.42	5.21	75.3	$8.22 \cdot 10^7$
Monomer Basic	0.0083	$1.57 \cdot 10^{-04}$	$6.08 \cdot 10^{-4}$	1.91	6.90	75.3	$8.22 \cdot 10^7$
HMW 1	0.0083	$3.60 \cdot 10^{-06}$	$3.50 \cdot 10^{-6}$	2.40	8.23	210	$2.14 \cdot 10^8$
HMW 2	0.0083	$7.72 \cdot 10^{-06}$	$3.90 \cdot 10^{-5}$	5.70	5.20	287	$2.10 \cdot 10^8$

at 300 nm, the scaling factor from 300 to 280 nm and the results from SEC and IEC analysis of the feed at 280 nm.

From the available data, the gradient and the highest and lowest salt steps were used for estimation, as the peak shape did not change much for the intermediate steps.

Absorbance-based modelling is able to determine the non-linear parameters σ_i and a_i uniquely from single-component curves [58]. These are available for all impurities, but not for the monomer charge variants. As the variants are indistinguishable in SEC, we can assume them to have equal steric shielding coefficients and absorption coefficients.

Curve fitting finished with a very good match of measurement and simulation, considering the complex elution behavior with long tailing step elutions and blunt gradient top. The result is shown in Figure 7.4.

The found parameter set in Table 7.2 is reasonable, the characteristic charges ascend with the molecule size and in the monomer case with charge variant type. Steric shielding factors and absorption coefficients ascend approximately with molecule size as expected. Sorption kinetics and film diffusion are fast, as indicated by the steep elution fronts.

7.3.4 Optimization

Again, the genetic algorithm was employed to determine the optimal salt step height together with the fractionation boundaries. The optimization of load conditions was performed with traditional high-throughput screening beforehand. Hence, comparison to a non-model-based approach in this particular scale was not possible.

Results of the genetic algorithm are plotted in Figure 7.5. Although the model was calibrated only with the gradient and the 190 mM and 230 mM steps, the results resemble the findings in section 7.3.2 closely: only step concentrations below 210 mM allow a purity above 99 % and only step concentrations below 200 mM achieve high yields above 95 %. The yield values are slightly higher in the model-based optimization results as some parts of the reference elution peaks were not analyzed by SEC and could not be considered when calculating the reference optimum (cf. Fig. 7.1).

A compromise between yield and purity is found at approximately 200 mM, closely followed by 210 mM, just like in the reference analysis. The admissible volume of 100 ml would be fully exploited by a 195 to 200 mM step. A 210 mM step is predicted to achieve a yield of 91 % at the required purity of 99 % using only 60 ml.

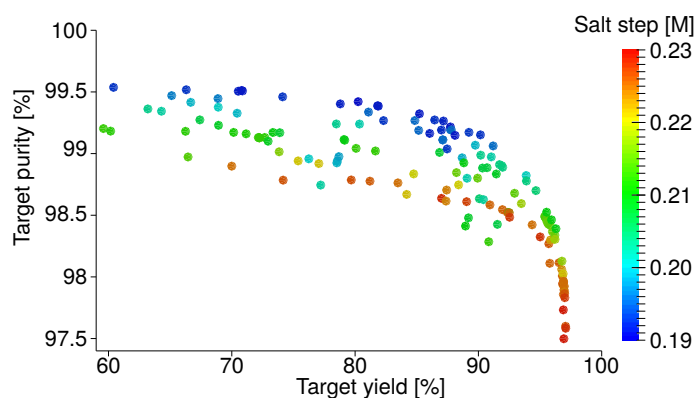


Figure 7.5: Intermediate values of salt step optimization with a genetic algorithm. Step concentrations below 210 mM allow a purity above 99 %. Highest yield values are achieved by step concentrations above 200 mM.

7.4 Concluding Remarks

The benefit of model based optimization compared to the traditional approach is foremost given by the fast adaptation to changes in the feed composition and the possibilities of further optimization. For example, salt profiles can be constructed consisting of several steps in combination with a gradient.

The reduction of the number of experiments in this case is not significant, as conventional optimization was straight forward and the model-based optimum would have to be verified by an additional experiment.

Fractionation itself is a necessity for both approaches, where further studies should examine if good results can be obtained with lower resolution.

Acknowledgment

The research leading to these results was partly funded by EUROTRANS-BIO (grant agreement no. 0316071B, EC's Seventh Framework Programme).

The authors have declared no conflict of interest.

8 | Model-based Integrated Optimization and Evaluation of a Multi-step Ion Exchange Chromatography

Thiemo Huuk¹, Tobias Hahn¹, Anna Osberghaus¹, Jürgen Hubbuch¹

¹ Karlsruhe Institute of Technology (KIT), Institute of Process Engineering in Life Sciences, Section IV: Biomolecular Separation Engineering, Karlsruhe, Germany

Abstract

Current approaches to downstream process development in the biopharmaceutical industry are commonly based on a combination of platform technology, high-throughput experimentation, and 'rules of thumb'. These empirical strategies conflict with demands for a mechanistic process understanding and a rational definition of design space, issued by the *Quality by Design* approach (QbD). Model-based process simulation and optimization are options for implementation of QbD. A model-based process optimization approach has to consider the complexity of biopharmaceutical downstream processes, especially the interactions of multiple chromatographic operations.

We present a case study on model-based concerted process optimization of two consecutive ion exchange chromatographies (Poros 50HS and Q Sepharose FF). Our optimization approach includes a process flowsheet optimization, the shape of the salt gradient, and the boundaries of fraction collection for both columns. The superiority of the presented concerted process optimization approach is demonstrated by comparison to a sequential approach that optimizes the two ion exchange chromatographies (IEX) consecutively. Verification is carried out with a set of three model proteins (cytochrome *c*, chymotrypsin, ribonuclease A).

The *in silico* optimum is reproduced in lab experiments and the modeling tool is successfully employed for the identification and characterization of critical process parameters (CPP).

Nomenclature

Abbreviation	Unit	Definition
$c_{p,i}$	M	concentration of protein i in the pores of the adsorber
$c_{p,salt}$	M	salt concentration in the pores of the adsorber
c_i	M	protein concentration i in the interstitial phase
c_{in}	M	protein concentration i at the column inlet
c_{out}	M	protein concentration i at the column outlet
D_{ax}	mm^2s^{-1}	axial dispersion coefficient
ε_b		voidage of the bed
ε_p		particle voidage
ε_t		total voidage of the bed
$HETP_{Dex}$	mm	height equivalent of a theoretical plate calculated from dextran injection
$k_{ads,i}$		adsorption coefficient of protein i in the SMA isotherm
$k_{des,i}$		desorption coefficient of protein i in the SMA isotherm
$k_{eq,i}$		$k_{ads,i} \cdot k_{des,i}^{-1}$
$k_{eff,i}$	mm^2s^{-1}	effective mass transfer coefficient of protein i
$k_{kin,i}$		$k_{des,i}^{-1}$
L	mm	length of the column
Λ	M	total ionic capacity per adsorber skeleton volume
ν_i		characteristic charge of protein i in SMA isotherm
q_i	M	protein concentration i on the adsorber skeleton phase
r_p	mm	radius of adsorber particles
σ_i		steric shielding coefficient of protein i in the SMA isotherm
t	s	time
$u(t)$	$mm s^{-1}$	interstitial velocity of the fluid
x	mm	axial position in the column

8.1 Introduction

Nowadays, the majority of downstream processes (DSP) for biopharmaceuticals are based on multiple chromatographic and non-chromatographic separation techniques. The use of chromatography is by large due to its mild conditions, the diversity of possible interaction modes, and the long history of chromatographic operations in industry and regulatory authorities. Aside from chromatography, non-chromatographic techniques such as micro- or ultra-filtration or pH conditioning operations are necessary to prepare the process solutions for a chromatographic operation or to ensure bacterial or viral safety and to remove insoluble particles [100; 145]. Industrial DSP development, especially for monoclonal antibodies (mAb), is commonly based on platform processes which are slightly adapted to new entities [35; 100; 145], high-throughput experimentation or 'rules of thumb' [122]. On

the one hand, platform approaches ensure fast process development and reduce the time to market. On the other hand, it has to be assumed that the strongly reduced exploration of design space during adaptation of platform processes to new entities is prone to lead to suboptimal processes [118; 164]. In addition, the limited mechanistic knowledge might account for an increased number of batch failures [27]. Model-based process understanding and optimization are sensible and important additions to platform processes [62; 66]. The integration of modeling tools into process development is an essential part of the strategy for implementation of the *Quality by Design* (QbD) approach [27; 62; 74]. Consequently, modeling tools are increasingly gaining the attention of the pharmaceutical industry [19; 36; 92].

Most experimental and modeling approaches focus on single chromatographic operations [30; 35; 51; 124; 127], or optimize consecutive operations in a sequential manner [54], or with strong simplifications such as non-mechanistic peak shapes (triangles instead of peaks) [132; 133] or short-cut methods [106]. However, industrial downstream processes (DSP) are commonly based on chromatographic and non-chromatographic operations, which are arranged in a sequential manner to meet the ambitious purity requirements [145; 158]. An approach that only focuses on single-unit operations will probably be unable to identify the global process optimum with respect to yield, purity or economic considerations [66; 119]. To meet the growing requirements of industry to integrate modeling tools into industrial DSP, the commonly used modeling approach has to be extended from single chromatographic operations to concerted multi-step optimization tasks.

In 2012, Helling et al. [66] presented a chromatographic sequence of hydrophobic interaction chromatography (HIC) and cation exchange chromatography (CEX) to justify the need for integrated optimization of a two-column sequence. The presented approach is restricted to optimization of the fraction boundaries and disregards optimization of the salt elution gradients or a process flowsheet optimization. Furthermore, the approach only mentions one set of isotherm parameters to predict the retention behavior of a whole crude antibody feedstock.

Nfor et al. [119] presented a model-based optimization of a multi-step downstream sequence, focusing on the optimal arrangement of several different chromatographic modes. The approach is restricted to a partial fraction of possible operational variables (linear flow, gradient length, loading factor). The implications of intermediate operations in between the chromatographic operations are only considered under economic aspects.

An approach disregarding the dynamics of interaction between the single-column processes (e.g. salt gradient, flow, fractionation, etc.) for all unit operations in a concerted manner including a process flowsheet optimization will most probably be unable to identify the global process optimum [118; 164].

In this manuscript, an integrated modeling approach for two consecutive ion exchange operations and an intermediate buffer exchange is presented. This approach is capable to identify the global process optimum for the separation of several protein species and is demonstrated by a case study combining cation and anion exchange chromatography (CEX: Poros 50HS, AEX: Q Sepharose FF). A ternary mixture of chymotrypsin (Chy), cytochrome *c* (Cyt), and ribonuclease A (RibA) is chosen as model system for the separation problem. This set of model proteins covers a narrow pI range of 8.7, 9.5, and

9.6, respectively, constituting a great challenge to the presented separation task. Inverse calibration of a lumped rate model for chromatography, combined with steric mass action isotherm, is carried out on linear gradient elution data and breakthrough curves [124]. First the column parameters are determined experimentally (e.g. voidage). Afterwards, the isotherm parameters are estimated iteratively by minimizing the discrepancy between the experimental and simulated chromatograms. Alternatively, the isotherm parameters could also be determined experimentally from isocratic, gradient, and frontal experiments and correlations (e.g. [129; 144]). In this case study we decided to use the model-based inverse calibration due to its better compatibility with industrial process development workflows, the waiver of correlations, and the faster process development. For a comparison of the inverse calibration and correlation approach we refer to [124]. The calibration is done separately for both chromatographic operations. A subsequent *in silico* optimization is used to identify the global process optimum for an objective function with respect to cytochrome *c* purity, yield, and a minimal volume of the fraction collected from the final column. The optimization includes the shape of the salt gradient and the boundaries of fraction collection. In addition, the optimization accounts for an arbitrary order of the two IEX (flowsheet optimization), namely an AEX→CEX and a CEX→AEX process flow-sheet. The optimization of all parameters for both columns is carried out in a concerted manner. The advantage of this concerted optimization approach is demonstrated by a comparison with a conventional sequential optimization of the two IEX. The use of three linear gradient elutions and one breakthrough curve for model calibration reduces the sample consumption for this case study, as compared to classical approaches using *Design of Experiments* (DoE). This case study bases on a two-column process, but the presented modeling approach is extendable to more complex arrangements of unit operations and larger sets of protein species.

8.2 Theory

8.2.1 Transport-dispersive Model

The transport-dispersive model (TDM) [109] depicted in Eqs. (8.1),(8.2) is used to model the macroscopic mass transport through the column. The system is of convection-diffusion-reaction (CDR) type. The rate of change of a protein concentration $c_i(x, t)$ in the interstitial phase consists of convective mass transport in space with respect to the average interstitial velocity $u(t)$ of the flowing fluid. Peak broadening effects are modeled as dispersion in space with respect to a lumped coefficient D_{ax} , and transition from the interstitial concentration into the particle pore concentration $c_{p,i}(x, t)$ depending on the voidage of the bed ε_b , the radius of adsorber particles r_p , and an effective transfer coefficient $k_{eff,i}$. The model is one-dimensional, such that the concentrations depend on the axial position in the column $x \in [0, L]$ and time. Hence, the axial dispersion coefficient D_{ax} can be calculated from the height equivalent of a theoretical plate ($HETP_{Dex}$) of a dextran injection and the interstitial velocity ($D_{ax} = HETP_{Dex} \cdot u(t)/2$) [109]. The approach to determine D_{ax} from the *HETP* stems from the van Deemter equation and works well, but correlation for film and pore diffusion coefficients (e.g. [79]) often do not describe the behavior for high and low concentrations at the same time. Hence we rather estimate the effective mass transfer coefficient k_{eff} or set it constant if the axial dispersion is dominant and we do not see a change in peak shape.

The second equation models the accumulation of mass in the pore phase $c_{p,i}$ and stationary phase q_i (protein binding to the adsorber) depending on the particle voidage ε_p . The model is complemented with Danckwerts boundary conditions, Eqs. (8.3),(8.4), and an isotherm equation modeling the stationary phase concentration q_i .

$$\frac{\partial c_i(x, t)}{\partial t} = -u(t) \frac{\partial c_i(x, t)}{\partial x} + D_{ax} \frac{\partial^2 c_i(x, t)}{\partial x^2} - \frac{1 - \varepsilon_b}{\varepsilon_b} k_{eff,i} \frac{3}{r_p} (c_i(x, t) - c_{p,i}(x, t)) \quad (8.1)$$

$$\varepsilon_p \frac{\partial c_{p,i}(x, t)}{\partial t} + (1 - \varepsilon_p) \frac{\partial q_i(x, t)}{\partial t} = k_{eff,i} \frac{3}{r_p} (c_i(x, t) - c_{p,i}(x, t)) \quad (8.2)$$

$$\frac{\partial c_i}{\partial x}(0, t) = \frac{u(t)}{D_{ax}} (c_i(0, t) - c_{in,i}(t)) \quad (8.3)$$

$$\frac{\partial c_i}{\partial x}(L, t) = 0 \quad (8.4)$$

8.2.2 Steric Mass Action Isotherm

The steric mass action isotherm (SMA) introduced by Brooks and Cramer in 1992 [23] is a commonly used semi-mechanistic isotherm in ion exchange chromatography, involving one or more macromolecules with steric hindrance, in this case of proteins. It is capable to reproduce the influence of counter ions on the retention behavior of protein species, using the proteins' characteristic charges ν_i . Besides this, it considers column properties like the total ionic capacity Λ and steric shielding effects σ_i of the proteins, blocking an amount of binding sites greater than the actual number of sites it interacts with. The kinetic SMA isotherm is given in Eq. (8.5), with q_i and $c_{p,i}$ being the concentration of the protein i adsorbed and in solution, respectively. $c_{p,salt}$ is the salt concentration of the solution. $k_{ads,i}$ and $k_{des,i}$ are the adsorption and desorption coefficients.

$$\frac{\partial q_i(x, t)}{\partial t} = k_{ads,i} \underbrace{\left(\Lambda - \sum_{j=1}^k (\nu_j + \sigma_j) q_j(x, t) \right)}_{\bar{q}_{salt}(x, t)} c_{p,i}(x, t) - k_{des,i} c_{p,salt}^{\nu_i}(x, t) q_i(x, t) \quad (8.5)$$

This formulation is not well suited for inverse parameter estimation as the change of k_{ads} or k_{des} always affects peak height and retention at the same time. In order to alter peak height unimpededly, the isotherm equation was modified as shown in Eq. (8.6). In this isotherm equation, parameters for kinetic effects ($k_{kin} = 1/k_{des}$) and equilibrium ($k_{eq} = k_{ads}/k_{des}$) are separated, such that a change in k_{kin} strongly affects peak height, while the retention time is preserved to a large extent; vice versa for k_{eq} [61].

$$\underbrace{\frac{1}{k_{des,i}}}_{k_{kin,i}} \frac{\partial q_i(x, t)}{\partial t} = \underbrace{\frac{k_{ads,i}}{k_{des,i}}}_{k_{eq,i}} \bar{q}_{salt}^{\nu_i}(x, t) c_{p,i}(x, t) - c_{salt}^{\nu_i}(x, t) q_i(x, t) \quad (8.6)$$

According to our experience, correlations for determining the linear isotherm parameters from the gradient elution results [129; 168] only determine the characteristic charge parameter well. A previous study [124] showed that this parameter can be found accurately

with chromatogram fitting as well, and that estimation of k_{eq} is inevitable for simulation. For an elaborate discussion on the applicability of correlations we refer to the Handbook of Process Chromatography by Hagel, Jagschies and Sofer [56].

8.2.3 Numerical Solution

Following the method of lines, the equation system is first discretized in space on given nodes, using the finite element method (FEM). FEM is a highly versatile method with strong mathematical foundation and well suited for CDR equations. The solution procedure starts with the weak formulation, incorporating the boundary conditions and representing the variables with basis functions from the respective spaces. A Galerkin ansatz was used here, choosing basis and test functions from the same spaces, specifically first- and second-order polynomials. The discretization in time is performed with the Crank-Nicolson method, a semi-implicit procedure providing second-order accuracy. Finally, the non-linearity of the equation system introduced by the isotherm must be treated with an iterative procedure, here Picard iteration or Newton's Method. The resulting linear systems are solved depending on their dimension with a direct method (e.g. LU factorization) or iterative method (e.g. GMRES). For a general overview of numerical methods for PDEs, we refer to [136].

8.2.4 Estimation and Optimization

Because of the system's non-linearity, finding a global optimum for parameter estimation and subsequently for process optimization is challenging. Deterministic methods cannot leave local minimums and only provide quadratic convergence when starting sufficiently near the optimum. Heuristic methods such as simulated annealing, genetic or evolutionary algorithms cover a larger search space by performing random jumps, but give no guarantee on the convergence rate. A common approach is to start with a heuristic method to identify candidates for global optima and find the final solution using a deterministic algorithm. For parameter estimation, the objective is constituted by curve fitting, such that the goal function is given by the sum of square errors between simulation and measurement data. The simulation uses molar concentrations. Therefore, the measured UV traces are converted from absorption units to molar concentrations using the known molar protein amounts injected to the column and the recorded peak areas. For process optimization, the found parameter estimates are fixed and a system parameter such as salt concentration is used as optimization variable. In this case study, the objective consists of the product-related quality attributes, namely loss, purity, and dilution of the target component cytochrome *c*.

8.3 Materials

8.3.1 Chromatographic Instrumentation

The chromatographic experiments were carried out using an ÄKTApurifier 10 fast protein liquid chromatography (FPLC) equipped with Pump P-903, UV (10mm path length), conductivity and pH monitor UPC-900, an autosampler A-900 and a fraction collector Frac-950 (all GE Healthcare, Little Chalfont, Buckinghamshire, UK). The instrument was controlled with UNICORN 5.10 (GE Healthcare, Little Chalfont, Buckinghamshire, UK).

8.3.2 Adsorbers, Buffers, and Proteins

For ion exchange chromatography (IEX), a 1mL column (8x20mm) prepacked with Poros 50HS strong cation exchange adsorber (Applied Biosystems, Carlsbad, CA, USA, column packing by Atoll, Weingarten, Germany) was used. A second 1mL column (7x25mm) prepacked with the strong anion exchange resin Q Sepharose FF (QFF) was supplied by GE Healthcare (Carlsbad, CA, USA). Between the runs, the columns were stored in a bacteriostatic solution. After storage, the columns were pre-charged by a prolonged equilibration with low and high salt buffer. For cation exchange chromatography, a 50mM sodium citrate buffer (Merck, Darmstadt, Germany) with 0 and 1M additional NaCl (Merck, Darmstadt, Germany) was used at pH 5.0. For the anion exchange experiments, a 50mM 1-methylpiperazine buffer (Sigma, St. Louis, MO, USA) supplemented with 0 or 1M NaCl was used at pH 9.8. All solutions were prepared using ultra-pure water (UPW) (arium pro UV, Sartorius, Göttingen, Germany). Buffers were 0.22 μ m-filtrated and degassed by sonification.

Lyophilized α -chymotrypsin (bovine pancreas, no. C4129), ribonuclease A (bovine pancreas, no. R5503), and cytochrome *c* (bovine heart, no. 30398) were used as model proteins (all from Sigma, St. Louis, MO, USA). All protein solutions were prepared using the respective low salt buffer and were 0.22 μ m-filtrated prior to usage.

8.3.3 Software

Isotherm parameter estimation, chromatogram simulation, and process optimization were carried out using the in-house developed software ChromX. ChromX provides numerical tools for solving various kinds of chromatography models, including the model combination of TDM and SMA. The discretization scheme chosen was a linear finite element ansatz in space using 100 equidistant nodes, which provided a high simulation speed and maintained accuracy as compared to runs with quadratic elements and a higher number of computational nodes. The aforementioned Crank-Nicolson scheme was used for time-discretization with the time step set constant to one second. A Picard iteration was employed for the non-linearity together with UMFPACK as linear solver. ChromX was used for a first evaluation of results, the final chromatograms were exported as comma-separated values and plotted with Matlab R2012b (The Mathworks, Natick, ME, USA) and CorelDRAW X5 (Corel, Ottawa, Canada). For parameter estimation and process optimization, ChromX offers interfaces to various libraries. The implementations used here were *levmar* [101] as deterministic method, based on the Levenberg-Marquardt algorithm (LMA), and the genetic algorithm optimizer *GAlib* [161] as heuristic counter-part (GA).

8.4 Methods

8.4.1 Extra Column Effects

The chromatographic system and the two columns were characterized with 25 μ L tracer injections at a linear flow of 100cm/h. This corresponds to a volumetric flow of 0.838 and

0.641 mL/min for the CEX and AEX, respectively. 1%(v/v) acetone (Merck, Darmstadt, Germany) injections were used to determine the system dead volume. As pore-penetrating, not interacting tracer, 1M NaCl and acetone were applied to the Poros 50HS and QFF column, respectively. The determined dead volumes calculated from the 280nm and conductivity signals were used for the correction of the measured raw data. 25 μ L injections of a filtrated 10g/L dextran 2000kDa solution (Sigma, St. Louis, MO, USA) onto the two columns were used to determine the volume of the inter-particle space. Furthermore, the dextran signals at 215nm were used to calculate the axial dispersion coefficient using UNICORN.

8.4.2 Column Titration

Acid-base titration was carried out to determine the total ionic capacity Λ of the two columns. In brief, the CEX column was flushed with a 0.5M HCl solution until a constant UV and conductivity signal was achieved. Afterwards, the column was washed with UPW until a constant UV and conductivity baseline was reached. After that, the column was titrated at a flow of 100cm/h with a 0.01M NaOH solution until an increase in conductivity signal was recorded. From the Na-ion concentration of the titrant and the volume of the applied titrant, the total number of exchangeable ions was calculated. In the procedure for the AEX, the HCl and NaOH solutions were exchanged.

8.4.3 Linear Gradient Elution

Linear gradient elution (LGE) data were used for isotherm parameter estimation. The whole method was carried out at a linear flow of 100cm/h. After a two-column volume (CV) equilibration with the respective low salt buffer, 25 μ L of a 0.6mM pure protein solution was automatically injected onto the column. Ribonuclease A was applied in a concentration of 1.2mM due to its lower extinction coefficient. Unbound protein was removed from the column during a 2CV flushing with low salt buffer. Afterwards, 15CV linear gradient elutions with a final NaCl concentration of 500, 600 and 700mM for the CEX and 300, 400 and 500mM for the AEX were carried out. The final NaCl concentrations for ribonuclease A on the AEX were 200, 300 and 400mM, and for cytochrome *c* on the CEX 400, 500, 600mM. A subsequent 2CV wash with the final gradient concentration buffer and an additional 2CV regeneration step using the respective buffer with 1M NaCl were applied. The 280nm traces plotted over the volume were exported with UNICORN in Microsoft Excel format.

8.4.4 Breakthrough Curves

Breakthrough curves (BC) were used for the estimation of the shielding parameter σ in the SMA isotherm. For the BC, a 0.6mM protein or 1.2mM ribonuclease A solution in low salt buffer, respectively, was applied to the equilibrated column with a SuperLoop (GE Healthcare, Little Chalfont, Buckinghamshire, UK). The flow was chosen to 100cm/h. The 280nm traces plotted over the volume were exported with UNICORN in Microsoft Excel format.

8.4.5 Buffer Exchange

A buffer exchange was carried out between the CEX and AEX step during the experimental process evaluation. For buffer exchange purposes, a VivaSpin 20 centrifugal concentrator (Sartorius, Göttingen, Germany) equipped with a 3kDa molecular weight cut-off (MWCO) polyethersulfone (PES) membrane was used. The fraction collected from CEX was twofold concentrated and adjusted with the target buffer. This procedure was repeated three times to exchange the buffer.

8.4.6 Parameter Estimation

The SMA isotherm parameters k_{kin} , k_{eq} , and the charge ν were estimated from the three linear gradient elution data using the software ChromX. The gained set of parameters was completed by the estimation of the shielding parameter σ from the breakthrough curves. Due to the appearance of multiple protein signals for ribonuclease A, ribonuclease was treated as two protein species, represented by two different sets of isotherm parameters (RibA1 and RibA2). For the AEX, a blank subtraction due to a salt-induced baseline drift of the buffer was carried out. For estimation, the GA and LMA algorithms were used. The 280nm traces plotted over the volume, exported with UNICORN, have been imported into ChromX respecting the FPLCs dead volume.

8.4.7 *In silico* Process Optimization

The reviewed model process consists of one CEX and one AEX in arbitrary order. A ternary protein mixture containing 0.6mM of cytochrome *c* and chymotrypsin and 1.2mM ribonuclease A is applied to the first column *in silico*. The initial gradient condition, the gradient length and slope are *in silico* optimized for both IEX. In addition, the start and end of fraction collection are optimized *in silico* for both columns. The fraction collected from the first column is *in silico* desalted, doubled, and injected to the second column. Within the concerted optimization approach, the process parameters are optimized for both columns at once, just evaluating the fraction collected from the second column with respect to an objective function. The order of CEX and AEX is kept arbitrary. The concerted optimization approach is illustrated in Figs. 8.4 A and 8.5 A.

To evaluate whether the concerted approach is superior to conventional sequential optimization, the CEX→AEX process optimization is repeated using a sequential optimization. In the sequential approach, the first column is optimized with respect to the objective function. Afterwards, the fraction from the first column is virtually injected to the second column for its optimization. The sequential optimization approach is illustrated in Fig. 8.6 A. The parameters to be optimized and their ranges are illustrated in Fig. 8.1. The overlapping ranges for the start and end concentration of the salt gradient allow linear gradient and isocratic elution. The lower limit of the starting time for fraction collection is zero. Therefore, a flow-through operation is allowed besides bind-elute.

The objective function used in all approaches intends to achieve a great molar purity and a great molar yield of the target protein cytochrome *c* and a low dilution of cytochrome *c*

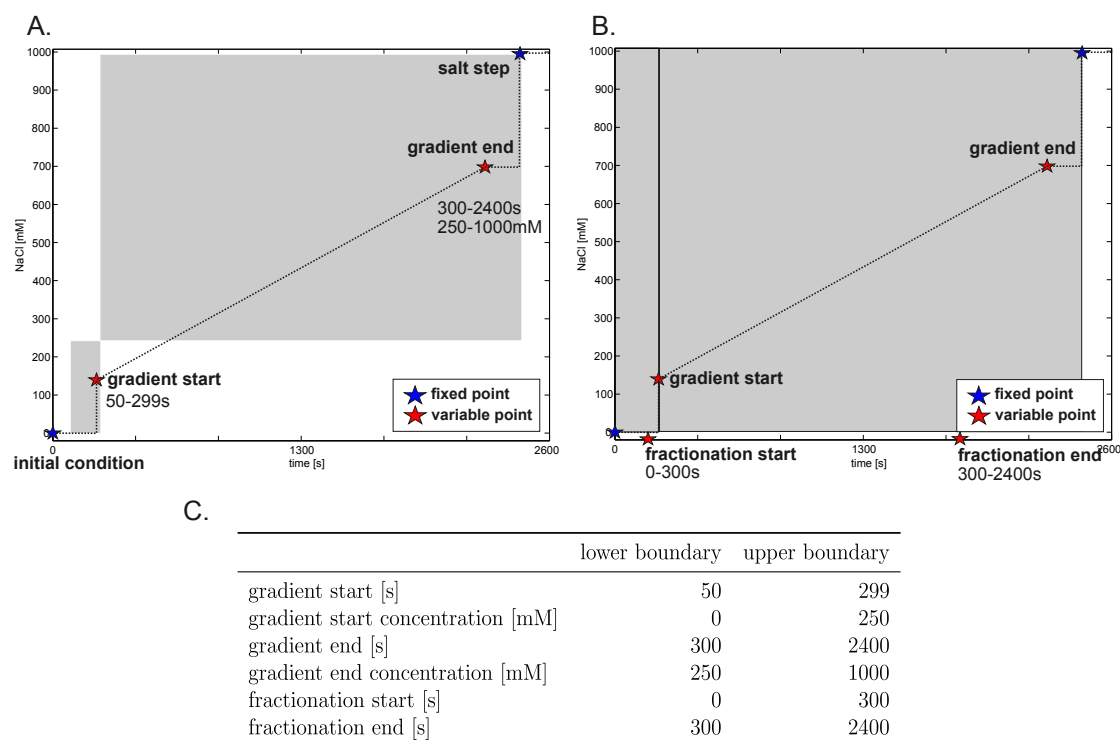


Figure 8.1: Parameters with ranges for the optimization of the IEX salt gradient (A) and the boundaries for the collection of fractions (B) in AEX and CEX. The gray boxes indicate the ranges of the specified parameters. Table C lists the boundaries for parameter optimization.

in the evaluated fraction. With weighting factors, the objective function is given by

$$\begin{aligned}
 \text{purity}[\text{mol/mol}] &\in [0, 1] \\
 \text{yield}[\text{mol/mol}] &\in [0, 1] \\
 \text{fraction}[\text{s}] &\in [0, 2400]
 \end{aligned}$$

$$\min_{\bar{p}} \left(\underbrace{(1 - \text{purity})}_{\text{impurity}} + 0.5 \cdot \underbrace{(1 - \text{yield})}_{\text{loss}} + 0.01 \cdot \frac{\text{fraction}}{\text{mL}} \right) \quad (8.7)$$

with \bar{p} depicting the variable parameter set. The terms refer to cytochrome *c* in the chosen fraction. The weighting terms were introduced to compensate the different magnitudes of the three factors. The range of time, respectively volume values is much larger than purity and yield, such that it has been weighted with 0.01. The model describes concentration over time, therefore the boundaries for fraction collection are given in seconds. Irrespective of this calculation, the objective of 'fraction' is calculated using volumes instead of times, therefore the fraction size within the objective function is given in *mL*. The first column is run in duplicate and the fractions are pooled and directed to the second column. The factor 0.5 for yield equalizes this intermediate pooling. Due to its insensitivity to local minimums of the objective function, the GA was used for process optimization.

Table 8.1: Voidages are calculated from tracer injections. The total ionic capacity is measured by acid-base titration. The axial dispersion coefficient is calculated from dextran injections.

		Poros 50HS	Q Sepharose FF
bed voidage	ε_b	0.341	0.315
particle voidage	ε_p	0.449	0.851
total voidage	ε_t	0.638	0.898
total ionic capacity per adsorber volume/ M	Λ	0.165	2.117
axial dispersion coefficient/ $\frac{mm^2}{s}$	D_{ax}	0.135	0.176

8.4.8 Experimental Process Evaluation

The best process in the *in silico* optimization was reproduced in lab experiments on the Äkta FPLC, namely the concerted optimized sequence of CEX→AEX. The ternary protein mixture was applied to the CEX and the optimized salt gradient and peak fractionation were executed. The collected fractions from two identical runs were pooled and the buffer was exchanged to the low salt AEX buffer. Afterwards, the sample was applied to the AEX, executing the optimized salt gradient and fraction collection. The performances of the experimental systems were evaluated with respect to the data predicted in the modeling approach.

8.5 Results

8.5.1 System Characterization

The FPLC dead volume of $70\mu L$ was determined by tracer injections without a column attached to the system. All other data were corrected with respect to this dead volume. The column voidages were calculated from injections of a pore-penetrating, non-interacting and a non-pore-penetrating, non-interacting tracer. The total ionic capacity was determined by acid-base titration. The calculated voidages and capacities are given in Tab. 8.1.

8.5.2 Parameter Estimation

Estimation of the isotherm parameters was carried out using the Levenberg-Marquart (LMA) and genetic algorithm (GA). First, the kinetic, equilibrium and charge parameters were estimated from the three linear gradient elution (LGE) data. Afterwards, the shielding parameter was estimated from the three LGE and the breakthrough curve (BC). After estimation of the shielding parameter, a comparison of the model response and the experimental data revealed that for the presented case study, film diffusion has a negligible impact on the model quality. Therefore, k_{eff} was set to $r_p \cdot 3^{-1}$ (ref. Eq. (8.1)).

The measured data and the model responses from parameter estimation are given in Figs. 8.2 and 8.3 for Poros 50HS and Q Sepharose FF, respectively. The estimated parameters for both columns are summarized in Tab. 8.2.

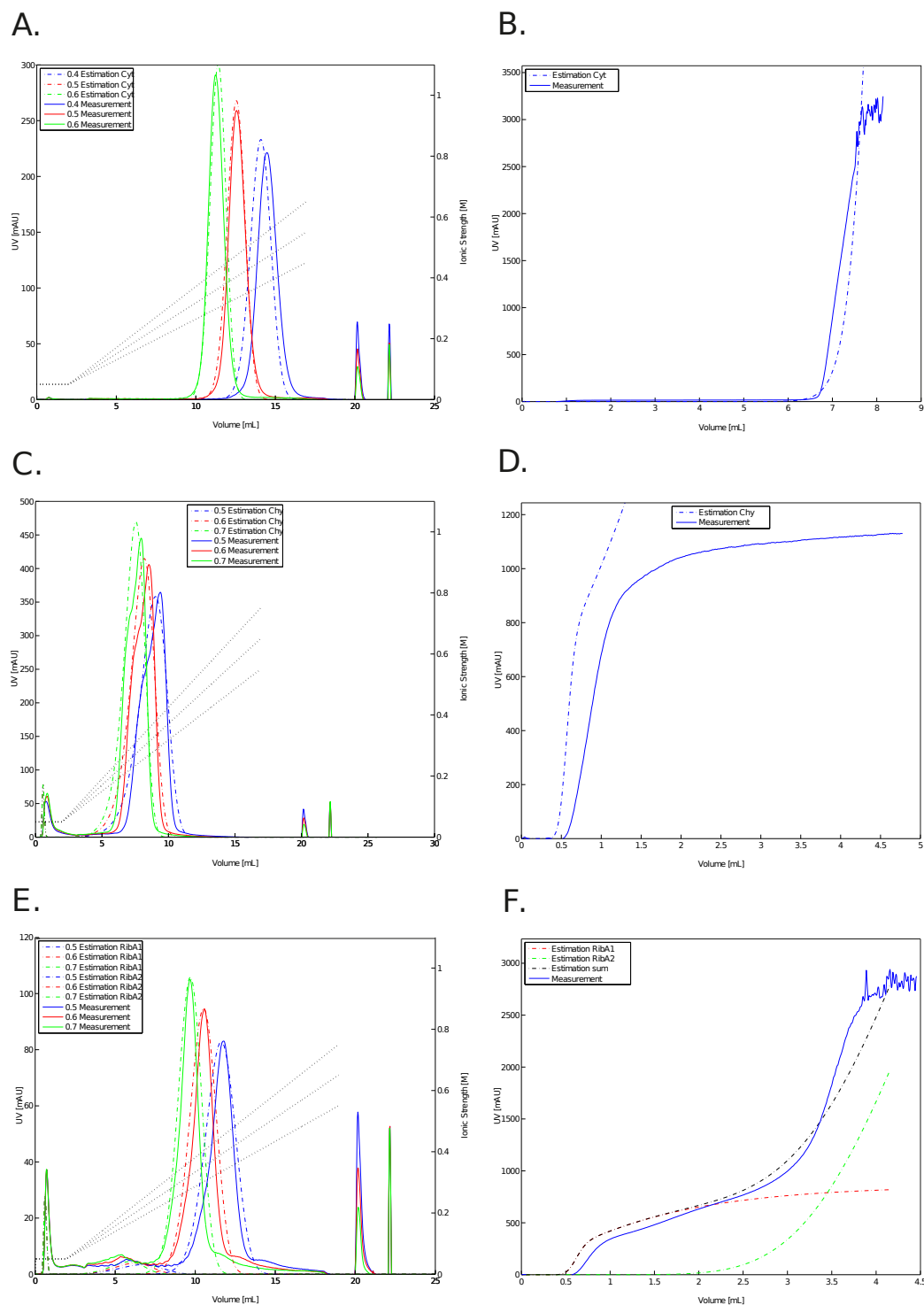


Figure 8.2: Results of the estimation of the isotherm parameters for Poros 50HS. A., C., and E. show the measured (solid lines) and estimated (dashed lines) data for the linear gradient elution experiments. B., D., and F. present the corresponding breakthrough curve data. A. and B. represent the cytochrome *c* data, C. and D. the chymotrypsin data, and E. and F. the ones for ribonuclease A.

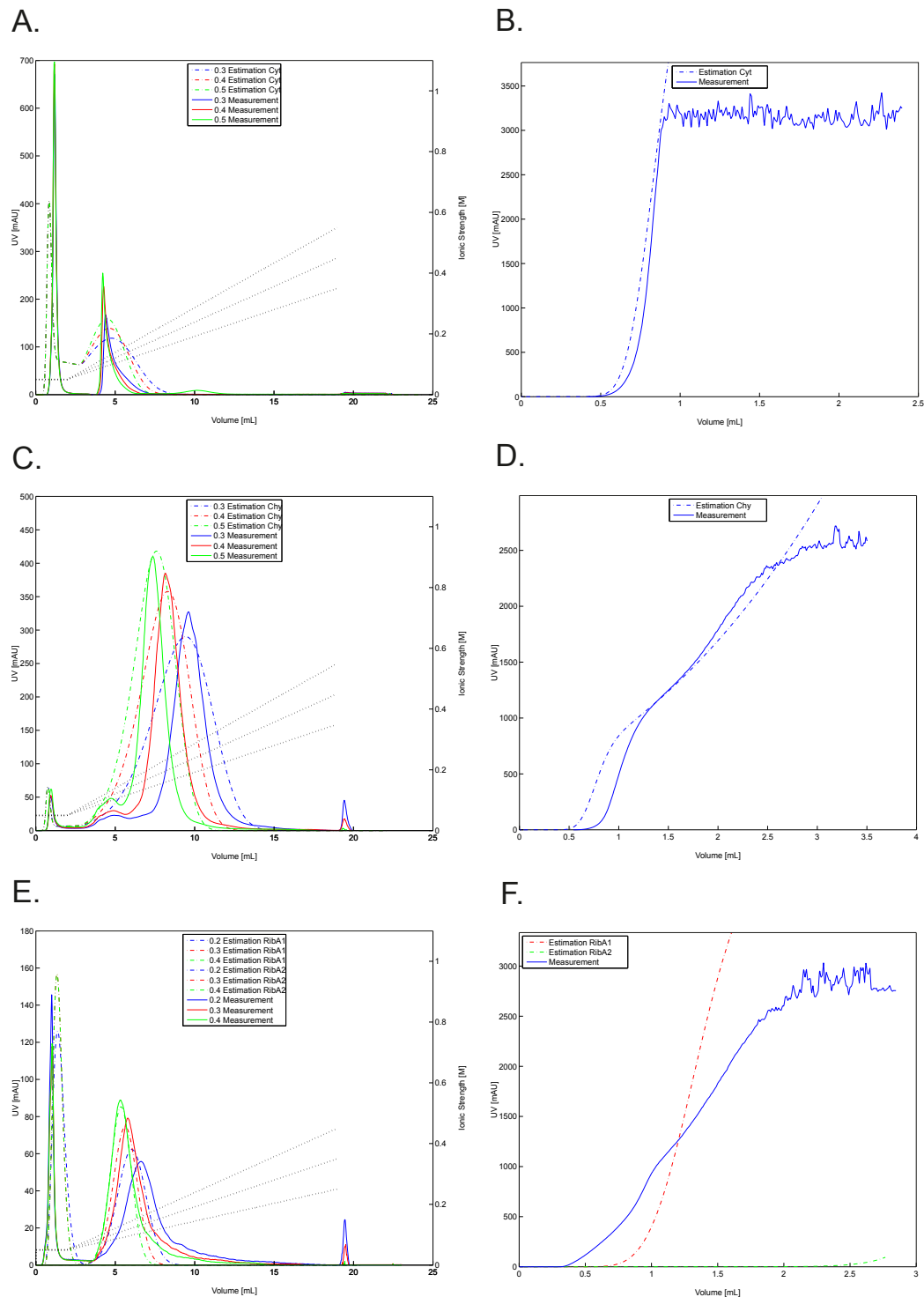


Figure 8.3: Results of the estimation of the isotherm parameters for Q Sepharose FF. A., C., and E. show the measured (solid lines) and estimated (dashed lines) data for the linear gradient elution experiments. B., D., and F. present the corresponding breakthrough curve data. A. and B. represent the cytochrome *c* data, C. and D. the chymotrypsin data, and E. and F. the ones for ribonuclease A.

Table 8.2: Estimated isotherm parameters for cytochrome *c* (Cyt), chymotrypsin (Chy) and the two ribonuclease A components (RibA1 and RibA2) on the Poros 50HS and the Q Sepharose FF column.

Poros 50HS		Cyt	Chy	RibA1	RibA2
kinetic	k_{kin}	0.054	0.049	0.1	0.203
equilibrium	k_{eq}	497.327	32.213	3.128	55.527
charge	ν	4.447	4.575	3.673	3.128
shielding	σ	5.001	0.1	53.245	2.964
Q Sepharose FF		Cyt	Chy	RibA1	RibA2
kinetic	k_{kin}	0.3	0.465	2	0.067
equilibrium	k_{eq}	0.009	0.033	3.722	0.22
charge	ν	2.25	2.61	0.066	1.545
shielding	σ	1	16.131	40.441	15.842

8.5.3 *In silico* Process Optimization

8.5.3.1 Concerted Flowsheet Optimization

After characterization of the Poros 50HS and Q Sepharose FF column with respect to the retention behavior of the model proteins, given in the estimation section, the isotherm parameters were used for *in silico* optimization of the process sequence. In this sequence, the salt gradients' starting point in time and concentrations and the gradient slopes and lengths were optimized within predefined ranges for both columns (for details ref. to Fig. 8.1). In addition, the boundaries of fraction collection were optimized for both columns. The fraction collected from the final column was evaluated with respect to the objective function given in Eq. (8.7). The results of concerted optimization after 2300 iterations using a genetic algorithm are given in Figs. 8.4 and 8.5 for the two process flowsheets CEX→AEX and AEX→CEX, respectively. Subfigure A illustrates the optimization approach, Table B presents the optimized parameters. The chromatograms of the optimized IEX are given in C and D for the first and second column, respectively. The gray boxes indicate the boundaries for fraction collection. E presents the protein amounts injected to the first column and the ones collected from the first and second column. Table F summarizes the purity, yield, and fraction volumes for both IEX and gives the calculated objectives.

The concerted optimization of the CEX→AEX process flowsheet leads to a steep gradient starting at 65s at 196mM NaCl and ending at 627s at 992mM (Fig. 8.4 C). In the optimized fraction collected from the CEX, chymotrypsin and ribonuclease A1 can be separated from the target protein cytochrome *c*. Ribonuclease A2 can only be partly separated from the target protein. The fraction collected from the CEX is virtually buffer exchanged to the buffer of the AEX, the protein amount is doubled, and the sample is injected to the AEX. The optimized parameters for the AEX represent a flat gradient starting at 237s at 68mM NaCl and ending at 2378s at 394mM (Fig. 8.4 D). The fraction collection from the AEX starts with the first increase of the cytochrome *c* trace and stops fractionation before the elution of the remaining contaminant ribonuclease A2. The cytochrome *c* purity can be

increased from initially 25% to nearly 90%, accepting a loss of about 45%. The objective function which has to be minimized starts at a value of 0.75 for the initial sample, decreases after the CEX to 0.53, and finally gives a value of 0.36.

The concerted optimization of the AEX→CEX process flowsheet leads to a gradient starting at 151s at 93mM NaCl and ending at 1522s at 571mM (Fig. 8.5 C). In the optimized fraction collected from the AEX, chymotrypsin and ribonuclease A2 can be partly separated from the target protein cytochrome *c*. Ribonuclease A1 cannot be separated from the target protein. The fraction collected from the AEX is virtually buffer exchanged to the buffer of the CEX, the protein amount is doubled, and the sample is injected to the CEX. The optimized parameters for the CEX represent a steep gradient starting at 83s at 91mM NaCl and ending at 551s at 979mM (Fig. 8.5 D). The boundaries for fraction collection from the CEX are capable to separate chymotrypsin and ribonuclease A1 almost completely from the target protein. The amount of residual ribonuclease A2 remains almost constant. The cytochrome *c* purity can be increased from initially 25% to nearly 66%, accepting a loss of about 31%. The objective function which has to be minimized starts at a value of 0.75 for the initial sample, falls in quality after the AEX to 0.78, and finally gives a value of 0.60.

Comparing the two process flowsheet options, the CEX→AEX sequence leads to an objective of 0.36 and the AEX→CEX sequence to an objective of 0.60. Therefore, the CEX→AEX sequence is superior to the alternative IEX arrangement based on the given objective function. In the following Section 8.5.3.2, the found process optimum for the CEX→AEX sequence using a concerted optimization approach is compared to the same IEX arrangement, however using a sequential optimization approach.

8.5.3.2 Sequential Process Optimization

In the sequential process optimization approach given in Fig. 8.6 A, the CEX is optimized separately. Afterwards, the optimal fraction collected from the CEX is subjected to the AEX optimization.

The sequential optimization of the CEX→AEX process flowsheet was carried out for 2300 iterations on the CEX and the same number of iterations for the AEX to ensure comparability to the concerted optimizations with 2300 iterations for the whole process.

The optimization leads to a steep gradient starting at 50s at 195mM NaCl and ending at 724s at 915mM (Fig. 8.6 C). In the optimized fraction collected from the CEX, chymotrypsin and ribonuclease A1 can be separated from the target protein cytochrome *c*. Ribonuclease A2 can only be partly separated from the target protein. The fraction collected from the CEX is virtually buffer exchanged to the buffer of the AEX, the protein amount is doubled, and the sample is injected to the AEX. The optimized parameters for the AEX represent a flat gradient starting at 51s at 172mM NaCl and ending at 2279s at 234mM (Fig. 8.6 D). The fraction collection from the AEX exhibits the same purity as the fraction collected from the CEX (60%), but a lower yield of the target protein. The cytochrome *c* purity can be increased from initially 25% to nearly 60%, accepting a loss of about 27%. The objective function which has to be minimized starts at a value of 0.75 for the initial sample, decreases after the CEX to 0.46, and finally gives a value of 0.59. The decline of

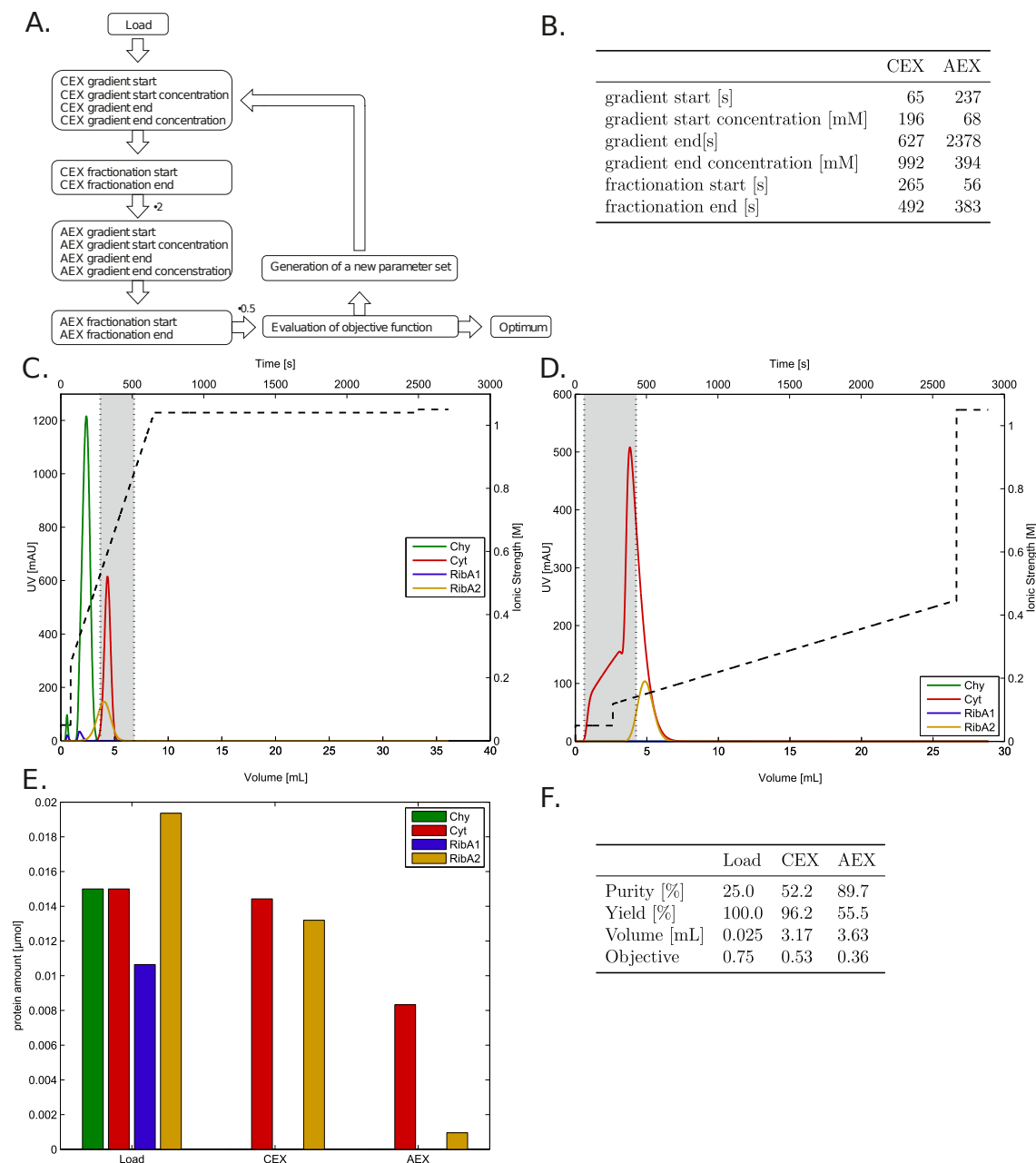


Figure 8.4: Results of the concerted *in silico* optimization of Poros 50HS (CEX) and Q Sepharose FF (AEX). The optimization principle is given in A. Table B summarizes the results of the parameter optimization. C. and D. present the corresponding chromatograms of the CEX and AEX, respectively. The gray boxes illustrate the boundaries of fraction collection. E. indicates the protein amounts injected to the first column and the ones collected from each column. Table F. summarizes the outcome of the process optimization.

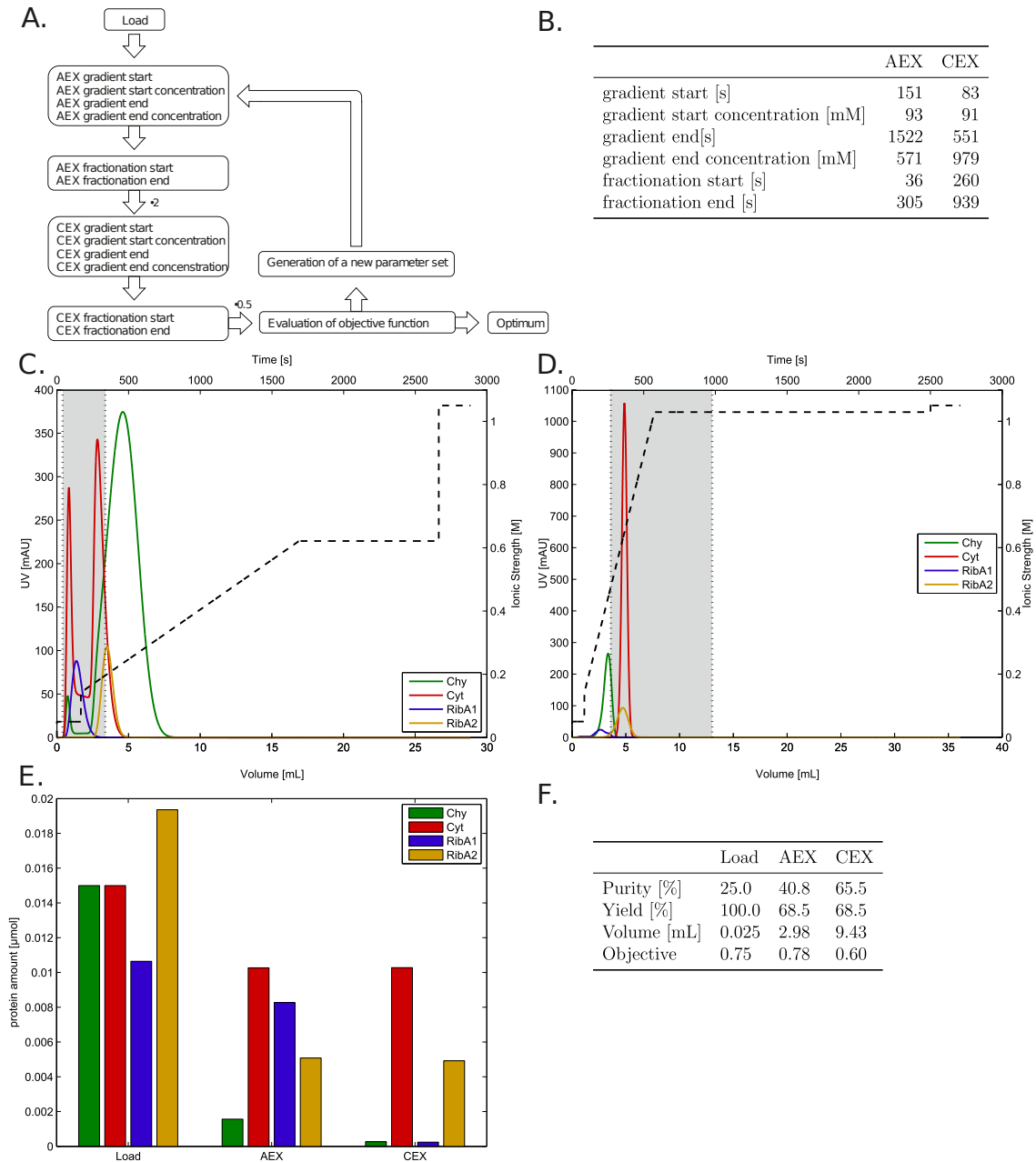


Figure 8.5: Results of the concerted *in silico* optimization of Q Sepharose FF (AEX) and Poros 50HS (CEX). The optimization principle is given in A. Table B summarizes the results of the parameter optimization. C. and D. present the corresponding chromatograms of the AEX and CEX, respectively. The gray boxes illustrate the boundaries of fraction collection. E. indicates the protein amounts injected to the first column and the ones collected from each column. Table F. summarizes the outcome of the process optimization.

process performance from CEX to AEX is due to the failure to enhance the product purity on the final column, while accepting a loss of product. From a practical point of view, the process would have been stopped after the initial CEX, but this case study focuses on the comparison of a concerted and a sequential multi-column process optimization.

In comparison with the concerted optimization approach of the CEX→AEX process flow-sheet which gave an objective of 0.36, the sequential optimization shows an objective of 0.59. Therefore, the concerted optimization approach achieved a superior process in comparison to the sequential approach, based on the given objective function.

8.5.4 Experimental Process Evaluation

To validate the best *in silico* chromatographic sequence, namely Poros 50HS→Q Sepharose FF, this process is reproduced in lab experiments. In the *in silico* process, the buffer is exchanged virtually, the salt concentration is adjusted to the initial condition of the QFF, and the protein amount is doubled. In the experimental evaluation, the Poros operation is carried out twice, the two fractions are pooled and the buffer is exchanged using a UF/DF spin filter. Afterwards, the sample is injected to the QFF column. Fig. 8.7 presents the experimental results of the reproduced sequence. The blue line corresponds to the 280nm protein sum signal. The red 527nm signal equates to cytochrome *c*. The ratio of high salt buffer applied to the column entrance and the conductivity trace recorded at the column outlet are given by the dashed and dotted black curves. Fig. 8.7 A presents the experimental results of the Poros 50HS run, corresponding to the *in silico* optimum given in Fig. 8.4 C. In the experimental chromatogram, there is a minor flow-through fraction of proteins apart from cytochrome *c*. The *in silico* optimum reveals a fraction of chymotrypsin and ribonuclease A1 being apparent in the flow-through. The *in silico* optimization predicts the majority of proteins, eluting within two peaks in the increasing salt gradient. The first one contains chymotrypsin, ribonuclease A1 and a minor fraction of ribonuclease A2. The second peak, which corresponds to the *in silico* collected fraction, equates to the residual ribonuclease A2 and the target component cytochrome *c*. The experimental validation of this prediction is given in Fig. 8.7 A. In the validation, the two peaks are less resolved than in the simulation. The experimental peak size and the distribution of the target component cytochrome *c* is in accordance with the model prediction. The boundaries for fraction collection cover the cytochrome *c* peak.

The buffer of the collected fraction is exchanged with a spin filter and the doubled protein amount is injected to the Q Sepharose FF column. The *in silico* and experimental chromatograms are given in Figs. 8.4 D and 8.7 B, respectively. The model predicts that about half of the cytochrome *c* flows through the column without binding. The residual cytochrome *c* co-elutes with the remaining contaminant ribonuclease A2 at the beginning of the salt gradient. The experimental validation revealed greater deviations from the model prediction, but the overall peak composition still matches. Cytochrome *c* elutes in the flow-through and at the beginning of the salt gradient. The amount of protein besides cytochrome in the second peak is still predominant. The elevated baseline in Fig. 8.7 B results from the 1-methylpiperazine buffer and the increased salt concentration. However, the peak resolution and shape do not match to the model predictions acceptably.

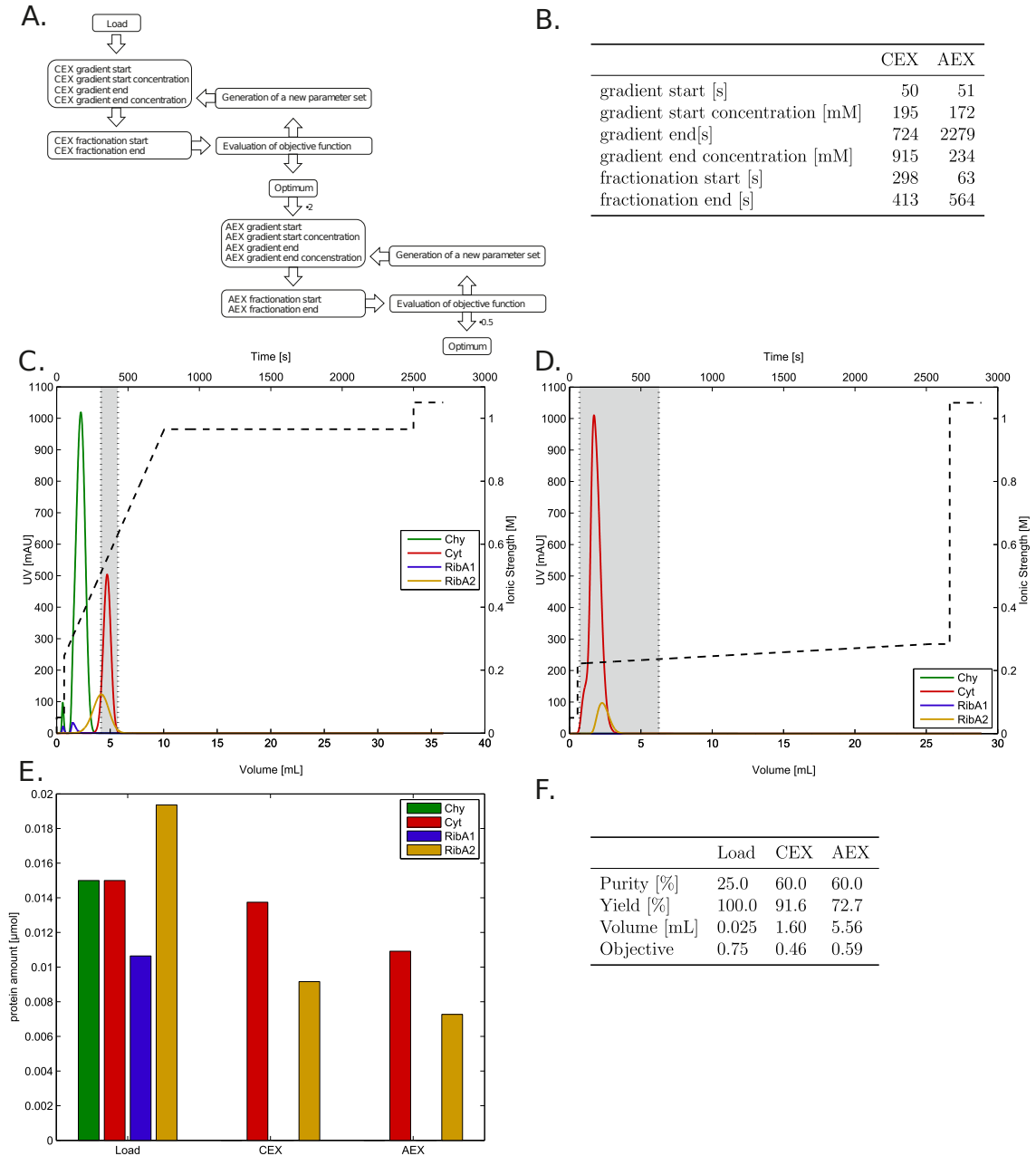


Figure 8.6: Results of the sequential *in silico* optimization of Poros 50HS (CEX) and Q Sepharose FF (AEX). The optimization principle is given in A. Table B summarizes the results of the parameter optimization. C. and D. present the corresponding chromatograms of the CEX and AEX, respectively. The gray boxes illustrate the boundaries of fraction collection. E. indicates the protein amounts injected to the first column and the ones collected from each column. Table F. quantifies the outcome of the process optimization.

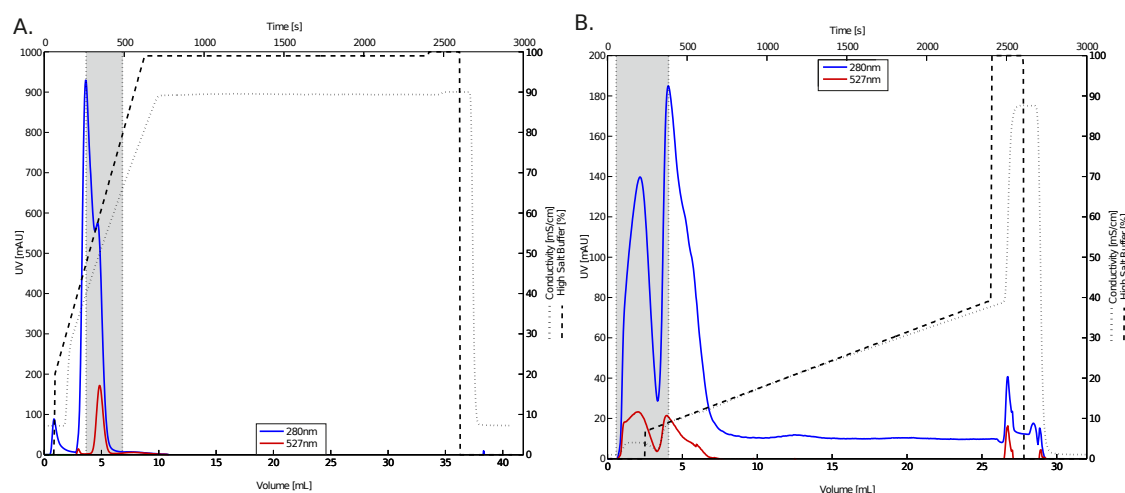


Figure 8.7: Experimental validation of the *in silico* optimized process. A presents the Poros 50HS and subfigure B the Q Sepharose FF chromatogram. The blue 280nm signal corresponds to the sum of proteins, the red 527nm signal is cytochrome *c* specific. The dashed and dotted black curves represent the ratio of high salt buffer applied to the column inlet and the conductivity trace, detected at the column outlet. The gray boxes indicate the boundaries for fraction collection.

8.5.5 Model-based Error Analysis

To evaluate the reasons for this mismatch between experimental data and the model prediction in AEX, the conductivity traces in Fig. 8.7 B were examined in more detail. Fig. 8.8 A presents the ratio of high salt buffer at column inlet (dashed line) and the conductivity trace recorded at the outlet (dotted line) in the experimental validation. The dotted conductivity trace exhibits an increase during the sample injection from about one to four mS/cm . The *in silico* optimized AEX step given in Fig. 8.4 D, does not account for this elevation of conductivity. To correct the model with respect to the experimental reality, the salt concentration of the sample injected to the Q Sepharose FF column, was *in silico* estimated and adjusted to 30mM NaCl. The resulting model prediction of the ionic strength traces is given in Fig. 8.8 B. It is obvious that the introduction of 30mM NaCl to the injected sample, leads to a correction of the predicted traces. The effect of the modified salt concentration to the *in silico* chromatogram is given in Fig. 8.8 C. For clarity, only the two remaining major proteins, cytochrome *c* and ribonuclease A2 are shown. The appearance of two poor-resolved peaks, both containing cytochrome *c* and just the latter one containing ribonuclease A2, matches the model prediction better.

8.6 Discussion

The model-based concerted optimization showed the superiority of the process flowsheet combining CEX→AEX as compared to the AEX→CEX process. Within the CEX→AEX process, the Poros 50HS exhibits a steep salt gradient. The majority of contaminants elute in the flow-through after sample injection and at the beginning of the salt gradient. The optimized boundaries for fraction collection match the peak of the target component cytochrome *c*. The collected fraction contains residual ribonuclease A2, which is difficult

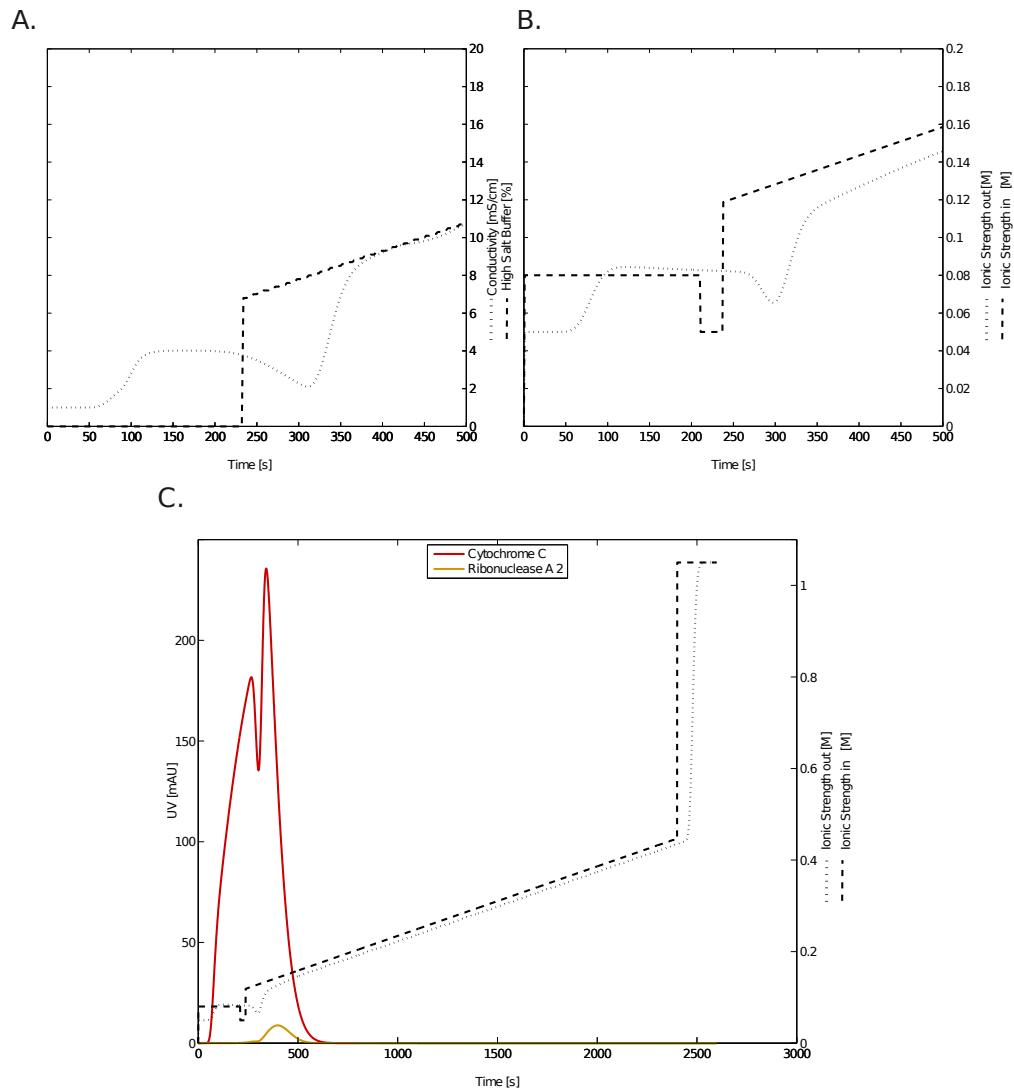


Figure 8.8: Evaluation of an elevated ionic strength of the protein sample, injected to the Q Sepharose FF column. Subfigure A presents the experimental traces for the ratio of high salt buffer applied to the column inlet (dashed line) and the conductivity trace recorded at the column outlet (dotted line). Subfigure B shows the effect of an elevated ionic strength of the injected protein sample. The dashed line shows the *in silico* ionic strength at the column entrance, the dotted line the *in silico* ionic strength at the column outlet. Subfigure C presents the effect of an elevated ionic strength of the injected sample to the chromatogram recorded *in silico* from Q Sepharose FF.

to separate from the target protein due to similar physico-chemical properties. In the subsequent AEX, the cytochrome *c* purity can be increased from 52% to nearly 90%, accepting a loss of half of the target species. After the final AEX, the achieved objective is 0.36 in comparison to the inferior AEX→CEX process with an objective of 0.6. The optimized process flowsheet is strongly influenced by the composition of the objective function and the introduced weighting factors. If protein purity or a high yield is the more important attribute, this can be considered by the modification of weighting factors.

To prove the necessity of a concerted process optimization, we reproduced the best column arrangement found in the concerted optimization within a sequential process optimization. In the sequential approach, the CEX was optimized independently and afterwards, the found optimum was used in a subsequent optimization of the AEX (for more details, ref. to Fig. 8.6 A).

In comparison to the concerted CEX→AEX process with a purity of 52%, a yield of 96%, and an objective of 0.53 after the initial CEX, the sequential optimization results in a purity of 60%, a yield of 92%, and an objective of 0.46 after the CEX. Therefore, the optimization of the CEX solely is superior to the intermediate result of the concerted process optimization. This finding coincides with the general expectation, because the concerted optimization intends to achieve a minimal objective after the final AEX, disregarding the quality of intermediate results like the fraction collected from the CEX. After the final AEX, the concerted optimization leads to a purity close to 90%, a yield of 56%, and an objective of 0.36. In contrast, the sequential optimization results in a final purity of 60%, a yield of 73%, and an objective of 0.59. Therefore, the result of the concerted optimization for the final AEX is superior to the one found for the sequential optimization. In addition, the objective for the concerted optimization is also superior to the intermediate result of the sequential optimization. This finding underlines the impressive capability of the concerted process optimization approach to avoid an over- or under-optimization of single intermediate states, as occurred for the sequential optimization. The latter one over-optimizes the intermediate CEX, indeed achieving an excellent intermediate result, but being clearly inferior when looking at the overall process performance.

The number of 2300 iterations in the optimization algorithm was kept constant for the two concerted processes. For the sequential process optimization, 2300 iterations per single IEX were used. Therefore, comparability of the found optima should be given with respect to an equal computational effort. However, it remains unclear whether the late termination of fraction collection in the sequential AEX (ref. Fig. 8.6 D) in comparison with the concerted CEX→AEX process (ref. Fig. 8.4 D) is coincidental.

To verify the *in silico* process optimization, the best process, namely the concerted optimized sequence of CEX→AEX, is reproduced in lab experiments.

The experimental reproduction of the *in silico* optimum for the CEX matches the model-derived data. The model predicts the flow-through and the two peaks within the salt gradient accurately. Minor differences occur with respect to the resolution of the two major peaks.

The *in silico* optimization of the subsequent Q Sepharose FF leads to a flat salt gradient elution profile. The contaminants exhibit a slightly greater affinity to the resin. About half of the target component cytochrome *c* elutes in the flow-through during sample injection.

The flow-through is collected as target fraction. The residual cytochrome *c* and the major contaminant ribonuclease A2 co-elute at the begin of the salt gradient. The co-eluting proteins are discharged due to the requirement of cytochrome purity in the objective function. The experimental validation of the optimized AEX operation reveals aberrations from the model prediction. In the experimental chromatograms, the flow-through peak and the one eluting at the beginning of the salt gradient achieve a better peak separation. In conjunction with this finding, there are differences in the overall peak shape.

We attribute the accurate prediction of the CEX and the difficulties with the AEX to the poorer model parameter estimation for the QFF in contrast to the Poros 50HS runs. The assumption that e.g. ribonuclease A consists of just two different species simplifies the more heterogeneous composition of ribonuclease species. This simplification has a negative impact on the quality of the estimation. In analytical chromatographic runs of the different model proteins, in AEX there are more protein peaks visible (data not shown). In addition, effects of propagation of uncertainty have to be considered. In practice, there are minor experimental process uncertainties apparent during the Poros 50HS run. These inaccuracies, e.g. in the collection of the target fraction, will propagate during the second column. To account for this finding, a term considering the process robustness or insensitivity against minor process changes might be introduced into the objective function in future experiments.

In addition to this general difficulty of considering the propagation of uncertainties [19; 124], we review the model-based approach to analyze the impact of potential contributors to the inaccurate fit of the experimental to the *in silico* data. The conductivity traces from the AEX validation experiments revealed an increase from one to four mS/cm during the sample injection (ref. Fig 8.7 B). The *in silico* process optimization does not exhibit this increase in conductivity during sample injection (ref. Fig. 8.4 D), because it assumes a complete buffer exchange in between the two IEX. To prove that the incomplete exchange of buffer during the experimental process validation is the major contributor to the uncertainty of the modeling approach, we estimated and adjusted the protein sample injected to the AEX *in silico* to a NaCl concentration of $30mM$. Fig. 8.8 presents the consequence of an elevated salt concentration of the sample injected to the AEX onto the AEX chromatogram. The increased salt concentration shifts the elution profile of cytochrome *c* in a manner that the *in silico* chromatogram and the one obtained during the experimental validation achieve an excellent degree of similarity. This finding indicates that the application of model-based tools within protein purification tasks is not only restricted to process development, but also capable of identifying critical process parameters or critical unit operations. Such an approach could probably support a QbD-driven approval of pharmaceuticals [19; 30; 165]. In the presented *in silico* optimized model process, the imperfectness of buffer exchange in between the two IEX seems to be the most critical operation to be considered. In comparison to classical process development using DoE, the overall sample consumption is reduced. For the three linear gradient elutions, $25\mu L$ of a $0.6mM$ protein solution were required per gradient ($1.2mM$ for ribonuclease A). The breakthrough curves (BC) constitute the major contributor to the overall protein consumption, as volumes from 5 to $10mL$ protein solution per BC were required. The BC is only necessary to estimate the shielding parameter σ within the SMA isotherm, so BCs are only required if the model has to extrapolate to the non-linear adsorption range of the isotherm. Otherwise, the protein consumption can be reduced extremely.

In addition, the time requirement can probably be minimized in contrast to classical DoE approaches to process optimization. An additional advantage of model-based process optimization in contrast to DoE approaches is that the lab experiments and parameter estimation have to be carried out just once. Testing, for example, different objective functions or column arrangements only demands multiple *in silico* process optimization cycles. In contrast, classical DoE approaches would require additional lab experiments, e.g. to incorporate the different possibilities of salt gradient profiles.

The model system used in this case study consists of two pure proteins (cytochrome *c* and chymotrypsin) and ribonuclease A which was treated as a two-component mixture. Beside the estimation of two isotherm parameter sets from one chromatogram, the presented modeling approach is also capable of predicting more heterogeneous protein mixtures. The latter case is just dependent on adequate analytics for fraction analysis.

In this study we used the SMA isotherm to model the interaction of the proteins with the adsorber surface. The use of a 'simpler isotherm' such as Langmuir is not practical because of the need to respect salt gradients. The SMA isotherm would reduce to Langmuir isotherm for $c_{salt} = const.$ and $\nu = 1$. According to Parente and Wetlaufer [129] $\nu = 1$ implies that the retention volumes of the species would have to fulfill $V_r \cdot (c_{gradient,end} - c_{gradient,begin}) = const.$ This is not the case in our results. Furthermore, some of the breakthrough experiments show a short steep ascent followed by a slower rise (Figs. 8.2 F, 8.3 D). This behavior could only be modeled with slow kinetics (steep ascent) and non-zero shielding parameter (slower rise). Equilibrium models or a pure stoichiometric displacement model would not have been sufficient.

8.7 Conclusion

We presented an approach to a model-based integrated downstream process optimization, considering a flowsheet optimization, the salt gradient elution profile, and the boundaries for fraction collection for two subsequent IEX steps. The modeling and process optimization approach was successfully applied to the task of global optimization of the chromatographic operations. The systematic comparison of sequential and concerted process optimization proved that a concerted process optimization approach prevents over- or under-optimization of single-unit operations. The time and effort to calibrate a model for concerted or two models for sequential optimization is identical.

The drawback of this concerted optimization approach is the impossibility to do the computation for the two columns in parallel, e.g. by the distribution across multiple computers, to reduce the overall time consumption.

Difficulties with the intermediate operation of exchanging the buffer system highlighted the need for an integration of such operations into the modeling approach. In future, intermediate operations such as ultra-/diafiltration will be integrated into our modeling approach, e.g. by inclusion of black-box models in between the chromatographic operations.

In addition, we applied our modeling tool to the evaluation of the impact of an imperfect buffer exchange operation in between the two IEX. The presented methodology might be

a useful tool in QbD-based approvals of biopharmaceuticals, especially for identification and characterization of critical process parameters.

The presented optimization approach using an in-house developed software toolbox is extendable to greater process sequences, including commonly used platforms in DSP. Furthermore, our modeling approach and the implemented software are capable of handling larger numbers of protein species (e.g. mAb heterogeneity or sets of host cell proteins) and are not restricted to small-scale chromatographic columns. Concluding, model-based optimization is open to coping with industrial downstream process development.

Acknowledgment

We kindly thank Anna Bogutzki who contributed to the experimental data acquisition for model calibration. The authors gratefully acknowledge financial support and technical advice by Roche Diagnostics GmbH (Penzberg, Germany). The research leading to these results has partly received funding from EUROTRANS-BIO (grant agreement no. 0316071B, EC's Seventh Framework Program).

9 | Conclusion and Outlook

In this thesis we implemented a methods portfolio which can support downstream process development based on mechanistic modeling. The software ChromX was introduced as a tool for model-based process development, enabling the application of the technology in teaching and in academic research. As a contribution to a more sophisticated way of model calibration, we established an alternative experimental method to determine the ionic capacity in column chromatography and extended the technology to batch chromatography. By the way this method is capable to quantify the amount of adsorber in batch chromatography, opening up the possibility for future hybrid approaches, linking mechanistic modeling and high-throughput process development. Model parameters are commonly estimated based on experimental data. We addressed the problem of planning and selecting the experiments with the highest information content. Chromatographic processes are usually monitored and controlled based on uv signals. Mechanistic modeling is carried out based on molar or mass concentrations. We resolved this limitation, by introducing a reformulation of the model equations, enabling the direct usage of uv signals in model calibration. High-throughput process development (HTPD) is a further key technology in downstream process development, that was until now, mostly used apart from mechanistic modeling. HTPD can pose a huge challenge on the throughput of subsequent analytical techniques. We addressed this challenge by the adaptation of a photometric high-throughput analytical method to batch chromatography, enabling the integrated generation of multi-component batch isotherms on a robotic work station. In a first application case study we compared the traditional process development approach, based on DoE with mechanistic modeling. Finally, we extended the commonly employed single column modeling technology to the modeling of multi-column processes.

Summing up, we could implement several technologies, which can serve as a kind of building blocks for future process development concepts. Nevertheless, the fields of mechanistic modeling, HTPD, and future hybrid approaches are rapidly developing. From an academic and probably also from an industrial perspective, the model equations have to be extended continuously. Effects such as reactions on the adsorber surface, leading to an aggregate formation and dissolution or the consideration of proteins, exhibiting multiple binding orientations are not addressed adequately. With respect to future hybrid approaches, combining model-based approaches and HTPD, the definition of a technology interface has to be focused in future research. Mechanistic modeling can probably simplify the current way of designing high-throughput experiments, while maximizing the knowledge derived from the experimental data.

A | Supporting Information

A.1 Supporting Information for: Simulating and Optimizing Preparative Protein Chromatography with ChromX

Tobias Hahn¹, Thiemo Huuk¹, Vincent Heuveline², Jürgen Hubbuch¹

¹ Karlsruhe Institute of Technology (KIT), Institute of Process Engineering in Life Sciences, Section IV: Biomolecular Separation Engineering, Karlsruhe, Germany

² Heidelberg University, Interdisciplinary Center for Scientific Computing, Engineering Mathematics and Computing Lab, Heidelberg, Germany

A.1.1 List of Model Parameters

Symbol	Unit Type	Recommended Unit	Description
c	Conc.	M	Mobile phase concentration in interstitial volume
c_p	Conc.	M	Mobile phase concentration of protein in pore volume
$c_{p,s}$	Conc.	M	Mobile phase concentration of salt in pore volume
r_p	Length	mm	Particle radius of adsorbent
D_{app}	$\frac{\text{Length}^2}{\text{Time}}$	$\frac{\text{mm}^2}{\text{s}}$	Apparent dispersion coefficient
D_{ax}	$\frac{\text{Length}^2}{\text{Time}}$	$\frac{\text{mm}^2}{\text{s}}$	Axial dispersion coefficient
D_{pore}	$\frac{\text{Length}^2}{\text{Time}}$	$\frac{\text{mm}^2}{\text{s}}$	Pore diffusion coefficient
ε_{Col}	-	-	Column/bed porosity
ε_{Bead}	-	-	Stationary phase porosity
ε_{Tot}	-	-	Total porosity
k_{eff}	$\frac{\text{Length}}{\text{Time}}$	$\frac{\text{mm}}{\text{s}}$	Effective film/pore transfer coefficient
k_{eq}	-	-	Adsorption equilibrium coefficient
$k_{eq,L}$	Conc. ⁻¹	M ⁻¹	Adsorption equilibrium coeff. for Langmuir isotherm
k_{kin}	Time·Conc. ^ν	sM ^ν	Adsorption rate coefficient
L_{Col}	Length	mm	Column length

Λ	Conc.	M	Stationary phase ionic capacity
ν	-	-	Characteristic charge for SMA isotherm
q	Conc.	M	Stationary phase concentration of protein
q_{max}	Conc.	M	Single-component max. conc. for Langmuir isotherm
q_s	Conc.	M	Stationary phase concentration of salt
σ	-	-	Steric shielding coefficient for SMA isotherm
t	Time	s	Time dimension
u_{int}	$\frac{\text{Length}}{\text{Time}}$	$\frac{\text{mm}}{\text{s}}$	Interstitial mobile phase velocity
x	Length	mm	Space dimension

A.1.2 Experimental Parameter Determination

In the laboratory course, initial experiments were conducted to determine system properties. Afterwards, four experiments in the bind/elution mode were performed for parameter estimation, i.e. one step elution and two gradient elutions with a low sample volume and one gradient elution with a large sample volume.

First, the necessary system and column parameters were determined and verified by checking the agreement of the simulated salt elution profile and conductivity signal. Then, the isotherm parameters were determined by chromatogram fitting.

A.1.2.1 Dead Volumes

The system's dead volumes from the auto-sampler to the UV detector and to the conductivity detector were determined with an acetone pulse injection without column to be $V_{dead,cond} = 140 \mu L$ and $V_{dead,UV} = 122 \mu L$.

A.1.2.2 Column and Bead Dimensions

In this case study, a pre-packed SP Sepharose FF column (GE Healthcare, $L_{Col} = 25 \text{ mm}$, $V_{Col} = 0.962 \text{ mL}$) was used. The radius of the adsorber beads is 0.045 mm according to the manufacturer.

A.1.2.3 Linear Flow Rate

The pump flow was set to $u_{Vol} = 0.962 \text{ mL/min}$. In ChromX, we have to specify the flow in distance/time. We use the units mm and s below, as they fit the process scale best. The linear flow rate can be calculated easily as shown below.

$$u \left[\frac{\text{mm}}{\text{s}} \right] = \frac{L_{col}}{V_{col}} \cdot \frac{u_{vol} \left[\frac{\text{mL}}{\text{min}} \right]}{60} = \frac{25}{0.962} \cdot \frac{0.962}{60} \frac{\text{mm}}{\text{s}} = 0.4167 \frac{\text{mm}}{\text{s}} \quad (\text{A.1})$$

A.1.2.4 Porosities

20 μL pulse injections of 1 M NaCl (pore-penetrating) and 10 g/L dextran (2000 kDa, non-pore-penetrating) at the same flow rate were used to determine the porosities. The measured retention volumes were $V_{NaCl,rt} = 0.98 \text{ mL}$ and $V_{Dex,rt} = 0.38 \text{ mL}$. We first subtract the respective system dead volumes

- $V_{NaCl} = V_{NaCl,rt} - V_{dead,cond} = 0.84 \text{ mL}$,
- $V_{Dex} = V_{Dex,rt} - V_{dead,UV} = 0.258 \text{ mL}$,

and then calculate the porosities

- Total porosity: $\varepsilon_{tot} = \frac{V_{NaCl}}{V_{col}} = \frac{0.84}{0.962} = 0.873$,
- Column porosity: $\varepsilon_{col} = \frac{V_{Dex}}{V_{col}} = \frac{0.258}{0.962} = 0.268$,
- Bead porosity: $\varepsilon_{bead} = \frac{V_{NaCl} - V_{Dex}}{V_{col} - V_{Dex}} = 0.827$.

A.1.2.5 Axial Dispersion

The axial dispersion coefficient D_{ax} can be derived from the broadening of the dextran pulse. Moment analysis for the injection of an ideal Dirac pulse of a non-pore-penetrating, non-interacting tracer yields the following Eq. (A.2) for the parameter σ_{Dex} of the resulting Gaussian peak that can be solved for D_{ax} . [156]

$$\sigma_{Dex}^2 = 2D_{ax}L_{Col} \left(\frac{\varepsilon_{Col}}{u} \right)^3. \quad (\text{A.2})$$

Typically, the control software of the chromatography system includes peak analysis tools that calculate this value automatically or the height equivalent of a theoretical plate (HETP), which is defined as the rate of increase of the Gaussian peak profile per unit length, and can be written as in Eq. (A.3). [109; 156]

$$HETP = \frac{\sigma_{Dex}^2}{L_{Col}} \left(\frac{u}{\varepsilon_{Col}} \right)^2 = 2D_{ax} \left(\frac{\varepsilon_{Col}}{u} \right). \quad (\text{A.3})$$

Here, we obtained the value $HETP = 0.4798 \text{ mm}$. Using the linear flow rate and the column porosity from above, we can now calculate the axial dispersion coefficient

$$D_{ax} = HETP \cdot \frac{u}{2 \cdot \varepsilon_{col}} = 0.373 \text{ mm}^2/\text{s}. \quad (\text{A.4})$$

Table A.2: Bind/elute experiments.

Elution Mode	Sample Volume (mL)	Vol-Gradient/Step Height (% Buffer B)	Length of Elution (CV)
Step	0.5	15	10
Gradient	0.5	50	10
Gradient	0.5	100	10
Gradient	60	50	10

A.1.2.6 Ionic Capacity

The total ionic capacity Λ of the packed resin was determined by acid-base titration.[72] The column is flushed with 0.5 M HCl, such that all ligands are saturated with H⁺ ions and then washed with ultrapure water. We then inject 0.1 M NaOH ($= c_{NaOH}$) solution to replace H⁺ by Na⁺ ions. The conductivity signal starts to increase at $V_{NaOH} = 3.27 \text{ mL}$. Consequently, $c_{NaOH} \times V_{NaOH} = 0.327 \text{ mol}$ are exchanged. To obtain the capacity of the stationary phase, we divide by its volume, expressed by total column volume and total porosity:

$$\Lambda = \frac{V_{NaOH} \cdot c_{NaOH}}{V_{col} (1 - \varepsilon_{tot})} = 2.677 \text{ M}. \quad (\text{A.5})$$

A.1.2.7 Bind/Elute Experiments

Three experiments with a low sample volume (0.5 mL) and one with a breakthrough (60 mL) were conducted with the mixture of antibody, lysozyme, and myoglobin. The used buffers were Buffer A (20 mM Bicine, 0 mM NaCl, pH 8.2) and Buffer B (20 mM Bicine, 1000 mM NaCl, pH 8.2). Elution was initiated 5.2 mL after the end of injection with the settings given in Table A.2, followed by washing with 100 % Buffer B after 9.5 mL \approx 10 column volumes (CV). As salt was not injected via the auto-sampler, but via a mixing chamber, an additional dead volume of 1.35 mL had to be added to the event in ChromX. In case of steps, the additional dead volume is only 1.10 mL, if a pump wash was performed prior to the step.

The results were exported from the control software as XLS files, including volume, UV 280 nm, and conductivity data columns.

A.1.2.8 Component-specific Parameters

The column parameters were first checked by comparing the simulated salt elution profile with the recorded conductivity signal. Film transfer and pore diffusion parameters for the salt component were estimated.

The proteins' SMA parameters were determined by chromatogram fitting. First, the parameters that are active in the linear range of the isotherm were estimated from the

experiments with a low sample volume. Two gradient experiments are sufficient to determine the characteristic charge and equilibrium parameter by their effect on retention time.[129; 143] The kinetic parameter is responsible for additional peak broadening and can also be determined from low-sample-volume experiments.[86] A step elution experiment was included as well, as film transfer and pore diffusion parameters have a stronger influence on the peak shape in this mode. The steric shielding parameter cannot be estimated from experiments with a low sample volume, as it occurs only in the sum of Eq. (??) which is then close to zero. It was estimated from the experiment with a high sample volume, while keeping the other parameters constant.

A.1.3 Master's Degree Program and Software Exercises

The lecture series on chromatography modeling is well-established in the curriculum of the bioengineering master's degree program at KIT. It shifts the focus from finding a workable solution in the lab to understanding the effects that lead to a certain peak shape in the chromatogram. At first, the partial differential equations seem to have several parameters, but in the course of the lecture series, the influences of void volumes and diffusion effects become more obvious. Relating isotherm parameters to elution peak shapes provides for a connection to practical laboratory experience. The software exercises accompany the lecture series on chromatography modeling and are intended to provide a deeper understanding of the mathematical operators and parameters in the differential equations.

Surveys on the lecture series were conducted by the Executive Support Department of KIT, Section III: Quality Management. In 2014, seven students responded to the survey on the last day of class. From the 28 questions, one of the most important aspects in this context was that the students recognized the importance of the lecture for further study (4.86/5, standard deviation (SD) 0.38, 0=very low, 5=very high). They felt that difficult issues could be presented, liked the practical examples, and were encouraged to work on their own outside class (each 4.71/5, SD 0.49). One student commented that he/she particularly liked the ChromX exercises. In comparison, 14 students performed the software exercises with the Chromulator in 2011. They rated the practical examples and encouragement to learn on their own with 3.93/5 (SD 0.92), and 4.43/5 (SD 0.65). Larger comparative studies would be necessary to find the most effective way to use ChromX in the classroom.

In the following, we present exemplary exercises performed with the Langmuir isotherm.

A.1.3.1 Single-component Ideal Model

Analyze and simulate the following system with a single-component equilibrium Langmuir isotherm:

- Column length = 25 mm, • $k_{eq,L} = 1 \text{ M}^{-1}$,
- Column volume = 0.962 mL, • $q_{max} = 20 \text{ M}$,
- Total porosity = 0.82, • $c(x, 0) = 0 \text{ M}$,
- Flow rate = 1 mm/s, • $c(0, 0 \leq t < 5 \text{ s}) = 0.001 \text{ M}$,
- $D_{app} = 0.01 \text{ mm}^2/\text{s}$, • $c(0, t \geq 5 \text{ s}) = 0 \text{ M}$.

Start a new ChromX session and set the model to *EquilibriumDispersive, NoPoreModel*, and *Langmuir*. For a better resolution, increase the *Axial Cells* to 200 and reduce the *Initial Step* to 0.1. Copy the column parameters from above and remove the Salt component. Set the Langmuir parameters as above and kinetics to zero to obtain the equilibrium model. Adjust the injection start concentration and time of the end of injection.

1. Do your observations agree with the theoretical retention time for an ideal model?
2. Set the injection end to 200 s. Does the time of breakthrough agree with the retention time of a shock?
3. What is the sample concentration that generates a breakthrough at 80.5 s? Validate your result by simulation.
4. Reduce the injection end to 30 s. Describe the result.
5. Estimate when the rear of the peak will reach the base line. Explain deviations.
6. What happens when the capacity doubles and q_{max} increases to 40? Explain.

A.1.3.2 Competitive Adsorption and Displacement

Keep the simulation and column setup of the previous section and simulate two single-component experiments and one with both components:

- Component 1: $k_{eq,L} = 1 \text{ M}^{-1}$, $q_{max} = 20 \text{ M}$,
- Component 2: $k_{eq,L} = 3 \text{ M}^{-1}$, $q_{max} = 10 \text{ M}$,

Both components shall be injected for 20 s with a sample concentration of 0.05 M.

7. Compare the peaks. Explain the result.
8. Increase the injection time to 200 s to simulate a two-component breakthrough experiment. Explain the behavior of the first component.
9. What happens, when adding a third component with $k_{eq,L} = 5 \text{ M}^{-1}$, $q_{max} = 10 \text{ M}$?

A.1.3.3 Proposed Solutions

1. The equation correctly predicts the peak maximum at 113 s (Fig. A.1a).
2. Yes, the inflection point of the breakthrough at 0.0005 M is exactly at 110.5 s (Fig. A.1a).
3. The concentration is 0.5 M (Fig. A.1b).
4. The shock front stays at 80.5 s. We observe a short plateau and a diffuse rear. The peak ends at 145 s (Fig. A.1b).

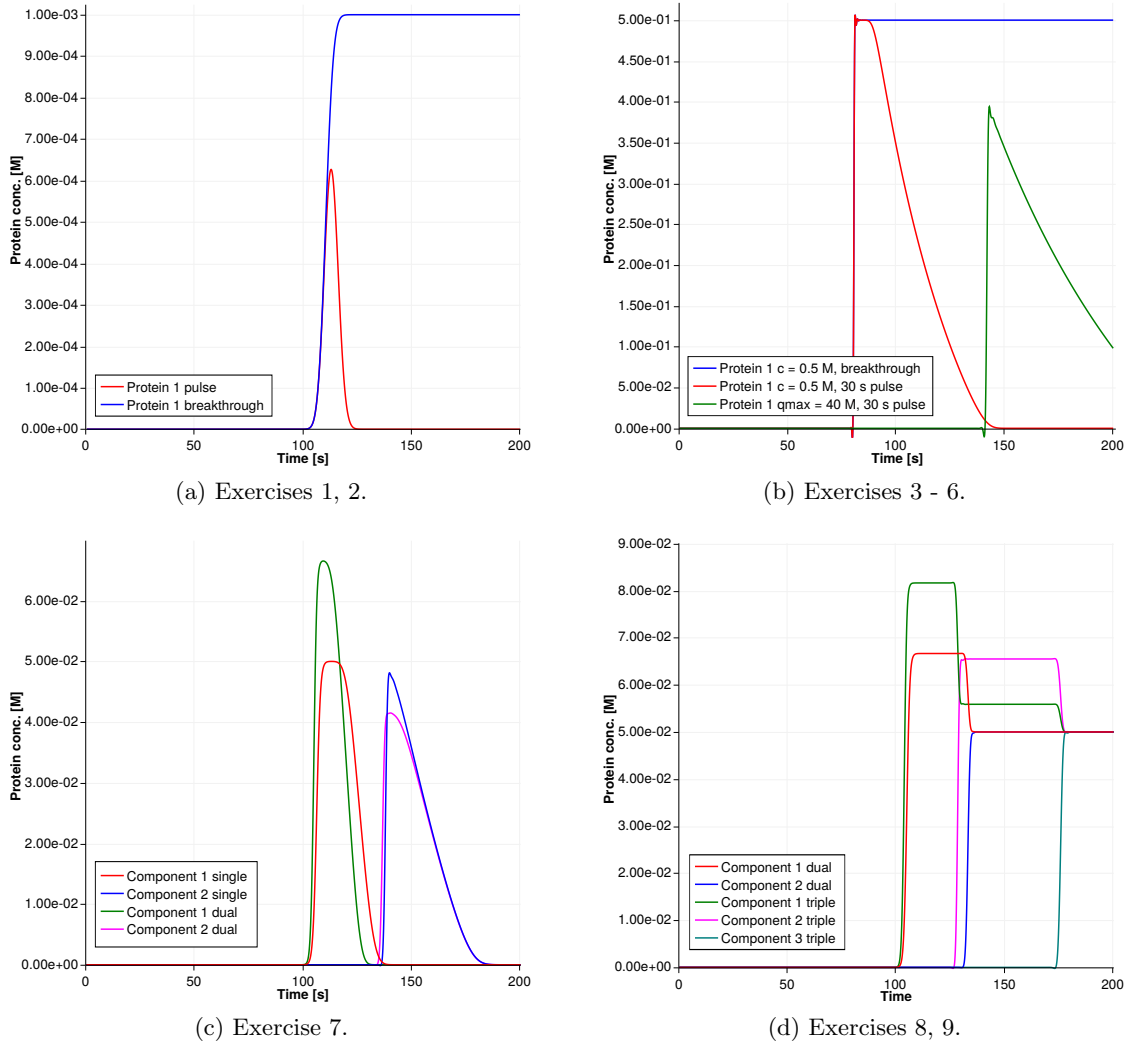


Figure A.1: Plots of simulation results

- The rear of the pulse is to migrate according (with t_{inj} instead of $t_{inj}/2$) and reach the base line at 140.5 s. Because of the non-zero dispersion, additional broadening occurs. The value of $0.01 \text{ mm}^2/\text{s}$ leads to an approximate broadening of 0.05 mm/s in each axial direction. The contact time of $140.5 \text{ s} - 30 \text{ s} = 110.5 \text{ s}$ leads to a total broadening of 5.525 mm . At an interstitial flow rate of $u/\varepsilon_{Tot} = 1/0.82 \text{ mm/s}$, this equals 4.5 s .
- Theoretically, the shock retention time is 110 s and 215.5 s for a symmetrical peak. We observe a shock at 143 s with a height of 0.4 M . Obviously, the intra-column concentrations were not sufficient to develop the whole shock (Fig. A.1b).
- In preparative chromatography, the system response to multi-component feedstocks is not just a superposition of the single-component breakthroughs or peaks. Component 1 competes with Component 2 for binding sites, while having the smaller $k_{eq,L}$ value. It does not adsorb as much as in the single-component case and, thus, migrates faster through the column, resulting in a slightly earlier and higher peak. Component 2 also moves slightly faster, as it cannot bind with the same amount in

the beginning. Again, the concentration migrates faster. As Component 2 follows the even faster moving Component 1, binding sites are constantly freed at the front of the band of Component 2, leading to a less strong shock build-up and a smoother top (Fig. A.1c).

8. Because of its smaller $k_{eq,L}$, Component 1 adsorbs more slowly and the concentration front migrates faster. The following Component 2 partly displaces the first component and the desorbed concentration accumulates in a faster-moving plateau. Because of the nonlinear adsorption behavior described by the Langmuir isotherm, the additional concentration cannot fully re-adsorb.
9. The effect is increased in the three-component setting. Component 1 is displaced even more strongly and also Component 2 shows this behavior. Component 3 having the largest $k_{eq,L}$, follows the others and adsorbs in the three-component equilibrium state.

A.2 Supporting Information for: A Versatile Noninvasive Method for Adsorber Quantification in Batch and Column Chromatography Based on the Ionic Capacity

Thiemo Huuk¹, Till Briskot¹, Tobias Hahn¹, Jürgen Hubbuch¹

¹ Karlsruhe Institute of Technology (KIT), Institute of Process Engineering in Life Sciences, Section IV: Biomolecular Separation Engineering, Karlsruhe, Germany

Table 1: Column chromatography data of Poros 50HS. The means and standard deviations of triplicates per column volume (CV) are given. Gravimetry was carried out as a single measurement. The means and standard deviations of all CVs are shown below the table.

CV / μL	$\varepsilon_{\text{column}}$	$\varepsilon_{\text{particle}}$	$\varepsilon_{\text{total}}$	$\Lambda_{\text{his}}^{\text{skeleton}} / \frac{\text{mol}}{\text{L}}$	$\Lambda_{\text{his}}^{\text{CV}} / \frac{\text{mol}}{\text{L}}$	$\Lambda_{\text{AcB}}^{\text{skeleton}} / \frac{\text{mol}}{\text{L}}$	$\Lambda_{\text{AcB}}^{\text{CV}} / \frac{\text{mol}}{\text{L}}$	$m_{\text{dry}} / \text{g}$
164	0.45	0.55	0.75	$0.402 \pm 1.9 \cdot 10^{-2}$	$0.100 \pm 4.8 \cdot 10^{-3}$	$0.355 \pm 4.0 \cdot 10^{-4}$	$0.088 \pm 9.9 \cdot 10^{-5}$	0.051
227	0.38	0.52	0.70	$0.390 \pm 3.9 \cdot 10^{-2}$	$0.116 \pm 1.2 \cdot 10^{-2}$	$0.283 \pm 1.2 \cdot 10^{-4}$	$0.084 \pm 3.6 \cdot 10^{-5}$	0.071
320	0.39	0.49	0.69	$0.386 \pm 1.6 \cdot 10^{-2}$	$0.121 \pm 5.0 \cdot 10^{-3}$	$0.239 \pm 4.2 \cdot 10^{-4}$	$0.075 \pm 3.3 \cdot 10^{-4}$	0.094
448	0.39	0.51	0.70	$0.385 \pm 1.1 \cdot 10^{-2}$	$0.116 \pm 3.2 \cdot 10^{-3}$	$0.248 \pm 1.1 \cdot 10^{-3}$	$0.075 \pm 3.3 \cdot 10^{-4}$	0.134
566	0.41	0.49	0.70	$0.369 \pm 1.7 \cdot 10^{-3}$	$0.110 \pm 5.0 \cdot 10^{-4}$	$0.253 \pm 1.1 \cdot 10^{-4}$	$0.076 \pm 3.3 \cdot 10^{-5}$	0.168
mean \pm sd				$0.387 \pm 1.1 \cdot 10^{-2}$	$0.113 \pm 7.0 \cdot 10^{-3}$	$0.276 \pm 4.2 \cdot 10^{-2}$	$0.080 \pm 5.6 \cdot 10^{-3}$	

Table 2: Column chromatography data of SP Sepharose FF. The means and standard deviations of triplicates per column volume (CV) are given. Gravimetry was carried out as a single measurement. The means and standard deviations of all CVs are given below the table.

CV / μL	ϵ_{column}	$\epsilon_{\text{particle}}$	ϵ_{total}	$\Lambda_{\text{his}}^{\text{skeleton}} / \frac{\text{mol}}{\text{L}}$	$\Lambda_{\text{his}}^{\text{CV}} / \frac{\text{mol}}{\text{L}}$	$\Lambda_{\text{AcB}}^{\text{skeleton}} / \frac{\text{mol}}{\text{L}}$	$\Lambda_{\text{AcB}}^{\text{CV}} / \frac{\text{mol}}{\text{L}}$	$m_{\text{dry}} / \text{g}$
173	0.40	0.91	0.95	$5.585 \pm 1.9 \cdot 10^{-1}$	$0.305 \pm 1.0 \cdot 10^{-2}$	$4.033 \pm 1.1 \cdot 10^{-2}$	$0.220 \pm 6.0 \cdot 10^{-4}$	0.023
246	0.32	0.92	0.95	$4.965 \pm 7.6 \cdot 10^{-2}$	$0.262 \pm 4.0 \cdot 10^{-3}$	$3.850 \pm 1.6 \cdot 10^{-2}$	$0.203 \pm 8.2 \cdot 10^{-4}$	0.031
400	0.42	0.91	0.95	$5.272 \pm 6.0 \cdot 10^{-2}$	$0.267 \pm 3.1 \cdot 10^{-3}$	$3.671 \pm 1.0 \cdot 10^{-2}$	$0.186 \pm 5.2 \cdot 10^{-4}$	0.042
434	0.39	0.91	0.94	$5.147 \pm 5.7 \cdot 10^{-2}$	$0.290 \pm 3.2 \cdot 10^{-3}$	$4.268 \pm 1.7 \cdot 10^{-2}$	$0.240 \pm 9.8 \cdot 10^{-4}$	0.059
487	0.37	0.91	0.94	$5.379 \pm 3.0 \cdot 10^{-2}$	$0.303 \pm 1.7 \cdot 10^{-3}$	$3.823 \pm 2.6 \cdot 10^{-2}$	$0.216 \pm 1.5 \cdot 10^{-3}$	0.055
mean \pm sd				$5.269 \pm 2.1 \cdot 10^{-1}$	$0.285 \pm 1.8 \cdot 10^{-2}$	$3.929 \pm 2.1 \cdot 10^{-1}$	$0.213 \pm 1.8 \cdot 10^{-2}$	

Table 3: Additional parameters and settings used for the simulations of the column breakthrough curves. The case study was carried out using an alternative adsorber lot.

	Unit	Value
Column model		Transport dispersive
Pore model		General rate
Isotherm		Steric mass action
Number of axial cells		50
Number of radial cells		10
Time step	s	1
Length	mm	20.8
Volume	mL	0.711
Column porosity		0.44
Bead porosity		0.8
Axial dispersion	$\frac{mm^2}{s}$	0.1
Ionic capacity	$\frac{mol}{L}$	1.86
Salt: Film diffusion	$\frac{mm}{s}$	$1.5 \cdot 10^{-2}$
Salt: Pore diffusion	$\frac{mm^2}{s}$	$1 \cdot 10^{-4}$
Lysozyme: Film diffusion	$\frac{mm}{s}$	$1.5 \cdot 10^{-2}$
Lysozyme: Pore diffusion	$\frac{mm^2}{s}$	$4 \cdot 10^{-5}$
Lysozyme: k_{kin}		0.5

A.3 Supporting Information for: Deconvolution of High-throughput Multi-component Isotherms Using Multi-variate Data Analysis of Protein Spectra

Pascal Baumann^{1,*}, Tobias Hahn^{1,*}, Thiemo Huuk^{1,*}, Anna Osberghaus¹, Jürgen Hubbuch¹

¹ Karlsruhe Institute of Technology (KIT), Institute of Process Engineering in Life Sciences, Section IV: Biomolecular Separation Engineering, Karlsruhe, Germany

* Contributed equally to this work

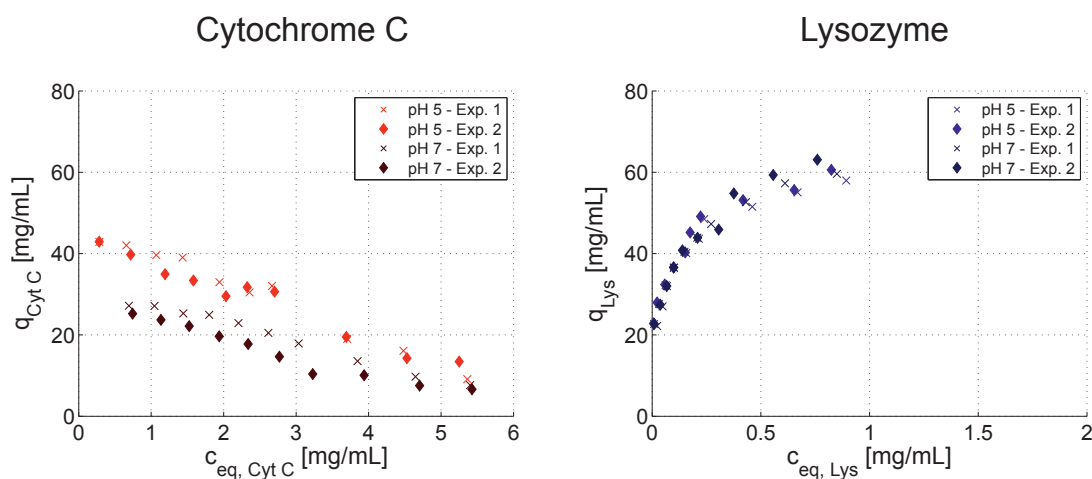


Figure A.2: Comparison of isotherm data for determination of the experimental robustness and model performance. Duplicates of the isotherm experiments performed at 90 mM ionic strength for pH 5 and pH 7. The duplicates are indicated as diamonds and crosses, respectively. The results for cytochrome c are shown in red (left) and for lysozyme in blue (right).

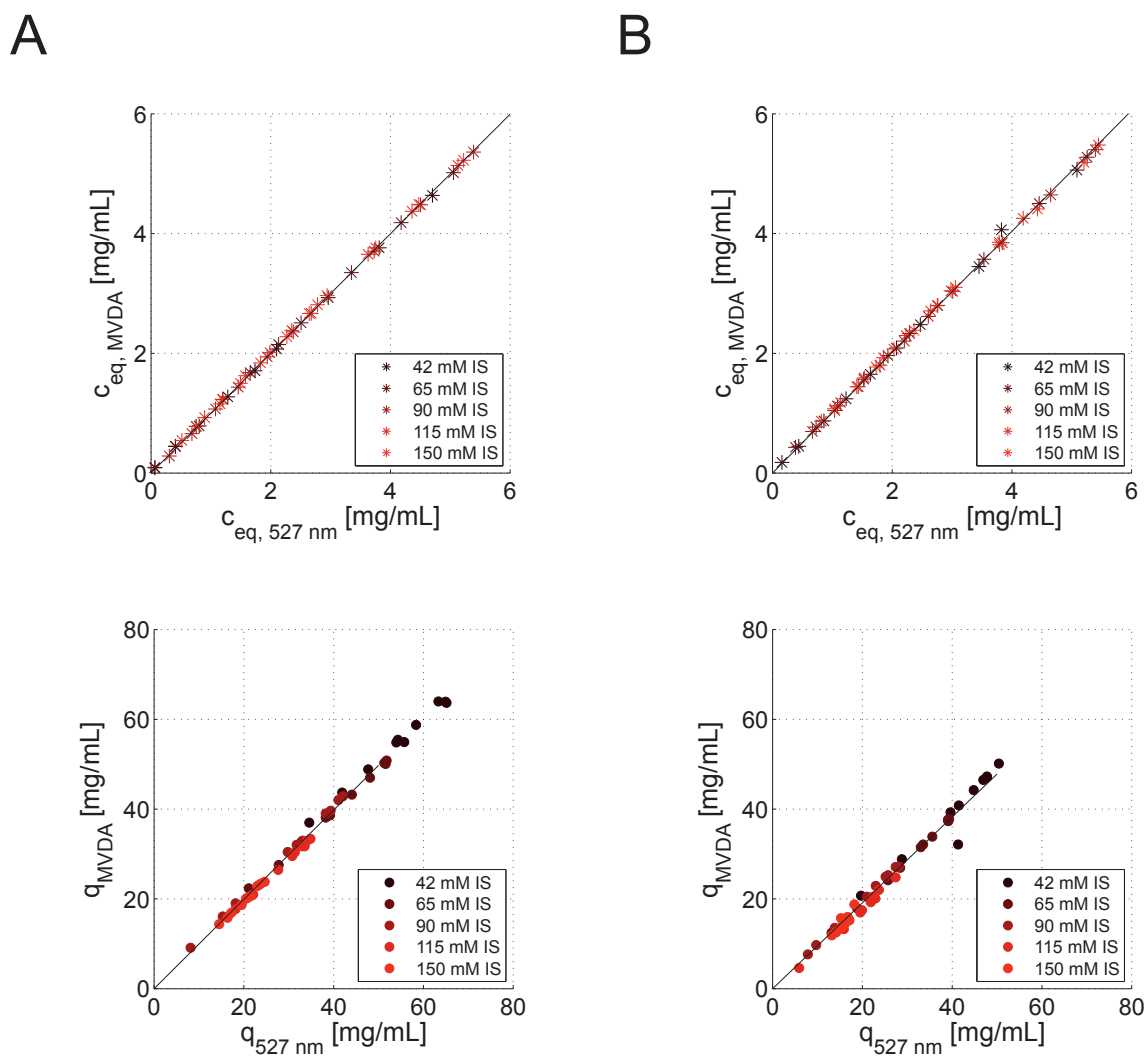


Figure A.3: Comparison of cytochrome c isotherm data points at pH 5 (A) and pH 7 (B) derived from the MVDA model and the selective 527 nm wavelength as a secondary analytics for validation. The agreement of the different data point is shown in parity plots for the equilibrium concentration of cytochrome in solution and bound to the adsorbent.

Bibliography

1. ABEL, S.; ERDEM, G.; AMANULLAH, M.; MORARI, M.; MAZZOTTI, M.; AND MORBIDELLI, M., 2005. Optimizing control of simulated moving beds—experimental implementation. *Journal of chromatography. A*, 1092, 1 (2005), 2–16. doi:10.1016/j.chroma.2005.04.101.
2. AHRENS, J.; GEVECI, B.; AND LAW, C., 2005. 36 - ParaView: An End-User Tool for Large-Data Visualization. In *Visualization Handbook* (Ed. C. D. H. R. JOHNSON), 717 – LXXII. Butterworth-Heinemann, Burlington. ISBN 978-0-12-387582-2. doi: 10.1016/B978-012387582-2/50038-1.
3. APPLIED BIOSYSTEMS, 2013. *POROS 50 μ m Resin - General Column Packing*. <https://tools.thermofisher.com/content/sfs/manuals/4468731.pdf>.
4. ARELLANO-GARCIA, H.; SCHÖNEBERGER, J.; AND KÖRKEKEL, S., 2007. Optimale Versuchsplanung in der Chemischen Verfahrenstechnik. *Chemie-Ingenieur-Technik*, 79, 10 (2007), 1625–1638. doi:10.1002/cite.200700110.
5. ASPEN TECHNOLOGY. Aspen Chromatography. <http://www.aspentech.com/products/aspen-chromatography.aspx>. Accessed May 2015.
6. ATKINSON, A.; DONEV, A.; AND TOBIAS, R., 2010. *Optimum Experimental Designs, With SAS*. Oxford University Press. ISBN 13: 9780199296606. doi: 10.1198/jasa.2008.s258.
7. BARKER, G.; CALZADA, J.; OUYANG, Z.; DOMAGALSKI, N.; HERZER, S.; AND RIEBLE, S., 2015. A systematic approach to improve data quality in high-throughput batch adsorption experiments. *Eng. Life Sci.*, (2015). doi:10.1002/elsc.201400242.
8. BARZ, T.; LÖFFLER, V.; ARELLANO-GARCIA, H.; AND WOZNY, G., 2010. Optimal determination of steric mass action model parameters for β -lactoglobulin using static batch experiments. *Journal of Chromatography A*, 1217, 26 (2010), 4267–4277. doi: 10.1016/j.chroma.2010.04.001.
9. BAUER, I.; BOCK, H. G.; KÖRKEKEL, S.; AND SCHLÖDER, J. P., 2000. Numerical methods for optimum experimental design in DAE systems. *Journal of Computational and Applied Mathematics*, 120, 1-2 (2000), 1–25. doi:10.1016/S0377-0427(00)00300-9.
10. BAUMANN, P.; BLUTHARDT, N.; RENNER, S.; BURGHARDT, H.; OSBERGHAUS, A.; AND HUBBUCH, J., 2015. Integrated development of up- and downstream processes supported by the Cherry-Tag™ for real-time tracking of stability and solubility of proteins. *Journal of Biotechnology*, 200 (2015), 27–37. doi:10.1016/j.jbiotec.2015.02.024.

11. BAUMGARTNER, K.; OELMEIER, S.; AND HUBBUCH, J., 2015. The influence of mixed salts on the capacity of hic adsorbers: A predictive correlation to the surface tension and the aggregation temperature. *Biotechnol. Progr.*, (2015). doi:10.1002/btpr.2166.
12. BEACHKOFSKI, B. K. AND GRANDHI, R. V., 2002. Improved Distributed Hypercube Sampling. In *AIAA Paper*, 1–8. doi:10.2514/6.2002-1274.
13. BENSCH, M.; SCHULZE WIERLING, P.; VON LIERES, E.; AND HUBBUCH, J., 2005. High throughput screening of chromatographic phases for rapid process development. *Chemical Engineering and Technology*, 28, 11 (2005), 1274–1284. doi:10.1002/ceat.200500153.
14. BENSCH, M.; SELBACH, B.; AND HUBBUCH, J., 2007. High throughput screening techniques in downstream processing: Preparation, characterization and optimization of aqueous two-phase systems. *Chemical Engineering Science*, 62, 7 (2007), 2011 – 2021. doi:http://dx.doi.org/10.1016/j.ces.2006.12.053.
15. BERGANDER, T.; KRISTINA NILSSON-VÄLIMAA, K. Ö.; AND LACKI, K. M., 2008. High-throughput process development: Determination of dynamic binding capacity using microtiter filter plates filled with chromatography resin. *Biotechnol. Progr.*, 24 (2008), 632–639. doi:10.1021/bp0704687.
16. BERGANDER, T. AND LACKI, K. M., 2015. High-throughput process development: Chromatography media volume definition. *Eng. Life Sci.*, (2015). doi:10.1002/elsc.201400240.
17. BHAMBURE, R.; KUMAR, K.; AND RATHORE, A., 2011. High throughput process development for biopharmaceutical drug substances. *Trends in Biotechnology*, 29, 3 (2011), 127–135. doi:10.1016/j.tibtech.2010.12.001.
18. BORG, N.; BRODSKY, Y.; MOSCARIELLO, J.; VUNNUM, S.; VEDANTHAM, G.; WESTERBERG, K.; AND NILSSON, B., 2014. Modeling and robust pooling design of a preparative cation-exchange chromatography step for purification of monoclonal antibody monomer from aggregates. *J. Chromatogr. A*, 1359 (2014), 170–181. doi: 10.1016/j.chroma.2014.07.041.
19. BORG, N.; WESTERBERG, K.; ANDERSSON, N.; VON LIERES, E.; AND NILSSON, B., 2013. Effects of uncertainties in experimental conditions on the estimation of adsorption model parameters in preparative chromatography. *Computers and Chemical Engineering*, 55 (2013), 148–157. doi:10.1016/j.compchemeng.2013.04.013.
20. BOSWELL, P. G.; STOLL, D. R.; CARR, P. W.; NAGEL, M. L.; VITHA, M. F.; AND MABBOTT, G. A., 2013. An advanced, interactive, high-performance liquid chromatography simulator and instructor resources. *Journal of Chemical Education*, 90, 2 (2013), 198–202. doi:10.1021/ed300117b.
21. BRESTRICH, N.; BRISKOT, T.; OSBERGHAUS, A.; AND HUBBUCH, J., 2014. A tool for selective inline quantification of co-eluting proteins in chromatography using spectral analysis and partial least squares regression. *Biotechnology and Bioengineering*, 111, 7 (2014), 1365–1373. doi:10.1002/bit.25194.

-
22. BRESTRICH, N.; SANDEN, A.; KRAFT, A.; MCCANN, K.; BERTOLINI, J.; AND HUBBUCH, J., 2015. Advances in inline quantification of co-eluting proteins in chromatography: Process-data-based model calibration and application towards real-life separation issues. *Biotechnology and Bioengineering*, 112, 7 (Jul. 2015). doi:10.1002/bit.25546.
 23. BROOKS, C. A. AND CRAMER, S. M., 1992. Steric mass-action ion exchange: Displacement profiles and induced salt gradients. *AIChE Journal*, 38, 12 (Dec. 1992), 1969–1978. doi:10.1002/aic.690381212.
 24. CABALLERO, S.; DIEZ, J. M.; BELDA, F. J.; OTEGUI, M.; HERRING, S.; ROTH, N. J.; LEE, D.; GAJARDO, R.; AND JORQUERA, J. I., 2014. Robustness of nanofiltration for increasing the viral safety margin of biological products. *Biologicals*, 42 (2014), 79–85. doi:10.1016/j.biologicals.2013.10.003.
 25. CHARTRAIN, M. AND CHU, L., 2008. Development and production of commercial therapeutic monoclonal antibodies in mammalian cell expression systems: An overview of the current upstream technologies. *Current Pharmaceutical Biotechnology*, 9 (2008), 447–467. doi:10.2174/138920108786786367.
 26. CHEN, J.; TETRAULT, J.; ZHANG, Y.; WASSERMAN, A.; CONLEY, G.; DI LEO, M.; HAIMES, E.; NIXON, A. E.; AND LEY, A., 2010. The distinctive separation attributes of mixed-mode resins and their application in monoclonal antibody downstream purification process. *Journal of Chromatography A*, 1217, 2 (2010), 216–224. doi:10.1016/j.chroma.2009.09.047.
 27. CHHATRE, S.; FARID, S. S.; COFFMAN, J.; BIRD, P.; NEWCOMBE, A. R.; AND TITCHENER-HOOKER, N. J., 2011. How implementation of quality by design and advances in biochemical engineering are enabling efficient bioprocess development and manufacture. *Journal of Chemical Technology and Biotechnology*, 86, 9 (2011), 1125–1129. doi:10.1002/jctb.2628.
 28. CHROMWORKS. ChromWorks. <http://chromworks.com>. Accessed May 2015.
 29. CHUNG, W. K.; FREED, A. S.; HOLSTEIN, M. A.; MCCALLUM, S. A.; AND CRAMER, S. M., 2010. Evaluation of protein adsorption and preferred binding regions in multimodal chromatography using NMR. *Proceedings of the National Academy of Sciences of the United States of America*, 107, 39 (2010), 16811–16816. doi:10.1073/pnas.1002347107.
 30. CLOSE, E. J.; SALM, J. R.; BRACEWELL, D. G.; AND SORENSEN, E., 2014. Modelling of industrial biopharmaceutical multicomponent chromatography. *Chemical Engineering Research and Design*, 92, 7 (2014), 1304–1314. doi:10.1016/j.cherd.2013.10.022.
 31. COFFMAN, J. L.; KRAMARCZYK, J. F.; AND KELLEY, B. D., 2008. High-throughput screening of chromatographic separations: I. method development and column modeling. *Biotechnology and Bioengineering*, 100, 4 (2008), 605–618. doi:10.1002/bit.21904.
 32. CORNEL, J.; TARAFDER, A.; KATSUO, S.; AND MAZZOTTI, M., 2010. The direct inverse method: A novel approach to estimate adsorption isotherm parameters. *Journal*

-
- of Chromatography A*, 1217, 12 (2010), 1934–1941. doi:DOI10.1016/j.chroma.2010.01.063.
33. CRAMER, H., 1957. *Mathematical Methods of Statistics*. Princeton University Press. ISBN 9780691005478. doi:10.2307/2280199.
34. DANCKWERTS, P., 1953. Continuous flow systems. *Chemical Engineering Science*, 2, 1 (Feb. 1953), 1–13. doi:10.1016/0009-2509(53)80001-1.
35. DEGERMAN, M.; JAKOBSSON, N.; AND NILSSON, B., 2006. Constrained optimization of a preparative ion-exchange step for antibody purification. *Journal of Chromatography A*, 1113, 1-2 (Apr. 2006), 92–100. doi:10.1016/j.chroma.2006.01.121.
36. DEGERMAN, M.; WESTERBERG, K.; AND NILSSON, B., 2009. A Model-based approach to determine the design space of preparative Chromatography. *Chemical Engineering and Technology*, 32, 8 (2009), 1195–1202. doi:10.1002/ceat.200900102.
37. DEVERNAY, F. C/C++ Minpack, ver. 1.3.2. <http://devernay.free.fr/hacks/cminpack/>.
38. DZIENNIK, S. R.; BELCHER, E. B.; BARKER, G. A.; AND LENHOFF, A. M., 2005. Effects of ionic strength on lysozyme uptake rates in cation exchangers. I: Uptake in SP sepharose FF. *Biotechnology and Bioengineering*, 91, 2 (Jul. 2005), 139–153. doi:10.1002/bit.20503.
39. FAHRNER, R. L.; KNUDSEN, H. L.; BASEY, C. D.; GALAN, W.; FEUERHELM, D.; VANDERLAAN, M.; AND BLANK, G. S., 2001. Industrial purification of pharmaceutical antibodies: Development, operation, and validation of chromatography processes. *Biotechnology and Genetic Engineering Reviews*, 18 (2001), 301–327. doi:10.1080/02648725.2001.10648017.
40. FLATMAN, S.; ALAM, I.; GERARD, J.; AND MUSSA, N., 2007. Process analytics for purification of monoclonal antibodies. *Journal of Chromatography B*, 848 (2007), 79–87. doi:10.1016/j.jchromb.2006.11.018.
41. FORSCHUNGSZENTRUM JÜLICH. CADET. <https://github.com/modsim/CADET>. Accessed May 2015.
42. FORSSÉN, P.; ARNELL, R.; AND FORNSTEDT, T., 2006. An improved algorithm for solving inverse problems in liquid chromatography. *Computers & Chemical Engineering*, 30, 9 (Jul. 2006), 1381–1391. doi:10.1016/j.compchemeng.2006.03.004.
43. GAGNON, P., 2011. Technology trends in antibody purification. *Journal of chromatography A*, 1221 (2011), 57–70. doi:10.1016/j.chroma.2011.10.034.
44. GALLANT, S. R.; KUNDU, A.; AND CRAMER, S. M., 1995. Modeling non-linear elution of proteins in ion-exchange chromatography. *Journal of Chromatography A*, 702, 1-2 (May 1995), 125–142. doi:10.1016/0021-9673(94)00992-I.
45. GALLANT, S. R.; KUNDU, A.; AND CRAMER, S. M., 1995. Optimization of step gradient separations: Consideration of nonlinear adsorption. *Biotechnology and Bioengineering*, 47, 3 (1995), 355–372. doi:10.1002/bit.260470310.

-
46. GAVARA, P. R.; CABRERA, R.; VENNAPUSA, R. R.; GRASSELLI, M.; AND FERNANDEZ-LAHOPE, M., 2012. Preparation, characterization, and process performance of composite fibrous adsorbents as cation exchangers for high throughput and high capacity bioseparations. *J. Chromatogr. B*, 903 (2012), 14–22. doi:10.1016/j.jchromb.2012.06.027.
 47. GLOWINSKI, R., 2003. Finite element methods for incompressible viscous flow. In *Numerical Methods for Fluids (Part 3)* (Eds. P. CIARLET AND J. LIONS), vol. 9 of *Handbook of Numerical Analysis*, 3 – 1176. Elsevier. doi:10.1016/S1570-8659(03)09003-3.
 48. GOODWIN, GRAHAM C, PAYNE, R. L., 1977. *Dynamic System Identification: Experiment Design and Data Analysis*. Academic Press. ISBN 9780080956459.
 49. GOTTSCHALK, U. (Ed.), 2009. *Process Scale Purification of Antibodies*. John Wiley and Sons.
 50. GU, T., 1995. Multicomponent Radial Flow Chromatography. In *Mathematical Modeling and Scale-up of Liquid Chromatography*, 102–110. Springer Berlin Heidelberg. ISBN 978-3-642-79543-5.
 51. GUÉLAT, B.; STRÖHLEIN, G.; LATTUADA, M.; DELEGRANGE, L.; VALAX, P.; AND MORBIDELLI, M., 2012. Simulation model for overloaded monoclonal antibody variants separations in ion-exchange chromatography. *Journal of Chromatography A*, 1253 (2012), 32–43. doi:10.1016/j.chroma.2012.06.081.
 52. GUERRIER, L.; FLAYEUX, I.; AND BOSCHETTI, E., 2001. A dual-mode approach to the selective separation of antibodies and their fragments. *Journal of Chromatography B: Biomedical Sciences and Applications*, 755, 1-2 (2001), 37–46. doi:10.1016/S0378-4347(00)00598-3.
 53. GUERRIER, L.; GIROT, P.; SCHWARTZ, W.; AND BOSCHETTI, E., 2000. New method for the selective capture of antibodies under physiological conditions. *Bioseparation*, 9, 4 (2000), 211–221. doi:10.1023/A:1008170226665.
 54. GUIOCHON, G. AND BEAVER, L. A., 2011. Separation science is the key to successful biopharmaceuticals. *Journal of Chromatography A*, 1218, 49 (2011), 8836–8858. doi:10.1016/j.chroma.2011.09.008.
 55. GUIOCHON, G.; SHIRAZI, D. G.; FELINGER, A.; AND KATTI, A. M., 2006. *Fundamentals of Preparative and Nonlinear Chromatography*. Academic Press. ISBN 9780123705372.
 56. HAGEL, L.; JAGSCHIES, G.; AND SOFER, G., 2008. *Handbook of Process Chromatography*. Elsevier Academic Press, Amsterdam, 2. ed. edn. ISBN 9780123740236. doi:10.1016/B978-012374023-6.50010-5.
 57. HAHN, R.; BAUERHANSL, P.; SHIMAHARA, K.; CHRISTOPHERWIZNIEWSKI; TSCHELIESSNIG, A.; AND JUNGBAUER, A., 2005. Comparison of protein a affinity sorbents ii. mass transfer properties. *J. Chromatogr. A*, 1093 (2005), 98–110. doi:10.1016/j.chroma.2005.07.050.

58. HAHN, T.; BAUMANN, P.; HUUK, T.; HEUVELINE, V.; AND HUBBUCH, J., 2015. UV absorption-based inverse modeling of protein chromatography. *Engineering in Life Sciences*, (May 2015). doi:10.1002/elsc.201400247.
59. HAHN, T.; HUUK, T.; HEUVELINE, V.; AND HUBBUCH, J., 2015. Simulating and Optimizing Preparative Protein Chromatography with ChromX. *Journal of Chemical Education*, 0 (2015), 150623161654001. doi:10.1021/ed500854a.
60. HAHN, T.; HUUK, T.; OSBERGHAUS, A.; DONINGER, K.; NATH, S.; HEPBILDIKLER, S.; HEUVELINE, V.; AND HUBBUCH, J., 2015. Calibration-free inverse modeling of ion-exchange chromatography in industrial antibody purification. *Engineering in Life Sciences*, (2015). doi:10.1002/elsc.201400248.
61. HAHN, T.; SOMMER, A.; OSBERGHAUS, A.; HEUVELINE, V.; AND HUBBUCH, J., 2014. Adjoint-based estimation and optimization for column liquid chromatography models. *Computers and Chemical Engineering*, 64 (2014), 41–54. doi:10.1016/j.compchemeng.2014.01.013.
62. HANKE, A. T. AND OTTENS, M., 2014. Purifying biopharmaceuticals: Knowledge-based chromatographic process development. *Trends in Biotechnology*, 32, 4 (2014), 210–220. doi:10.1016/j.tibtech.2014.02.001.
63. HANSEN, S. K.; SKIBSTED, E.; STABY, A.; AND HUBBUCH, J., 2011. A label-free methodology for selective protein quantification by means of absorption measurements. *Biotechnology and Bioengineering*, 108, 11 (2011), 2661–2669. doi:10.1002/bit.23229.
64. HARDIN, A. M.; HARINARAYAN, C.; MALMQUIST, G.; AXEN, A.; AND VAN REIS, R., 2009. Ion exchange chromatography of monoclonal antibodies: Effect of resin ligand density on dynamic binding capacity. *J. Chromatogr. A*, 1216 (2009), 4366–4371. doi:10.1016/j.chroma.2008.08.047.
65. HELDIN, E.; GRÖNLUND, S.; SHANAGAR, J.; HALLGREN, E.; ERIKSSON, K.; XAVIER, M.; TUNES, H.; AND VILELA, L., 2014. Development of an intermediate chromatography step in an insulin purification process. the use of a high throughput process development approach based on selectivity parameters. *J. Chromatogr. B*, 973 (2014), 126–132. doi:10.1016/j.jchromb.2014.09.024.
66. HELLING, C.; BORRMANN, C.; AND STRUBE, J., 2012. Optimal Integration of Directly Combined Hydrophobic Interaction and Ion Exchange Chromatography Purification Processes. *Chemical Engineering and Technology*, 35, 10 (2012), 1786–1796. doi:10.1002/ceat.201200043.
67. HERRMANN, T.; SCHRÖDER, M.; AND HUBBUCH, J., 2006. Generation of equally sized particle plaques using solid-liquid suspensions. *Biotechnology Progress*, 22, 3 (2006), 914–918. doi:10.1021/bp050296i.
68. HOOVER, T. B., 1982. Multiple eluent and pH effects on ion chromatography of phosphate and arsenate. *Sep. Sci. Technol.*, 17, 2 (1982), 295–305. doi:10.1080/01496398208068540.

-
69. HORSTMANN, B. J.; KENNEY, C. N.; AND CHASE, H. A., 1986. Adsorption of proteins on sepharose affinity adsorbents of varying particle size. *J. Chromatogr.*, 361 (1986), 179–190. doi:10.1016/S0021-9673(01)86905-3.
70. HOU, Y. AND CRAMER, S. M., 2011. Evaluation of selectivity in multimodal anion exchange systems: A priori prediction of protein retention and examination of mobile phase modifier effects. *Journal of Chromatography A*, 1218, 43 (2011), 7813–7820. doi:10.1016/j.chroma.2011.08.080.
71. HUBBUCH, J.; LINDEN, T.; KNIEPS, E.; THÖMMES, J.; AND KULA, M.-R., 2002. Dynamics of protein uptake within the adsorbent particle during packed bed chromatography. *Biotechnol. Bioeng.*, 80 (2002), 359–368. doi:10.1002/bit.10500.
72. HUUK, T. C.; HAHN, T.; OSBERGHAUS, A.; AND HUBBUCH, J., 2014. Model-based integrated optimization and evaluation of a multi-step ion exchange chromatography. *Separation and Purification Technology*, 136 (Nov. 2014), 207–222. doi:10.1016/j.seppur.2014.09.012.
73. ICH, 1999. Viral Safety evaluation of biotechnology products derived from cell lines of human or animal origin Q5A(R1). In *International Conference on Harmonisation of Technical Requirements for Registration of Pharmaceuticals for Human Use*.
74. ICH, 2011. ICH-Endorsed Guide for ICH Q8/Q9/Q10 Implementation. In *International Conference on Harmonisation of Technical Requirements for Registration of Pharmaceuticals for Human Use*.
75. ICH, 2011. Pharmaceutical Development Q8(R2). In *International Conference on Harmonisation of Technical Requirements for Registration of Pharmaceuticals for Human Use*.
76. ICH, 2012. Development and manufacture of drug substances (Chemical entities and biotechnological/Biological Entities) Q11. In *International Conference on Harmonisation of Technical Requirements for Registration of Pharmaceuticals for Human Use*.
77. JAKOBSSON, N.; KARLSSON, D.; AXELSSON, J. P.; ZACCHI, G.; AND NILSSON, B., 2005. Using computer simulation to assist in the robustness analysis of an ion-exchange chromatography step. *Journal of Chromatography A*, 1063, 1-2 (2005), 99–109. doi:10.1016/j.chroma.2004.11.067.
78. JOHANSSON, B. L.; BELEW, M.; ERIKSSON, S.; GLAD, G.; LIND, O.; MALOISEL, J. L.; AND NORRMAN, N., 2003. Preparation and characterization of prototypes for multi-modal separation media aimed for capture of negatively charged biomolecules at high salt conditions. *Journal of Chromatography A*, 1016, 1 (2003), 21–33. doi:10.1016/S0021-9673(03)01140-3.
79. JUNGBAUER, A., 1996. Insights into the chromatography of proteins provided by mathematical modeling. *Current Opinion in Biotechnology*, 7, 2 (1996), 210–218. doi:10.1016/S0958-1669(96)80015-2.
80. JUNGBAUER, A.; MACHOLD, C.; AND HAHN, R., 2005. Hydrophobic interaction chromatography of proteins: III. Unfolding of proteins upon adsorption. *Journal of Chromatography A*, 1079 (2005), 221–228.

-
81. KALLBERG, K.; BECKER, K.; AND BÜLOW, L., 2011. Application of a pH responsive multimodal hydrophobic interaction chromatography medium for the analysis of glycosylated proteins. *Journal of Chromatography A*, 1218, 5 (2011), 678–683. doi:10.1016/j.chroma.2010.11.080.
82. KARGER, B. L. AND BLANCO, R., 1989. The effect of on-column structural changes of proteins on their HPLC behavior. *Talanta*, 36, 1-2 (Jan. 1989), 243–248. doi:10.1016/0039-9140(89)80102-X.
83. KARKOV, H. S.; SEJERGAARD, L.; AND CRAMER, S. M., 2013. Methods development in multimodal chromatography with mobile phase modifiers using the steric mass action model. *Journal of Chromatography A*, 1318 (2013), 149–155. doi:10.1016/j.chroma.2013.10.004.
84. KARLSRUHE INSTITUTE OF TECHNOLOGY (KIT). ChromX. <http://www.chromx.org>. Accessed Mar 2015.
85. KARLSSON, D.; JAKOBSSON, N.; AXELSSON, A.; AND NILSSON, B., 2004. Model-based optimization of a preparative ion-exchange step for antibody purification. *Journal of Chromatography A*, 1055, 1-2 (2004), 29–39. doi:10.1016/j.chroma.2004.08.151.
86. KARLSSON, D.; JAKOBSSON, N.; BRINK, K.-J.; AXELSSON, A.; AND NILSSON, B., 2004. Methodologies for model calibration to assist the design of a preparative ion-exchange step for antibody purification. *Journal of Chromatography A*, 1033, 1 (Apr. 2004), 71–82. doi:10.1016/j.chroma.2003.12.072.
87. KEENER, R. N.; MANEVAL, J. E.; AND FERNANDEZ, E. J., 2004. Toward a robust model of packing and scale-up for chromatographic beds. 1. Mechanical compression. *Biotechnol. Prog.*, 20 (2004), 1146–1158. doi:10.1021/bp034279.
88. KELLEY, B. D.; SWITZER, M.; BASTEK, P.; KRAMARCZYK, J. F.; MOLNAR, K.; YU, T.; AND COFFMAN, J., 2008. High-throughput screening of chromatographic separations: IV. Ion-exchange. *Biotechnology and Bioengineering*, 100, 5 (Aug. 2008), 950–963. doi:10.1002/bit.21905.
89. KENNEDY, L. A.; KOPACIEWICZ, W.; AND REGNIER, F. E., 1986. Multimodal liquid chromatography columns for the separation of proteins in either the anion-exchange or hydrophobic-interaction mode. *Journal of Chromatography A*, 359 (Jan. 1986), 73–84. doi:10.1016/0021-9673(86)80063-2.
90. KITTELMANN, J.; OTTENS, M.; AND HUBBUCH, J., 2015. Robust high-throughput batch screening method in 384-well format with optical in-line resin quantification. *J. Chromatogr. B*, 988 (2015), 98–105. doi:10.1016/j.jchromb.2015.02.028.
91. KNÄBLEIN, J., 2013. *Twenty Thousand Years of Biotech - From "Traditional" to "Modern Biotechnology"*, 1–38. Wiley-VCH Verlag GmbH & Co. KGaA. ISBN 9783527669417. doi:10.1002/9783527669417.ch1.
92. KONTORAVDI, C.; SAMSATLI, N. J.; AND SHAH, N., 2013. Development and design of bio-pharmaceutical processes. *Current Opinion in Chemical Engineering*, 137 (2013), 1–7. doi:10.1016/j.coche.2013.09.007.

-
93. LADIWALA, A.; REGE, K.; BRENNEMAN, C. M.; AND CRAMER, S. M., 2005. A priori prediction of adsorption isotherm parameters and chromatographic behavior in ion-exchange systems. *Proceedings of the National Academy of Sciences of the United States of America*, 102, 33 (2005), 11710–11715. doi:10.1073/pnas.0408769102.
94. LAMPINEN, J.; RAITIO, M.; PERÄELÄ, A.; ORANEN, H.; AND HARINEN, R.-R., 2012. Microplate based pathlength correction method for photometric DNA quantification assay. Technical report, Thermo Fisher Scientific.
95. LEE, S.; RYU, K.-H.; KIM, Y.-G.; JUNG OH AHN AND, H. L.; JUNG, J.-K.; AND LEE, E. G., 2015. Radial scale-down of packed bed chromatography in a thin cylindrical tube for preparative media. *Process Biochem.*, 50 (2015), 839–845. doi:10.1016/j.procbio.2015.01.024.
96. LENDERO, N.; VIDIC, J.; BRNE, P.; FRANKOVIC, V.; STRANCAR, A.; AND PODGORNİK, A., 2008. Characterization of ion exchange stationary phases via pH transition profile. *J. Chromatogr. A*, 1185 (2008), 59–70. doi:10.1016/j.chroma.2008.01.023.
97. LENDERO, N.; VIDIC, J.; BRNE, P.; PODGORNİK, A.; AND STRANCAR, A., 2005. Simple method for determining the amount of ion-exchange groups on chromatographic supports. *J. Chromatogr. A*, 1065 (2005), 29–38. doi:10.1016/j.chroma.2004.10.072.
98. LEVY, N. E.; VALENTE, K. N.; CHOE, L. H.; LEE, K. H.; AND LENHOFF, A. M., 2014. Identification and characterization of host cell protein product-associated impurities in monoclonal antibody bioprocessing. *Biotechnol. Bioeng.*, 111 (2014), 904–912. doi:10.1002/bit.25158.
99. LIU, H.; GAZA-BULSECO, G.; FALDU, D.; CHUMSAE, C.; AND SUN, J., 2008. Heterogeneity of monoclonal antibodies. *Journal of Pharmaceutical Sciences*, 97 (2008), 2326–2447. doi:10.1002/jps.21180.
100. LIU, H. F.; MA, J.; WINTER, C.; AND BAYER, R., 2010. Recovery and purification process development for monoclonal antibody production. *mAbs*, 2, 5 (2010), 480–499. doi:10.4161/mabs.2.5.12645.
101. LOURAKIS, M., 2004. levmar: Levenberg-Marquardt nonlinear least squares algorithms in C/C++. <http://www.ics.forth.gr/~lourakis/levmar/>.
102. LUND UNIVERSITY. pcs. <http://www.chemeng.lth.se/pcs>. Accessed May 2015.
103. MA, J. K.-C.; M.W.DRAKE, P.; AND CHRISTOU, P., 2003. The production of recombinant pharmaceutical proteins in plants. *Nature Reviews Genetics*, 4 (2003), 794–805. doi:10.1038/nrg1177.
104. MAISER, B.; KRÖNER, F.; DISMER, F.; BRENNER-WEISS, G.; AND HUBBUCH, J., 2012. Isoform separation and binding site determination of mono-PEGylated lysozyme with pH gradient chromatography. *Journal of Chromatography A*, 1268 (2012), 102–108. doi:10.1016/j.chroma.2012.10.047.
105. MANNALL, G. J.; MYERS, J. P.; LIDDELL, J.; TITCHENER-HOOKER, N. J.; AND DALBY, P. A., 2009. Ultra scale-down of protein refold screening in microwells: Challenges, solutions and application. *Biotechnology and Bioengineering*, 103, 2 (2009), 329–340. doi:10.1002/bit.22245. <http://dx.doi.org/10.1002/bit.22245>.

-
106. MAREK, W.; MUCA, R.; WOŚ, S.; PIATKOWSKI, W.; AND ANTOS, D., 2013. Isolation of monoclonal antibody from a Chinese hamster ovary supernatant. II: Dynamics of the integrated separation on ion exchange and hydrophobic interaction chromatography media. *Journal of Chromatography A*, 1305 (2013), 64–75. doi:10.1016/j.chroma.2013.06.076.
107. MATASCI, M.; HACKER, D. L.; BALDI, L.; AND WURM, F. M., 2008. Recombinant therapeutic protein production in cultivated mammalian cells: current status and future prospects. *Drug Discovery Today: Technologies*, 5 (2008), 37–42. doi:10.1016/j.ddtec.2008.12.003.
108. MCNAY, J. L. AND FERNANDEZ, E. J., 1999. How does a protein unfold on a reversed-phase liquid chromatography surface? *Journal of Chromatography A*, 849, 1 (1999), 135–148. doi:10.1016/S0021-9673(99)00546-4.
109. MICHEL, M.; EPPING, A.; AND JUPKE, A., 2005. *Modeling and Determination of Model Parameters*, chap. 6, 215–312. Wiley-VCH Verlag GmbH & Co. KGaA. ISBN 9783527306435. doi:10.1002/3527603484.ch6.
110. MOLLERUP, J. M., 2006. Applied thermodynamics: A new frontier for biotechnology. *Fluid Phase Equilibria*, 241, 1-2 (2006), 205–215. doi:10.1016/j.fluid.2005.12.037.
111. MOLLERUP, J. M., 2008. A review of the thermodynamics of protein association to ligands, protein adsorption, and adsorption isotherms. *Chemical Engineering and Technology*, 31, 6 (2008), 864–874. doi:10.1002/ceat.200800082.
112. MOLLERUP, J. M.; HANSEN, T. B.; KIDAL, S.; SEJERGAARD, L.; AND STABY, A., 2007. Development, modelling, optimisation and scale-up of chromatographic purification of a therapeutic protein. *Fluid Phase Equilibria*, 261, 1-2 (Dec. 2007), 133–139. doi:10.1016/j.fluid.2007.07.047.
113. MOLLERUP, J. M.; HANSEN, T. B.; KIDAL, S.; AND STABY, A., 2008. Quality by design-Thermodynamic modelling of chromatographic separation of proteins. *Journal of Chromatography A*, 1177, 2 (2008), 200–206. doi:10.1016/j.chroma.2007.08.059.
114. MOVITZ, J., 1974. A study on the biosynthesis of protein a in staphylococcus aureus. *Eur. J. Biochem.*, 48 (1974), 131–136. doi:10.1111/j.1432-1033.1974.tb03750.x.
115. MUCA, R.; PIATKOWSKI, W.; AND ANTOS, D., 2009. Altering efficiency of hydrophobic interaction chromatography by combined salt and temperature effects. *Journal of Chromatography A*, 1216, 50 (2009), 8712–8721. doi:10.1016/j.chroma.2009.04.046.
116. NASH, D. C. AND CHASE, H. A., 1998. Comparison of diffusion and diffusion-convection matrices for use in ion-exchange separations of proteins. *J. Chromatogr. A*, 807 (1998), 185–207. doi:10.1016/S0021-9673(98)00076-4.
117. NEVILLE, D. C. A.; DWEK, R. A.; AND BUTTERS, T. D., 2009. Development of a single column method for the separation of lipid- and protein-derived oligosaccharides. *Journal of Proteome Research*, 8, 2 (Feb. 2009), 681–687. doi:10.1021/pr800704t.

-
118. NFOR, B. K.; AHAMED, T.; VAN DEDEM, G. W. K.; VAN DER WIELEN, L. A. M.; VAN DE SANDT, E. J. A. X.; EPPINK, M. H. M.; AND OTTENS, M., 2008. Design strategies for integrated protein purification processes: Challenges, progress and outlook. *Journal of Chemical Technology and Biotechnology*, 83, 2 (2008), 124–132. doi:10.1002/jctb.1815.
119. NFOR, B. K.; AHAMED, T.; VAN DEDEM, G. W. K.; VERHAERT, P. D. E. M.; VAN DER WIELEN, L. A. M.; EPPINK, M. H. M.; VAN DE SANDT, E. J. A. X.; AND OTTENS, M., 2013. Model-based rational methodology for protein purification process synthesis. *Chemical Engineering Science*, 89 (2013), 185–195. doi:10.1016/j.ces.2012.11.034.
120. NFOR, B. K.; NOVERRAZ, M.; CHILAMKURTHI, S.; VERHAERT, P. D. E. M.; VAN DER WIELEN, L. A. M.; AND OTTENS, M., 2010. High-throughput isotherm determination and thermodynamic modeling of protein adsorption on mixed mode adsorbents. *Journal of Chromatography A*, 1217, 44 (2010), 6829–6850. doi:10.1016/j.chroma.2010.07.069.
121. NFOR, B. K.; RÍPIĆ, J.; VAN DER PADT, A.; JACOBS, M.; AND OTTENS, M., 2012. Model-based high-throughput process development for chromatographic whey proteins separation. *Biotechnology Journal*, 7, 10 (2012), 1221–1232. doi:10.1002/biot.201200191.
122. NFOR, B. K.; VERHAERT, P. D. E. M.; VAN DER WIELEN, L. A. M.; HUBBUCH, J.; AND OTTENS, M., 2009. Rational and systematic protein purification process development: the next generation. *Trends in Biotechnology*, 27, 12 (2009), 673–679. doi:10.1016/j.tibtech.2009.09.002.
123. OELMEIER, S. A.; DISMER, F.; AND HUBBUCH, J., 2010. Application of an aqueous two-phase systems high throughput screening method to evaluate mab HCP separation. *Biotechnology and bioengineering*, 108, 1 (2010), 69–81. doi:10.1002/bit.22900.
124. OSBERGHAUS, A.; BAUMANN, P.; HEPBILDIKLER, S.; NATH, S.; HAINDL, M.; VON LIERES, E.; AND HUBBUCH, J., 2012. Detection, quantification, and propagation of uncertainty in high-throughput experimentation by Monte Carlo methods. *Chemical Engineering and Technology*, 35, 8 (2012), 1456–1464. doi:10.1002/ceat.201100610.
125. OSBERGHAUS, A.; DRECHSEL, K.; HANSEN, S.; HEPBILDIKLER, S.; NATH, S.; HAINDL, M.; VON LIERES, E.; AND HUBBUCH, J., 2012. Model-integrated process development demonstrated on the optimization of a robotic cation exchange step. *Chem. Eng. Sci.*, 76 (2012), 129–139. doi:10.1016/j.ces.2012.04.004.
126. OSBERGHAUS, A.; HEPBILDIKLER, S.; NATH, S.; HAINDL, M.; VON LIERES, E.; AND HUBBUCH, J., 2012. Determination of parameters for the steric mass action model-A comparison between two approaches. *Journal of Chromatography A*, 1233 (2012), 54–65. doi:10.1016/j.chroma.2012.02.004.
127. OSBERGHAUS, A.; HEPBILDIKLER, S.; NATH, S.; HAINDL, M.; VON LIERES, E.; AND HUBBUCH, J., 2012. Optimizing a chromatographic three component separation: A comparison of mechanistic and empiric modeling approaches. *Journal of Chromatography A*, 1237 (2012), 86–95. doi:10.1016/j.chroma.2012.03.029.

128. OSBORNE, R., 2013. Fresh from the biotech pipeline-2012. *Nature biotechnology*, 31 (2013), 100–103. doi:10.1038/nbt.2498.
129. PARENTE, E. S. AND WETLAUFER, D. B., 1986. Relationship between isocratic and gradient retention times in the high-performance ion-exchange chromatography of proteins. *Journal of Chromatography A*, 355, 1 (Jan. 1986), 29–40. doi:10.1016/S0021-9673(01)97301-7.
130. PEREZ, H. L.; CARDARELLI, P. M.; DESHPANDE, S.; GANGWAR, S.; SCHROEDER, G. M.; VITE, G. D.; AND BORZILLERI, R. M., 2014. Antibody-drug conjugates: current status and future directions. *Drug Discovery Today*, 19 (2014), 869–881. doi:10.1016/j.drudis.2013.11.004.
131. PEZZINI, J.; JOUCLA, G.; GANTIER, R.; TOUEILLE, M.; LOMENECH, A.-M.; SENECHAL, C. L.; GARBAY, B.; SANTARELLI, X.; AND CABANNE, C., 2011. Antibody capture by mixed-mode chromatography: A comprehensive study from determination of optimal purification conditions to identification of contaminating host cell proteins. *J. Chromatogr. A*, 1218 (2011), 8197–8208.
132. POLYKARPOU, E. M.; DALBY, P. A.; AND PAPAGEORGIOU, L. G., 2012. A novel efficient optimisation system for purification process synthesis. *Biochemical Engineering Journal*, 67 (2012), 186–193. doi:10.1016/j.bej.2012.06.012.
133. POLYKARPOU, E. M.; DALBY, P. A.; AND PAPAGEORGIOU, L. G., 2012. An MILP formulation for the synthesis of protein purification processes. *Chemical Engineering Research and Design*, 90, 9 (2012), 1262–1270. doi:10.1016/j.cherd.2011.11.021.
134. PROCESS SYSTEMS ENTERPRISE. gProms. <http://www.psenterprise.com/gproms.html>. Accessed May 2015.
135. PRZYBYCIEN, T. M.; PUJAR, N. S.; AND STEELE, L. M., 2004. Alternative bioseparation operations: life beyond packed-bed chromatography. *Current opinion in biotechnology*, 15 (2004), 469–478. doi:10.1016/j.copbio.2004.08.008.
136. QUARTERONI, A. AND VALLI, A., 1994. *Numerical approximation of partial differential equations*. Springer; Berlin, Heidelberg, 1st ed. edn. ISBN 9783540852674. doi:10.1007/978-3-540-85268-1.
137. QURESHI, Z. H.; NG, T. S.; AND GOODWIN, G. C., 1980. Optimum experimental design for identification of distributed parameter systems. *International Journal of Control*, 31, 1 (1980), 21–29. doi:10.1080/00207178008961025.
138. SAHDEV, S.; KHATTAR, S. K.; AND SAINI, K. S., 2007. Production of active eukaryotic proteins through bacterial expression systems: a review of the existing biotechnology strategies. *Molecular and Cellular Biochemistry*, 307 (2007), 249–264. doi:10.1007/s11010-007-9603-6.
139. SALINAS, B. A.; SATHISH, H. A.; BISHOP, S. M.; HARN, N.; CARPENTER, J. F.; AND RANDOLPH, T. W., 2010. Understanding and modulating opalescence and viscosity in a monoclonal antibody formulation. *J. Pharm. Sci.*, 99 (2010), 82–93. doi:10.1002/jps.21797.

-
140. SAMRA, H. S. AND HE, F., 2012. Advancements in high throughput biophysical technologies: Applications for characterization and screening during early formulation development of monoclonal antibodies. *Mol. Pharmaceutics*, 9 (2012), 696–707. doi:10.1021/mp200404c.
141. SCHMIDT-TRAUB, H., 2005. *Preparative Chromatography: Of Fine Chemicals and Pharmaceutical Agents*, 1–458. Wiley-VCH Verlag GmbH & Co. KGaA, Weinheim, FRG. ISBN 9783527306435. doi:10.1002/3527603484.
142. SHALLIKER, R. A.; KAYILLO, S.; AND DENNIS, G. R., 2008. Optimizing Chromatographic Separation: An Experiment Using an HPLC Simulator. *Journal of Chemical Education*, 85, 9 (Sep. 2008), 1265. doi:10.1021/ed085p1265.
143. SHUKLA, A. A.; BAE, S. S.; MOORE, J. A.; BARNTHOUSE, K. A.; AND CRAMER, S. M., 1998. Synthesis and Characterization of High-Affinity, Low Molecular Weight Displacers for Cation-Exchange Chromatography. *Industrial & Engineering Chemistry Research*, 37, 10 (1998), 4090–4098. doi:10.1021/ie9801756.
144. SHUKLA, A. A.; BARNTHOUSE, K. A.; BAE, S. S.; MOORE, J. A.; AND CRAMER, S. M., 1998. Structural characteristics of low-molecular-mass displacers for cation-exchange chromatography. *Journal of Chromatography A*, 814, 1-2 (Dec. 1998), 83–95. doi:10.1016/S0021-9673(98)00374-4.
145. SHUKLA, A. A.; HUBBARD, B.; TRESSEL, T.; GUHAN, S.; AND LOW, D., 2007. Downstream processing of monoclonal antibodies—Application of platform approaches. *Journal of Chromatography B: Analytical Technologies in the Biomedical and Life Sciences*, 848, 1 (Mar. 2007), 28–39. doi:10.1016/j.jchromb.2006.09.026.
146. STABY, A.; SAND, M.-B.; HANSEN, R. G.; JACOBSEN, J. H.; ANDERSEN, L. A.; GERSTENBERG, M.; BRUUS, U. K.; AND JENSEN, I. H., 2006. Comparison of chromatographic ion-exchange resins III. Strong cation-exchange resins. *J. Chromatogr. A*, 1118 (2006), 168–179. doi:10.1016/j.chroma.2004.01.026.
147. STONE, D. C., 2007. Teaching Chromatography Using Virtual Laboratory Exercises. *Journal of Chemical Education*, 84, 9 (Sep. 2007), 1488–1495. doi:10.1021/ed084p1488.
148. STRAUSS, D. M.; CANO, T.; CAI, N.; DELUCCHI, H.; PLANCARTE, M.; COLEMAN, D.; BLANK, G. S.; CHEN, Q.; AND YANG, B., 2010. Strategies for developing design spaces for viral clearance by anion exchange chromatography during monoclonal antibody production. *Biotechnology progress*, 26 (2010), 750–755. doi:10.1002/btpr.385.
149. SUSANTO, A.; KNIEPS-GRÜNHAGEN, E.; VON LIERES, E.; AND HUBBUCH, J., 2008. High Throughput Screening for the Design and Optimization of Chromatographic Processes: Assessment of Model Parameter Determination from High Throughput Compatible Data. *Chemical Engineering & Technology*, 31, 6 (2008), 1846–1855. doi:10.1002/ceat.200800457.
150. SUSANTO, A.; TREIER, K.; KNIEPS-GRÜNHAGEN, E.; VON LIERES, E.; AND HUBBUCH, J., 2009. High throughput screening for the design and optimization of chromatographic processes: Automated optimization of chromatographic phase systems. *Chem. Eng. Technol.*, 32 (2009), 140–154. doi:10.1002/ceat.200800350.

-
151. TELEN, D.; LOGIST, F.; VAN DERLINDEN, E.; TACK, I.; AND VAN IMPE, J., 2012. Optimal experiment design for dynamic bioprocesses: A multi-objective approach. *Chemical Engineering Science*, 78 (Aug. 2012), 82–97. doi:10.1016/j.ces.2012.05.002.
152. TOUEILLE, M.; UZEL, A.; DEPOISIER, J.-F.; AND GANTIER, R., 2011. Designing new monoclonal antibody purification processes using mixed-mode chromatography sorbents. *Journal of Chromatography B*, 879 (2011), 836–843. doi:10.1016/j.jchromb.2011.02.047.
153. UCINSKI, D., 2004. *Optimal measurement methods for distributed parameter system identification*. CRC Press LLC. ISBN 9780203026786.
154. UNIVERSITY OF OHIO. Chromulator. <http://www.ohio.edu/people/gu/CHROM>. Accessed May 2015.
155. VALLIERE-DOUGLASS, J.; WALLACE, A.; AND BALLAND, A., 2008. Separation of populations of antibody variants by fine tuning of hydrophobic-interaction chromatography operating conditions. *Journal of chromatography A*, 1214 (2008), 81–89. doi:10.1016/j.chroma.2008.10.078.
156. VAN DEEMTER, J.; ZUIDERWEG, F.; AND KLINKENBERG, A., 1956. Longitudinal diffusion and resistance to mass transfer as causes of nonideality in chromatography. *Chemical Engineering Science*, 5 (1956), 271 – 289. doi:[http://dx.doi.org/10.1016/0009-2509\(96\)81813-6](http://dx.doi.org/10.1016/0009-2509(96)81813-6). <http://www.sciencedirect.com/science/article/pii/0009250996818136>.
157. VAN LIEROP, M. J. C.; WIJNANDS, F.; LOKE, Y. W.; EMMER, P. M.; LUKASSEN, H. G. M.; BRAAT, D. D. M.; VAN DER MEER, A.; MOSSELMAN, S.; AND JOOSTEN, I., 2002. Detection of HLA-G by a specific sandwich ELISA using monoclonal antibodies G233 and 56B. *Molecular human reproduction*, 8, 8 (2002), 776–784. doi:10.1093/molehr/8.8.776.
158. VÁZQUEZ-REY, M. AND LANG, D. A., 2011. Aggregates in monoclonal antibody manufacturing processes. *Biotechnology and Bioengineering*, 108, 7 (2011), 1494–1508. doi:10.1002/bit.23155.
159. VELAYUDHAN, A. AND HORVÁTH, C., 1988. Preparative chromatography of proteins : Analysis of the multivalent ion-exchange formalism. *J. Chromatogr. A*, 443 (1988), 13–29. doi:10.1016/S0021-9673(00)94779-4.
160. VOITL, A.; MÜLLER-SPÄTH, T.; AND MORBIDELLI, M., 2010. Application of mixed mode resins for the purification of antibodies. *Journal of Chromatography A*, 1217, 37 (2010), 5753–5760. doi:10.1016/j.chroma.2010.06.047.
161. WALL, M., 1996. GALib: A C++ library of genetic algorithm components. <http://lancet.mit.edu/ga/>.
162. WALTER, E. AND PRONZATO, L., 1997. *Identification of Parametric Models: from Experimental Data*. Springer-Verlag. ISBN 3540761195.
163. WANKAT, P. C., 2006. Using a commercial simulator to teach sorption separations. *Chemical Engineering Education*, 40, 3 (2006), 165.

-
164. WESTERBERG, K.; BROBERG-HANSEN, E.; SEJERGAARD, L.; AND NILSSON, B., 2013. Model-based risk analysis of coupled process steps. *Biotechnology and Bioengineering*, 110, 9 (2013), 2462–2470. doi:10.1002/bit.24909.
165. WESTERBERG, K.; DEGERMAN, M.; AND NILSSON, B., 2010. Pooling control in variable preparative chromatography processes. *Bioprocess and Biosystems Engineering*, 33, 3 (2010), 375–382. doi:10.1007/s00449-009-0335-8.
166. WIENDAHL, M.; VÖLKER, C.; HUSEMANN, I.; KRARUP, J.; STABY, A.; SCHOLL, S.; AND HUBBUCH, J., 2009. A novel method to evaluate protein solubility using a high throughput screening approach. *Chemical Engineering Science*, 64, 17 (2009), 3778 – 3788. doi:http://dx.doi.org/10.1016/j.ces.2009.05.029.
167. WIENDAHL, M.; WIERLING, P. S.; NIELSEN, J.; CHRISTENSEN, D. F.; KRARUP, J.; STABY, A.; AND HUBBUCH, J., 2008. High throughput screening for the design and optimization of chromatographic processes miniaturization, automation and parallelization of breakthrough and elution studies. *Chem*, 31 (2008), 893–903. doi: 10.1002/ceat.200800167.
168. YAMAMOTO, S., 2005. Electrostatic interaction chromatography process for protein separations: Impact of engineering analysis of biorecognition mechanism on process optimization. *Chemical Engineering and Technology*, 28, 11 (2005), 1387–1393. doi: 10.1002/ceat.200500199.
169. YIN, J.; LIB, G.; RENA, X.; AND HERRLER, G., 2007. Select what you need: A comparative evaluation of the advantages and limitations of frequently used expression systems for foreign genes. *Journal of Biotechnology*, 127 (2007), 335–247. doi:10.1016/j.jbiotec.2006.07.012.
170. ZHOU, J. X. AND DEPARTMENT, T. T., 2006. Basic concepts in q membrane chromatography for large-scale antibody production. *Biotechnology progress*, 22 (2006), 341–349. doi:10.1021/bp050425v.